THE UNIVERSITY *of* EDINBURGH

Technoeconomic Analysis of Offshore Green Hydrogen Production Re-using Oil and Gas Infrastructure.

Diana Jeleňová

Thesis submitted in partial fulfilment of the requirements for the award of an Engineering Doctorate

The University of Edinburgh

30th June 2022

ABSTRACT

With more industries realising the decarbonisation potential of green hydrogen, and more countries introducing their future hydrogen strategies, large scale hydrogen production will soon become a number one priority to meet growing hydrogen demand. For this reason, offshore wind farms are being proposed for large scale hydrogen production.

There are two routes to transfer energy generated by offshore wind farms to shore. A more conventional way through cables in the form of electricity, and a more novel route, by building new or re-using existing gas pipelines to transfer renewable electricity in the form of green hydrogen.

This work compares the two approaches for energy transfer and provides a technoeconomic assessment of a large scale offshore green hydrogen production for non-grid connected wind farms. With over 6000km of existing oil and gas pipelines in the UK continental shelf of the North Sea to be decommissioned in the next 10 years, the methodology developed within this work has been applied to a case study in the Northern part of the North Sea.

The methodology firstly identifies and maps areas of interest that match offshore renewable resource and oil and gas infrastructure. Once the area has been identified, the wind resource can be assessed in this area and the energy yield determined for a particular floating wind farm size. The volume of green hydrogen that can be produced from the floating wind farm can then be determined and consequently the requirements for the hydrogen pipeline infrastructure can be calculated. The final stage in the methodology is to conduct a techno-economic assessment to allow realistic and informed decisions to be made regarding the use of hydrogen as an energy vector at the chosen location.

This work demonstrates that it is possible to re-use oil and gas pipelines from a thermo-hydraulic perspective even without requiring the use of a compressor on the platform. However, substantial summer and winter hydrogen production differences cause efficiency issues, leading to significant storage requirements. It also shows that building new pipelines to shore only adds 2% to LCOH and might be preferred from pipeline integrity perspective. It was established that using pipelines is cheaper than using cables in low and central cost scenarios, when the cost for building a new topside is not included.

The methodology presented within can be applied to any future large scale non-grid connected windfarms enabling countries to reach their 2050 net zero goals.

LAY SUMMARY

Hydrogen is an energy carrier, that can decarbonise many sectors such as transportation, heating, and heavy industry to name a few. This is because unlike fossil fuels, when pure hydrogen burns, the only product is water and heat, which is the same for when hydrogen is converted to electricity. When produced from renewable energy, hydrogen carbon emissions decrease even further, and this hydrogen is often called green. With more sectors realising the decarbonisation potential of green hydrogen, and more countries introducing their future hydrogen strategies, large scale hydrogen production will soon become a number one priority to meet growing hydrogen demand. For this reason, offshore wind farms are being proposed for large scale hydrogen production.

There are two routes to transfer energy generated by offshore wind farms back to shore. A more conventional way through cables in the form of electricity, and a more novel route, by building new or re-using existing gas pipelines to transfer renewable electricity in the form of green hydrogen.

This work compares the two approaches for energy transfer and provides a technoeconomic assessment of a large scale offshore green hydrogen production for floating offshore wind farms that are not connected to the electrical grid. With over 6000km of existing offshore UK oil and gas pipelines to be removed in the next 10 years, the methodology developed within this work has been applied to a case study in the Northern part of the North Sea.

The methodology firstly identifies and maps offshore renewable resource (tide, waves and wind) and oil and gas infrastructure (pipelines and platforms). Once suitable area for hydrogen production has been identified, the wind resource is assessed in this area and the energy production determined for a model floating offshore wind farm. The volume of green hydrogen that can be produced from the floating wind farm can then be determined and consequently the requirements for the hydrogen pipeline infrastructure can be calculated. The final stage in the methodology is to conduct a techno-economic assessment to allow realistic and informed decisions to be made regarding the use of hydrogen as an energy carrier at the chosen location.

This work demonstrates that it is possible to re-use oil and gas pipelines for hydrogen transportation. However, substantial summer and winter hydrogen production differences cause efficiency issues, leading to significant storage requirements. It also

shows that building new pipelines to shore only adds 2% to the levelised cost of hydrogen. It was established that using pipelines is cheaper than using cables when the cost for building a new topside is not included.

The methodology presented within can be applied to any future large scale windfarm that is not connected to the electrical grid, enabling countries to reach their 2050 net zero goals.

ACKNOWLEDGMENTS

I would like to thank the following for making this thesis possible:

- All the IDCORE team and students as it is an amazing programme, full of education, industrial experience but also friendships and great adventure. Special thanks go to Katrina and David for always being there for me when needed.
- My industrial supervisor Alan Mortimer for choosing me during the Company Days and allowing me to pursue a project in hydrogen as well as any other initiatives I came up with, always supporting me, believing in me and being a great mentor.
- My lead academic supervisor Julia Race for always being available for a meeting and making me keep my work on track as well as my articles in check.
- My other academic supervisors Dimitri Mignard for providing detailed feedback and Philipp Thies for providing an industrial point of view and keeping the 'Eng' in my doctorate.
- Wind analysis, pipeline, electrical, hydrogen and other teams at Wood plc for always answering any questions I had regarding different challenges. Special thanks go to Marta Cholota who spent substantial time teaching me to work with GIS, and wind analysis software. Hooman Haghighi and Callum Peace, who always answered any questions regarding pipelines I had. David Hair, Jim Morrison and Ian Laidlow for providing information on oil and gas infrastructure. Kohan Kourosh and Ben Carroll for providing estimates on topsides, and Islay Duboulay for providing images that have been later adjusted for the purpose of this thesis (as well as late evening coffee breaks and chats).
- My family for always letting me do whatever I wanted and supporting me in my life decisions even if it meant moving very far from home.
- All my amazing friends that have always been there for me to celebrate great achievements as well as mourn any mishaps by enjoying our outdoor trips and all the black metal and grind concerts and festivals that kept me sane during these five very intense years.
- The staff at The Disability & Wellbeing Service at the Strathclyde University who were always very helpful and welcoming.

DECLARATION

I declare that this thesis has been composed solely by myself and that it has not been submitted, in whole or in part, in any previous application for a degree. Except where states otherwise by reference or acknowledgment, the work presented is entirely my own.

TABLE OF CONTENTS

LIST OF FIGURES

LIST OF TABLES

ABBREVIATIONS AND NOMENCLATURE

a	Measure of the attraction between particles
α_i	Wind speed over Weibull shape factor
$A_1^{(R)}$	Area of downwind turbine
AC	Alternating current
AE	Alkaline Electrolyser
AE_U	Average Electrolyser Utilisation
AHP	Annual Hydrogen Production
$A_{heat\ loss}$	Heat loss area
AoS	Areas of Search
$A_{overlap}$	The overlapping area between $A_1^{(R)}$ and the wind deficit downwind area
API	American Petroleum Institute
ASME	American Society of Mechanical Engineers
ATR	Autothermal Reforming
AWFU	Average Wind Farm Utiliation
b	Volume occupied by a particle, excluded from volume of the pipeline
BEIS	Department for Business, Energy and Industrial Strategy
c	Weibull shape parameter
C_0	CAPEX at year 0
C3S	Copernicus Climate Change Service

CAPEX	Capital Expenditure
C_C	Cable CAPEX
CCC	The Climate Change Committee
CCS	Carbon Capture and Storage
CCUS	Carbon Capture Use and Storage
C_D	Desalination unit CAPEX
C_E	Electrolyser CAPEX
CE	AC-DC Conversion Efficiency
CF	Capacity Factor
CFD	Computational Fluid Dynamics
C_{FOWF}	Floating Offshore Wind Farm CAPEX
C_{H0}	Hydrogen Production CAPEX at year 0
CL	Cable Length
CO_2	Carbon dioxide
COP	Conference of the parties
COP26	Conference of the parties under the UNFCCC that happened in Glasgow in 2021
C_P	Pipeline CAPEX
CPUC	California Public Utility Commission
C_T	Topside CAPEX
C_t	thrust coefficient

D	Pipeline Diameter
D_0	Rotor diameter of upwind turbine
D_{31}	DECEX at year 31
D_C	Cable DECEX
DC	Direct Current
DEC	Desalination Electricity Consumption
DECEX	Decommissioning expenditure
DESAL	Desalination
DFIG	Doubly-Fed Induction Generators
D_{FOWF}	Floating offshore wind farm DECEX
D_{H31}	Hydrogen production DECEX at year 31
DOLPHYN	The Deepwater Offshore Local Production of Hydrogen
D_o	Outside diameter
D_P	Pipeline DECEX
DPO	Draft Plan Options
D_T	Topside DECEX
DTU	Technical University of Denmark
E	Potential energy term
e	Electron
EA	Electrolyser Availability
ECMWF	European Centre for Medium-Range Weather Forecasts

EDI	Energy Delta Institute
EEC	Electrolyser Electricity Consumption
EIC	Energy Industries Council
EIGA	European Industrial Gases Association
EL	Electrolysis Losses
EoS	Equation of state
EPA	Environmental Protection Agency
E_T	Electricity output in year t
E_U	Electrolyser Utilisation
EU	European Union
f	Skin friction coefficient
F	Location factor
FCH 2 JU	Fuel Cell and Hydrogen Joint Undertaking 2
FCHJU	Fuel Cell and Hydrogen Joint Undertaking
FLAGS	Far North Liquids and Associated Gas System
FOWF	Floating offshore wind farm
FOWT	Floating Offshore Wind Turbine
Eo	Electrolyser operation
erf	Gaussian error function
F_T	Thrust force
g	Gravitational acceleration

G	Gas gravity
GAEP	Gross Annual Energy Production
GHG	Greenhouse Gas
GIS	Geographic Information System
$G_k(\alpha_i)$	Inverse Weibull scale parameter *k*
ΔH	Elevation change
H_2	Hydrogen
H_2O	Water
HGV	Heavy Goods Vehicle
H_t	Hydrogen produced in year t
HVAC	High Voltage Alternating Current
HVDC	High Voltage Direct Current
IAC	Inflation Adjusted Cost
ID	Internal Diameter
IEA	International Energy Agency
INTOG	Innovation and Targeted Oil and Gas Decarbonisation
IPCC	Intergovernmental Panel on Climate Change
IR	Inflation Rate
IRR	Internal Rate of Return
k	Weibull scale parameter
K	Roughness factor

ksi	Kilopound per square inch
k_W	Wake effect decay constant
L	Length
LBC	Lohrenz-Bray-Clark
LC	Levelised Cost
LCOE	Levelised Cost of Energy
LCOH	Levelised Cost of Hydrogen
LFAC	Low Frequency Alternating Current
μ	Mean
m	Mass
MGO	Marine Gas Oil
MOP	Maximum operating pressure
MPP	Mean Power Production
MPPE	Mean Power Production available for the Electrolyser
MWS	Mean Wind Speed
nmol	Number of moles
n	Total operational lifetime
NAEP	Net Annual Energy Production
NCDC	National Climatic Data Centre
NCF_t	Net Cash Flow in year t

NFPA	National Fire Protection Association
NIST	National Institute of Standards and Technology
NP	New pipeline
NPT	New pipeline+topside
NPV	Net Present Value
NS	North Sea
NSTA	North Sea Transition Authority
n_{STACK}	Operational lifetime of one stack in hours
O&G	Oil and Gas
O&M	Operation and maintenance
O_C	Cable OPEX
OD	Outer diameter
O_D	Desalination unit OPEX
O_E	Electrolyser OPEX
OFGEM	Office of Gas and Electricity Markets
O_{FOWF}	Floating offshore wind farm OPEX
OFTO	Offshore Transmission Operator
OGA	Oil and Gas Authority
O_{Ht}	Hydrogen production operational expenditure in year t

OGTC	Oil and Gas Technology Centre
O_P	Pipeline OPEX
OPEX	Operational Expenditure
OPRED	Offshore Petroleum Regulator for Environment and Decommissioning
ORE	Offshore Renewable Energy
OREC	Offshore Renewable Energy Converter
OSPAR	Oil Spill Prevention, Administration and Response
O_T	Topside OPEX
O_t	Operational expenditure in year t
OWF	Offshore wind farm
OWT	Offshore wind turbine
OWPB	Offshore wind programme board
p	Pressure
P	Mean Power Production
P1	Gas inlet pressure
P2	Gas outlet pressure
Pave	Average pressure
Pb	Pressure at base condition
PC	Past cost
PEM	Proton Exchange Membrane/ Polymer Electrolyte Membrane
PM	Pipeline material

PSU	Practical Salinity Units
PtG	Power to Gas
PV	Photovoltaic
q	Overall heat transfer coefficient
Q	Heat transfer
Qb	Gas flow rate at base condition
QGIS	Quantum Geographic Information System
ρ_{AIR}	Air density
ρ	Fluid density
ρ_{PM}	Pipeline material density
r	Discount rate
R	Gas constant
R_E	The cost of equity
RE	Renewable Energy
REC	Renewable Energy Converter
R_D	The cost of debt
RU	Re-used pipeline
RUT	Re-used pipeline+ topside
σ	Standard deviation
S	Salinity
SHFCA	Scottish Hydrogen Fuel Cell Association

SMR	Steam Methane Reforming
SMYS	Specified Minimum Yield Strength
SNG	Synthetic Natural Gas
SOE	Solid Oxide Electrolyser
SRC	Stack replacement cost
SR	Stack replacement
SRK	Soave-Redlich-Kwong
t	Individual year from 1 to n
τ	Wall stress
T	Temperature
T_a	Ambient temperature
Tave	Average temperature
Tb	Temperature at base conditions
TDS	Total Dissolved Solids
TEA	Total Electrolysis Availability
TEL	Total Electrolysis Losses
T_f	Fluid temperature
TLP	Tension leg platform
TNUoS	Transmission network use of system charges
TR	Asset Tax Rate
TSO	Transmission system operator

TWFA	Total Wind Farm Availability
TWFL	Total Wind Farm Losses
U	Mean fluid velocity
u_0	Undisturbed wind speed
$u_c(y)$	Combined Uncertainty
$u_i(x_i)$	Uncertainty of x
UK	United Kingdom
UKCS	UK Continental Shelf
UNFCCC	United Nations Framework Convention on Climate Change
v_1	Effective wind speed faced by the down-wind turbine
VD	Market Value of Debt
VE	Value of Equity
vi	Wind speed
V_P	Pipeline volume
WACC	Weighted Average Cost of Capital
WEC	Wave Energy Converter
WFL	Wind Farm Losses
WFU	Wind Farm Utilisation
WR	Water Required
WT	Wall thickness
WTG	Wind Turbine Generator

X	Number of observations
$\bar{x}$	The mean value of all observations
X_{01}	Downwind horizontal distance between the two turbines
x_i	The value of one observation
yr	Year
z	Height
Z_{ave}	Average compressibility factor

CHAPTER 1 - INTRODUCTION

1.1 Decarbonisation

It is widely accepted that climate change poses a threat to the planet and humans living on it with the driver being human greenhouse gas (GHG) emissions to the atmosphere [1], [2]. According to the Intergovernmental Panel on Climate Change (IPCC) any further delay in mitigation and adaptation will lead to missed opportunity for sustainable and liveable future for all [1]. To avoid this scenario, many countries have met in Glasgow in 2021 for Conference of the parties (COP) under the United Nations Framework Convention on Climate Change (UNFCCC) better known as COP26. The result of COP26 was Glasgow Climate Pact proposing to close the 2030 emissions gap with the aim to reach net zero by 2050 [3], where net zero means that the total emissions removed from the atmosphere offset the emissions produced [2]. To set the scene and link the importance of this research in large scale offshore green hydrogen production to current affairs, next section describes decarbonisation efforts and legislation within European geopolitical region, namely in Scotland, the United Kingdom, and the European Union. These areas were chosen as they are the most relevant to the location of the case study carried out within this thesis.

1.1.1 The European Union

In Europe, the European Green Deal is looking to reduce GHG emissions by at least 55% by 2030, with no net GHG emissions by 2050 [4]. On top of the European Green Deal, the EU has also introduced the RePowerEU Plan in May 2022, after Russian military aggression against Ukraine, to rapidly reduce dependence on Russian fossil fuels by accelerating the green transition, saving energy, and diversifying suppliers. RePowerEu is looking to lower natural gas consumption by 30% by 2030 by meeting energy efficiency targets. The plan also increases renewable energy targets to 45% (1236 GW) by 2030; and sets target of 10 million tonnes of domestic and 10 million tonnes of imported renewable hydrogen by 2030. According to The Commission, hydrogen will be key to replacing natural gas, coal and oil in hard to decarbonise industries and transportation [5].

1.1.2 The United Kingdom

The UK is aiming to be net zero by 2050. In April 2022, the UK government released the British Energy Security Strategy [6] that builds on the Ten Point Plan for green industrial revolution by the Department for Business, Energy and Industrial Strategy (BEIS) [7] and the Net Zero Strategy [8]. Some of the goals that the UK is looking to achieve are fully decarbonising the power system by 2035, with 40 GW of offshore wind 1GW of which to be floating by 2030, installing carbon capture and storage to tackle industrial emissions, ensuring low carbon heating in buildings, and all cars being fully zero emissions capable by 2035 [8]. As part of the strategy, 5GW of hydrogen production should be delivered by 2030, whilst halving Oil and Gas (O&G) emissions [8].

By providing step-by-step guide to large scale offshore green hydrogen production, this thesis is in line with these decarbonisation goals and helps to accelerate UK hydrogen production. It aligns with several points on The Ten Point Plan such as:

- Point 1- Advancing offshore wind by enabling storage and energy transportation even to grid constrained areas.
- Point 2- Driving the growth of low carbon hydrogen by producing green hydrogen at large scale.
- Points 4, 5, 6, and 7- Accelerating the shift to zero emission vehicles, green public transport, jet zero and green ships as well as greener buildings by growing hydrogen supply.

1.1.3 Scotland

To tackle climate change, in 2019 Scotland has set a new net zero emissions target by 2045 based on the recommendations by The Climate Change Committee (CCC) [2]. The new interim targets for Scotland are at least 75% lower emissions than the baseline by 2030 and 90% lower emissions than the baseline by 2040 [9]. The GHGs reported in the greenhouse gas account are carbon dioxide, methane, nitrous oxide, perfluorocarbons, sulphur hexafluoride, nitrogen trifluoride and hydrofluorocarbons [10]. The baseline for carbon dioxide, methane, and nitrous oxide is set as the emissions in the year 1990, while the baseline for all the rest of the reported gases is the year 1995 [10]. In 2019, the greenhouse gas account reduced by 51.5%, which caused Scotland to miss their 2019 interim target of 55% reduction in comparison to the baseline by 3.5% [10].

Figure 1.1 summarises total Scottish emissions by sector for 2019 as published by the CCC [11]. As can be seen in Figure 1.1, surface transportation is the highest emitting sector in Scotland with 56% of emissions coming from cars, and 18% each from HGVs and vans [11]. Second most emitting sector includes both residential and non-residential buildings, where energy efficiency improvements have decreased direct emissions by 22% since 1990. While the power generation now only accounts for 4% of total emissions, fuel supply contributed 9% where 48% comes from O&G production and 41% from refining. The 2020 greenhouse gas account will be published in June 2022.

The next section discusses, the role of hydrogen in helping to reduce the carbon footprint of the afore mentioned sectors, including existing examples of key hydrogen projects.

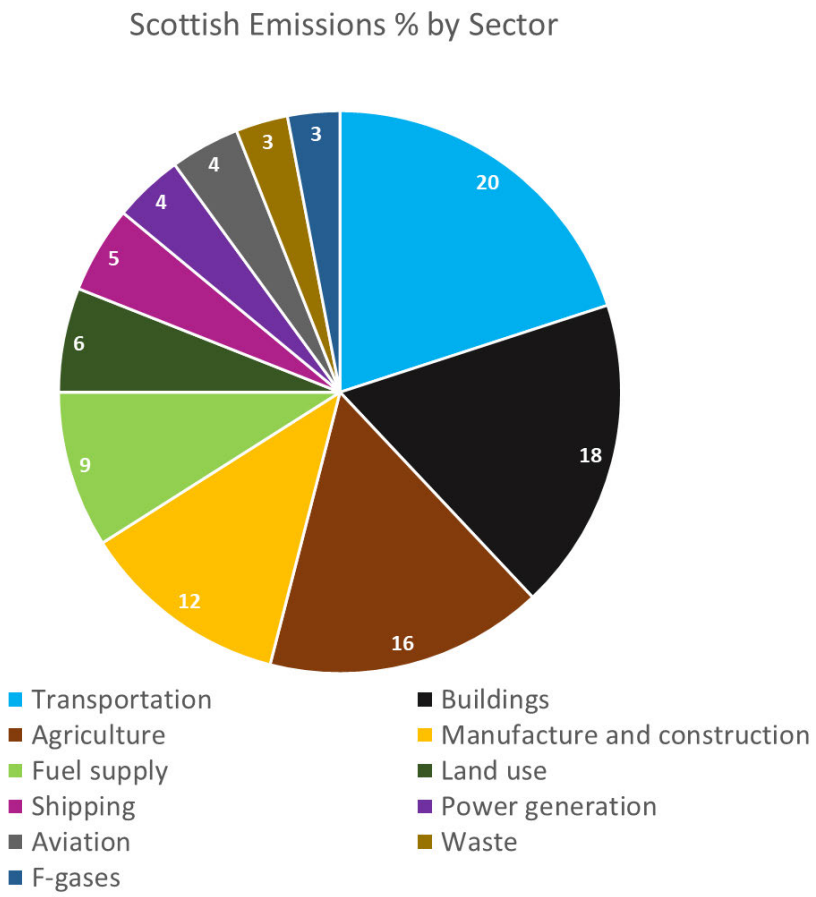

Figure 1.1: Scottish emissions % by sector.

1.2 Hydrogen

Hydrogen is the most abundant element in the Universe. It is an odourless and nontoxic energy carrier, with the highest energy content by weight when compared to common fuels like gasoline, diesel and MGO (marine gas oil). Hydrogen is an important low carbon replacement for natural gas, with the potential to reduce emissions from a variety of sectors such as heating, transportation, heavy industry, power production and others. Unlike fossil fuels, when pure hydrogen burns, the only product is water and heat, which is the same for when hydrogen is converted to electricity. When produced from renewable feedstocks such as renewable energy, hydrogen has an even higher potential for carbon reduction than when produced from fossil fuels as the carbon savings from production add up to the savings from avoided tailpipe emissions [12].

1.2.1 Hydrogen Strategies

The fact that hydrogen is a future strategic enabler to decarbonisation and energy transition is evidenced by the number of countries that have released their hydrogen strategies and roadmaps in the past five years. Japan, leading the way in 2017 [13], South Korea and Australia in 2019 [14], [15], have been followed by a significant number of European countries as well as Chile and Canada in 2020 [16]–[18]. The Scottish Government's hydrogen policy statement was released in 2020 [19], followed by The UK hydrogen strategy in 2021 [20].

By 2030, the EU is aiming to have sufficient electrolyser capacity to produce 10 million tons of green domestic hydrogen, Scotland is aiming for 5GW of renewable and low carbon hydrogen and the UK is targeting 42 TWh/yr of low carbon hydrogen production [5], [19], [20].

1.2.2 Types of Hydrogen

1.2.2.1 Grey, Blue and Brown Hydrogen

In 2020, over 99% of the 90 Mt of world hydrogen demand, was generated from fossil fuels [18]. This includes hydrogen obtained from steam methane reforming (SMR), from cracking, and from coal gasification [21]. In SMR, natural gas reacts with steam at high temperatures over a catalyst resulting in syngas, from which the so-called grey hydrogen is separated at a later stage [22]. Steam methane reforming and water-gas shift reactions are shown in Equations (1.1) and (1.2).

It is the most widely used as well as the cheapest method of hydrogen production with the lowest carbon dioxide emissions of the fossil fuel H_2 production methods [23]. In theory, around 90% of the carbon dioxide from the SMR process can be captured by the CCS (carbon capture and storage) or CCUS (carbon capture usage and storage) system turning grey hydrogen into blue hydrogen [22], [24]. From existing projects, Sturgeon refinery in Canada captures 70% of its CO_2 emissions, producing blue hydrogen required for refinery operation and selling carbon dioxide for further use in enhanced oil recovery [25], [26].

$$CH_4 + H_2O \rightarrow 3H_2 + CO \quad \textbf{(1.1)}$$

$$CO + H_2O \rightarrow H_2 + CO_2 \quad \textbf{(1.2)}$$

There is another blue hydrogen production process called autothermal reforming (ATR) with CCS. It also uses natural gas to form hydrogen but should have a higher conversion efficiency and 95% CO_2 capture rate in theory. It is not currently used due to lack of CO_2 transportation and storage infrastructure.[27]. ATR uses pure oxygen rather than air for partial combustion and thus avoids CO_2 nitrogen separation as in SMR [27].

Coal gasification producing brown hydrogen on the other hand, has cheaper fuel costs but higher carbon footprint than SMR due to lower hydrogen production efficiency, which is around 60% [22], [23].

1.2.2.2 Green Hydrogen

According to Velazquez Abad & Dodds [28], there is no universally accepted definition for green hydrogen yet. However, most of the definitions do mention renewable source or constrain the amount of GHG emissions released [28]. Thus, for the purpose of this thesis, green hydrogen (or renewable hydrogen) refers to hydrogen produced from renewable sources such as wind or solar energy. To produce hydrogen from renewable energy, a process called electrolysis is used. Electrolysis is a chemical process in which electricity is used to split water into hydrogen and oxygen gas.

There are three types of electrolysers including alkaline (61% of total installed capacity), Polymer Electrolyte Membrane often referred to as PEM (31%), and solid oxide electrolysers (0.8%) [18] shown in Figure 1.2 a) b) and c) respectively. When direct current (DC) is applied to a chemical cell in the presence of water, hydrogen evolves at the cathode, while oxygen evolves at anode for low temperature electrolysers such as alkaline and PEM (60-90°C) (Figure 1.2 a) and b)) and vice versa for high temperature electrolysers such as solid oxide electrolyser (700-900°C) (Figure 1.2 c)) [29], [30].

The major difference between PEM and alkaline electrolyser is that a PEM electrolyser has an acidic electrolyte separated by a membrane instead of a basic electrolyte through which the hydrogen cations pass from the anode to the cathode. (See Figure 1.2). More detail on different types of electrolysers and their suitability for offshore hydrogen production can be read in Chapter 3. Green hydrogen produced by electrolysis of water contributed less than 0.5% of global hydrogen supply in 2020 [18]. However, according to IEA, there are enough projects at different development stages that could boost electrolytic hydrogen supply to 8Mt by 2030 [18].

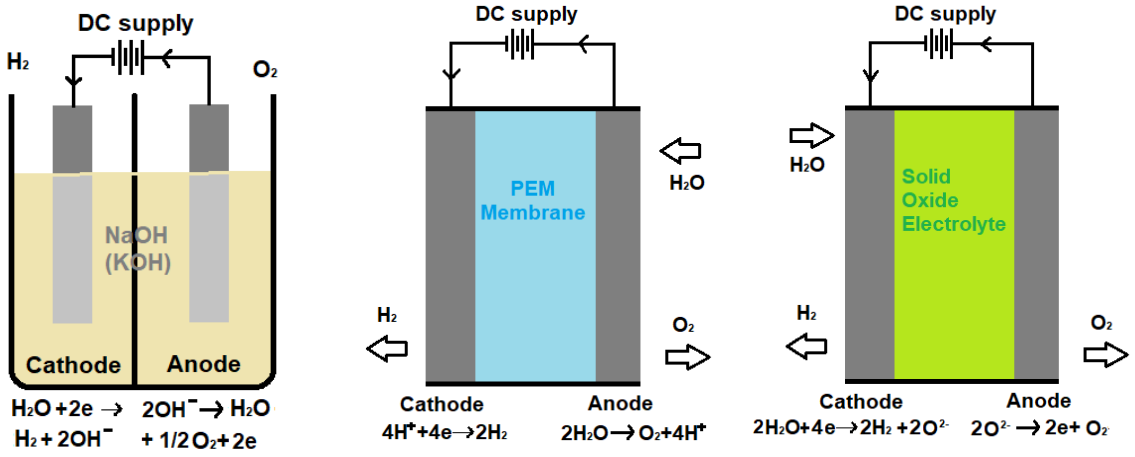

a) Alkaline electrolyser **b) PEM electrolyser** **c) Solid oxide electrolyser**

Figure 1.2: Diagram of an a) alkaline, b) PEM and c) solid oxide electrolyser

To convert hydrogen back to electricity, reverse reaction to the one described in Figure 1.2 occurs in which hydrogen reacts with oxygen to create water vapour while forcing the electrons to pass through the electric circuit, Equations (1.3) to (1.5). The device in which reverse electrolysis occurs is called a fuel cell, with the most common type being the PEM fuel cell.

$$Anode: H_2 \rightarrow 2H^+ + 2e^- \quad \textbf{(1.3)}$$

$$Cathode: \frac{1}{2}O_2 + 2H^+ + 2e^- \rightarrow H_2O \quad \textbf{(1.4)}$$

$$Overall\ reaction: H_2 + \frac{1}{2}O_2 \rightarrow H_2O \quad \textbf{(1.5)}$$

There is also pink and yellow hydrogen, which are both types of electrolytic hydrogen powered by nuclear reactors (pink) or solar power (yellow). The least common type of hydrogen is turquoise hydrogen that is produced via methane pyrolysis, which is a catalytic process resulting in decomposition of natural gas into hydrogen and solid carbon as shown in Equation (1.6) [31].

$$CH_4 \rightarrow 2H_2 + C \quad \textbf{(1.6)}$$

The last type of hydrogen discussed within this section is hydrogen obtained through CCUS enabled biomass gasification. During this process, the biomass consisting of any organic material such as agricultural, commercial or sewage waste, is heated in air, oxygen or steam to create syngas consisting of combination of carbon monoxide, carbon dioxide and hydrogen, from which hydrogen is separated at a later stage [27]. While gasification is a mature technology, the CCUS application is new and so this type of hydrogen is likely to be produced in 2030s to 2050s once CCUS infrastructure is installed [27].

1.2.3 Hydrogen Application

The following section outlines sectors that hydrogen can help to decarbonise, describing the role of hydrogen as well as examples of relevant hydrogen projects.

1.2.3.1 Heavy Industry

Hydrogen could decarbonise industrial processes that require gas to create high temperatures such as cement, aluminium, iron and steel production [32] or be used as a green reducing agent in the steel production process [33]. The iron and steel making industry is the second largest industry energy consumer and largest CO_2 emitter in the world contributing 2.6 gigatonnes of carbon dioxide per year [32].

Iron and steel making accounts for up to 7% of global CO_2 emissions [32]. There is a Swedish joint venture, HYBRIT that is aiming to replace coal with hydrogen in the steel making process. In this case, HYBRIT is suggesting using hydrogen Equation (1.7) rather than natural gas or coke Equation (1.8) as a main reductant, which can reduce 85-90% of total carbon dioxide emissions in ore-based steel making process [34]. Steel manufacturers can also use hydrogen as energy storage allowing for reliable renewable energy supply to power electric furnaces and ovens, reducing the carbon footprint of steelmaking even further [33].

$$\frac{1}{3}Fe_2O_3 + H_2 \rightarrow \frac{2}{3}Fe + H_2O \quad \textbf{(1.7)}$$

$$\frac{1}{3}Fe_2O_3 + CO \rightarrow \frac{2}{3}Fe + CO_2 \quad \textbf{(1.8)}$$

1.2.3.2 Chemical Industry

The chemical sector is the largest industrial energy consumer when counted together with the petrochemical industry [35]. Green hydrogen could be used as a feedstock for synthesis of ammonia, Equation (1.9), avoiding 1.7t of CO_2 per ton of product, and synthesis of methanol, Equation (1.10), avoiding 1.5t of CO_2 per ton of product [36]. Using green hydrogen in these processes would lead to decarbonisation of further processes such as production of propylene, benzene, toluene and xylene, which can be synthetised using green hydrogen based methanol and then again used as feedstocks for different polymers [36].

$$3H_2 + N_2 \rightarrow 2NH_3 \quad \textbf{(1.9)}$$

$$CO + 2H_2 \rightarrow CH_3OH \quad \textbf{(1.10)}$$

A good example of industrial use of hydrogen is project Refhyne that is aiming to decarbonise refinery products as well as investigate opportunities in decarbonising refinery processes [37]. Hydrogen could be used for example as a fuel for high heat [38].

1.2.3.3 Heat

Hydrogen could replace natural gas in the gas grid providing heat to homes with some adjustments to the end user appliances. BEIS is planning to enable 20% hydrogen blending into the natural gas supply by 2023, which could save up to 6 million tonnes of carbon dioxide equivalent every year, transitioning to 100% hydrogen gas network in the future [39].

There are already several existing projects involving hydrogen gas networks, two examples of which include H100 and Hy4Heat. H100 project is a world-first demonstration of its kind looking to provide 300 local homes in Fife with a 100% hydrogen gas grid with hydrogen sourced from a local offshore wind turbine [40]. Hy4Heat project carried out a safety assessment for using 100% hydrogen for heating and cooking and helped to mobilise industry and academia to collaborate and develop new domestic hydrogen boilers, meters, cookers, heaters and other appliances that will be essential to replacing natural gas with hydrogen in the gas grid [41].

1.2.3.4 Transportation

Different means of transportation such as ships, airplanes, trains, road transportation like buses, heavy freight vehicles, vans, passenger vehicles, specialised machinery such as agricultural machinery, refuse vehicles, road gritters, etc can all in theory be decarbonised by hydrogen. There is a potential to retrofit existing vehicles and use hydrogen or hydrogen derivatives in combustion engines or powering electric vehicles using fuel cells.

An example of an existing retrofitted hydrogen ferry is HyDime project operating a dual-fuel hydrogen-diesel commercial passenger and vehicle ferry between Kirkwall and Shapinsay in Orkney [42]. Other transportation initiatives are H_2 Bus Europe, a consortium looking to deploy at least 1000 hydrogen buses to cities in Europe by 2023, with buses already operating in the UK, Denmark and Latvia [43], hydrogen-electric power trains for aircrafts by ZeroAvia [44], and Alstom hydrogen trains [45].

1.2.3.5 Power

There are several roles hydrogen and its derivatives could play in decarbonisation of the power sector. Hydrogen is one of the leading options for long term renewable energy storage helping to smooth the power supply as well as helping to export renewable energy worldwide [46]. Both hydrogen and ammonia could be used in gas

turbines as a blend as well as sole gasses for power generation. Other options are using fuel cells as back up and alternative to diesel generators in off-grid scenarios such as remote locations or offshore oil and gas platforms.

One example of hydrogen in the power sector is the BIG HIT project, where a 75kW hydrogen fuel cell is being used as a generator in Kirkwall providing heat and power for several harbour buildings as well as supplying ferries with power when docked [47]. An example of hydrogen storage is the HYPSTER project funded by the Fuel Cells and Hydrogen Joint Undertaking (FCH JU), which is a hydrogen storage pilot project funded by the EU looking to store hydrogen in underground salt caverns in France [48].

Other sectors that could be decarbonised via hydrogen are agriculture through 'green' fertilisers produced from green ammonia and whiskey distilling industry using hydrogen to decarbonise whiskey production [49].

1.2.4 Offshore Wind and Hydrogen

With renewable energy expanding further offshore to access good wind resource, and significant expenses for decommissioning of oil and gas infrastructure approaching, hydrogen production which re-uses offshore oil and gas assets is becoming of more interest to countries around the North Sea, such as UK, Norway and the Netherlands. An estimated £16.6 billion is forecast to be spent on decommissioning in the UK continental shelf in the next decade, the majority of which will take place around Scotland [50].

There are several studies carried out in the Netherlands by Energy Delta Institute (EDI), The World Energy Council and North Sea Energy looking into synergies between different offshore fields and repurposing of oil and gas infrastructure to be used for carbon storage and hydrogen production [51]–[55].

There are also ongoing industrial projects around the North Sea that are further described in Section 1.2.5 such as the Deep Purple, PosHydon or GigaStack projects.

The major advantage of producing hydrogen offshore would be the potential of repurposing the pre-existing oil and gas infrastructure for transporting the power to shore in the form of hydrogen rather than building new cables to connect to an already constrained grid. Another advantage is that producing hydrogen offshore is often perceived safer than producing it onshore, resulting in higher public acceptance and support [55]. A full literature review on offshore hydrogen production is provided in Chapter 3.

There are three different methods to produce green hydrogen from offshore wind, based on the location of the electrolyser as shown in Figure 1.3. There is onshore hydrogen production, offshore hydrogen production with the electrolyser co-located with the wind turbine (decentralised hydrogen production) and centralised offshore hydrogen production.

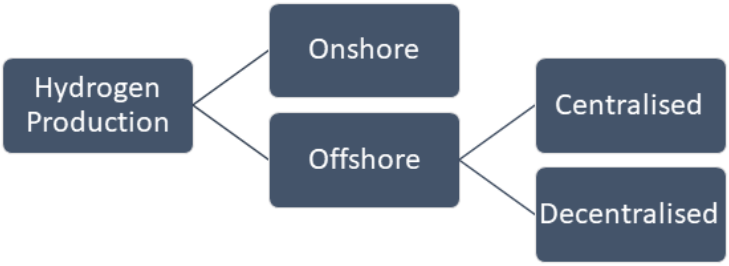

Figure 1.3: Diagram showing different ways of green hydrogen production form offshore wind.

Onshore hydrogen production is closest to current “business as usual” where the power from an offshore wind farm is transmitted to shore through power cables and connected to a hydrogen production site onshore. The major advantage of producing hydrogen onshore is that it avoids costly offshore operations and allows electrolysers to be connected to a fresh water source.

This option is currently the most advanced in comparison to other options for producing hydrogen from offshore wind. However, challenges include a near-shore corrosive marine environment that will require adjustments to the electrolyser.

When it comes to offshore hydrogen production, electrolysers could be ‘centralised’, where they are all placed on an offshore substation, a re-used oil and gas platform, a newly built offshore platform, or an artificial island, or ‘decentralised’ where each electrolyser is on an individual wind turbine structure. Advantages of offshore hydrogen production are the reduction of power transmission cables that are more expensive than hydrogen pipelines [56], and greater public acceptance [55] while the disadvantages include a harsh offshore environment, need for costly offshore operations and the requirement for desalination units to provide a supply of high quality water.

When comparing centralised and decentralised hydrogen production, a major challenge of having centralised offshore hydrogen production is the limited space on a platform, requiring advancement in electrolyser technology for bulk hydrogen production (i.e. vertically stackable electrolysers) [57]. The major advantage of centralised hydrogen production is the ability to apply system level management strategy options that will significantly drive down all cost elements and improve the efficiency of the system. Another advantage of centralised offshore hydrogen production is the potential of re-using oil and gas infrastructure and deferring the cost of decommissioning.

On the other hand, co-locating hydrogen production with each individual wind turbine allows the power output of an entire wind farm to be captured for conversion to green hydrogen. This is because it is easier to fit an electrolyser and a desalination unit with the capacity of an individual WTG onto the structure of the WTG than fit all the electrolysers covering capacity of the whole windfarm onto a platform. This is the major advantage of this option. However, there will be increased efficiency loses as the electrolysers will not be centrally managed. Other advantages include easier installation and decommissioning when the electrolyser system is directly attached to the structure, which is specifically applicable to floating wind turbines.

The challenges associated with decentralised hydrogen production are the necessary adjustments to the electrolysers to make them suitable for offshore operation on a floating or a fixed platform. This might include motion compensation technology when placed on a floating substructure as well as including marinisation aspects. Key disadvantages are the loss of economies of scale, loss of centralised system management and operation and maintenance (O&M). During O&M each electrolyser will have to be attended to individually in comparison to onshore and centralised options where the electrolyser(s) are located on the same site. This will significantly prolong the time needed for maintenance, which is costly when operating offshore.

1.2.5 Relevant Offshore Wind to Hydrogen Projects

1.2.5.1 Gigastack Project (UK)

The Gigastack project is looking into using renewable energy from the Hornsea 2 Ørsted offshore windfarm to produce hydrogen with a 100 MW PEM type electrolyser supplied by ITM Power to decarbonise the nearby Phillips 66 Refinery on the Humber. The project is looking to deploy the electrolyser in 2025 [58].

1.2.5.2 Westkuste 100 Project (Germany)

The project includes building a 700 MW green hydrogen plant by 2030, powered by a dedicated Ørsted offshore wind farm. The windfarm is currently unbuildable due to grid constraints, so in order to be built, hydrogen is required to transfer the energy to land. The plant is intended for synthetic fuels production for airplanes. Companies involved include Ørsted, EDF, Thyssenkrupp and others [59].

1.2.5.3 PosHydon (Netherlands)

The PosHydon project is aiming to install and operate a 1 MW PEM electrolyser on a Q-13a oil and gas platform in the Dutch section of the North Sea, transferring the produced hydrogen to land through an existing gas pipeline. This platform has been previously electrified with a cable from land and thus has been found to be fit for purpose. The companies involved are Neptune Energy, Nexstep, TNO, Gasunie DEME Offshore and others [60]. This pilot project was scheduled to start at the end of 2021 and run for two years [61]. However, there is no publicly available information, at the time of writing, confirming that the electrolyser has been already installed.

1.2.5.4 Deep Purple (Norway)

This project offers an alternative storage solution to batteries and is looking into installing subsea hydrogen storage onto the seabed. The electrolysers at wind turbine generator (WTG) level will produce hydrogen, which can then be stored in the tanks on the seabed and converted back to electricity via the fuel cells. The full-scale pilot should be running by 2025 [62].

1.2.5.5 Dolphyn Project (UK)

The Deepwater Offshore Local Production of Hydrogen (Dolphyn) project, is ERM's concept for large scale green hydrogen production from offshore floating wind. ERM is looking to install a PEM electrolyser on a moored floating semi-submersible sub-structure and transfer the hydrogen to land through hydrogen pipelines [63]. The project is initially designed for the North Sea, looking to install a 2 MW prototype by 2024 and 10 MW full scale precommercial model by 2027 [63].

1.3 Offshore Oil and Gas Infrastructure

Since the commercial extraction of oil and gas began, extensive networks of offshore O&G infrastructure have been installed globally. As a lot of these structures are now nearing the end of their lifetime, this work investigates potential of their re-use for the purpose of offshore green hydrogen production. This section briefly introduces existing oil and gas infrastructure, mainly platforms, as Chapter 4 describes the pipelines in great detail. This section then ends with the discussion on current regulations for decommissioning and re-use of oil and gas infrastructure.

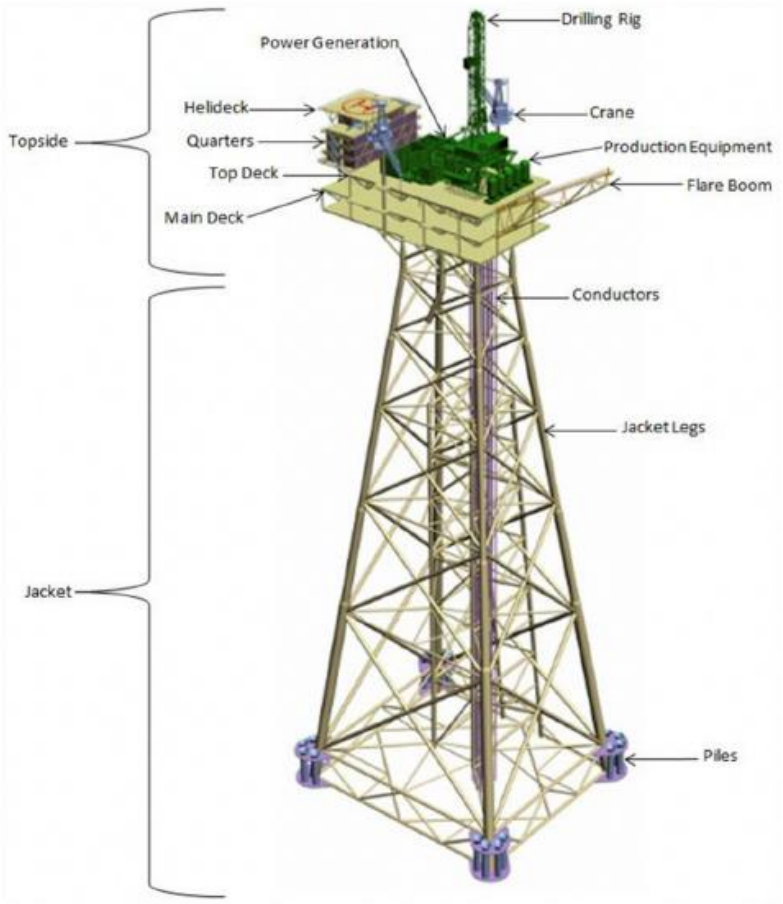

Figure 1.4: Steel jacket oil and gas platform [64].

Oil and gas platform typically consists of a topside and a substructure that holds the topside above the sea level (see Figure 1.4). As shown in Figure 1.4, typical topside contains a drilling rig for oil and gas extraction, a power generation to supply the platform with electrical energy, a helideck, a crane, production equipment, a flare boom to burn excessive gas, and living quarters in case the platform is manned [64]. There are two ways to divide O&G platforms, based on material, and attachment to the sea floor. O&G platforms can be fixed or floating, and steel or concrete. Fixed platforms can be further subdivided into piled structures (typically made of steel) and gravity based (typically made of concrete). Out of 522 O&G structures in the North Sea, the majority of them have steel substructure [65].

Figure 1.4 shows an example of most common oil and gas structure, which is jacket type platform [64]. Jacket is a piled steel structure consisting of tubular steel legs that are piled into the seabed. Other types of O&G platforms are presented in Figure 1.5. The choice between these depends on the water depth.

Once the platform reaches end of its life, it goes through the process of decommissioning, which means the platform is removed and the seabed is returned to its previous condition. Rather than issues with structural integrity, the platforms are often decommissioned due to well depletion or the extraction from the field the platform serves being no longer commercially viable. As mentioned in Section 1.2.4, an estimated £16.6 billion is forecast to be spent on decommissioning in the UK continental shelf in the next decade, the majority of which will take place around Scotland [50]. Thus, following section discusses decommissioning.

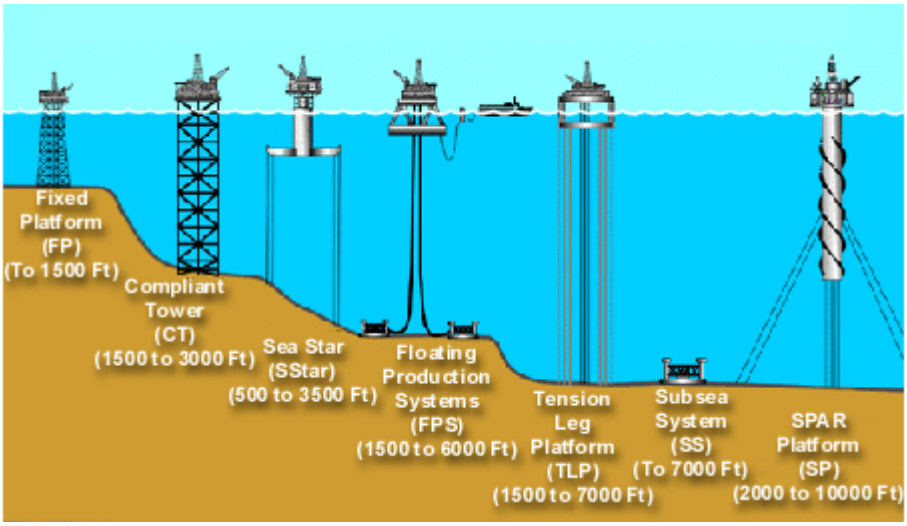

Figure 1.5: Different types of platform substructures based on water depth [64].

1.3.1 Decommissioning

Under OSPAR Decision 98/3, it is prohibited to leave wholly or partly disused offshore installations in-situ offshore. The only exceptions are all concrete installations, and steel jacket installations weighing more than 10,000 tonnes in air, in which case companies can apply for derogation (leaving structures in place) [66]. The topsides of all installations however, must be removed to shore [67].

The expected cost of topside removal is estimated at £1 billion (6.6% of overall decommissioning cost) [66]. There are three approaches to decommissioning of the topsides [66];

- ‘Single-lift’ which uses large lift vessels to remove the topside with all equipment in one lift up to 48,000 tons [68].
- ‘Reverse installation’ where modules are removed one by one
- ‘Piece small’ where the topside is broken into small pieces and removed to shore

The decision as to what approach to take usually depends on the availability of vessels and technical constraints of the structure like weight and configuration. If a heavy lift vessel is available and the topside can be removed in one piece, this is usually the preferred way as it decreases the amount of expensive offshore operations. When heavy lift vessels are not available, or the topsides are too heavy to be removed in one go, the other two methods are chosen [69].

For the purposes of reuse for offshore hydrogen production, reverse installation and single-lift are preferred. The reverse installation method leaves the topside deck in place and available for re-use, if suitable, from a structural integrity point of view. Single-lift removes the entire topside and allows a new topside, including hydrogen production equipment to be installed on the substructure. While the reverse-installation method can save money on building a new topside, it will be more costly during decommissioning as it will involve more offshore operations than single lift and vice versa. Piece small decommissioning is inappropriate for re-use of platforms for hydrogen production as it involves breaking the modules on the topside, which in contrast to reverse installation, can cause damage to the topside. The topside might then end up needing to be replaced, resulting in further costs and delay. Regardless of whether the topside is replaced, it is notable that leaving the substructure in situ can defer expenditure of £1 billion, which is estimated for total substructure removal within the UK continental shelf [66].

In line with Offshore Petroleum Regulator for Environment and Decommissioning (OPRED) regulations, all decommissioning programmes must demonstrate that all potentials for re-use have been examined and discussed with the North Sea Transition Authority (former OGA, which stands for The Oil and Gas Authority) [67].

Some challenges identified by the Department for Business, Energy and Industrial Strategy (BEIS) for preventing re-use of offshore oil and gas infrastructure for other commercial purposes are:

- Liability – currently the Secretary of State can make the previous owner of the infrastructure liable for decommissioning of the structure if the current owner is unable to meet the decommissioning requirements [70]. This makes the current operators of the platforms reluctant to sell the structures for re-use as they cannot completely pass on the liability.
- Cost of deferring decommissioning - deferring decommissioning in order to re-use the infrastructure in the future will still incur costs for maintenance and monitoring that will have to be paid by someone whether it is the current asset owner, the new asset owner or the government [70].

1.4 This Work

With increasing emergency to tackle the climate change and growing interest in hydrogen as a key contributor to decarbonisation, this thesis addresses the question of a large-scale green hydrogen supply that will be crucial to meeting decarbonisation goals as outlined within this chapter.

With renewable energy expanding further offshore, the research question being addressed in this work is:

i. is it ***technically*** feasible to produce green hydrogen offshore in large scale, whilst repurposing existing O&G infrastructure to transport power back to shore in the form of hydrogen and
ii. is it ***economically*** feasible to produce green hydrogen offshore in large scale, whilst repurposing existing O&G infrastructure to transport power back to shore in the form of hydrogen?

Thus, the aim of this research is to investigate the techno-economic feasibility of future offshore hydrogen production with a case study applied to Scotland. This will be achieved through following objectives:

- Mapping and matching areas for offshore wind farms and oil and gas platforms around Scotland (**Chapter 2**)
- Estimating annual energy production of a model floating offshore windfarm (**Chapter 2** and **Chapter 3**)
- Investigating offshore hydrogen production (**Chapter 3**)
- Investigating transportation of hydrogen through existing O&G pipelines in the North Sea (**Chapter 4**)
- Conducting economic analysis of offshore hydrogen production (**Chapter 5**)

1.4.1 Thesis Layout

First Chapter outlines the challenges and current interest in hydrogen as well as the role hydrogen could play in decarbonisation. Later the second chapter talks about mapping of offshore oil and gas infrastructure and potential offshore renewable energy sites. It describes the methodology and applies it to a case study in the Scottish part of the North Sea. The second part of the second chapter goes through reasoning and methodology of resource assessment in which a 1.5GW floating offshore windfarm has been designed and annual energy yield has been calculated. Further it describes four scenarios that show the effect of availability of the windfarm on the capacity factor for non-grid connected wind farms.

As shown in Figure 1.6, the results of Chapter 2 then feed into Chapter 3 which introduces offshore hydrogen production in more detail and shows methodology for calculating hourly hydrogen production and flow rates, which then feed into Chapter 4.

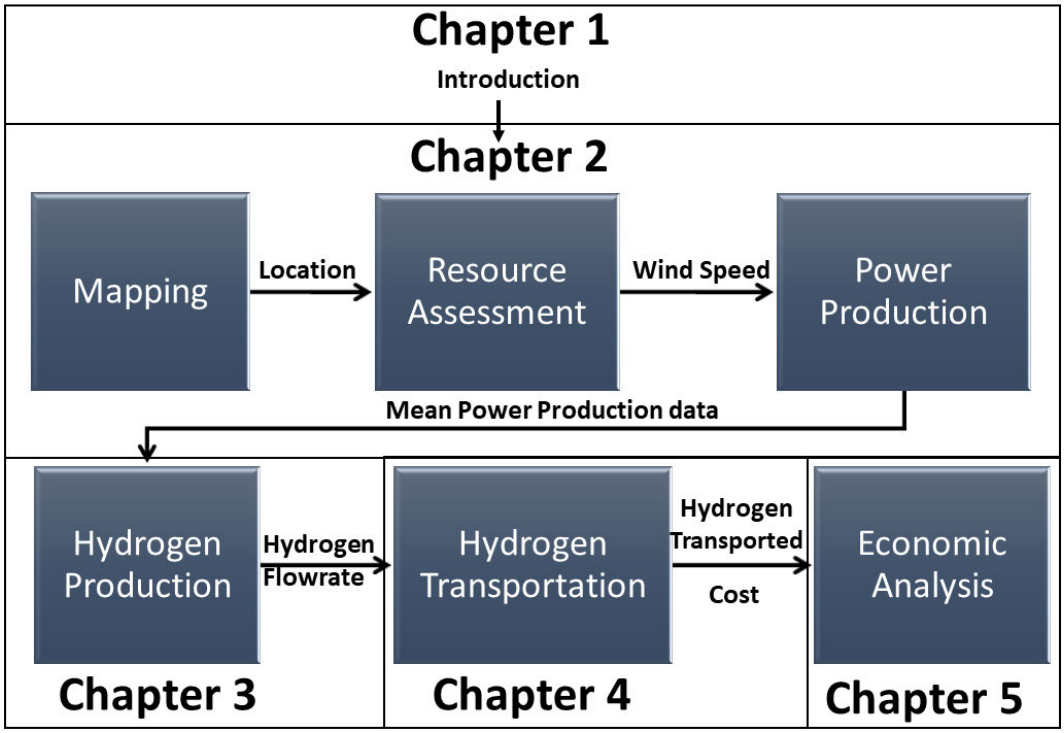

Figure 1.6: Diagram of the layout of this thesis.

Chapter 4 describes hydrogen transportation through pipelines and different associated challenges such as failure modes, difference in materials between purpose build hydrogen pipelines and existing pipelines in the North Sea. Further the chapter contains methodology and results for pressure drop calculations done on software PIPESIM that determine suitability of existing offshore gas pipelines for hydrogen transportation.

Last Chapter contains economic analysis to answer the second part of the research question whether offshore hydrogen production is economically feasible. It contains comparison between levelised cost of hydrogen (LCOH) and levelised cost of electricity (LCOE) from the modelled wind farm described in Chapter 2 and describes which is more feasible and why including sensitivity analysis.

1.4.2 Constraints

The work focuses on large scale centralised green hydrogen production via PEM electrolysis from a non-grid connected offshore floating wind farm. It investigates re-use of oil and gas infrastructure such as platforms, to produce hydrogen, and natural gas pipelines, to transport hydrogen to shore. This work does not investigate re-use of existing pipelines or building new pipelines onshore. The research focuses entirely on hydrogen production and transportation and does not cover any other aspects of hydrogen economy such as storage or other hydrogen carriers such as ammonia or methanol. This is because many different topics needed to be covered in the timeframe of this EngD for completeness of the techno-economic analysis, and there are other IDCORE students investigating hydrogen storage and hydrogen derivatives. The work investigates the feasibility of offshore green hydrogen production in the year 2030, as commercial offshore hydrogen production is likely to happen further in the future based on the current pace of energy transition and growth of hydrogen demand, the improvements and marinisation of green hydrogen production technologies and the timelines for building new windfarms. Scotland has been chosen for the case study as with its vast offshore wind resources, decarbonisation goals and hydrogen ambitions, it is uniquely placed for large scale offshore green hydrogen production.

1.4.3 Contributions to Knowledge

To be able to produce green hydrogen offshore, techno-economic assessment like the one developed in this work is an essential first step to identify challenges and help industry and academia to progress decarbonisation goals at pace.

The major contributions of this work are:

a) Mapped areas around Scotland with oil and gas infrastructure near areas with existing wind farms or areas suitable for future offshore wind farm developments including information on weight, decommissioning, and expected cease of operation for the platforms nearby. This can be utilised by the O&G platform operators to determine possible use of their platforms and pipelines after the cease of production as well as to evaluate their decarbonisation options. This information can be also used by the wind farm developers and hydrogen supply developers to establish areas suitable for large scale hydrogen production.

b) Full detailed methodology on resource assessment and impact of offshore hydrogen production on the capacity factor of the windfarm, which was also published in conference proceedings [71] and used in a journal paper [72]. This work gives information to wind farm developers on potential impacts of hydrogen production on the capacity factor of non-grid connected windfarms that is highly relevant to grid constrained areas.

c) Full methodology on existing pipeline re-use for hydrogen, which is relevant to offshore gas pipelines operators on options after cease of O&G production as well as analysis of low pressure pipeline operation without compressors, which is of interest to the future hydrogen producers due to the limited space offshore.

d) Full offshore green hydrogen production analysis as well as levelised cost of offshore green hydrogen calculations that can be used by the wind farm developers to provide them with information on alternative options of sending power to land when building wind farms near grid constrained areas with good resource.

Additionally to the interest of the industrial sponsor Wood plc, other organisations interested in this research were Crown Estate Scotland, Net Zero Technology Centre (former Oil and Gas Technology Centre), Shetland Islands Council, and North Sea Transition Authority (former Oil and Gas Authority).

This research has been also presented at the Scottish Hydrogen and Fuel Cell Association (SHFCA) Annual Conference in 2019, Wind Europe 2019 Conference, Tech20 for Net Zero Technology Centre in 2020, and to the MPs at the House of Commons in 2020 to highlight a few events.

With the overarching way this thesis covers major points of offshore green hydrogen production, it serves as a steppingstone towards large scale offshore green hydrogen production in the future. It provides information crucial to enabling re-use of oil and gas infrastructure for green hydrogen production and provides alternative to windfarm operators to the way they transfer their power to land. With the current growth in hydrogen demand and supply, this thesis is well placed and timed to provide important answers in the novel but growing field of offshore green hydrogen production.

CHAPTER 2 - MAPPING AND RESOURCE ASSESSMENT

Parts of this chapter were published as proceedings for Wind Europe 2019 [71] *and in Journal of Applied Energy* [72].

2.1 Overview

Chapter 2 shows the process used to determine the energy yield for a theoretical offshore floating wind farm for offshore green hydrogen production. It first discusses mapping methodology to determine suitable location for offshore hydrogen production. Then, using a case study from the Northern part of the North Sea, the chapter takes the reader through the process of resource assessment, wind farm design and power production calculations to determine energy yield available for hydrogen production. This process can be applied anywhere in the world and the results feed into offshore green hydrogen production, which is discussed in Chapter 3 (See Figure 2.1). The main contribution and novelty of this chapter is taking the standard resource assessment and energy production methodology for offshore windfarms and using it for non-grid connected wind farms supplying hydrogen production as well as the application of this methodology to a case study in Scotland.

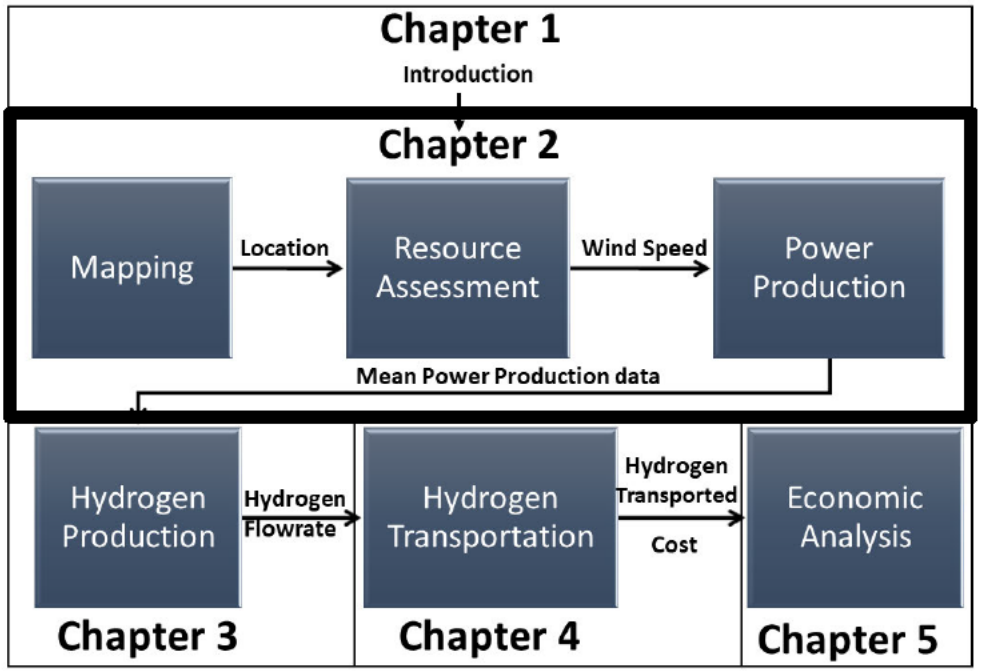

Figure 2.1: Thesis flow diagram.

2.2 Methodology

Figure 2.2 shows the methodology for selecting an area for offshore green hydrogen production, through resource assessment all the way to annual energy production calculations. Each section of the process shows attributes needed, to evaluate each of the sections, which will be first discussed in more detail in sections below and then applied to a case study in Scotland also referred to as the Magnus case study due to its location near the Magnus platform.

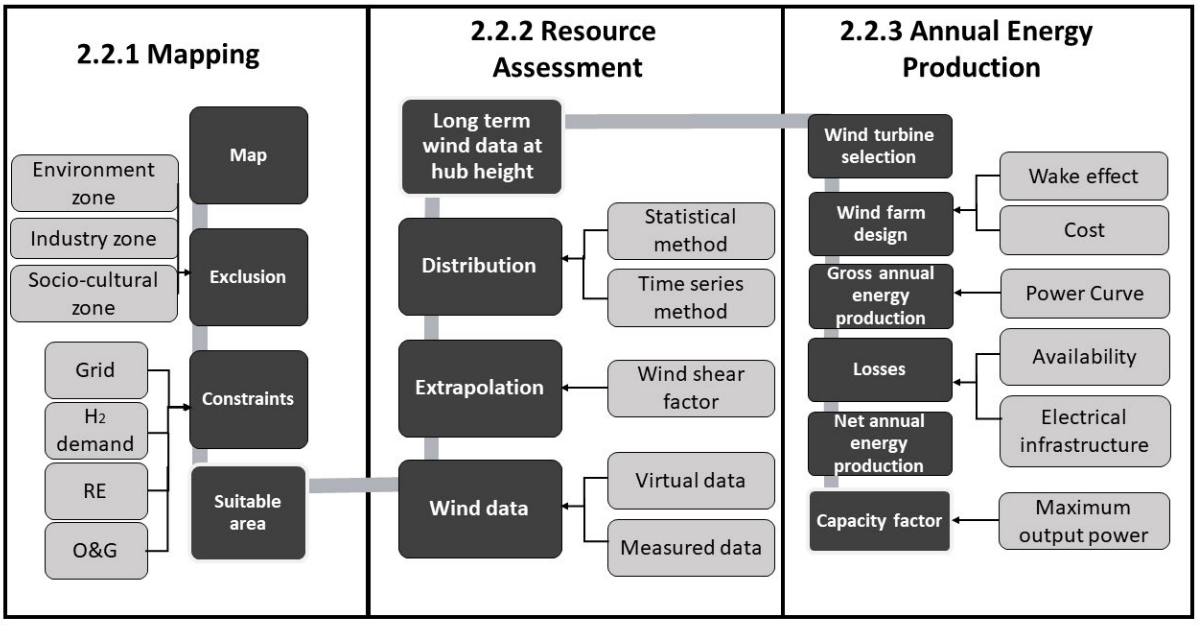

Figure 2.2: Methodology diagram.

2.2.1 Mapping

Several aspects need to be considered to select an appropriate site for offshore green hydrogen production while re-using oil and gas infrastructure. There are exclusion areas which are used by other users and constraints that make certain areas more suitable than others (see Figure 2.2). Exclusion aspects as well as some constraints are similar to those considered for any offshore structure and are well described by Marine Scotland [73].

Marine Scotland [73] divides exclusion zones, that limit areas available for new offshore production facilities, into three categories. These are industry, environment, and socio-cultural zones. The industrial users are military, aviation (where relevant for

hydrogen production in combination with wind farms), shipping, and fishing. Environmental aspects include nature protection zones, as well as potential collision zones with sea species and seabird. Socio-cultural aspects include leisure activities such as water sports, aesthetics, but also areas of special cultural and/or local community interest. For example, projects that aim to be built near beaches or cliffs that bring tourists to the local area or have sentimental meaning to the local community are unlikely to go ahead. However, in certain cases, the structures can become desirable from socio-cultural aspect as in case of Whitelee windfarm that has an interactive visitor's centre as well as cycle routes for people to use [74].

Technical aspects that need to be considered and are a constraint rather than exclusion are renewable energy (RE), grid, physical features, O&G infrastructure, and hydrogen demand hubs. RE considers the quality of renewable energy resource (when considering building RE converter as well as hydrogen production facility) or existing or planned offshore renewable energy converters (ORECs) (when planning to co-locate hydrogen production facility with existing ORECs). Grid aspect includes distance from substations, cable landings and the size and 'stability' of the closest grid. Lack of these means the area may be more suitable for hydrogen production rather than grid connection. Physical features include bathymetry and water depth, which can also be an exclusion factor if considering fixed ORECs or depending on anchoring system chosen if OREC is floating. O&G infrastructure includes existing O&G infrastructure such as platforms and pipelines, including their expected cease of production. The last constraint to consider is the proximity to potential hydrogen demand hubs that includes areas onshore and offshore that have potential offtakers of hydrogen. These could be ports, distilleries, refineries, as well as big cities and other offtakers described in Section 1.2.3 of Chapter 1.

The data needed to determine appropriate location are usually obtained through different surveys such as environmental survey (to obtain information on species in the area, bathymetry, depth), resource assessment (installing wind masts and/or weather buoys to gain information on RE resource), stakeholder engagement (information on industry, environment, and socio-cultural aspects). However, most of these data are already publicly available through different databases or are provided by different institutions such as Energy Industries Council (energy related data), NATS (world air traffic data), ESRI (miscellaneous world data) [75], Marine Scotland (Scotland specific offshore data) [76], etc. The data are usually in the form of a

shapefile, which is a data storage format that stores geographic information such as location, shape and physical attributes [77]. These can be processed by geographic information system (GIS) tools that create, manage and map data and connect it to a geographic location [77].

2.2.2 Resource Assessment

Whilst the mapping section was applicable to all ORECs, this section will focus on offshore wind assessment as this thesis is focused on large scale hydrogen production. Current tidal and wave energy converters have lower power output and technology readiness level.

2.2.2.1 Wind Data

Cantero [78] describes typical resource assessment and energy production methodology that has been applied in this thesis. To calculate annual energy production, either measured or virtual wind data are used. Typical meteorological measurement masts from which data can be sourced include anemometers for measuring wind speed, wind vanes for measuring wind direction, plus a thermometer, barometer, hygrometer and pyranometer to measure air temperature, pressure, moisture and solar irradiation [78]. The data used for energy production calculations such as wind speed and wind direction time series need to be measured or extrapolated to the hub height (the distance from the platform to the rotor) of interest [78]. The equation below shows the extrapolation method used when wind data are not available at desired height [79].

$$v_i = v_0 \left(\frac{h_i}{h_0}\right)^s \quad \textbf{(2.1)}$$

Where

$v_i = wind\ speed\ at\ hub\ height\ (m/s)$

$v_0 = wind\ speed\ at\ reference\ height\ (m/s)$

$h_i = height\ at\ which\ wind\ speed\ is\ desired\ (m)$

$h_0 = reference\ height\ (m)$

$s = shear\ factor\ (0.1\ offshore\ [80])$

If reliable measured wind data are not available, reanalysis datasets are used. These are created by assimilating historical observations of wind speed, wind direction and pressure from sources, such as satellites, ground stations, weather balloons etc. and are used in climate and weather modelling as a source of meteorological information [81]. There are different global reanalysis options available such as ERA-5, ERA-Interim, MERRA-2 and CFSR [81]. Out of these options, ERA-5 is often preferred as it has the best spatial resolution (30 km), good temporal resolution (hourly data) and is freely available [82], [83]. It covers the period from 1950 to present and is being developed through the Copernicus Climate Change Service (C3S) by European Centre for Medium-Range Weather Forecasts (ECMWF) [84], [85].

2.2.2.2 Wind Data Analysis

To reduce the uncertainty of wind power production predictions, it is essential to understand the wind speed distribution characteristics [86]. Shi *et al.*[87] describes two ways to determine the wind speed distribution, the time series method, and the statistical analysis method. The time series method is more accurate and allows for calculation of hourly power production, but includes processing of large datasets [87]. The statistical analysis method is faster and more widely used in industry as it determines annual energy production (AEP) and capacity factor (CF) directly.

This chapter discusses the industry-preferred statistical analysis method as published in Offshore Wind Europe 2019 Conference Proceedings [71], while Chapter 3 discusses the time series method as pipeline simulations described in Chapter 4 required maximum and minimum hourly hydrogen flow rates that could not be accurately determined from AEP and CF obtained through a statistical analysis method.

Weibull Distribution

When considering statistical methods, the Weibull distribution is most widely used and provides a good fit to the wind speed data [88]–[92].

The Weibull distribution is a two parameter function and it is represented in Equation (2.2) [89].

$$P(v < vi < v + dv) = P(v > 0)\left(\frac{k}{c}\right)\left(\frac{vi}{c}\right)^{k-1} exp\left[-\left(\frac{vi}{c}\right)^{k}\right]dv \quad \textbf{(2.2)}$$

Where k is a Weibull scale parameter (in m/s) and c is a unitless Weibull shape parameter. $P(v < vi < v + dv)$ represents the probability that wind speed (vi) is between wind speed v and $v + dv$ while $P(v > 0)$ is the probability that wind speed exceeds 0 [89]. Wind manufacturers often provide standard performance figures using the Rayleigh function, which is a type of Weibull distribution where c is equal to 2 [91].

2.2.3 Annual Energy Production

Net annual energy production (NAEP) is generally estimated to determine the feasibility of building a windfarm from the financial perspective [93]. It shows how much actual power the windfarm produces that can be sold and whether it is enough to generate return on investment. This chapter determines gross and net annual energy production as shown in Figure 2.2 (where gross AEP is NAEP without subtracting the losses) to determine the amount of power available for hydrogen production. Wind farm generation is often represented by capacity factor (CF), which is a ratio between NAEP and maximum theoretical energy output of the windfarm, see Equation (2.3) [94].

$$CF = \frac{NAEP}{Maximum\ output\ power} \quad \textbf{(2.3)}$$

While maximum output power is just the rated power of individual WTGs multiplied by their number, there is a complex process to determine NAEP, which is described in full in this section and applied to a case study in Scotland in the next section. It should be noted that the maximum output power is not the same as gross annual energy production (GAEP). GAEP is smaller than maximum output power, as GAEP incorporates wind resource analysis, and windfarm layout and is part of the NAEP determination process.

2.2.3.1 Windfarm design

To predict GAEP, it is necessary to select an appropriate wind turbine generator (WTG) as well as design the layout of the wind farm.

The choice of suitable WTG is based on its power curve (PC) provided by the WTG manufacturer [95]. The PC shows the relationship between wind speed at hub height and rated power of the WTG [95], indicating how much gross power the WTG produces at given wind speed. For example, a small wind turbine with a cut off wind speed of 10 m/s (wind speed at which WTG no longer operates to avoid damage) would not be chosen for an offshore wind site with average wind speeds above 10 m/s and a large WTG with rated power at wind speed of 10 m/s and above, would not be installed in areas with lower average windspeeds.

The windfarm layout firstly depends on the wind direction. The WTGs should be facing the prevailing wind direction. Secondly, wind farm layout is a trade-off between minimising the wake effect (reduction of wind speed behind the rotor) and minimising the cost [93], [96]. The problem is that while wake effect can be minimised by maximising the distance between the individual wind turbines, allowing the wind speed to recover, the cost increases when the distance between wind turbines increases due to increased length of inter-array cables as well as increased time of maintenance [93], [96]. To read more on different existing windfarm layout optimisation models, Shakoor *et al.*[97] summarises layout models focusing on power production optimisation (minimising wake effect), whilst Hou *et al.* [98] summarises the layout models based on electrical system optimisation.

Wake Effect

Rather than treating each turbine individually expecting full power production as per the power curve, wake effects need to be taken into consideration. Wake loss is a decreased wind power capacity in the space behind a wind turbine caused by the turbine extracting energy from the wind to turn the blades (Figure 2.3). Thus, each wind turbine which is downstream from other wind turbines faces wake loss, unless large distances between turbines are established to minimise the wake effects. This is depicted in Figure 2.3. A way to calculate the wake effect described by Katic *et al.* [99] is shown in Equation (2.4).

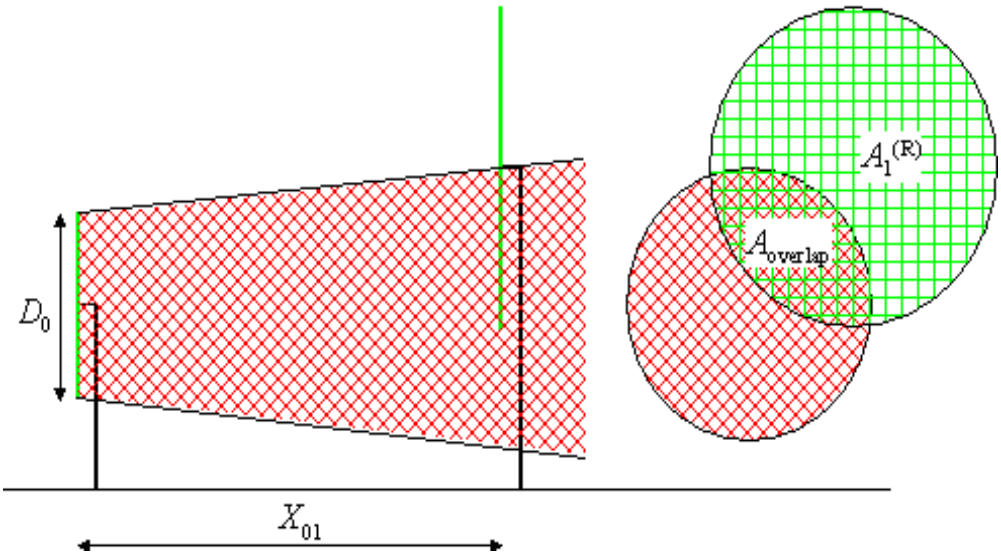

Figure 2.3: Graphical representation of wake effect [100]**.**

$$v_1 = u_0\left(1-\sqrt{1-C_t}\right)\left(\frac{D_0}{D_0+2k_W X_{01}}\right)^2 \frac{A_{overlap}}{A_1^{(R)}} \quad \textbf{(2.4)}$$

$$C_t = \frac{2F_T}{\rho_{AIR}\frac{\pi}{4}{D_0}^2{u_0}^2} \quad \textbf{(2.5)}$$

The effective wind speed in m/s faced by the down-wind turbine (v_1) is calculated using Equation (2.4), where u_0 is undisturbed wind speed in m/s, C_t is thrust coefficient, D_0 is rotor diameter in m of upwind turbine, X_{01} is the downwind horizontal distance in m between the two turbines, k_W is the wake effect decay constant, which is 0.04 for offshore wind farms, $A_1^{(R)}$ is the area of downwind turbine in m^2 and $A_{overlap}$ is the overlapping area in m^2 between $A_1^{(R)}$ and the wind deficit downwind area as shown in Figure 2.3 [100]. C_t, depends on the thrust force F_T in N and is inversely proportional to the air density ρ_{AIR} in kg/m^3, D_0 in m and u_0 in m/s squared as shown in Equation (2.5) [100].

2.2.3.2 Gross Annual Energy Production

Equation (2.6) shows how to calculate gross annual energy production (GAEP), by multiplying the power curve (power generated as a function of wind speed, $f(vi)$) with the probability of occurrence of the wind speed, $P(vi)$ and the number of hours in a year [101], [102].

$$GAEP = \int_{0}^{\infty} f(vi)P(vi)dvi \times 8760.25 \quad \textbf{(2.6)}$$

Equation (2.6) can be written as Equation (2.7) when the probability of occurrence of the wind speed is represented by the Weibull distribution [102].

$$GAEP = \int_{0}^{\infty} \left(\frac{k}{c}\right)\left(\frac{vi}{c}\right)^{k-1} exp\left[-\left(\frac{vi}{c}\right)^{k}\right] P(vi)dvi \times 8760.25 \quad \textbf{(2.7)}$$

2.2.3.3 Net Annual Energy Production

To get actual or net AEP (NAEP), losses must be subtracted from GAEP, Equation (2.8). Typical losses include electrical infrastructure losses, non-availability (turbine downtime), hydrogen production losses, and wake effect [78]. The electrical losses include AC to DC conversion and any other cable losses. The reasons for WTG downtime are mostly weather conditions and maintenance (which can be a significant factor due to limited accessibility offshore) [78].

$$NAEP = GAEP - Losses \quad \textbf{(2.8)}$$

2.2.3.4 Uncertainty

Root sum square method, Equation (2.9), has been used to estimate the uncertainty of the annual energy yield as per Beach *et al.* [103].

$$u_c(y) = \sqrt{\sum_{i=1}^{n} [u_i(x_i)]^2} \quad \textbf{(2.9)}$$

Where

$u_i(x_i)$ = *uncertainty of x*

$u_c(y)$ = *combined uncertainty*

Annual energy production is often represented using probability figures such as P50, P75 or P90, etc. P50 is the average level of generation with output forecasted to exceed P50, 50% of the project lifetime. P90 value mean that the system will generate value over P90, 90% of the time. Thus, P90 has a smaller value than P10 as P10 value is only exceeded 10% of the windfarm lifetime [104]. The P values can be calculated using Equation (2.10), where μ is mean, σ is standard deviation and erf stands for Gaussian error function of the data set. P90 occurs when $f(x- \mu / \sigma)$ is equal to 0.1 [104].

$$f\left(\frac{x-\mu}{\sigma}\right) = \frac{1}{2}\left[1 + erf\left(\frac{x-\mu}{\sigma}\frac{1}{\sqrt{2}}\right)\right] \quad \textbf{(2.10)}$$

2.3 The Case Study

2.3.1 Mapping

To make an overall map of offshore O&G infrastructure and planned and existing offshore renewable sites as the one in Figure 2.4 different shapefiles from Marine Scotland [105] and NSTA & OceanWise [106] were updated using information from the Offshore petroleum regulator for environment and decommissioning [107] and combined using a Quantum Geographic Information System (QGIS 2.18) [108].

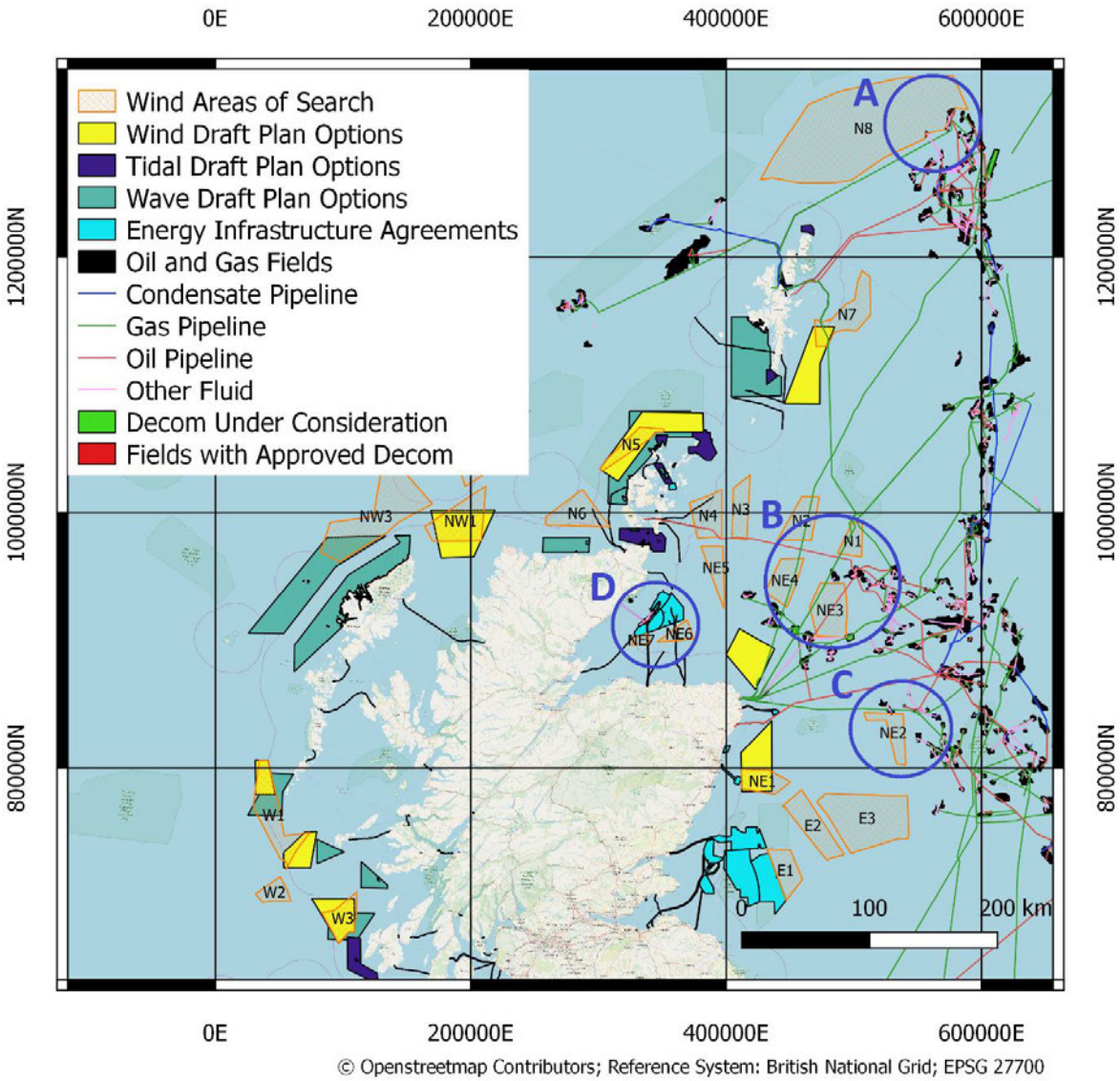

Figure 2.4: Map of offshore O&G and RE infrastructure around Scotland with the blue circles showing the indicative sites for potential offshore green hydrogen production (circles not to scale).

At the time of carrying out the research within this chapter, the draft plan options (DPO) for Scotwind leasing round were not yet finalised and so the shape files of areas of search (AoS) based on the scientific study conducted by Marine Scotland Science [109] were used instead as the next best alternative [105].

AoS are sites recommended by Marine Scotland to offshore wind developers as a result of weighting 20 relevant GIS layers looking into potential areas of opportunity and constraint. These layers featured the following aspects: bathymetry, wind resource, fishing, aviation, defence, shipping, protected areas, cultural heritage, social considerations, future trends, supply chains and O&G installations. These sites should have appropriate resource and face the least obstructions during consenting and licensing [109], [110].

Once an AoS with oil and gas infrastructure in the vicinity was determined, all oil and gas platforms and pipelines were mapped and are all listed in the Appendix A.

The Rystad database was used to estimate the date when platforms are ceasing production [111] and the OSPAR Inventory for Offshore installations was used for topside and substructure weight data [112].

As shown in Figure 2.4 four areas have been identified as potential sites for offshore hydrogen production due to the presence of both, oil and gas infrastructure and offshore renewable energy. Area A is north of Shetland, area B is northeast of St Fergus with three wind AoS, area C is east of Aberdeen and D is in Moray Firth. The RE and O&G infrastructure count for each area is summarised in Table 2.1 and a more detailed map for each of the areas is shown in Figure 2.5. Specific platforms within 50 km radius of AoS and pipelines coming from the platforms are listed in Tables A1-A9 in the Appendix A.

Table 2.1: Summary of AoS and O&G infrastructure in Areas A, B, C and D.

	A	*B*		*C*	*D*
Wind AoS	N8	NE3	NE4	N1	NE2	NE6 & NE7
O&G platforms within 50km radius	3	6	1	4	2	2
O&G pipelines from platforms	3	10	1	4	4	1
Offshore Wind Developments	-	-		-	4	

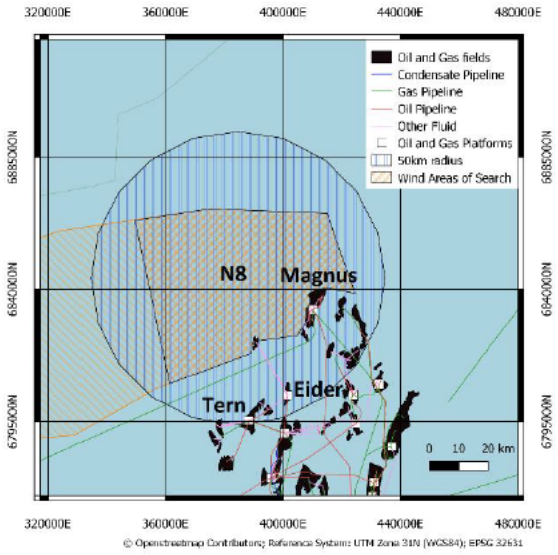

a) Area A

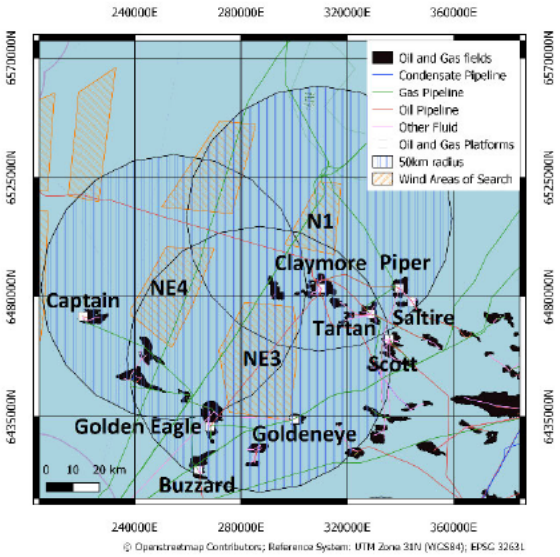

b) Area B

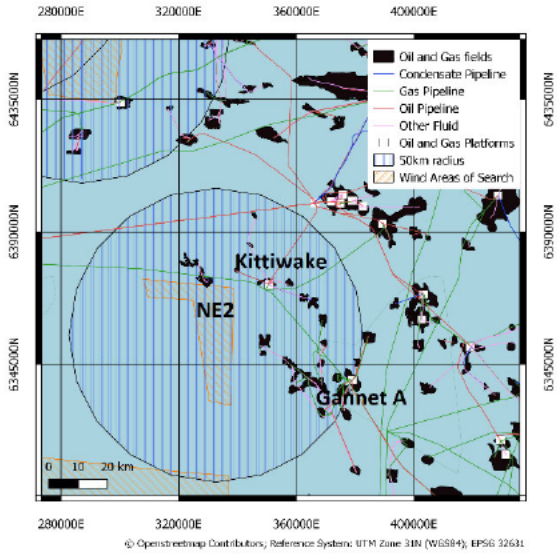

c) Area C

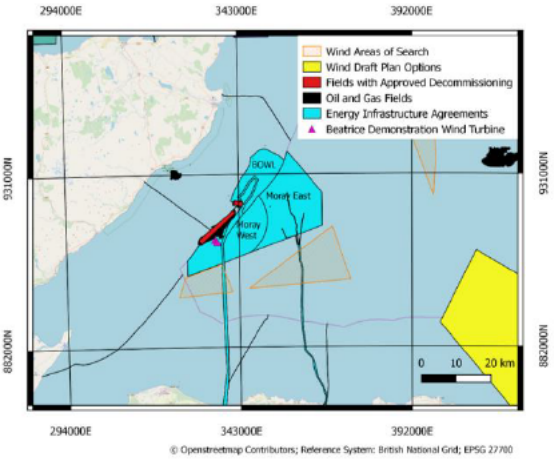

d) Area D

Figure 2.5: Four identified areas with AoS and O&G infrastructure in the vicinity.

Out of the four areas identified, area A has been selected for the case study due to distance from land (more than 100 km), grid constraints in closest cable landing point (Shetland Islands) [113], and potential future hydrogen demand in Shetland [114]. Area A will be referred to as the Magnus case study throughout the thesis as per Magnus platform near the AoS N8. Although areas B, C and D have higher potential future hydrogen market due to their proximity to mainland, ports, and cities such as Aberdeen that already has many existing hydrogen projects, they were not chosen for the case study in this work. This is because these sites are closer to shore than area A with cables being the likely transportation route chosen as is the case in area D with all existing and planned windfarms having cable connections (see Appendix A, Table A9 for existing and planned offshore windfarms in area D).

From the O&G pipelines listed in Table A2 in the Appendix A, two pipelines have been selected for the pipeline analysis in Chapter 4. These are PL164, a shorter feeder pipeline going from Magnus to Brent A and FLAGS (Far North Liquids and Associated Gas System), a longer transmission pipeline going from Brent A to St Fergus gas terminal. Both are highlighted in Figure 2.6. These were chosen as a representation of typical subsea gas pipelines that could be considered for hydrogen transportation in the future projects.

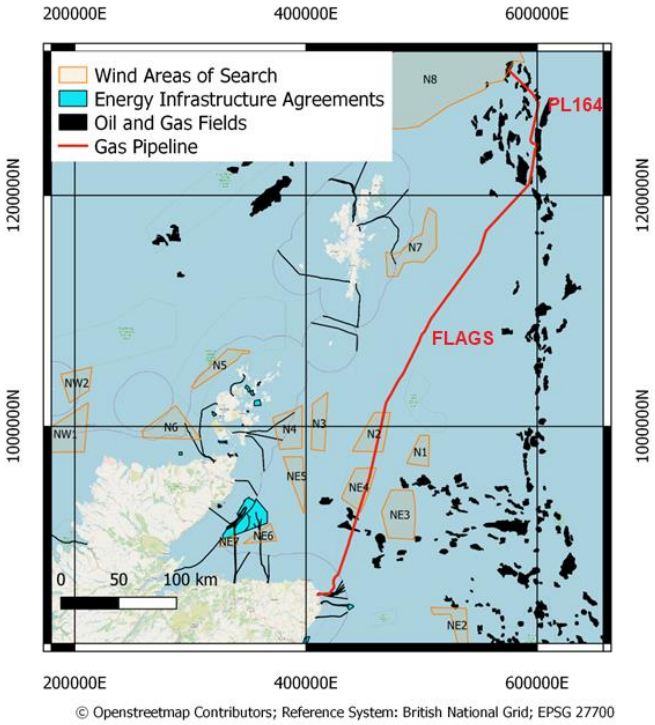

Figure 2.6: Map with highlighted PL164 and FLAGS pipelines.

2.3.1.1 Platform re-use

Figure 2.7 shows the weight distribution of existing oil and gas substructures around the areas identified above. Some of the platforms identified especially in Area A are with foundations heavier than 10, 000 tonnes such as Magnus, Tern, Eider (See Appendix A) meaning there might not be any economic advantage to the platform operator to re-use the foundations. However, there might be economic advantage to a hydrogen production operator not having to build new ones. The opposite applies to Areas C and D.

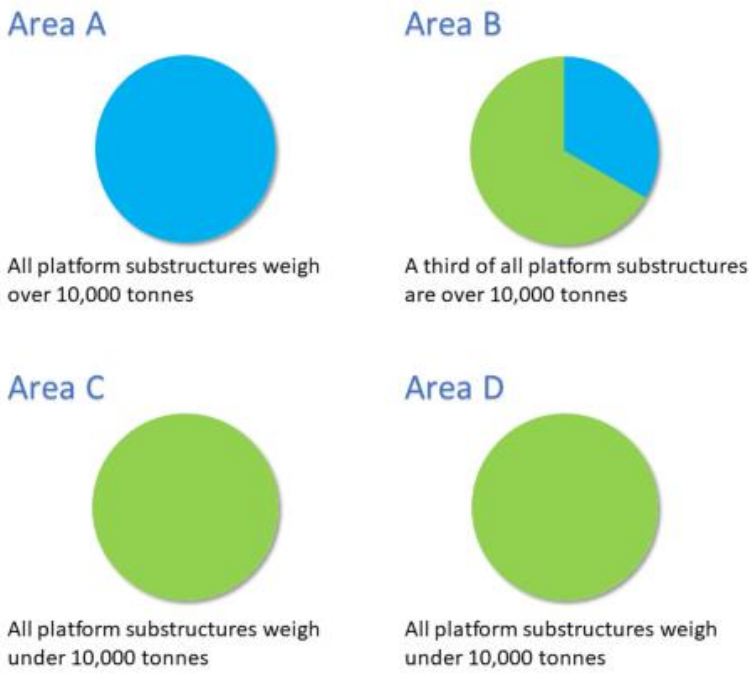

Figure 2.7: Graphic representation of platform substructure weight per area.

2.3.2 Resource Assessment

2.3.2.1 Wind Resource

To source measured wind data, several weather stations have been located on adjacent oil and gas platforms around area N8 with wind data available through the National Climatic Data Centre (NCDC) (Area A in Figure 2.4). However, these weather stations are for the purpose of confirming accessibility of heliports for maintenance and thus are not accurate and reliable enough for resource assessment. It was also not possible to access information on the type of instruments used for the measurement, surrounding environment effecting exposure of the mast and the effect of helicopter landings on the accuracy of the measurement. For these reasons, reanalysis data ERA-5 sourced from WindPro v3.0 [115] were used to estimate the wind resource.

To avoid introducing a trend in the long term data (from rare extreme weather events), the number of years selected for the analysis was based on the variance of the mean wind speed, Equation (2.11). The lowest variance in mean wind speed was for 21 years and so the long term wind distribution was based on 21 years (from 01/01/1998, 00:00 until 31/12/2018, 23:59) of hourly data. The last year considered is 2018 as the data collection and analysis was carried out in the early 2019.

$$Varriance = \frac{\sum(x_i - \bar{x})}{X - 1} \quad \textbf{(2.11)}$$

Where

$X = number\ of\ observations\ (years\ of\ data\ available)$

$x_i = the\ value\ of\ one\ observation\ (mean\ wind\ speed\ for\ specific\ number\ of\ years)$

$\bar{x} = the\ mean\ valueof\ all\ observations\ (mean\ wind\ speed\ for\ all\ years)$

2.3.2.2 Wind Analysis

A Weibull distribution as per Section 2.2.2.2 was used to fit wind speed data, with results presented in Figure 2.8. Figure 2.8 a) shows the wind rose for the Area A near Magnus platform. The area has a south-westerly wind, with prevailing wind direction of 220°. Figure 2.8 b) shows the Weibull distribution of wind speed in N8 area with average windspeed of 10.27 m/s.

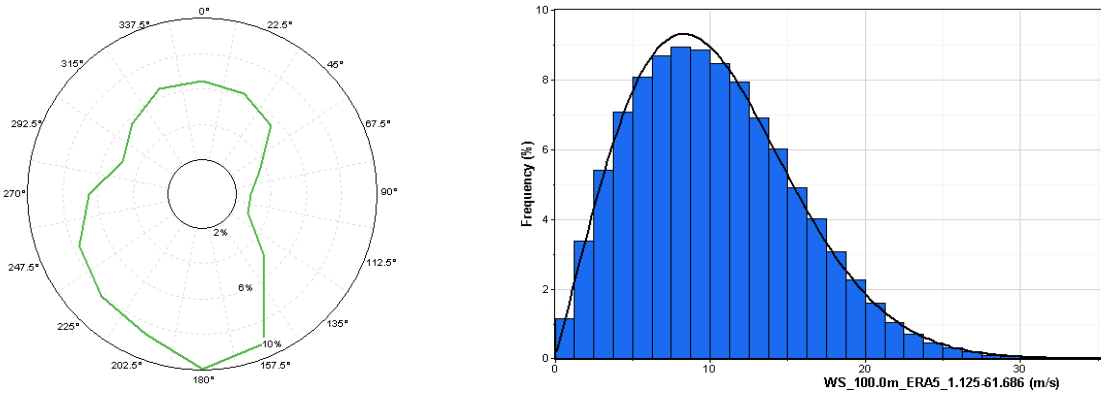

a) Wind rose **b) Weibull distribution**

Figure 2.8: Diagram of a) Wind rose and b) Weibull distribution.

2.3.3 Wind Farm Design

WindPro v3.0 [115] software for design and planning of windfarm projects was used to download the reanalysis data as well as modelling the layout of the wind farm.

2.3.3.1 Wind Turbine

As all sites identified (except Beatrice in area D) are in water depth greater than 60 m, floating offshore wind turbines are the likely technology to be installed in these locations. Thus, to future proof the results, the 10 MW Vestas V-164 turbine was chosen for the resource assessment.

All new planned floating wind projects are coming close to 10 MW. For example Equinor is currently installing 8 MW turbines for their Hywind Tampen project [116], Vestas has installed five of their V164-9.5MW turbines at Kincardine floating wind farm [117]. Principle Power and Senvion are planning to float a 10-MW turbine through a European Commission funded project [118].

The commercial version of the Vestas V-164 10MW is now available on the market with first turbine being installed as fixed in Scotland in 2021 [119] and the first floating installations due in 2023 in France [120]. The technical specifications for Vestas V-164 can be found in Table 2.2.

Table 2.2: Technical parameters for Vestas V164 [121].

Rated Power	10 MW
Rotor Diameter	164 m
Hub Height	105 m
Rotor Swept Area	21,124 m^2
Tip Height	187 m
Output	66kV, AC

2.3.3.2 Array

As the scaled area can fit 1,366 Vestas V-164 turbines resulting in 13.66 GW capacity, which is ten times the capacity of the largest offshore wind farm in the world, Hornsey 2, the windfarm layout was designed based on the latest leasing rounds specifications from The Crown Estate taking an upper limitation of 1.5 GW per wind farm [122].

To optimise the wake loss, aiming for no more than 10% as per a typical offshore windfarm [123], spacing between the wind turbines of 12 diameters in the prevailing wind direction and 8 diameters in the non-prevailing wind direction with staggered configuration was chosen. This layout of 150, 10 MW turbines, can be seen in Figure 2.9. Figure 2.9 also shows the distribution of wind speed across the analysed N8 area. Although the average wind speed is slightly better at the upper left corner, the windfarm has been placed closer to the Magnus platform.

The spacing used resulted in wake loss of 7.38%, which is good as average power loss for large offshore wind farms can be between 10-20% [124]. Throughout this work, the windfarm shown in Figure 2.9 is referred to as Magnus windfarm.

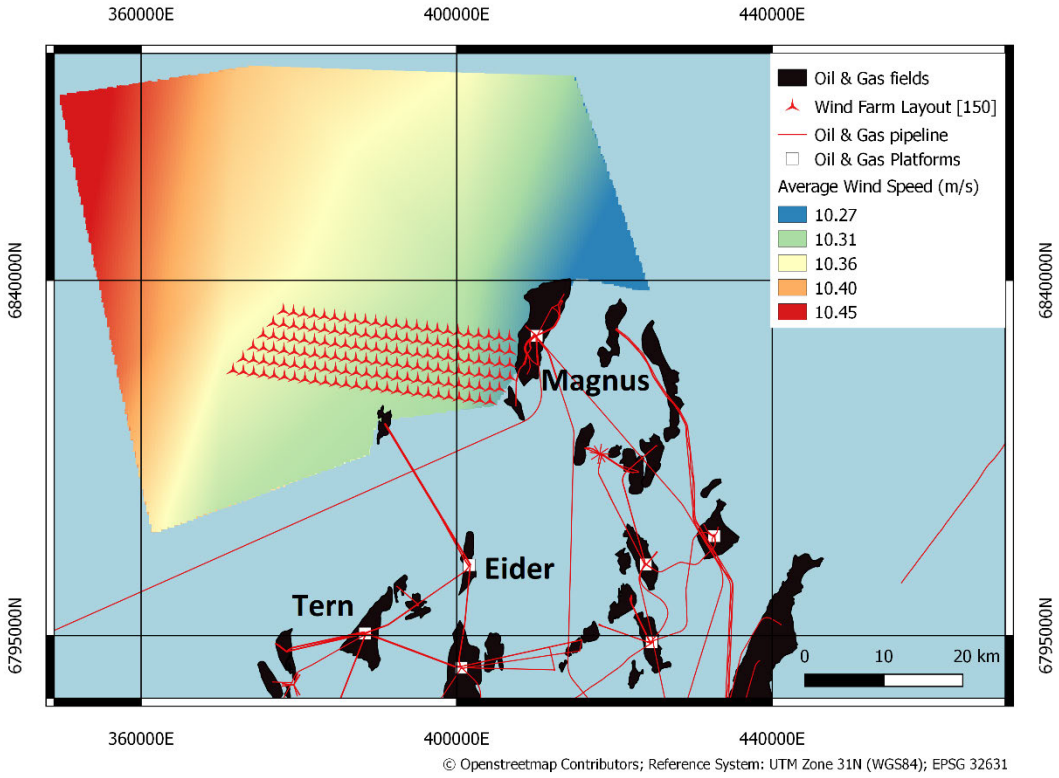

Figure 2.9: Scaled N8 area wind resource and the chosen layout for the 1.5 GW windfarm with staggered configuration.

2.3.4 Annual Energy Production

The AEP was calculated using a linear flow model in WAsP [125] that enables horizontal and vertical extrapolation of wind statistics in order to predict wind climate, wind resource and energy yield from individual wind turbines or entire wind farms. A linear flow model such as the one shown in Equation (2.6) in Section 2.2.3.2 is sufficient for an offshore wind farm, but it is recommended to use computational fluid dynamics (CFD) in case of complex terrain. The WAsP methodology consists of five main calculation blocks; analysis of raw wind data, generation of wind atlas data, wind climate estimation, estimation of wind power potential and calculation of windfarm production [102].

By providing WAsP with a power curve such as the one in Figure 2.10 a), it was possible to calculate gross annual mean energy production of the wind farm following the methodology outlined in Section 2.2.3.2. As the information needed for the annual energy yield prediction such as the power and thrust curves are confidential, the curves from the 10 MW reference wind turbine from the Technical University of Denmark were used [126]. The power curve and the thrust curve used are presented in Figure 2.10 a) and b).

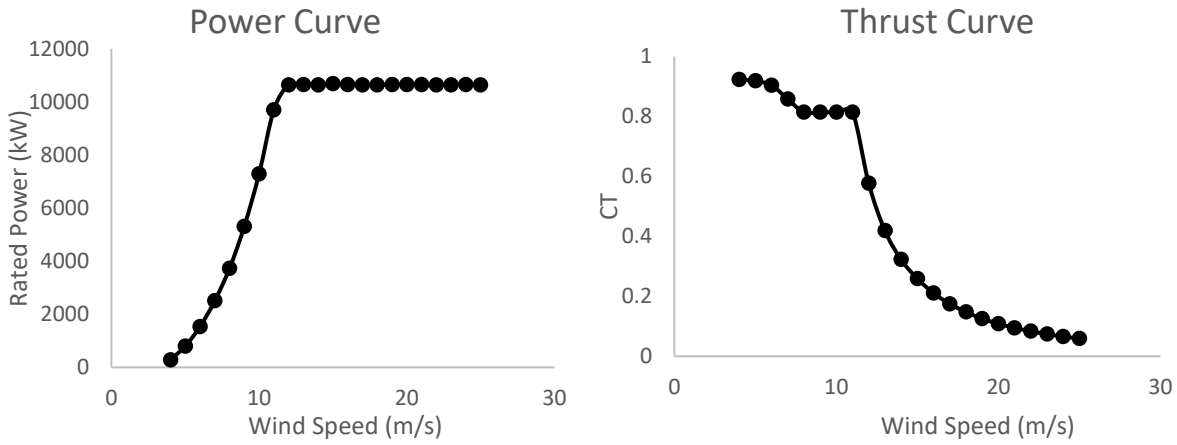

a) Power curve **b) Thrust curve**

Figure 2.10: a) Power curve b) Thrust curve [126].

WAsP uses a piece-wise linear function, Equation (2.12), to approximate mean power production [102].

$$P(v) = \frac{P_{i+1} - P_i}{v_{i+1} - v_i}(v - v_i) + P_i \quad \textbf{(2.12)}$$

Using Equation (2.12), Equation (2.7) can be simplified into Equation (2.13), where α_i is wind speed over Weibull shape factor, Equation (2.14), and $G_k(\alpha_i)$ is inverse Weibull scale parameter k, Equation (2.15) [127].

$$P = \sum_i \frac{P_{i+1} - P_i}{\alpha_{i+1} - \alpha_i} (G_k(\alpha_{i+1}) - G_k(\alpha_i)) \quad \textbf{(2.13)}$$

$$\alpha_i = \frac{vi}{c} \quad \textbf{(2.14)}$$

$$G_k(\alpha_i) = \frac{1}{k} \quad \textbf{(2.15)}$$

With the addition of the thrust coefficient curve (Figure 2.10 b) and the windfarm layout (Section 2.3.3.2), the wake loss of each turbine was estimated using methodology outlined in Section 2.2.3.1 [102].

2.3.4.1 Losses

Table 2.3 lists losses included in the NAEP calculation as described in Section 2.2.3.3. While the first two losses are related to power transfer and wind farm operation, wind hysteresis relates to delay in start-up after shutdown caused by wind reaching speed above cut off. 1% loss was applied due to the possibility of blade contamination and erosion. The percentage for blade contamination and hysteresis losses was determined based on industry practice and discussions with wind analysts. Wake effect loss is explained in Section 2.2.3.1.

Table 2.3: Wind farm losses

Loss	*Value*	*Source*
AC-DC conversion efficiency	90%	[128]
O&M Wind losses	6%	[129]
Wake effect	7.38%	[71]
Blade contamination	1%	[71]
Wind hysteresis	2.38%	[71]

2.3.4.2 Results

Table 2.4 summarises the wind farm energy yield calculated for the 1.5 GW wind farm using WaSP. The gross windfarm energy production was calculated to be 7607 GWh/year. Applying losses results in net annual energy production (P50) to come down to 5576.3 GWh/year.

Table 2.4: Summary of annual energy yield results for the Magnus wind farm.

Overall Conversion Efficiency [%]	73.3
Wind Farm Energy Yield [GWh/yr]	5576.3
Capacity Factor [%]	42.4
Standard Error in Energy Yield [%]	6.8
Standard Error in Energy Yield [GWh/yr]	378.7

2.3.5 Uncertainty

Combined uncertainty $u_c(y)$ has been calculated to be 5.1% for wind speed and 6.8% for energy based on Equation (2.9). $u_c(y)$ consist of several sources of uncertainty, $u_i(x_i)$, such as historic wind resource, wind data, future wind variability, spatial variation, and plant performance losses. Each source of uncertainty has been given a percentage contribution to the combined uncertainty based on discussion with wind analysts. Individual percentages for each source of uncertainty are kept confidential. Most of the uncertainty comes from the fact that the analysis is based on re-analysis data and there are no measurement data available for the site. This relates to uncertainty from wind data, historic wind resource and spatial variation. Future wind variability is the uncertainty expected from the effects of climate change on the wind climate.

Graphic representation of the uncertainties in the Magnus windfarm energy yield prediction at the proposed hub height for the WTG type considered are shown in

Figure 2.11. The red dashed line shows the predicted P50 yield for the Project. The blue lines represent the P10 / P90 uncertainty in the measurements and the energy yield prediction methodology; this uncertainty remains constant through the lifetime of the Project. The red solid lines represent the total uncertainty in energy yield when interannual variability is combined with the uncertainty in the yield prediction. This total uncertainty decreases over the lifetime of the Project.

The lower limit on the graph corresponds to the P90 and the upper limit corresponds to the P10.

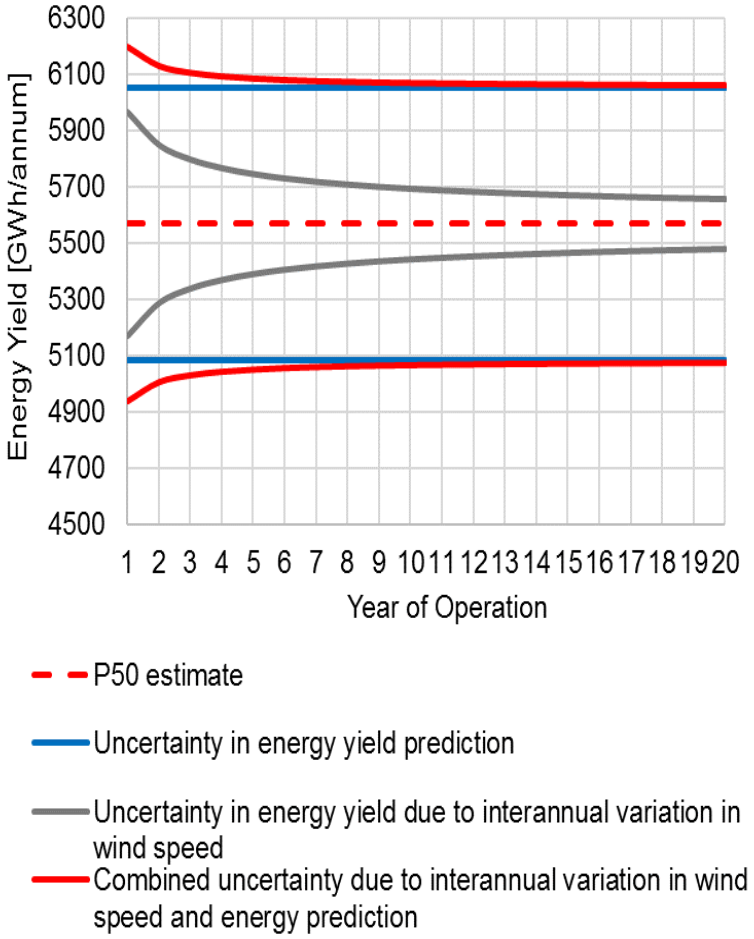

Figure 2.11: The uncertainty in the energy yield changing with the number of years of windfarm operation.

2.3.6 Capacity Factor

In this section, the effect of the availability of the electrolyser on the CF is investigated by changing the number of hours the electrolyser is available in comparison to the wind turbine generators (WTGs).

For the purpose of this study, WTG downtime is fixed at 6% based on the Crown Estate report [129]. To see the rate of change of the CF based on the electrolyser availability, different scenarios with varying electrolyser availability were considered and are presented in Table 2.5. Where electrolyser availability (EA) was calculated using Equation (2.16) and total maintenance was calculated using Equation (2.17).

Table 2.5: The summary of four scenarios with electrolyser availability noted for when the wind farm is operating.

Scenario	*Wind Farm Availability %*	*Electrolyser Availability %*	*Combined Maintenance %*	*Total Maintenance %*
1	94	100	6	6
2	94	97.3	6	8.7
3	94	94.2	2.9	11.8
4	94	91.3	0	14.7

$$EA = 100 - (Electrolyser\ Downtime - Combined\ Maintenance) \quad \textbf{(2.16)}$$

$$Total\ Maintenance = WF\ Downtime + Electrolyser\ Downtime \quad \textbf{(2.17)}$$

The most conservative scenario, Scenario 4, includes the instance where the electrolyser operates 8000 hours (91.3%) a year as in a typical chemical plant [130] and the maintenance is not coordinated with WTG maintenance. This is indicated in Table 2.5 by 0% for combined maintenance and by 14.7% for the total maintenance. This scenario results in lowest CF of 42.4% as shown in Table 2.6.

Table 2.6: Change in CF based on the availability of the electrolyser.

Scenario	*1*	*2*	*3*	*4*
CF %	46.5	45.2	43.7	42.4

In the most optimistic scenario, Scenario 1, the WTG maintenance takes place at the same time as the electrolyser's maintenance (coordinated approach assuming two separate teams for electrolysers and WTGs) and the electrolyser is down for 6% of the time or less, similar to the WTG.

The electrolyser availability represents the percentage relative to when the windfarm is operating rather than the total availability i.e. in Scenario 1 the electrolyser is 100% available when the windfarm is operating but there is maintenance taking place on the electrolyser during the WTG maintenance thereby resulting in total electrolyser availability of 94% or above.

The two scenarios between the two extremes have been calculated by incorporating the hourly windspeed data for the site for past 21 years. Ideally, the electrolyser's maintenance should be taking place during the time when the wind turbines are not operating to minimise energy loss. This happens during WTG maintenance but also when the windspeed is below cut-in speed or over cut-off speed. Occurrences when the windspeed is higher than cut-off were not considered as these are not suitable for maintenance. However, the windspeeds below cut-in speed will be ideal for maintenance activities.

The occurrences of windspeeds below 3 m/s used were during daylight between the months of April and September. The total hours calculated were 251.1 hours or 2.9% hours per year. Scenario 2 shows the electrolyser requiring 8.7% of maintenance time (operating 8000 hours) where 6% is done simultaneously with the WTG and 2.7% is done separately. Scenario 3 describes partially coordinated maintenance between the WTG and electrolyser where 2.9% of hours with windspeed below cut-in speed are used for maintenance of both and the rest of the maintenance is done separately for WTG and electrolyser throughout the year (with electrolyser operating 8000 hours). As can be seen in Table 2.6, CF varies as much as 4.1% between different scenarios for wind farms that are not connected to the grid.

2.4 Discussion

2.4.1 Mapping

None of the draft plan options for tidal and wave developments were located in proximity of O&G infrastructure (Refer back to Figure 2.4) and thus this work only concentrates on the wind technology. Currently wind turbines are more mature than wave and tidal, being able to harvest more energy and thus being more suitable for bulk hydrogen production. However, it may be worth considering wave and tidal technology in the future for smaller scale projects.

Four areas have been identified as being suitable for offshore hydrogen production in UKCS around Scotland. Three of these areas (A, B and C) are located in deep waters near areas of potential future floating wind developments. Area D, Moray Firth, is in shallow water with an existing grid connection to one of the platforms and existing and planned wind farms (Table A7 in Appendix A). If there was to be a pilot project for offshore hydrogen production in Scotland, the Beatrice platform (area D) would have been suitable as it was the first platform in Scotland to be electrified and connected to two 5MW wind turbines as well as the grid. The Beatrice platform already ceased production in 2015 and the decommissioning programme was published in December 2018. The removal of the Beatrice facilities is scheduled from 2024 to 2029 [131]. Unfortunately, it was not possible to select Area D for a case study to develop methodology for offshore hydrogen production within this work as it was not possible to establish a relationship with the owner of the Beatrice platform.

The majority of the platforms in the areas A, B and C are estimated to cease production by 2026 according to the Rystad database [111] (refer to Appendix A). With the current legislation, the infrastructure needs to be removed once abandoned [132]. Keeping the assets available after abandonment is expensive, so it is of crucial importance to consider offshore hydrogen production and initiate pilot projects now, before the O&G infrastructure is removed from the seabed. Better communication between O&G and RE sectors should be established, as once a decommissioning strategy is approved, it is hard to go back to have the operator consider alternative options as in the case of the Beatrice platform.

With the Oil and Gas Authority and Oil and Gas Technology Centre being rebranded to North Sea Transition Authority and Net Zero Technology Centre, there is an indication that the O&G sector is now opened to communication about decarbonisation and there might be projects re-using O&G infrastructure for hydrogen production in the UK in the future.

Out of the four areas identified, only one area was selected as a case study to develop a methodology for offshore hydrogen production. After excluding Area D for reasons mentioned earlier, area A was chosen based on the long distance from the nearest shore, and the insufficiency of electrical grid in the nearest shore as these are the prerequisites identified by World Energy Council [55] for converting power to gas rather than electricity.

AoS N8 has since been excluded from the DPO but could be still relevant for future offshore floating windfarm developments especially when combined with power to gas PtG or oil and gas sector decarbonisation. In fact, part of area N8 is now being considered for Sectoral Marine Plan for Offshore Wind for Innovation and Targeted Oil and Gas Decarbonisation (INTOG) [133].

2.4.2 Annual Energy Production

To carry out an approximate annual hydrogen production analysis, it is appropriate to use annual energy yield and capacity factor as the base for hydrogen production calculations. However, to determine pipeline suitability for hydrogen transportation and more in-depth analysis, maximum and minimum hourly hydrogen production and flow rates are required. The methodology for analysing hourly wind speeds and hourly power production as a feed into hydrogen production is discussed in Chapter 3.

2.4.3 Capacity Factor

The calculated capacity factor for the model windfarm connected to the electrolyser in area A is 42.4%, which is over 5% more than the average European offshore wind capacity factor [134]. One key finding of this study is that CF can be further optimised if the electrolyser’s maintenance is coordinated with the maintenance of the windfarm.

Scenario 1 results in the same value of capacity factor as in the case of a grid connected windfarm without curtailment or with several electrolyser units with alternating down time. Some literature suggests electrolyser availability over 98% [135], which if coordinated with windfarm maintenance would result in 46.5% CF, which is the same as in Scenario 1. This number however does not represent the harsh offshore environment and potential limitation with accessibility of the site, which will almost certainly decrease the availability of the electrolyser. Other studies quote availability of the electrolyser of 8,000 hours, which is typical for the majority of chemical plants and thus have been used in different ways in the rest of the Scenarios [130].

2.5 Conclusion and Future Work

The work presented in this chapter maps possible sites for offshore hydrogen production in Scotland, outlines the methodology for detailed resource assessment, wind farm design and introduces losses and uncertainty that need to be considered. There were 4 areas identified where existing O&G infrastructure coincides with already existing or potential offshore wind sites.

The majority of the sites are in deep water indicating the use of floating wind technology for production of offshore hydrogen on O&G infrastructure. To utilise the O&G infrastructure for hydrogen production, it is important to act now, before suitable sites are decommissioned. Some of the platforms identified especially in Area A have foundations heavier than 10,000 tonnes meaning there might not be any economic advantage to re-use the foundations for the asset operator. However, there might be an economic advantage to hydrogen production operator not having to build new ones. The opposite applies to Areas C and D.

The results presented also show the importance of integrating the design of the hydrogen plant with the windfarm at an early stage to optimise the performance of both as the availability of the electrolyser can have significant impact on CF when no grid is available. Future research could investigate the effects of connecting hydrogen plant to a wind farm on CF looking into connection issues, losses and availability issues in more detail.

None of the draft plan options for tidal and wave developments were located in proximity of O&G infrastructure, which is going to change with the upcoming INTOG. Thus, future research should include QGIS analysis with INTOG areas, or a completely new North Sea user accountancy map including areas that were under O&G exclusion zones during the time of this research as well as including tidal and wave energy converters.

CHAPTER 3 - OFFSHORE HYDROGEN PRODUCTION

3.1 Overview

The following chapter investigates different aspects of green hydrogen production offshore. The chapter presents the current position regarding the marinisation of electrolysers and describes how other research and industrial bodies are approaching the challenges of re-using oil and gas infrastructure for offshore hydrogen production. As mentioned in Chapter 2, this chapter discusses the time series method for mean hourly power production as pipeline simulations described in Chapter 4 required maximum and minimum hourly hydrogen flow rates that could not be accurately determined from AEP and CF obtained through a statistical analysis method described in Chapter 2. This chapter also describes a methodology for sizing the electrolyser and calculating the hydrogen flow rate based on the wind resource from Chapter 2. The results are first discussed within this chapter and then used in Chapters 4 and 5 as shown in Figure 3.1.

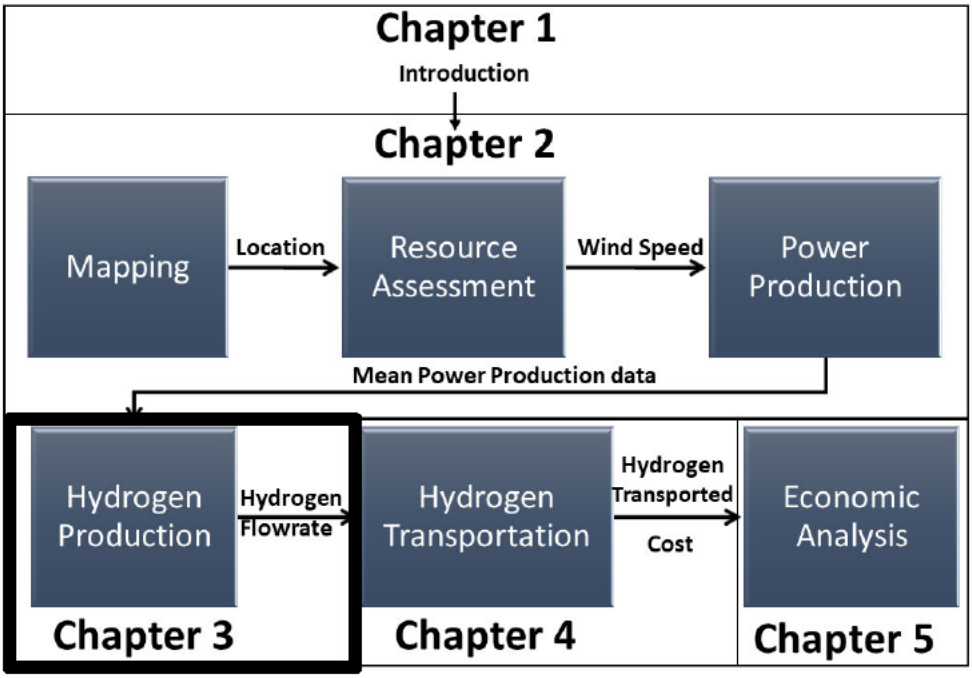

Figure 3.1: Thesis flow diagram.

3.2 Literature Review

In recent years, several areas across Europe have been investigated for the potential of re-using offshore oil and gas infrastructure for offshore hydrogen production. The areas include infrastructure in the North Sea [55], [136], Adriatic Sea [137] and Irish Sea [138]. While the areas around the North Sea mostly include offshore wind, wave and tidal as RE resources for hydrogen production, areas around the Adriatic Sea also consider floating solar [137]. Hydrogen production and synthesis of different hydrogen carriers, also called power to gas (PtG), are not the only potential use of oil and gas infrastructure. Other alternative uses that are mentioned in the literature specific to re-use of oil and gas infrastructure include electricity production, biofuel production from algae and artificial reefs [139]. Whilst the majority of the studies look into the techno-economic feasibility of offshore PtG as shown in Table 3.1, the environmental impact of offshore hydrogen production is also considered in the literature.

Table 3.1: Summary of offshore hydrogen and PtG literature based on type of study and renewable resource used.

Study Type	*Resource*	*Reference*
Technological and economic assessment	Wind	[51]–[53], [57], [63], [136]–[138], [140], [141]
Technological and economic assessment	Wave	[142], [143]
'Desk study'	Wind	[144], [145]
Environmental impact and risk assessment	Wind, wave, tidal	[139]

The different investigations discuss production of hydrogen, ammonia and synthetic methane as well as evaluating the optimal location of the infrastructure. Table 3.2 summarises the papers that investigate production of hydrogen, synthetic natural gas (SNG) and ammonia. All papers listed in Table 3.2 mention offshore production except Leporini *et al.* [137], who discuss hydrogen production offshore but methanation onshore. The studies in Table 3.2 also investigate other scenarios such as desalination [137] or biofuel production [139]. This work focuses entirely on hydrogen production as defined in Chapter 1.

Table 3.2: Summary of literature based on molecules produced.

Molecules produced	*Reference*
Hydrogen	[51]–[53], [137], [139]–[143]
SNG	[52], [138], [139], [145], [146]
Ammonia	[53], [139]

3.2.1 Decommissioning

3.2.2 The Use of Electrolysers Offshore

This section describes offshore electrolysis specifically. For more information on mechanisms and chemical reactions of electrolysis, revisit Chapter 1. Several papers investigating offshore hydrogen production through electrolysis describe three pathways to producing hydrogen offshore; direct sea water electrolysis, low temperature electrolysis (this includes a Proton Exchange Membrane (PEM) electrolysis and an Alkaline electrolysis) and high temperature electrolysis (solid oxide electrolysis) [141], [147].

Both Meier [141] and D'Amore-Domenech & Leo [147] identify low temperature electrolysers as currently the best option for green hydrogen production offshore. This is due to the better response of the electrolysers to the power variation of renewable energy converters. Direct seawater electrolysis was found inadequate for offshore hydrogen production due to much higher specific energy required in comparison to low temperature electrolysis combined with desalination, deeming this technology inefficient. Another argument against direct seawater electrolysis is the harmful impact of the process on the environment due to the production of chlorine and caustic soda (see Equations (3.1)-(3.3) [147]), which can have detrimental effects to marine life [148], [149]. Whilst brine (concentrated sea water, which is the by-product of desalination) can be also harmful to the environment, there are established brine disposal methods that can be applied offshore described in Ahmad and Baddour [150].

$$Anode: 2Cl^- \rightarrow Cl_2 + 2e^- \quad \textbf{(3.1)}$$

$$Cathode: 2H_2O + 2e^- \rightarrow H_2 + 2OH^- \quad \textbf{(3.2)}$$

$$Overall\ reaction: H_2O + 2NaCl \rightarrow Cl_2 + H_2 + 2NaOH \quad \textbf{(3.3)}$$

There are some new emerging technologies that claim to use sea water without the release of harmful by-products into the sea that might make offshore hydrogen production safer for the marine environment [151]. They also contain several features allowing operation in an offshore environment such as lightweight, polymer materials that are easily stackable [151].

Solid oxide electrolysis requires superheated vapour for its operation. SOE also has a very long cold start time, which would require it to run constantly, decreasing the overall efficiency of the process. D'Amore-Domenech & Leo [147] propose that high temperature electrolysis would operate more efficiently with a constant source of high temperature heat such as geo-thermal energy rather than wind energy [147].

When the question comes to PEM electrolyser versus alkaline electrolyser (AE), there are several parameters that need to be considered. These have been summarised by Buttler and Spliethoff [30] as flexibility, efficiency, capacity, lifetime, capital expenditure (CAPEX) and operational expenditure (OPEX). In general, when coupled with renewable energy converters it is important for the system to be able to cope with intermittent energy supply. This is not the case for AEs as they have poor partial load range with issues appearing already when load range drops below 40% [152]. With the decrease in load, the levels of hydrogen and oxygen evolved fall. This leads to dangerous potentially explosive concentrations of hydrogen, decreased purity of oxygen, decreased production of hydrogen and electrode degradation [152]. It is recommended that alkaline electrolysers run continuously to avoid short circuiting, shut-downs and slow start-ups [153]. However, adding storage systems such as batteries, and an AC to DC converter can smooth the power supply and enable AE to operate with offshore renewable energy without the aforementioned shortfalls [154].

A PEM electrolyser on the other hand has much better partial load range with most suppliers stating no limit for minimum load [30]. The PEM electrolyser offers high purity hydrogen at all loads with lower risk of hydrogen diffusing to the oxygen side [30]. Current interruptions were also found to reduce degradation of the electrolyser as they gave the electrolyser the time needed to recover from reversible degradation. Rakousky *et al.* [155] suggest that dynamic current density profiles, such as the ones from renewable energy sources, have the potential to positively affect the durability of the PEM electrolyser.

AE is more mature offering larger stack capacity and lower degradation rates [30]. However, the stack lifetime for PEM electrolyser and AE is comparable [30].

There are further advantages and disadvantages when considering the use of electrolysers specifically offshore. PEM electrolysers present lower size and weight due to greater current densities for the same operating efficiencies, while the alkaline electrolyser has lower CAPEX and uses inexpensive materials as electrodes [147], [156]. PEM’s compatibility advantage also stems from the fact that it can operate at higher pressures diminishing the need for post-production compression steps [152]. The operating pressure for AE is rather limited [152].

The disadvantage of the cheaper alkaline electrolyser technology is the risk of leakage of the corrosive electrolyte and the need to refill the electrolyte periodically, as this is lost during operation through product gases and contamination due to the corrosiveness of the marine environment [141], [147]. However, replacing the electrolyte and cleaning the electrolyser leads to recovery of the performance of AE. Also, recent research shows that the electrolyte replacement for an alkaline electrolyser can be sourced from the treated saturated brine, which is the by-product of seawater desalinisation [156]. This makes the alkaline electrolyser an attractive solution for use offshore in comparison to PEM electrolysers that suffer irreversible damage in the marine environment due to the presence of sodium chloride [147].

Another issue arises when it comes to the balance of plant. There is typically limited space on the offshore platform, which puts AE at a disadvantage. The alkaline electrolyser requires an electrolyte recirculatory system although as mentioned before, this might be joined with a water desalination plant. An alkaline electrolyser also produces lower purity hydrogen (especially when operating under irregular power source) thus an additional hydrogen purifier might be necessary. Also as previously mentioned, a separate compressor unit might be required when using AE rather than PEM electrolyser for easier hydrogen handling [152].

Table 3.3 shows electrolyser technology used in previous offshore hydrogen production studies.

Table 3.3: Electrolyser technology used in previous studies.

Model of electrolyser	*Electrolyser type*	*Reference*
1 MW Proton On site	PEM	[138]
Hylyzer-3000-30	PEM	[144]
Silyzer 300	PEM	[51], [53]
No particular model	PEM	[52], [63], [136], [141], [143]
No particular model	AE, PEM, SOE	[57]

No particular model or not clear	-	[137], [140], [142]

3.2.3 Sizing of the Electrolyser to the Platform

Not all literature considers spatial and weight requirements of the platform with regards to electrolysis and other equipment necessary for offshore hydrogen production.

O'Kelly-Lynch *et al.* [138] investigated offshore hydrogen production combined with methanation on the Alpha and Bravo platforms in the Irish Sea assuming a standard shipping container size per 1MW of electrolyser. No weight restrictions were taken into consideration. In their case study, they could fit up to 35 electrolysers on each platform allowing 2m spacing for maintenance assuming the platforms can be stripped to an empty deck.

The Energy Delta Institute has investigated weight and size restrictions of two gas platforms in the Netherlands for offshore hydrogen production. One was a smaller, satellite platform that could accommodate maximum of 60MW of a Silyzer 300 electrolyser capacity while the other platform could accommodate up to 250MW of the same electrolysers assuming all platform levels can be utilised. In their report they also show that the space is more limiting than weight and point to the fact that vertical distance between platform decks might pose an issue as the current height of the electrolysers is greater than the height available [53].

According to Gondal & Masood [145] the size of an artificial island would be required for all hydrogen production equipment to serve a 500MW offshore wind farm that would start at 15 000 m^2 reaching up to 5km^2 including residences and logistical platform.

A study conducted by DNV GL [157] also showed that there is insufficient amount of oil and gas platforms to be able to convert all of the energy from planned offshore wind farms to hydrogen. However, they estimated only 20-30MW of installed electrolyser capacity per platform, which is quite low when compared to results from The Energy Delta Institute but close to the numbers reported by O'Kelly-Lynch *et al.* [138]. According to their estimates, a 350MW windfarm requires 10-15 platforms considering electric losses of the wind turbine and convertors [157].

Thus, with different capacities reported it is clear that the capacity changes case by case according to the size of the available platform. It is also hard to future proof these estimations due to the fast progressing electrolyser technology. Thus, developing a methodology for companies to follow rather than providing numbers for specific cases will be a more useful outcome of this thesis.

For large scale non grid connected windfarms that are located far offshore, a scenario where electrolysers are located on a wind turbine could be more suitable, as this would allow for bigger electrolysis capacity than trying to fit them all on platforms. This has been suggested by Gondal [144], with the first commercial application being ERM's Dolphyn project [63] followed by the Oyster project [158] (refer back to Chapter 1 Section 1.2.4).

3.2.4 Desalination

As described in Section 3.2.2, both AE and PEM electrolysers require pure water input [147]. As there is no fresh water supply far offshore, sea water treatment will be necessary to provide water for the electrolysers. Sea water desalination is the most expensive type of water treatment [159] but sea water is the only type of water available offshore.

There are two types of desalination technologies, thermal and membrane. Thermal technologies use thermal energy as a primary source and electricity to drive associated pumps. Membrane technologies only use electricity. The most common processes for thermal type of desalination are multi-stage flash, multi-effect distillation and mechanical vapour compression. Unless there is a significant amount of waste heat, membrane desalination is more suitable than thermal as it has lower cost and energy demand [160]. Membrane desalination technology types are mostly Reverse Osmosis (RO), electro dialysis and electro dialysis reversal [161]. In line with the majority of studies in the PtG literature [51], [53], [137], [138], [143]–[145], RO has been chosen as the technique for desalination in this work. Its advantage is low energy consumption and it is the most economic desalination method for waters with TDS (total dissolved solids) higher than 5000 ppm (sea water is usually 35 000 ppm and above) [161].

RO is the most widely used desalination technique accounting for 66% of online desalination capacity [162]. RO desalination is a pressurised filtration of sea water through semi-permeable membrane separating fresh water from salt. The process consists of four phases as shown in Figure 3.2. Pre-treatment requires filtration to remove organic material, sterilization and addition of chemical to prevent biofouling [161]. Second phase requires high- pressure pump to force the sea water through the membrane. The AC electricity supplied for the pump, is the only form of energy RO requires. In order to obtain higher recovery ratio, this process is repeated second time with waste concentrated solution. Once water passes through the membrane (phase three), it requires phase four, post treatment, which adjusts the pH of clean water. Calculations on amount of water required and the electrical requirements/ losses are described in Sections 3.3.3.1 and 3.3.3.2.

Figure 3.2: Schematic for reverse osmosis desalination process [161]**.**

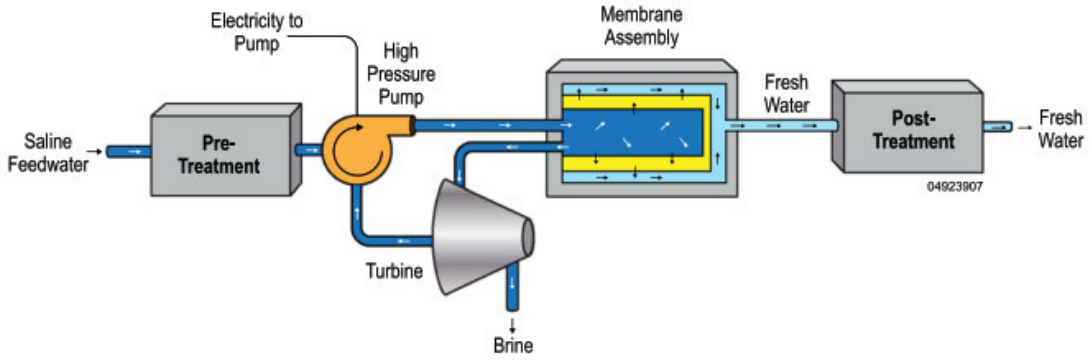

.

3.3 Methodology

This section ties in with the general methodology described in Section 2.2. of Chapter 2. This section shows the time series method of wind data analysis applied to the Magnus case study as pipeline simulations described in Chapter 4 require maximum and minimum hourly hydrogen flow rates that could not be accurately determined from AEP and CF obtained through a statistical analysis method described in Chapter 2.

3.3.1 Mean Power Production

Hourly mean wind speed (MWS) data, described in Chapter 2, from ERA-5 in m/s, averaged from the past 21 years (Figure B1 in Appendix B) were converted to mean power production (MPP) using an if statement algorithm as shown in Figure 3.3. The conditions are based on the best fit to the 10MW DTA wind turbine introduced in Section 2.3.4. of Chapter 2 in order to find the best curve that fits the PC to extrapolate between the data points provided by Bak *et al.* [126].

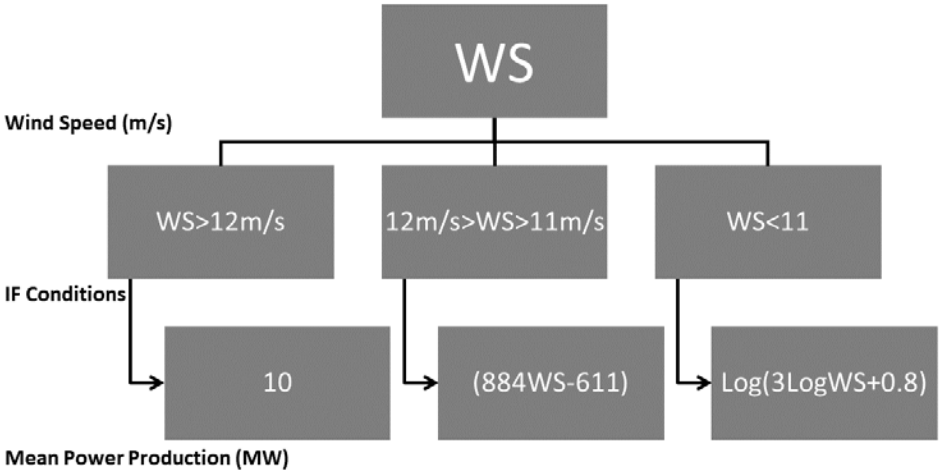

Figure 3.3: Algorithm used to calculate mean power production from wind speed.

As shown in Figure 3.4, this power curve was split into four sections. The rightmost section represents the region where wind speed reaches the maximum rated power. In this case, it is MWS greater than 12m/s (see Figure 3.4), past which mean power production is equal to 10MW, thus setting the condition to IF MWS>12, THEN MPP=10MW as shown in Figure 3.3. Depending on the shape of the power curve, the rest of the curve could be fitted using exponential function.

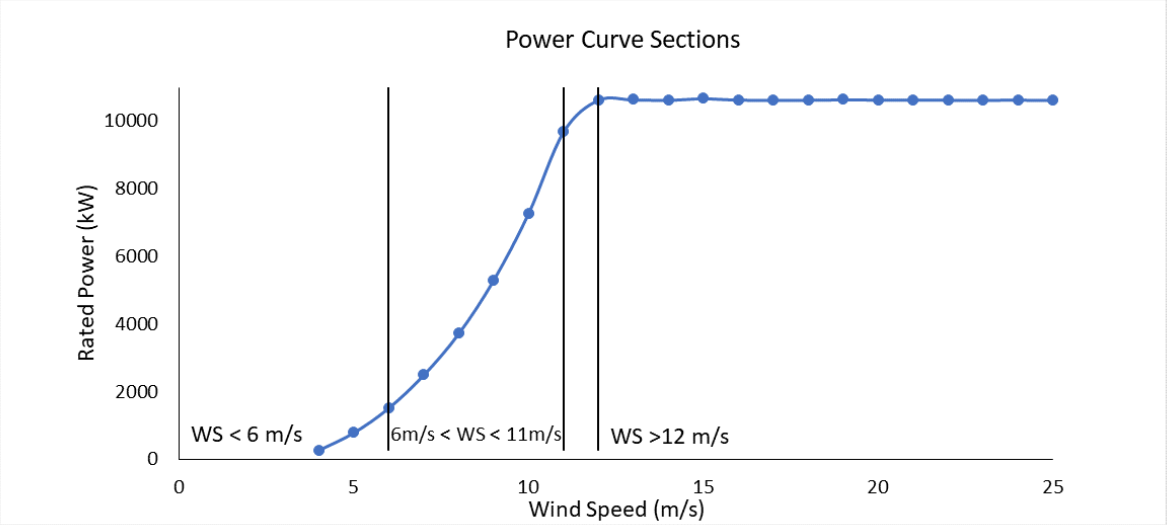

Figure 3.4: Power curve sections.

In here, the second section is between 6 m/s and 11 m/s, where a linear relationship was found between the logarithm of rated power and the logarithm of MWS (See Figure 3.5). The last two conditions that need to be included no matter the shape of the power curve consider the cut-in and the cut-off windspeeds, where IF MWS<Cut-in WS, THEN MPP=0, and IF MWS> cut-off WS, THEN MPP=0. The cut-off MWS of 25 m/s and cut-in wind speed (3 m/s) as well as 4m/s and 5m/s data points were omitted in this case as the MWS does not go above 13 m/s and below 7 m/s as shown in Figure B1 in Appendix B. The results of the mean power production are shown in Figure B2 in the Appendix B.

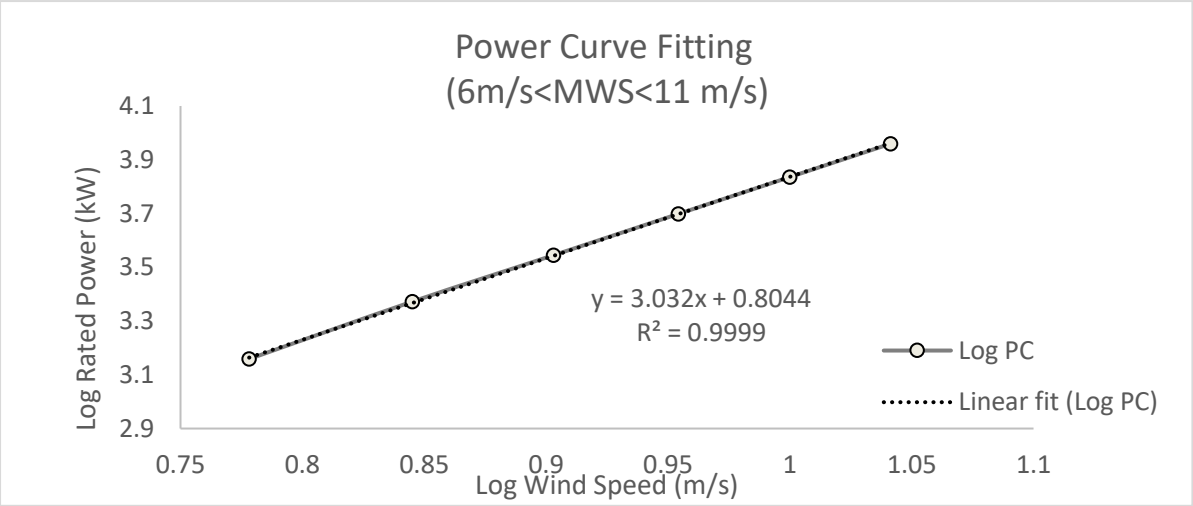

Figure 3.5: Linear fit to log rated power over log MWS.

3.3.2 Sizing the Electrolyser

This section describes the determination of the minimum and maximum gross electrolyser sizes (without losses), as these were needed to determine the minimum and maximum hydrogen flow rate for the pipeline analysis described in Chapter 4. The hydrogen production for further five electrolyser sizes between minimum and maximum with increments up to 150MW have been determined as an input to economic analysis presented in Chapter 5.3.3.3

The minimum electrolyser size in MW has been determined from the lowest (non-zero) mean power production hour. From the case study mean power production data, this occurs between 7pm and 8pm in July and is highlighted in Figure B2 in Appendix B. Summer months are typical for lowest power production due to low and discontinuous wind speeds. The minimum electrolyser size equals to 957.8 MW for the whole windfarm (i.e. when the lowest hourly MPP for individual turbine highlighted in Figure B2 in Appendix B is multiplied by the number of WTGs, which is 150 in this case) as shown in Equation (3.4).

$$Minimum\ electrolyser\ size = Lowest\ MPP \times Total\ number\ of\ WTGs \quad \textbf{(3.4)}$$

Where

$$Lowest\ MPP = lowest\ mean\ power\ production\ in\ MW\ per\ individual\ WTG$$

The electrolyser was scaled to 957.5MW to match electrolyser stack sizes (.5MW electrolysers available such as 17.5 MW and 3.5 MW [163]). However, this is depends on stack sizes available from selected provider. Sizing the electrolyser to the lowest MPP, allows the electrolyser to be utilised at 100% in theory (as no losses are included at this point), while the utilisation rate for the wind farm drops to 78% due to the windfarm running only at around 64% during the winter months (still no losses included). It should be noted that the utilisation rates are not the same as the capacity factor, as they only show utilization based on wind resource, with the losses being added at a later stage. The average utilisation rate for the windfarm (AWF_U) was calculated using Equation (3.5). To avoid exceeding 1 when the capacity of the electrolyser (EC) was greater than MPP, the condition in Equation (3.6) was used. The individual average utilisation rate for the windfarm (AWF_U) can be seen in Figure B3 in the Appendix B.

$$AWF_U = \frac{\sum \frac{EC}{MPP}}{Number\ of\ MPP\ data\ points} \quad \textbf{(3.5)}$$

Where

$EC = Electrolyser\ Capacity\ in\ kWh$

$MPP = Mean\ Power\ Production\ in\ kWh$

$$\boldsymbol{IF}\ EC > MPP\ \boldsymbol{THEN}\ AWF_U = 1\ \boldsymbol{ELSE}\ WF_U = \frac{EC}{MPP} \quad \textbf{(3.6)}$$

The maximum EC is equal to the full capacity of the wind farm, 1500 MW, as that was the highest mean power production hour for most of the winter months (refer back to Figure B2 in Appendix B). While utilisation for the windfarm without losses is 100% at maximum electrolyser size (no losses), the gross utilisation for the electrolyser was calculated using Equation (3.7) to be 84% mostly due to lack of wind in the summer months. Like AWF_U, condition shown in Equation (3.8) was set to avoid producing more than 100% when MPP is greater than EC. The individual average utilisation rates for the electrolyser (AE_U) can be seen in Figure B4 in the Appendix B.

$$AE_U = \frac{\sum \frac{MPP}{EC}}{Number\ of\ MPP\ data\ points} \quad \textbf{(3.7)}$$

$$\boldsymbol{IF}\ MPP > EC\ \boldsymbol{THEN}\ AE_U = 1\ \boldsymbol{ELSE}\ AE_U = \frac{MPP}{EC} \quad \textbf{(3.8)}$$

Where

$AE_U = Average\ electrolyser\ utilisation\ rate$

$EC = Electrolyser\ Capacity\ in\ kWh$

$MPP = Mean\ Power\ Production\ in\ kWh$

3.3.3 Hydrogen Production Rate

The following section first describes desalination plant and water requirements for the electrolysis, and then outlines methodology to determine annual and hourly hydrogen flow rates for Chapter 4.

3.3.3.1 Energy Requirement of Desalination Plant

To determine the energy consumption of a desalination plant, the salinity of the water treated is required. Based on information from Quante & Colijin [164], the North Sea salinity in the area of Shetland is 35.25 PSU (practical salinity units) with seasonal variability of ± 0.1.

Based on Equation (3.9), which is a polynomial equation for the energy consumption of the sea water reverse osmosis process with hydraulic pump for energy recovery from Caldera *et al*. [165], the energy consumption for the desalination unit in the region of the North Sea is 3.5 kWh/m^3.

$$DEC = 0.0003S^2 + 0.0018S + 2.6043 \quad \textbf{(3.9)}$$

Where

$DEC = Desalination\ energy\ consumption\ in\ kWh/m^3$

$S = salinity\ in\ PSU$

The recovery ratio, which is the percentage amount of desalinised water obtained from desalination, can be between 40%-60% for normal seawater desalination [166]. Normal seawater is defined as 35,000 mg/L of salinity, which is equivalent to 35 PSU and so 40-60% recovery ratio is applicable to the North Sea. A recovery ratio of 60% is also mentioned by Greenlee *et al.* [167] and Gude [168] as well as more recent research carried out by Shahzad *et al.* [169]. According to O'Kelly-Lynch *et al.* [138], any further improvement of the recovery ratio above 60% is unlikely due to osmotic pressure limitations and burst pressure of the membrane. However, Lenntech [170] mentions that there has been membranes developed which can take higher pressure and thus increase the recovery ratio. Their three-stage system is allegedly able to allow between 85-95% recovery, which is the highest for sea water desalination the author has come across during their review of desalination technologies.

Shahzad *et al.* [169] suggest that there is still potential to decrease the energy consumption from current 3.5kWh/m^3 for sea water reverse osmosis desalination. Caldera & Breyer [162] uses 3.0 kWh/m^3 for 2015 and 2030 simulations. According to the director of the International Desalination Association, electrical energy use is likely to go down to 2.1-2.4 kWh/m^3 by mid 2030s for medium to large desalination plants [171]. A commercial leaflet from 2016 from Lenntech already mentions electric consumption around 2.6 kWh/m^3 [172].

Thus, within this work, 2.5kWh/m^3 will be used including pre- and post-treatment, as they are included within the desalination system [172].

3.3.3.2 Water Requirements

Equation (3.10) represents a chemical reaction for production of hydrogen from water. Using Equations (3.10) and (3.11) it is possible to calculate that 1kg of hydrogen requires 9 litres of water.

$$2H_2O \rightarrow 2H_2 + O_2 \quad \textbf{(3.10)}$$

$$m = nmol \times RMM \quad \textbf{(3.11)}$$

Where

m= *mass in g*

$nmol$=*number of mols in mols*

RMM = *relative molecular mass in g/mol*

However, this calculation is only theoretical based on pure water and does not include any losses. In practice, more potable water is required as shown in Table 3.4. PEM electrolysers require high quality water with a maximum of 0.5 ppm total dissolved solids (TDS) [141], which is equivalent to pure or ultra-pure water. Some electrolyser vendors state that electrolysis requires demineralised water [163] (1-10ppm TDS). Sea water reverse osmosis produces water between 10-500ppm TDS [173] or 400-500 ppm [161], which is comparable to The Environmental Protection Agency (EPA) potable water standards [174]. Thus, deionisation treatment will be necessary if RO is used as a desalination treatment.

Some companies, such as ITM, have water treatment already included in their service [175]. Thus, more than 9L output from the desalination plant needs to be considered as for example the before mentioned arrangement from ITM requires 27L of potable water [175].

For this research, a figure of 15.6L of tap water per 1kg of hydrogen was used as it comes from information on large scale electrolysis and is close to the desalination output water quality [176]. 15.6L per kg of hydrogen is used rather than 27L as there should be improvements in the type and amount of water required for the electrolysis by 2030.

Table 3.4: Water requirements for PEM electrolysis.

Water/kg H_2	*notes*	*source*
27L	potable	[175]
10L	Ultra-high purity 5.0, demineralised water	[163], [177]
<15.6L	tap	[176]
9L	Pure water	Chemical calculation

3.3.3.3 Annual Hydrogen Flow Rate

Equations (3.12) to (3.22) show the methodology used to calculate the Annual Hydrogen Flow Rate (AHP) in kg. AHP is simply the mean power production available for the electrolyser in kWh ($MPPE$) divided by the electrolyser electricity consumption in kWh/kg (EEC), see Equation (3.12). EEC is set to 50 kWh/kg of hydrogen based on the EU key performance indicator for PEM electrolyser for 2030 [130].

$$AHP = \frac{MPPE}{EEC} \tag{3.12}$$

In Equation (3.12), the $MPPE$ depends on several factors as per Equations (3.13) - (3.15).

$$MPPE = EC \times AE_U \times TWFA \times TEA - DESAL \quad \textbf{(3.13)}$$

$$TWFA = 1 - TWFL \quad \textbf{(3.14)}$$

$$TEA = 1 - TEL \quad \textbf{(3.15)}$$

$MPPE$ depends on the full electrolyser capacity selected (EC) in kWh as determined in Section 3.3.2, the average electrolyser utilisation rate (AE_U) calculated based on MPP per hour (Section 3.3.2), the total wind farm availability rate ($TWFA$), the total electrolyser availability rate (TEA) and the desalination power requirements in kWh ($DESAL$).

Substituting Equations (3.13)-(3.15) into Equation (3.12), results in the full expression for AHP shown in Equation (3.16).

$$AHP = \frac{EC \times AE_U \times (1 - TWFL) \times (1 - TEL) - DESAL}{EEC} \quad \textbf{(3.16)}$$

Where $TWFL$ is total wind loss and can be calculated using Equation (3.17). $TWFL$ consists of wind farm loss (WFL), which are listed in Table 3.5, and average wind utilization (AWF_U), Section 3.3.2. TEL is total electrolyser loss and can be calculated using Equation (3.18). TEL consists of electrolyser loss (EL) (Table 3.5) and average electrolyser utilisation (AE_U) (Section 3.3.2).

$$TWFL = WFL/100 - (1 - AWF_U/100) \quad \textbf{(3.17)}$$

$$TEL = EL/100 - (1 - AE_U/100) \quad \textbf{(3.18)}$$

In order to take into consideration the spill-over capacity of the electrolyser when oversized (eg 1500MW) and wasted energy from the windfarm, when the electrolyser is sized at less than 1500MW, the following two IF, THEN, ELSE statements were included shown in Equations (3.19) and (3.20).

$$\textbf{IF } 1\text{-}AWF_U \geq WFL \textbf{ THEN } TWFL = 0 \textbf{ ELSE } TWFL = \text{Equation (3.17)} \quad \textbf{(3.19)}$$

$$\textbf{IF } 1\text{-}AE_U \geq EL \textbf{ THEN } TEL = 0 \textbf{ ELSE } TEL = \text{Equation (3.18)} \quad \textbf{(3.20)}$$

This means that wind farm losses are taken out of the spill-over power from the windfarm where available and that electrolyser maintenance is done when the units are not operating (i.e. when there is less wind than electrolysis capacity in the summer).

$DESAL$ is calculated by multiplying the amount of desalinised water required in m^3, which consists of water required in m^3 per kg of H_2 (WR) multiplied by amount of hydrogen produced in kg (AHP), by desalination electricity requirement (DEC) in kWh/m^3,Equations (3.21) and (3.22).

$$DESAL = Amount\ of\ Desalinised\ Water\ Required\ \times DEC \quad \textbf{(3.21)}$$

$$Amount\ of\ Desalinised\ Water\ Required = WR\ \times AHP \quad \textbf{(3.22)}$$

Table 3.5 shows the parameters that were used for the annual flow rate calculations. It includes hydrogen production and wind farm losses. All wind farm losses were added up and rounded to 27% and are abbreviated as WFL in Equations (3.17) and (3.19).

Table 3.5 Parameters included in annual hydrogen flow rate calculations.

Parameter	*Notes*	*Source*
Desalination electricity consumption (DEC)	2.5 kWh/Nm^3	Section 3.3.3.1
Water required (WR)	15.6 L/kg H_2	[176] Section 3.3.3.2
Hydrogen temperature at outlet	50°C	[178], [179]
Electrolyser electricity consumption (EEC)	50 kWh/kg of H_2	[130]

Electrolyser losses (EL)	8.7% (est 8000h annual operation)	[130]
AC-DC conversion efficiency	90% (10% included in WFL)	[128]
O&M Wind losses	6% (included in WFL)	[129]
Wake effect	7.38% (included in WFL)	[71]
Blade contamination	1% (included in WFL)	[71]
Wind hysteresis	2.38% (included in WFL)	[71]

3.3.3.4 Hourly Hydrogen Flow Rate

The maximum theoretical hourly flow rate in kg/hour, was calculated using Equation (3.23) by setting the losses to zero. For the minimum theoretical hourly flow rate, the annual losses listed in Table 3.5, apart from the electrical losses from desalination and AC to DC conversion, have not been deducted from the hourly flow rate as these are annual and would lead to skewing the hydrogen production towards lower numbers, Equation (3.24). In order to estimate the pipeline capacity, it is important to model the maximum potential hourly flow rate, to establish the pipeline size. Thus, only parameters listed in Table 3.6 were used as it allows to establish the uppermost limit of the pipeline, which will not be exceeded within the project. All annual losses have been included in economic analysis in Chapter 5 where annual flow rate was used.

$$Max\ Hourly\ H_2 Production = \frac{EC \times 1000}{EEC} \quad \textbf{(3.23)}$$

$$Min\ Hourly\ H_2 Production = \frac{Lowest\ MPP \times 1000 \times {}^{CE}/_{100} - DESAL}{EEC} \quad \textbf{(3.24)}$$

Where

EC= electrolyser capacity in MW

EEC= electrolyser electricity consumption in kWh/kg

Lowest MPP=lowest mean power production (for the whole wind farm) in MW

CE= AC-DC conversion rate in %

DESAL= desalination power requirement in kWh

Table 3.6: Summary of parameters used for hourly hydrogen flow rate calculations.

Parameter	*Notes*	*Source*
AC-DC conversion efficiency (CE)	90%	[128]
Hydrogen temperature at outlet	50°C	[178], [179]
Electrolyser electricity consumption (EEC)	50 kWh/kg of H_2	[130]
Desalination electricity consumption (DEC)	2.5 kWh/Nm3	Section 3.3.3.1
Water required (WR)	15.6 L/kg H_2	[176] Section 3.3.3.2

3.4 Results

3.4.1 Balance of Plant

Figure 3.6 shows a typical balance of plant for offshore green hydrogen production, which was used for this research. There is no information on size and weight of individual components due to confidentiality, but Chapter 5 provides cost estimates for offshore hydrogen production platforms.

First part is the FOWF described in Chapter 2, which consists of 150, 10 MW turbines, dynamic and array cables, and offshore substation for AC to DC conversion. Then it connects to a platform containing PEM electrolysers and desalination units.

A PEM electrolyser has been chosen for this study due to the better response of the PEM electrolyser to the power variation of wind energy, hydrogen output pressure above atmospheric pressure, and high purity as discussed in Section 3.2.2. This allows removing the compressor and hydrogen purifier from the balance of plant. Last part are the pipelines that can be either re-used or new built (more information on pipelines is included in Chapter 4). No storage, or accommodation has been considered in this work. Unmanned hydrogen production is standard for hydrogen projects such as Big Hit project [47] and is also considered for offshore hydrogen production platform based on DNV GL study on offshore hydrogen production [180]. The difference between cable and pipeline scenarios is the lack of export cable and onshore substation in pipeline scenario, and the lack of PEM electrolysers, desalination units and hydrogen production platform in cable scenario (See Figure 3.6 and **Error! Reference source not found.**).

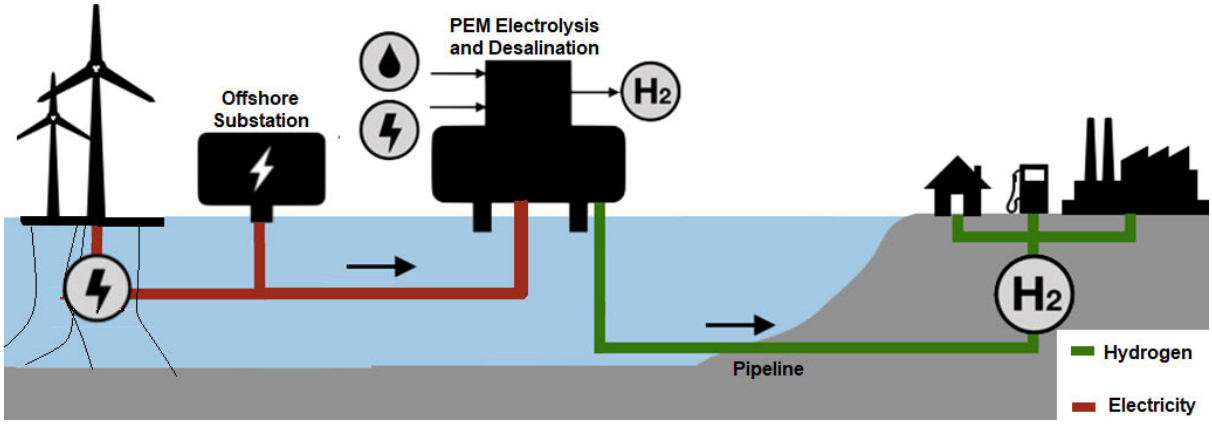

Figure 3.6: Offshore hydrogen production diagram, pipeline scenario (adapted with permission from Wood plc).

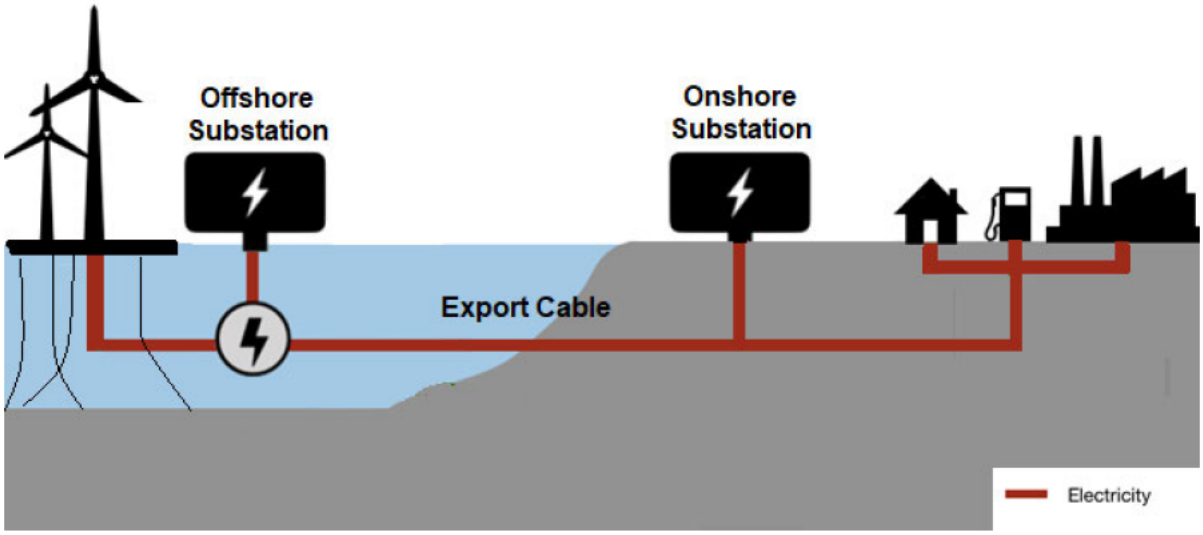

Figure 3.7: Cable scenario diagram (adapted with permission from Wood plc).

3.4.2 Sizing the Electrolyser

Table 3.7 shows the summary of utilisation rates for the electrolyser and wind farm at different sizes of electrolysers without losses. Full utilisation rates for the windfarm with 957.5 MW electrolyser size and electrolyser utilisation with 1500MW electrolyser size are presented in Figures B2 and B3 in the Appendix B.

Table 3.7 : Percentage utilisation of windfarm and electrolyser based on the size of electrolyser without losses.

Electrolyser size (MW)	*957.5*	*1000*	*1100*	*1250*	*1300*	*1400*	*1500*
Gross windfarm % utilisation average	78	82	87	93	95	98	100
Gross electrolyser % utilisation average	100	100	97	93	91	88	84

3.4.3 Hydrogen Flow Rates

Table 3.8 summarizes the hydrogen flow rates for different electrolyser sizes calculated as outlined in Section 3.3.3. The maximum hourly hydrogen flow rate used in Chapter 4 based on 1500MW electrolyser (with the utilization of the electrolyser just under 84%) and without any balance of plant (BoP) losses, was calculated to be 30,000 kg of H_2/hour (as per Equation (3.23) in Section 3.3.3.4). The minimum hourly flow rate used in Chapter 4 based on 957.5 MW electrolyser (with the utilization of the windfarm around 78%) and with losses from Table 3.6, was calculated to be 17,227 kg of H_2/hour (as per Equation (3.24) in Section 3.3.3.4). The minimum hourly flow rate is slightly higher for 1500MW electrolyser as it is limited by the least windy hour, rather than by the size of the electrolyser as for 957.5MW electrolyser case.

Table 3.8 Hydrogen flow rates based on electrolyser size

Electrolyser size (MW)	*957.5*	*1500*
Windfarm utilization average per year (%)	78.4	100
Electrolyser utilization average per year (gross) (%)	100	83.8
Electrolyser utilization average per year (net) (%)	85.9	56.8
Desalinised water required (m^3/h)	299-269	468-269
Hydrogen maximum and minimum flow rate (kg/h)	19,150-17,227	30,000-17,230

3.4.4 Electrical Challenges

This Section is based on interviews carried out with academics and industry specialists in electrical engineering [181]–[183]. Specifically with Dr Paul Judge from The University of Edinburgh, Damian McCool (former Wood Power Technical Manager) and Professor Olimpo Anaya- Lara from Strathclyde University. Major electrical challenges with the current set up of hydrogen production described within this thesis is the missing grid connection, large capacity of the windfarm, AC/DC conversions and cost. When looking at the wind farms far from shore, with no near stable cable landings, there will be several electrical challenges that will have to be overcome. As electrical challenges are outside of the scope of this thesis, following section summarises information from short literature review and the interviews with the industrial and academic specialists in order to highlight the need for further research into electrical aspects to enable offshore hydrogen production.

3.4.4.1 Black start capability

In the case of no wind, wind turbine requires power to start-up again from a complete shutdown, which is often referred to as black start. Göksu *et al.* [184] in their proceedings describe the requirements for non-grid connected wind turbine.

Firstly, the internal power supply should be large enough to start-up WTG controller, converters, wind speed and direction measurements as well as yaw and pitch mechanisms without any external supplies.

Secondly, WTG has to be able to continue producing power under fluctuating load and wind and lastly, all WTGs have to be synchronised within the wind farm. This power required for a start-up usually comes from the grid, but far-offshore wind farms without grid connection will require ability to self-start. Göksu *et al.* [184] list existing solutions in their proceedings. Some solutions include a small diesel generator, which could be co-located at the wind turbine. This however defeats the purpose of wind turbines being green way of energy transition from fossil fuels. Thus, the author would like to highlight solutions including batteries [185] and potentially hydrogen fuel cells, which have not yet been explored, but could be a way to start up a wind turbine. The timeliness and importance of black start capability is further confirmed by the existence of Offshore Wind Accelerator by Carbon Trust that funds R&D into electrical systems including black start capability [186].

3.4.4.2 AC to DC

Most of the current wind turbines use doubly-fed induction generators (DFIGs) containing AC/DC generator converter, DC link for rectification and DC/AC grid side inverter [187]. The electrolyser, on the other hand, uses DC [30]. While ERM [63] has not identified any challenges or extra costs associated with AC/DC rectification as electrolysers currently use AC electricity from UK transmission system, it is specific for their Dolphyn project design where an electrolyser is part of the wind turbine and the current requiring rectification is small. The challenge grows with large scale power production, where a large AC/DC conversion station will be required to supply large scale electrolysis, which is costly. It is possible for a wind turbine to generate DC, but this is very rare and would require extra protection in the form of expensive DC circuit breakers, and agreement with the manufacturers who might not want to be liable for the risk to the rest of the electric network within the windfarm and electrolysis plant. Thus AC/DC conversion for large scale electrolysis is another challenge that needs further research to enable large scale offshore hydrogen production.

3.4.4.3 Stability

Without the grid connection, there will be a challenge to keep the whole system stable. As the wind farm has variable power supply, it is important to match the demand. If the supply is greater than the load, frequency will increase potentially damaging the wind turbine as well as the electrolysis plant. If the supply is lower than the load, it should be less of an issue as the PEM electrolysers are flexible enough to handle changes in power supply. However, keeping the network balanced is still of an importance. Thus, proper sizing of the electrolyser to the wind farm and enabling storage will be crucial to ensure electrical stability of offshore hydrogen production.

3.4.4.4 Substations

In theory, it would be possible to have just one electrical substation as there are no electrical limits to the size. However, there is a limit on weight that can be installed in single lift by the installation vessels that might require 3-4 substations being installed instead to cover 1.5GW windfarm.

3.5 Discussion

3.5.1 Sizing the Electrolyser

As can be seen in Table 3.9 sizing the electrolyser at full capacity of the windfarm does not lead to the most hydrogen being produced. This is due to the way the model for calculating annual hydrogen production is set. First factor that effects amount of hydrogen produced outside of the size of the electrolyser is the wind turbine loss. At 1500MW, the electrolyser gross utilisation is at 84% and is also affected heavily by the windfarm losses (27%) as the windfarm utilisation is at 100%. This results in electrolyser net use to be 57% at 1500MW, which is comparable to the CF from Chapter 2 when deducting electrolyser availability of 8.7% and including uncertainty of 6.8% (Chapter 2, Section 2.3.4.2). This effect reduces as the size of the electrolyser decreases, as the utilisation of the electrolyser increases and some of the wind turbine losses use spill over electricity from the windfarm not 'taking' any electricity dedicated to the electrolyser as in case of 1500MW electrolyser. The most hydrogen is produced when the electrolyser is sized at 1300MW (87% of the windfarm capacity). This is due to electrolyser utilisation being at 91% allowing for O&M to take place during summer months when the electrolyser is not running at full capacity, while also wind farm not being 100% utilised and some of the losses being covered by spill-over electricity. Based on previous literature it is advised to size the electrolyser at 80% of the windfarm from economic perspective, which is similar to the lowest electrolyser size calculated within this work [53], [188].

Table 3.9: Annual hydrogen production based on electrolyser size.

Electrolyser size (MW)	*957.5*	*1000*	*1100*	*1250*	*1300*	*1400*	*1500*
Windfarm % utilisation average (gross)	78	82	87	93	95	98	100
Electrolyser % utilisation average (gross)	100	100	97	93	91	88	84
Electrolyser % net use	86	83	77	71	69	63	57

Annual H_2 production (Mkg)	145	146	152	160	162	161	161

3.5.2 Hydrogen Flow Rate

As shown in Table 3.8, the flow rate fluctuates based on the wind speed that fluctuates throughout the day and seasonally. The lowest flow rate within the fluctuations using the 1500MW electrolyser is expected to be 17,230 kg of H_2/hour including losses from AC to DC conversion and desalination plant power requirements. This means that the expected drop is nearly 13,000 kg of H_2 /hour in the month of July in comparison to winter months.

When sizing the electrolyser at approximately 82% of the windfarm capacity, (1000MW), we can expect smaller flow rate fluctuations with the maximum and minimum hydrogen flow rate expected to be 20,000-17,230 kg of H_2/hour.

There will be minimum fluctuations (19,150-17,227 kg of H_2 /hour) for the electrolyser sized at 957.5 MW as that is the minimum hourly energy production for the windfarm. This would result in 100% gross electrolyser utilisation and 78% gross utilisation of the windfarm.

3.6 Conclusion and Future Work

Chapter 3 looked into available literature investigating offshore hydrogen production, provided insights into balance of plant for offshore green hydrogen production and methodology to calculate the size of the electrolyser and hydrogen flow rate. These results later feed into the thermo-hydraulic pipeline investigation carried out in Chapter 4 and economic analysis in Chapter 5.

Major findings include that currently PEM electrolysis in combination with reverse osmosis desalination is the most suitable way to produce green hydrogen offshore.

For large scale non grid connected windfarms that are located far offshore, a scenario where electrolysers are located on a wind turbine could be more suitable, as this would allow for bigger electrolysis capacity, albeit individual electrolysers with their BoP would be required to fit on the turbine platforms.

Hourly hydrogen flow rate was calculated to vary between 30,000-17,230 kg/h for a 1500MW electrolyser, and 19,150-17,227 kg/h for 957.5MW electrolyser.

Future work could include techno economic analysis into different hydrogen carriers such as ammonia, synthetic natural gas, and liquid hydrocarbons. Other areas of offshore hydrogen production that would benefit from further research are direct sea water electrolysis, investigation into electrolysers suitable for offshore environment, and investigation into advantages and disadvantages of centralised electrolysis on a platform versus wind turbine co-located electrolysers.

Further research work into identified electrical challenges such as black start, AC to DC conversion and system stability and research into offshore hydrogen storage to help to offset the difference between summer and winter hydrogen production, would also allow for faster commercialisation of offshore hydrogen production.

CHAPTER 4 - RE-USE OF GAS PIPELINES FOR TRANSPORTATION OF HYDROGEN

4.1 Overview

One of the aims of this research is to identify if it is possible to re-use oil and gas pipelines for the transportation of green hydrogen. The following chapter contains information on pipeline theory and general methodology, which are then applied to two distinct existing pipelines in the North Sea, which were introduced in Section 2.3.1 in Chapter 2. A long transmission pipeline with large diameter, FLAGS, and a much shorter feeder pipeline PL164. These were chosen as a representation of typical subsea gas pipelines that could be considered for hydrogen transportation in the future projects. The chapter first introduces pipeline integrity challenges connected with transporting hydrogen and then discusses different codes recommendations on optimal steel grade and operating pressure for hydrogen transportation pipelines. Then it discusses equations of state and flow equations chosen for hydrogen transportation simulations, software chosen for the simulations and short validation results of the software. Further on, two existing pipelines are modelled to see whether they are suitable for hydrogen transportation. The modelling is based on thermo-hydraulic analysis using hydrogen flow rates calculated in Chapter 3 (see Figure 4.1). This work also investigates the sufficiency of the electrolyser outlet pressure (20-50 bar [30]) without added compressors for hydrogen gas transfer. Thus, the simulations are carried out at low pressures and the maximum hydrogen capacity at low pressures for the two pipelines is calculated. Lastly, three new purpose-built pipelines are investigated to compare to the existing PL164 and FLAGS for the 1.5GW Magnus windfarm case study. Many equations and values across the oil and gas industry are standardised in non-SI units such as diameters, yield strength etc. Thus, there are non-SI units used across this chapter with SI units quoted in the brackets.

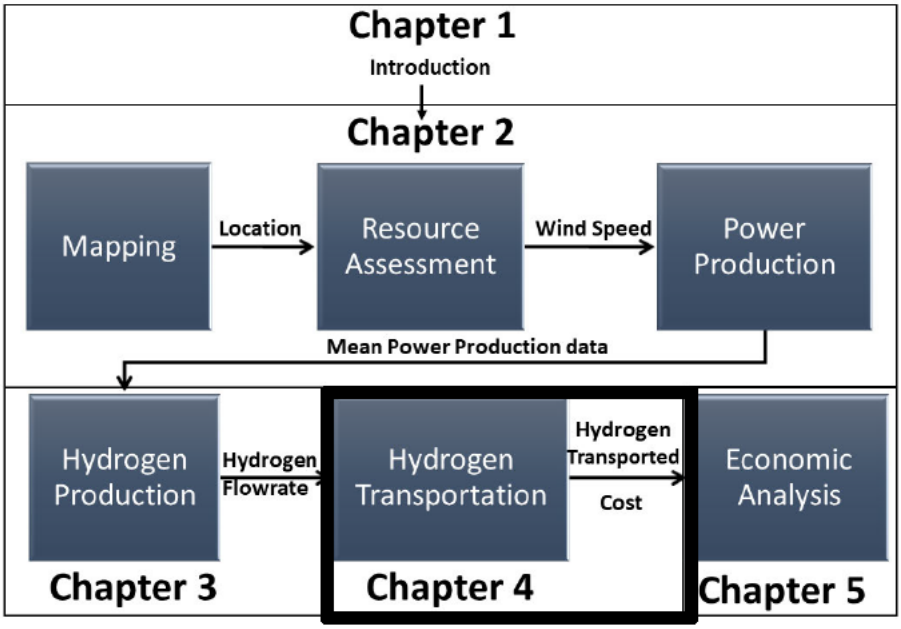

Figure 4.1: Thesis flow diagram.

4.2 Literature Review

4.2.1 Pipeline Integrity in the Presence of Hydrogen

The major issue with transporting hydrogen via existing oil and gas infrastructure is that hydrogen is highly volatile and tends to interact with the metals used to construct these pipelines [189]. There are several ways for hydrogen to migrate into the steel structure such as absorption of molecular hydrogen, introduction of hydrogen during fabrication process, and electrochemical reactions (such as corrosion) of hydrogen producing molecules (e.g. water or hydrogen sulphide) [190]. There are several pipeline failure modes stemming from the presence of hydrogen that are described in the following section.

4.2.1.1 Hydrogen Embrittlement

Hydrogen embrittlement is a reversible process occurring below 200°C (typically ambient temperature [191]) in which hydrogen reacts with steel causing deterioration in mechanical properties such as reduction in strength, toughness, ductility and load-carrying ability of the pipeline [189], [192]. There are still many unknowns regarding the process of hydrogen embrittlement [189], [193], but it is likely caused by adsorption of atomic hydrogen to the steel's surface, rather than chemical reaction of molecular hydrogen [191], [194], [195].

4.2.1.2 Hydrogen Attack

Hydrogen attack is an irreversible chemical reaction which occurs at combined high temperatures (above 200°C) and pressures in steel or copper pipelines [191], [195]. During hydrogen attack, hydrogen diffuses into steel, where it reacts with carbon to form methane. The process in which steel is depleted of carbon is called decarburisation, and it causes reduction of strength and ductility. Formed methane can also exert internal pressure that can cause internal cracks or fissures [189], [195]. Hydrogen attack failure is characterised at grain boundaries by fissures, bubbles, or decarburisation. The severity depends on pressure, temperature, stress, exposure time and pipeline composition.

Reducing pressure, temperature, stress, exposure time and adding molybdenum and chromium into the metal composition can reduce steel pipeline susceptibility to hydrogen attack [195].

It is unlikely to observe signs of hydrogen attack on pipelines transporting hydrogen offshore due to the elevated temperatures needed for hydrogen attack to occur.

4.2.1.3 Hydrogen Induced Cracking and Blistering

Hydrogen induced cracking is a sudden and brittle steel failure mode [189] occurring in a hydrogen environment during the application of stress below the pipeline steel's yield strength (maximum stress that can be applied to a material before it starts to irreversibly deform) [196]. The process involves the absorption of hydrogen into the steel structure and its diffusion into stressed regions of the crystal structure causing hydrogen induced cracking [196].

Hydrogen induced blistering normally occurs in environments containing hydrogen sulphide [196]. In this process a blister is formed by diffused hydrogen at the inclusion interfaces. This blister then cracks due to applied stresses and individual hydrogen atoms forming molecular hydrogen increasing the pressure within the structure [196].

Electrolytic charging experiments show that the ferrite-pearlite phases (steel phases), which can be found in pipeline steels like X52, X60 and X65, are highly susceptible to hydrogen induced cracking and blistering [190], [197].

4.2.1.4 Corrosion

The presence of water and oxygen from the electrolysis can cause pipeline corrosion as shown in simplified corrosion Equation 4.1. Thus, in order to avoid corrosion, EIGA code on hydrogen transportation pipelines advises water contamination in hydrogen to be less than 20 ppm [198]. Therefore, a hydrogen dryer and a deoxidiser should be included in the post electrolysis treatment.

$$4Fe + 3O_2 + 6H_2O \rightarrow 4Fe(OH)_3 \qquad \textbf{(4.1)}$$

Due to these failure modes listed in this section, the operating conditions discussed in in the next section are crucial for re-use of existing gas pipelines for transporting hydrogen.

4.2.2 Pipeline Operating and Design Criteria for Transporting Hydrogen

Mohitpour *et al.* [189] describe the design criteria for hydrogen gas service based on results from previously conducted lab testing and known information on operating hydrogen pipelines.

Oil and gas pipelines in the North Sea are mostly made of carbon steel due to its good properties, cost and fabrication [199]. One of the issues raised by OGTC [199] is the lack of publicly available information on the pipelines in the North Sea such as grade or wall thickness. According to discussions with different operators in the North Sea and pipeline engineers, the majority of the pipelines in the North Sea are of grade X65 [200]. That means that the material yield stress is 65 ksi (4480 bar). Figure 4.2 shows the maximum steel grade allowed for hydrogen transportation through steel pipelines to minimise hydrogen embrittlement based on laboratory tests, literature [199], and standards (European Industrial Gases Association [198]). The laboratory tests include fatigue crack growth rate tests [201], [202] and burst tests (testing at elevated pressures) [203].

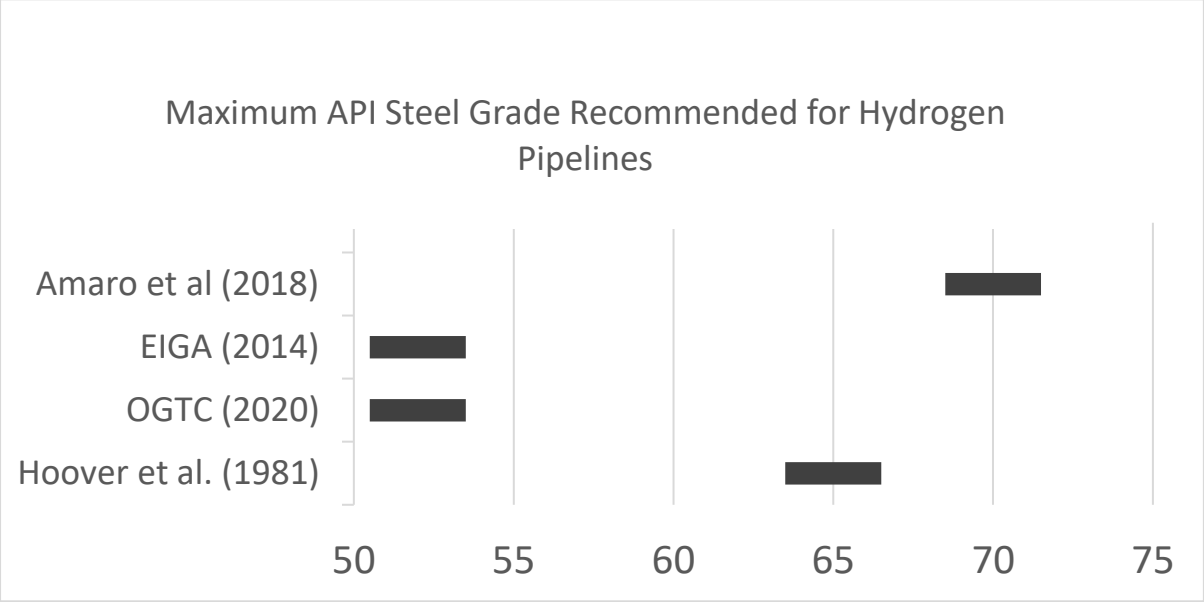

Figure 4.2: Maximum API steel grade recommended for hydrogen pipelines.

To certify pipeline steel for hydrogen, the American Society of Mechanical Engineers (ASME) standard B31.12-2019 provides two options for testing. Option A requires Charpy testing in air, which measures the amount of energy absorbed during fracture. It is readily available in many laboratories but requires addition of safety factors due to lack of testing in hydrogen. Option B requires testing in hydrogen determining fracture toughness, fatigue crack growth rate and stress intensity factor threshold, which is only available in a handful of laboratories [204].

Sandia National Laboratories, are able to provide hydrogen testing in situ, and have published a number of papers providing testing methodology and results for fracture toughness and crack growth propagation for different steel grades such as X80 [205], X70 [204] and X65 [206].

Mohitpour *et al.* [189] suggest that the majority of the existing hydrogen transmission lines are of steel grade API 5L X42 (API stands for American Petroleum Institute) or lower and operate between 30 and 60 bar with few failures reported. Similar conclusions were reached by OGTC with Xodus group according to ASME recommendations. The OGTC [199] concludes that the best pipelines for hydrogen re-use are the ones that were used for the transportation of natural gas, rather than oil (due to oil contamination in crude oil pipelines) and built between 1980-2000. This work also considers gas pipelines only. Pipelines built between 1980 and 2000 are more likely to be built from suitable material grades such as X52 that has been identified as most suitable for hydrogen storage and transportation by OGTC [199]. They suggest that the maximum operating pressure should lead to maximum stress in the walls to be between 30-50% of the specified minimum yield strength (SMYS) [199].

According to ASME B31.12-2019 [207], the maximum operational pressure (MOP) for hydrogen pipes of steel grade API 5L X60 and below, should be less than 207 bar. For all grades above X65, the MOP should be below 103 bar.

According to a French national project that carried out mechanical testing of an X80 pipeline in a hydrogen environment, [208], decreasing the operating pressure from 100 bar to 30 bar decreases the susceptibility of higher grade steel (X80) to hydrogen embrittlement.

Both EIGA 121/14 and ASME B31.12 standard recommend operating at a low utilisation, 30 and 40% of SMYS respectively, in case of lack of information on the actual state of pipelines intended for re-use [198], [207].

However, new laboratory tests conducted by National Institute of Standards and Technology (NIST) and Sandia National Laboratories that were used by ASME committee to review the B31.12 code has shown that it may be possible to use pipelines with steel grade up to X70 for hydrogen without a design penalty [202]. A revision has been proposed, so that the new ASME B31.12 code - allows the use of material with SMYS up to 70 ksi (4800bar) at design pressures up to 207bar [202].

Thus, based on the information summarised in this section, it is possible to re-use oil and gas pipelines for hydrogen considering material as a single factor even if they are of higher grade than X52, as long as the operating pressure is reduced. However, it should be noted that pipelines operating under reduced pressure are able to carry only a fraction of the hydrogen that they could at higher pressures, which reduces the design energy supply of the pipelines when transporting hydrogen rather than natural gas.

4.2.3 Pipeline Hydraulic Theory

To enable flow in the pipeline, a pressure difference is required, which is normally provided by pumps or compressors for export pipelines. Considering a single phase flow in a non-horizontal pipeline, there is a force exerted by the pressure difference over the cross section across the segment (first part of Equation (4.2), where D is diameter and p is pressure), a shear stress exerted by the wall on the fluid over the outer area of the cylinder (second part of Equation (4.2), where τ is wall stress and L is length of the pipeline), and the gravity force (third part of the Equation (4.2), where ρ is the gas density, g is gravitational acceleration and z is height), making it equal to zero as the fluid is moving at a uniform velocity. Rearranging Equation (4.2) gives the formula for pressure gradient, Equation (4.3), which is applied incrementally along the entire length of the pipeline to account for heat transfer, changes in height profile and variation in physical properties of the fluid due to changes in temperature and pressure. As shown in Equation (4.3) the pressure gradient can also be expressed using mean velocity by substituting Equation (4.4) into Equation (4.3), where f is skin friction coefficient and U is the mean fluid velocity.

$$0 = \left(\frac{\pi D^2}{4}\right) dp + \tau(\pi D dL) + \rho g \left(\frac{\pi D^2}{4}\right) dL \frac{dz}{dL} \quad \textbf{(4.2)}$$

$$\frac{dp}{dL} = -\frac{4\tau}{D} - \rho g \frac{dz}{dL} = -\frac{2\rho f U^2}{D} - \rho g \frac{dz}{dL} \quad \textbf{(4.3)}$$

$$\tau = \frac{1}{2} f \rho U^2 \quad \textbf{(4.4)}$$

4.2.3.1 Flow Equations

A variety of empirical flow equations exist to simplify Equation (4.3) and are used in programmes such as PIPESIM, UniSim or OLGA to calculate the flow rate with known inlet and outlet pressure or to calculate pressure drop when flow rate is known. These equations include, Weymouth, Panhandle A, Panhandle B, which are most widely used [209] and others such as Darcy-Weisbach [210], AGA and Colebrook-White [211].

Weymouth [212] is the oldest flow equation and is most accurate for short pipelines with small diameters (less than 12 inch (305 mm)) as it tends to overestimate the pressure drop for larger pipes [210]. Even so, this flow equation is normally used in gas pipeline design as an additional safety factor, as it provides more conservative numbers [209], [211].

The Panhandle A equation is mostly used for pipelines with medium to large diameters (12-60 inch (305-1524mm)) with moderate gas flow rates and medium to high pressures (55-103bar), while Panhandle B is used for pipelines with large diameters (36 inch (914 mm) plus), high flow rates and high pressure (69 bar plus) [209], [211].

The Darcy-Weisbach equation is an incompressible flow equation that can be used for any flow rate, diameter and pipeline length but does not account for gas compressibility [210].

The AGA flow equation has two versions, partially turbulent, which is used for medium diameter, medium flow and high pressure pipelines and fully turbulent, which is used for high pressure, high flow rate pipelines with medium to large diameter [211].

The Colebrook-White flow equation is used for similar systems as the AGA fully turbulent flow equation, but predicts higher pressure drops [211].

4.2.3.2 Equations of State

For hydraulics and general design calculations an equation of state (EoS) is necessary in order to predict compressibility, specific volume, density, thermal conductivity, viscosity, enthalpy, entropy, Joule-Thompson coefficient and sound velocity at various temperatures and pressures [189].

The parameters in flow equations depend on an EoS that is derived from the ideal gas law to describe phase behaviour. There are several EoSs that can be used to calculate hydrogen properties. While Mohitpour *et al.* [211] suggest the modified Benedict-Webb-Rubin, Włodek *et al.* [213] found Peng-Robinson sufficient in their work. Nasrifar [214] compares eleven EoS with experimental and tabular data from Vargaftik *et al.* [215] in their accuracy of predicting hydrogen properties. They reach the conclusion that all EoSs have comparable accuracy when predicting hydrogen properties at temperatures above 200K, which is the case for all pipelines operating offshore.

Thus, a good combination for pipeline analysis, based on this review of literature is the Peng-Robinson [216] EoS, Equation (4.5) as the most used EoS in industry [213], [214] and the Weymouth flow equation, Equations (4.6) and (4.7) as it tends to overestimate the pressure drop and is often used in distribution networks for additional safety [209], [211].

$$p = \frac{nRT}{V - b} + \frac{a}{(V + m_1 \times b) \times (V + m_2 \times b)} \quad \textbf{(4.5)}$$

$p = gas\ pressure$

$V_P = total\ volume\ of\ the\ pipeline\ containing\ the\ gas$

$a = measure\ of\ the\ attraction\ between\ particles$

$b = volume\ occupied\ by\ a\ particle\ excluded\ from\ V_P$

$n = number\ of\ moles$

$T = temperature$

$R = gas\ constant$

$m_1, m_2 = 1 + \sqrt{2}, 1 - \sqrt{2}$

$$Q_b = 432.7 \times \frac{T_b}{P_b} \sqrt{\left[\frac{P_1^2 - P_2^2 - E}{G \times L \times T_{ave} \times Z_{ave}}\right]} \times D^{2.667} \quad \textbf{(4.6)}$$

$$E = 0.0375G \times \Delta H \times \frac{P_{ave}^2}{T_{ave} \times Z_{ave}} \quad \textbf{(4.7)}$$

$Q_b = gas\ flow\ rate\ at\ base\ conditions, SCF/$

$T_b = temperature\ at\ base\ condition, 520\ °R$

$P_b = pressure\ at\ base\ condition, 14.7\ psia$

$P_1 = gas\ inlet\ pressure, psia$

$P_2 = gas\ outlet\ pressure, psia$

$G = gas\ gravity, dimensionless$

$E = potential\ energy\ term$

$\Delta H = elevation\ change, ft$

$P_{ave} = average\ pressure, psia$

$T_{ave} = average\ temperature, °R$

$Z_{ave} = average\ compressability\ factor, dimensionless$

$L = pipeline\ length, miles$

$D = pipeline\ inside\ diameter, inch$

4.2.3.3 Gas Velocity

When gas passes through a pipeline at high velocity, it can erode the pipeline and significantly reduce the life of the pipeline. The threshold velocity above which the fluid might cause damage to the pipeline is called the erosional velocity and is expressed by Equation (4.8) [211].

The hydrogen gas velocity should not exceed erosional velocity at peak conditions as it increases turbulence, pressure drop and internal erosion. Equation (4.8) can be changed into Equation (4.9) using recommended value of C=100 for gas transmission pipelines [217] and substituting the equation for gas density.

It is assumed that C=100 is also applicable to hydrogen transmission pipelines as no specific constant for hydrogen was found. For natural gas, the recommended velocity is 40-50% of erosional velocity (10-13 m/s) [211].

$$u_e = \frac{C}{\sqrt{\rho}} \tag{4.8}$$

$$u_e = \frac{100}{\sqrt{\frac{MP}{ZRT}}} \tag{4.9}$$

C=constant defined as 75<C<150

G= gas gravity

P=minimum pipeline pressure

R= universal gas constant

T= flowing gas temperature

u_e= erosional velocity

Z= compressibility factor at specified temperature and pressure

The erosional velocity changes along the pipeline with the change in elevation and depth effecting the temperature and pressure. As the flowing gas density decreases along the pipeline, the erosional velocity increases as shown in Equation (4.8). Diez *et al.* [218] recommend 15 m/s pure hydrogen gas flow rate, which is similar to industry recommendations for used pipelines and has been used for simulations within this work to determine the maximum pipeline capacity in Section 4.4.2.3.

4.2.4 PIPESIM

PIPESIM is a steady-state multiphase flow simulator used for well, pipeline and network design and optimization [219]. It was designed specifically for harsh environments such as the North Sea with first release in 1984 [219]. It enables modelling of multiphase flow, heat transfer and fluid behaviour [219]. Section 4.3.2.1 describes the PIPESIM process of calculating the pressure drop in more detail.

Although PIPESIM was originally designed for the purposes of oil and gas industry, same pipeline theory principles are applicable for all pipelines.

PIPESIM allows changing fluids from traditional oil and gas to other fluids such as hydrogen and carbon dioxide and was used for carbon dioxide flow simulations in pipelines in the past [220]. For the purpose of this research, using steady-state fluid simulations is adequate as they allow for pipeline sizing, calculating capacity and pressure drop.

During the time when pipeline modelling was carried out, a quick desk-based search indicated there was no specific software dedicated to hydrogen pipeline design. To the author's knowledge, the only commercially available software validated for hydrogen pipeline design and operation is Virtuoso [221]. Other examples of specific hydrogen software found are Simerics MP [222], FLOWNEX [223] for fuel cell stack simulations, and H2FillS [224] for hydrogen filling simulations.

Other examples of flow simulators are UniSim, OLGA, Synergi Pipeline Simulator, Virtuoso, HYSYS, etc. PIPESIM has been chosen for its extensive use in the industry, availability to research engineer, simple use with all relevant functionalities, and straightforward user interface.

4.3 Methodology

4.3.1 Pipeline Parameters

Table 4.1 shows parameters of the two North Sea pipelines used for simulation of hydrogen transportation in the case study area (see Section 2.3.1 in Chapter 2). The first pipeline, PL164, connecting the Magnus platform with Brent A since the year 2000 is an exposed, untrenched shorter pipeline with smaller diameter operated by EnQuest. The second pipeline, FLAGS, connecting Brent A platform with St Fergus gas terminal is a longer, larger diameter transmission pipeline operating since 1978 by Shell. Both are active gas pipelines. [225]

Table 4.1: Pipeline parameters

Parameter	*Units*	*PL164*	*FLAGS*	*Comments/Information Source*
OD	inch (mm)	20 (508)	36 (914)	[226]
ID	inch (mm)	18.74 (476)	34.74 (882)	Based on preferred wall thickness estimation using BS EN 10208-2:2009
WT	mm	16	16	BS EN 10208-2:2009
K	inch (mm)	0.0018 (0.046)	0.0018 (0.046)	As no further information on either of the pipelines is provided, a conservative value of 0.0018 inch effective roughness for aged pipeline is selected for the simulations [227].
L	km	79.2	452.13	[226]
P	bar	20, 50, 100		PEM electrolyser output pressure (20-50bar) [30] and ASME B31.12-2019 103bar P limit for steel grades X65 and above
T	°C	50		Hydrogen temperature at PEM electrolyser outlet [178], [179]

Mass flow rate	Kg/h	17,227-30,000	Based on the highest (winter) and lowest (summer) power production Chapter 3
Gas		hydrogen	Pure hydrogen assumed

4.3.2 Hydraulic and Thermal Analysis

4.3.2.1 Pressure Drop

The pressure drop, which is the difference in pressure between two points in a pipeline, was used to analyse suitability of existing pipelines PL164 and FLAGS for hydrogen transportation. As can be seen in Equation (4.10), pressure drop decreases with increasing diameter (D) of the pipeline and increases with increasing length ($L2$-$L1$) of the pipeline, skin friction coefficient (f), gas velocity (U) and gas density (ρ). The optimal pressure drop for natural gas pipelines is between 15-25 kPa/km (0.15-0.25 bar/km) [211]. However, this rule of thumb is hard to apply at low pressures and long pipelines such as the ones used here.

$$P2 - P1 = \frac{2\rho f U^2 (L2 - L1)}{D} \quad \textbf{(4.10)}$$

A similar algorithm as the one described by Włodek *et al.* [213] and Wetenhall *et al.* [220] shown in Figure 4.3 was used to calculate the pressure drop within the two hydrogen pipelines. First, inputs such as diameter, pressure, temperature, gas composition and summer and winter flow rates, (listed in Table 4.1) were entered into steady-state, multiphase flow simulator software, PIPESIM 2018.1 [228] based on the publicly available information on pipelines operating in the North Sea and operating parameters of existing hydrogen pipelines and electrolysers. As described by Wetenhall *et al.* [220], to calculate the steady state flow in pipelines, equations for conservation of mass, energy and momentum have to be solved simultaneously.

By adding fluid composition, inlet pressure and flow rate, it is possible to calculate pressure and temperature drop within the pipeline as shown in Figure 4.3 [220].

PIPESIM divides the pipeline into segments and solves the pressure and temperature drop for one segment at a time. Once converged PIPESIM moves on to an adjacent segment in the direction of flow [220].

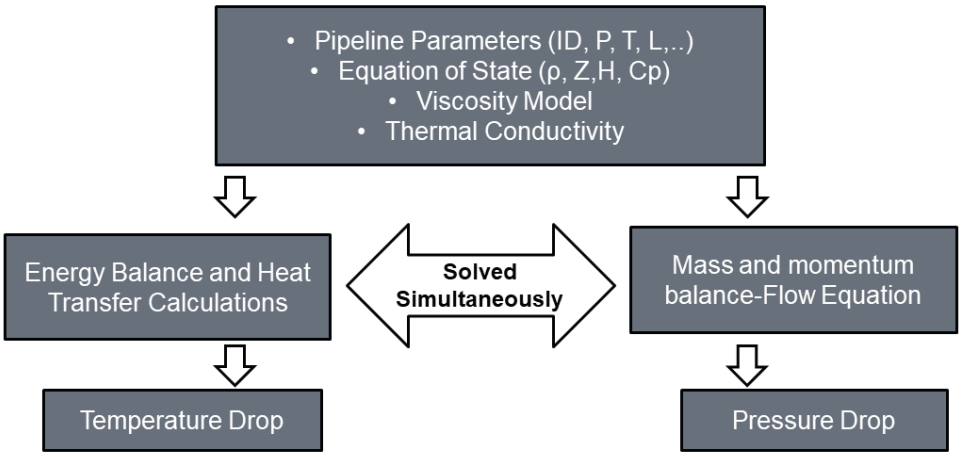

Figure 4.3: Hydraulic calculations flow diagram [220].

4.3.2.2 Maximum Capacity

The erosional velocity changes along the pipeline with the change in elevation and depth effecting the temperature and pressure. As the flowing gas density decreases along the pipeline, the erosional velocity increases (See Equation (4.8) in Section 4.2.3.3). Whilst for new pipeline design, it is possible to set the maximum velocity based on 40-50% of erosional velocity [211], used oil and gas pipelines require lower gas velocities for optimal operation and longer lifetime of the pipeline. By limiting the gas velocity to 15 m/s [218], to avoid erosion by any impurities such as sand or rust, which are likely to be present in re-used pipelines, maximum mass flow rates have been calculated for the PL164 and FLAGS pipelines at 20, 50 and 100 bar (See Section 4.4.2.3).

4.3.2.3 New Pipeline Design

Three new theoretical pipelines have been designed from Magnus to St Fergus, Flotta and Sullom Voe to compare the techno-economic case for new built pipelines with re-using existing pipelines, which is further described in Chapter 5. These have been designed using PIPESIM, summer and winter flow rates from the 1.5GW windfarm, and by balancing between pressure drop and time it takes the gas to reach the terminal

4.3.2.4 Hydrogen Properties

This research looked into hydrogen transportation by pipeline at operating pressures of 20, 50 and 100 bar and temperatures above 0°C (see yellow lines in Figure 4.4). This pressure range was chosen in order to assess the feasibility of hydrogen transfer at low pressure without compressors, The PEM electrolyser output pressure is between 20 and 50 bar [30] with 100 bar being set as upper maximum as to B31.12-2019 standard setting 103 bar as the MOP for pipelines with steel grades of X65 and above. Based on the yellow lines indicating operating temperatures and pressures on the simplified hydrogen phase diagram in Figure 4.4, there are no phase changes during hydrogen transportation. The research assumes that the hydrogen is pure and thus only single-phase flow equation is considered. Hydrogen properties were calculated using the pressure, volume, temperature (PVT) package Multiflash on PIPESIM [229] using Peng-Robinson EoS.

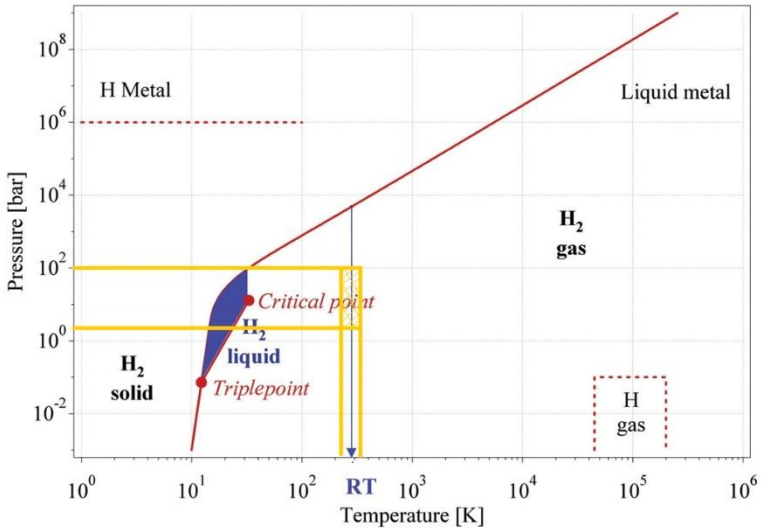

Figure 4.4: Simplified hydrogen phase diagram adjusted from [230].

4.3.2.5 Environmental Settings

The environmental data such as the water depth were included through a GIS option in PIPESIM. The metocean data of the North Sea such as water temperature and current velocity as a function of depth were sourced by PIPESIM from publicly available sources such as NORA [231], SIMORC [232] and NOAA [233]. For heat transfer, PIPESIM uses the method described by Kreith & Bohn [234] shown by Equation (4.11).

$$Q = qA_{heat\ loss}(T_f - T_a) \quad \textbf{(4.11)}$$

Where

Q= *heat transfer*

q=*overall heat transfer coefficient*

$A_{heat\ loss}$=*heat loss area based on outside diameter* (πD_o)

T_a=*ambient temperature*

T_f=*bulk fluid temperature*

4.3.3 Pipeline Model Validation and Sensitivity

Validation calculations have been carried out using PIPESIM 2018.1 software [228] to calculate pressure drop using Equation (4.3) on a 200km pipeline divided into 10 equal segments carrying hydrogen gas based on calculations by Włodek *et al.* [213]. The inlet pressure was set to 5MPa. There was no specified temperature in the paper, so 15 °C (typical temperature used for onshore pipelines) was used. As neither the wall thickness nor the roughness was specified, 12.7 mm and 0.0254 mm (PIPESIM pre-settings) were used respectively with zero elevation difference. The simple pipeline model was also used to investigate the sensitivity of pressure drop to flow equation and EoS.

4.3.3.1 Viscosity model

PIPESIM 2018.1 [228] offers four different models for determining viscosity. These are Pedersen [235], Lohrenz-Bray-Clark (LBC) [236], Pedersen Twu [237] and Super TRAPP [238]. In order to determine the best fit viscosity model for hydrogen, a quick test was performed similar to Wetenhall *et al.* [220] comparing results from four viscosity models to the viscosity of pure hydrogen from literature [239] available in Mohitpour *et al.* [189].

4.4 Results and Discussion

4.4.1 Pipeline Model Validation and Sensitivity

The following section presents and discusses results from the PIPESIM model validation using Peng-Robinson EoS and Panhandle A flow equation (Table 4.2). It also includes investigation of the pressure drop sensitivity to EoS and flow equations (Table 4.3), and the viscosity model comparison (Table 4.4).

As shown in Table 4.2, results from PIPESIM are comparable to the results of Włodek *et al.* [213], although many parameters were missing. However, it was still possible to compare the two as the majority of the parameters needed to calculate pressure drop as per Equation 4.10 were available, so the impact from missing parameters, values of which were assumed, was negligible. Simulating an existing hydrogen pipeline to validate the model and determine the best EoS and hydraulic equation from the ones previously used would have been preferable, but there were no publicly available data on operating hydrogen pipelines that would provide information such as pressure drop, inner diameter, flow rate, etc, so it was not possible to validate the model using existing hydrogen pipelines.

Table 4.2: Pressure drop comparison with Włodek *et al.* [213].

Flow m^3/h	*Internal Diameter /mm*	*Pressure drop /MPa*	
		[213]	*PIPESIM*
20,000	200	0.6	0.4
30,000	200	0.9	0.9
30,000	250	0.3	0.3

As shown in Table 4.3, there was only a small difference in pressure drop results between the 3-parameter Peng-Robinson [216] and the Soave-Redlich-Kwong (SRK) [240] EoS for Weymouth, Moody and Panhandle A simulation confirming observations reported by Nasrifar [214].

Table 4.3: A summary of pressure drop results showing differences between 2 EoS and 3 flow equations.

EoS	*Flow m^3/h*	*Internal Diameter /mm*	*Pressure drop/MPa*		
			Weymouth	*Moody*	*Panhandle A*
Peng-Robinson	20,000	200	0.46	0.43	0.39
Soave-Redlich-Kwong			0.47	0.44	0.39

Table 4.4: Viscosity model comparison.

		Viscosity (kg/m.s x 10^7)				
P/bar	*T/K*	*Pedersen*	*Pedersen Twu*	*LBC*	*Super TRAPP*	[189], [239]
50	280	77.59	77.59	87.74	88.86	79.97
50	300	81.01	81.01	91.69	92.56	82.34
20	300	80.41	80.41	91.20	92.56	81.75

As can been seen in Table 4.4, Pedersen and Pedersen Twu have comparable results and are closest to the literature values although slightly underestimating the viscosity. Both SuperTRAPP and LBC are overestimating the viscosity values, providing more conservative results. It should be noted that the SuperTRAPP model gave the same result for viscosity for 50 and 20 bar and thus it is not considered for the simulations as it is not as sensitive with change in pressure as other models.

LBC is chosen as a viscosity model within this research for its conservative values but greater sensitivity to change in pressure in comparison to SuperTRAPP. LBC is also suitable for modelling of non-polar molecule behaviour such as hydrogen [241].

4.4.2 Hydrogen Transportation Re-using Existing Gas Pipelines

4.4.2.1 Maximum hydrogen flowrate transportation (1.5 GW electrolyser)

Table 4.5 shows the results of the maximum flow rates for the PL164 and FLAGS pipelines. As can be seen in Table 4.5, the pressure drop is much smaller than the optimal pressure drop suggested by Mohitpour *et al.* [211] of 0.15-0.25 bar/km. This indicates that from the perspective of pressure drop, selected pipelines can be re-used for selected pressure and flow rate except for PL164 at 20 bar as it runs out of pressure upstream and requires higher pressure. However, low pressure drop also indicates that the pipelines are underutilised. (If the pressure drop was above the indicated range, the friction losses would be too high [211].) For the larger pipeline, FLAGS, the time it takes hydrogen to reach the gas terminal is significantly higher than for PL164 indicating sub-optimal gas velocity within the pipeline.

Table 4.5 Pressure drop for maximum hydrogen mass flow rate from a 1.5GW wind farm.

	PL164 (79.2 km, 20inch)			*FLAGS (452.13 km, 36 inch)*		
	*20 bar **	*50 bar*	*100 bar*	*20 bar*	*50 bar*	*100 bar*
H_2 mass flow rate (kg/h)	30,000	30,000	30,000	30,000	30,000	30,000
ΔP (bar)	-	5.95	2.87	2.9	1.0	0.45
ΔP (bar/km)	-	0.075	0.036	0.0065	0.002	0.00099
Time (hours)	-	1.7	3.6	14	38	75.6

*branch runs out of pressure upstream

Figure 4.5, which shows gas velocity for maximum hydrogen flow rate in FLAGS at 50 bar confirms that the gas velocity within the pipeline is sub-optimal. As can be seen in the figure, the actual gas velocity (purple line) is much smaller than the recommended gas velocity limit based on Mohitpour *et al.* [211], which can be applied to new built pipelines (the dashed red line) as well as the industry recommendation of 15m/s for re-used pipelines [218] (indicated by the dotted grey line). This suggests that while the maximum gross hourly hydrogen flow rate from 1.5 GW wind farm is sufficient for a small pipeline like PL164, it is not sufficient for a pipeline with much larger capacity such as FLAGS.

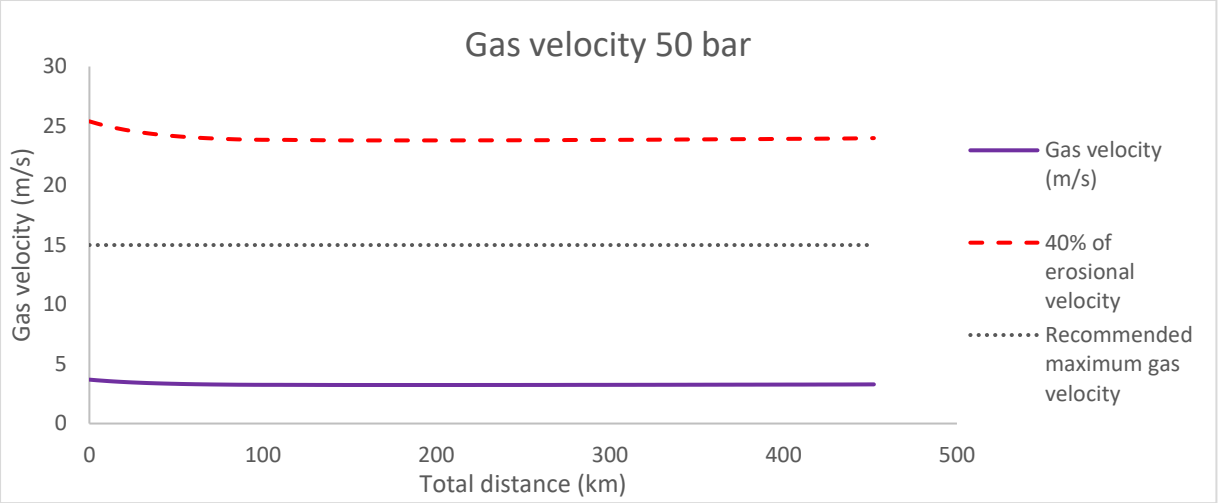

Figure 4.5 Change in gas velocity at 50 bar FLAGS.

Hydrogen Properties

The change of hydrogen gas properties at 50 bar with the distance travelled within the FLAGS pipeline is represented graphically in Figure 4.6 and Figure 4.7.

As the density increases in first the 100km (Figure 4.6), the erosional velocity slightly decreases as can be seen in Figure 4.5. As per Equation (4.9), the density initially increases due to decreasing temperature, which stabilises as the temperature stabilises (dash-dotted line in Figure 4.7).

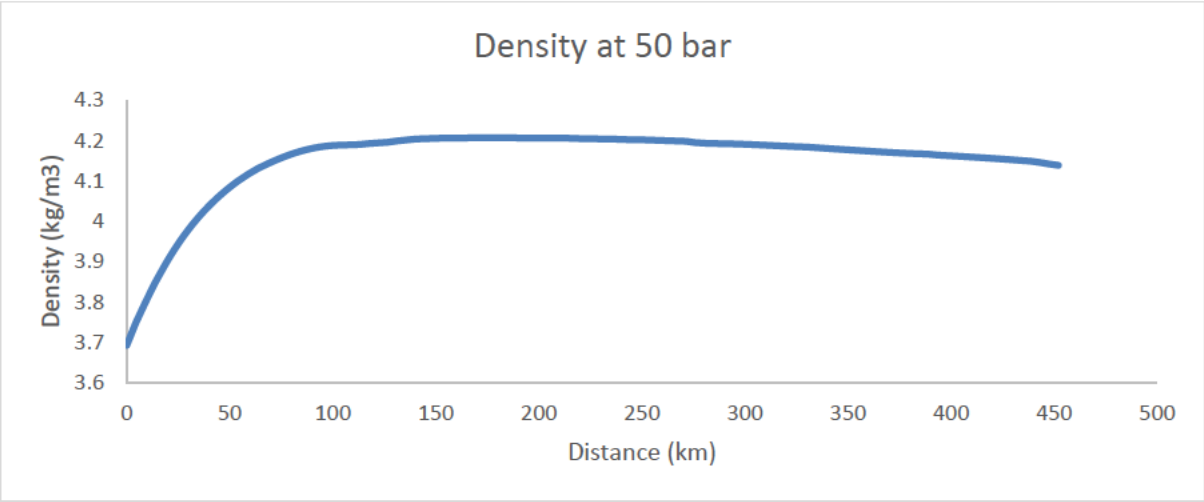

Figure 4.6 Change in density at 50 bar FLAGS

Figure 4.7 shows the decrease in temperature with increasing distance as the average temperature in the North Sea is around 11 °C [228], the hydrogen gas temperature slowly decreases with increasing depth and decreasing temperature of the North Sea. The temperature change of the North Sea with depth has been sourced from the PIPESIM database.

As per Equation (4.6), as the temperature decreases, the flow rate (yellow solid line) also decreases, which is visible in Figure 4.7.

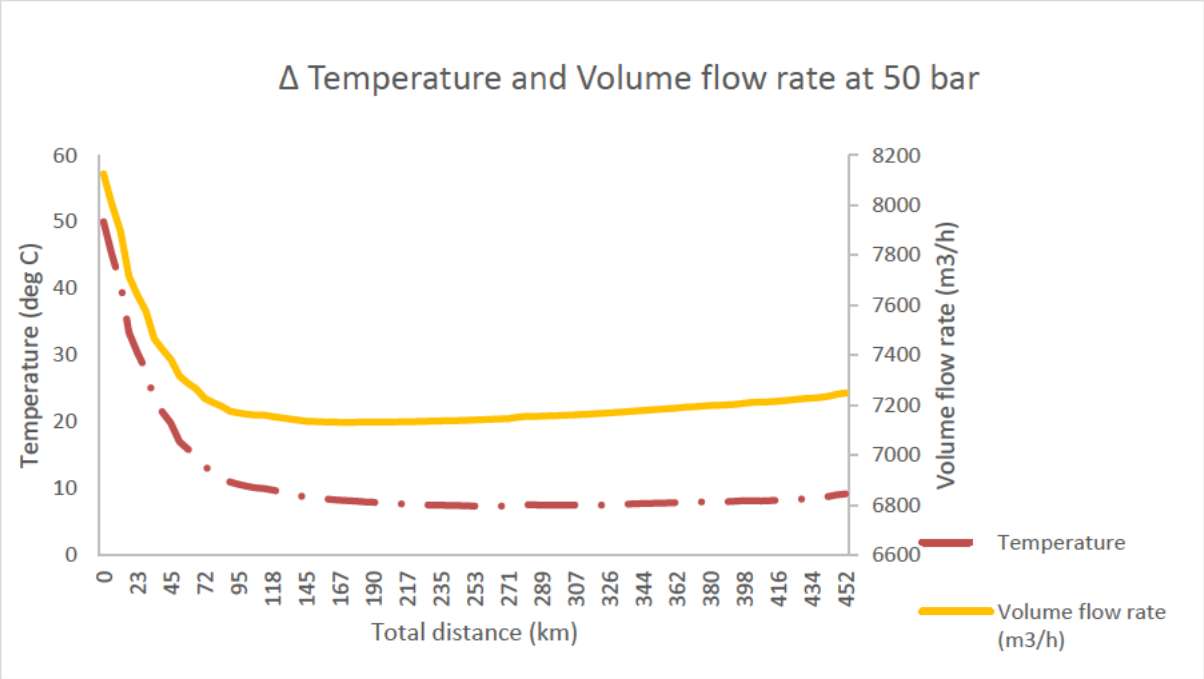

Figure 4.7 Change in T and V flow rate at 50 bar FLAGS

4.4.2.2 Minimum hydrogen flowrate transportation (957.5 MW electrolyser)

Table 4.6 shows the results of minimum flow rates for PL164 and FLAGS pipelines. As expected from the simulation results in Table 4.5, the pressure drop is even lower for lower mass flow rate. This is due to even lower gas velocities indicated by prolonged time it takes hydrogen gas to reach the gas terminal. The only exception is PL164 at 20 bar, which reaches average gas velocity above industry recommended 15 m/s and can lead to the erosion of the pipeline since the pipeline is re-used.

Table 4.6 Pressure drop for minimum hydrogen mass flow rate from 1.5GW wind farm.

	PL164 (79.2 km, 20inch)			*FLAGS (452.13 km, 36 inch)*		
	*20 bar **	*50 bar*	*100 bar*	*20 bar*	*50 bar*	*100 bar*
H_2 mass flow rate (kg/h)	17,227	17,227	17,227	17,227	17,227	17,227
ΔP (bar)	5.1	1.8	0.89	0.90	0.30	0.065
ΔP (bar/km)	0.064	0.022	0.011	0.0020	0.0007	0.00014
Time (hours)	1.2	3.2	6.4	27	67	133

*average gas velocity 19m/s with maximum gas velocity above 21 m/s

4.4.2.3 Maximum flow rates pipeline capacity

When sizing the maximum capacity, gas velocity is the limiting factor as the pressure drop is below the maximum optimal pressure drop range (0.15-0.25 bar/km) [211] as discussed in previous sections (Section 4.4.2.1 and 4.4.2.2).

Table 4.7 shows the maximum hydrogen hourly flow rate for existing gas pipelines PL164 and FLAGS. As can be seen, in most cases the pipelines are underutilised as indicated by gas velocity and pressure drop analysis in Sections 4.4.2.1 and 4.4.2.2.

The only case where this is not true is for PL164 at 20bar as the maximum flow rate the pipeline can transfer at 20 bar is 14,000 kg/hour. GW equivalents in Table 4.7 are assuming 50kWh/kg of hydrogen with no other losses included (refer back to Equation (3.23) in Section 3.3.3.4 in Chapter 3).

Table 4.7: Maximum suitable hourly hydrogen mass flow rates for PL164 and FLAGS.

	PL164			*FLAGS*		
	20 bar	*50 bar*	*100bar*	*20 bar*	*50 bar*	*100 bar*
ΔP (bar)	3.2	7.3	14	5.7	14.8	29
ΔP (bar/km)	0.04	0.093	0.18	0.01	0.03	0.06
Max mass flow rate (kgH_2/h)	14,000	33,000	64,000	40,000	100,000	194,000
Maximum velocity at any point (m/s)	15.25	14.9	15.1	14.8	15.2	15.1
Average gas velocity (m/s)	14.5	14.3	14.3	12.5	13.0	13.1
Time to the gas terminal (hours)	1.5	1.5	1.5	10	9.6	9.6
GW equivalent	0.7	1.65	3.2	2.0	5.0	9.7

4.4.2.4 Discussion

Figure 4.8 and Figure 4.9 show the pressure drop at minimum and maximum hydrogen mass flow rate at 20, 50 and 100 bar for PL164 and FLAGS respectively. There are no results for maximum flow rate at 20 bar for PL164 as the pipeline runs out of pressure halfway as the maximum optimum mass flow rate for the pipeline is 14,000 kg H_2/hour. It was possible to theoretically transport hydrogen gas at 17,227 kg/h with the maximum gas velocity above 21 m/s, which is too high, leading to higher pressure drop and pipeline erosion in practice.

As can be seen from the results summarised in Table 4.5 - Table 4.7, 20 bar would not be sufficient pressure to transport the hydrogen produced from the 1.5GW windfarm through a shorter feeder pipelines such as PL164. As shown in Table 4.7 the maximum capacity at 20 bar for the example feeder pipeline PL164 is 14,000 kg/h. With the electrolyser matching the least windy day, in the summer, mass flow rate equates to around 19,230 kg/h which is still more than the maximum mass flow rate PL164 can transport at optimum pressure drop and gas velocity.

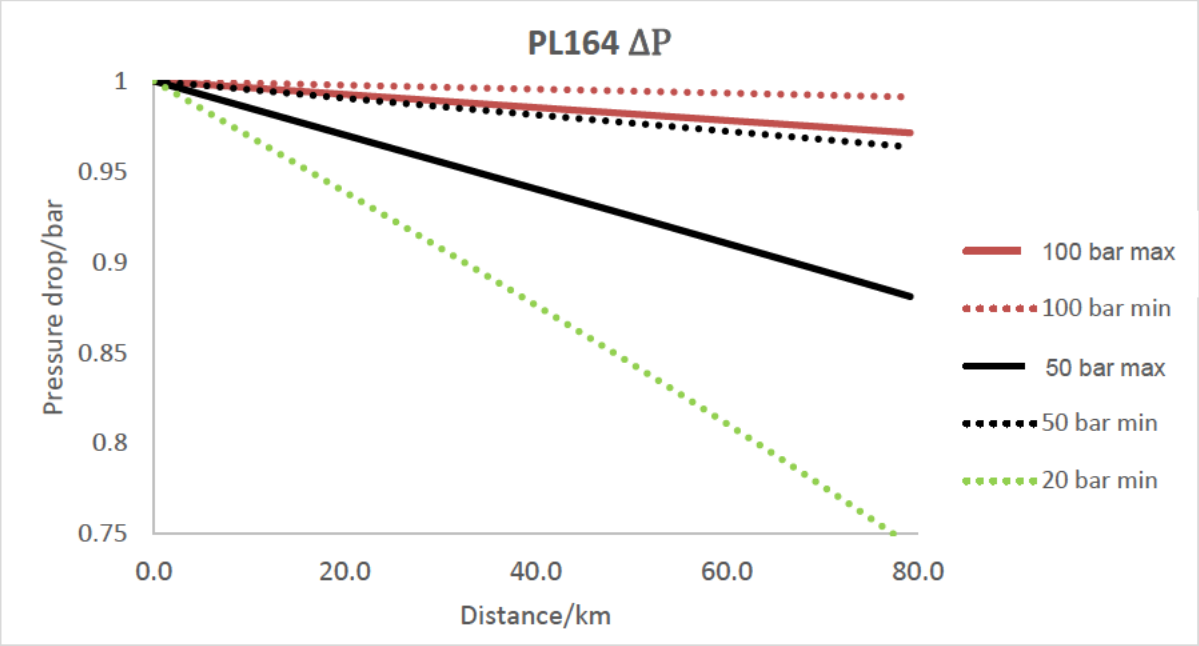

Figure 4.8: Pressure drop for PL164 at different pressures and flow rates.

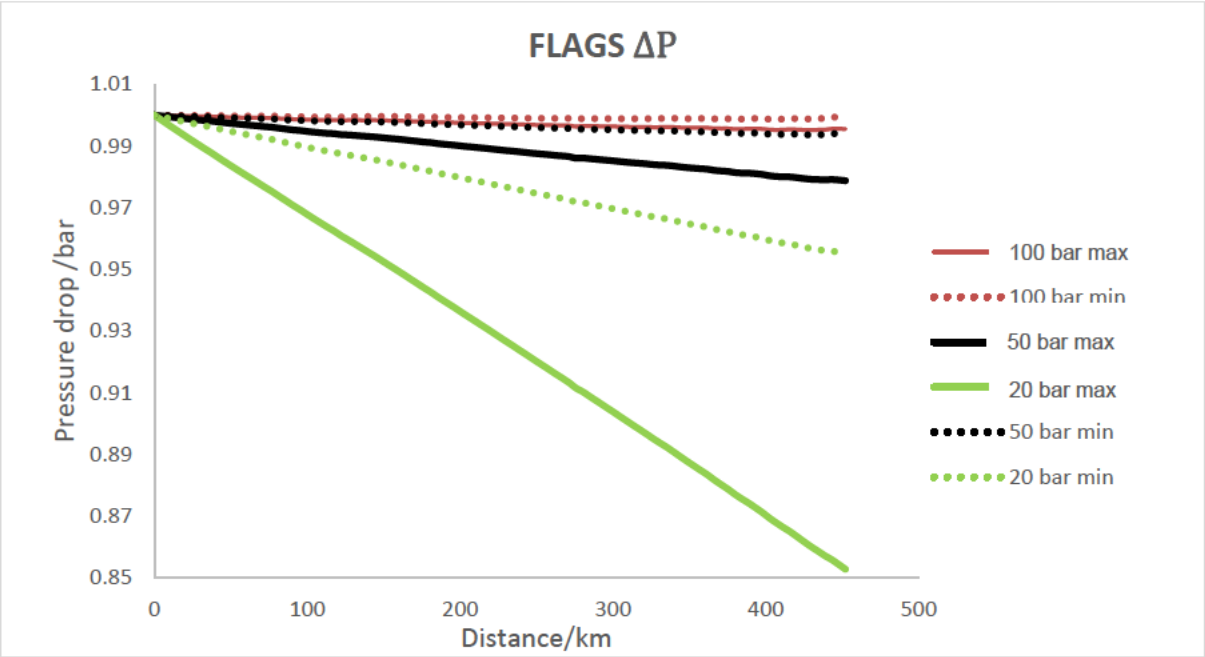

Figure 4.9: Pressure drop for FLAGS at different pressures and flow rates.

When avoiding the compressor in balance of plant to save space on the platform, the maximum assumed pressure for the PEM electrolyser is 50 bar [30]. This pressure allows the transportation of hydrogen from 1.5GW wind farm for both feeder and transmission pipelines such as PL164 and FLAGS.

For PL164, 50 bar is more suitable for the range of mass flow rates expected from a 1.5 GW windfarm. The problem comes with the longer transmission pipeline, FLAGS, where transportation of hydrogen at 50bar takes anywhere between 38-67 hours, which increases even further at 100bar (75.6-133 hours) due to the line being underutilised requiring more hydrogen flow rate.

This could be solved by including storage (for example in aquifers or porous rocks) to be able to transport higher flow rates in periods with lower wind in the summer.

While 100 bar significantly increases the maximum mass flow rate transferred through the pipelines, as shown in Table 4.7, which is important as hydrogen has lower heat capacity per volume in comparison to natural gas, it also significantly increases the transportation time, and would not be an optimal solution for a 1.5GW wind farm in current case study. In the current set up, PL164 is the limiting factor restricting the amount of hydrogen that can be produced.

While the pipeline is sufficient for 1.5 GW windfarm, if there were more windfarms around the Magnus platform in the future, a new pipeline would have to be built as currently FLAGS can transport three times the amount of hydrogen than PL164 at equivalent pressures.

4.4.3 New Pipeline Design

The advantage of building new pipelines is that new pipelines can be built from material with suitable steel grade operating at higher pressure and known pipeline integrity. The disadvantage of a purpose-built pipeline would be the limited capacity design, which would disable other future hydrogen production facilities in the vicinity to use it for hydrogen transport, unless it would be designed for larger amounts of hydrogen, which would increase the cost and decrease the efficiency until further hydrogen capacity is built up. Higher pressure would increase the amount of hydrogen flow rate but would also increase the time to the gas terminal. The suitability of the three possible routes for the Magnus case study are discussed within this section.

Figure 4.10 shows three potential pipelines if existing oil and gas pipelines were not re-used. The purpose-built pipelines could be shorter, approximately 485 km, by going straight to St Fergus, Figure 4.10b), rather than through Brent A platform like the combination of PL164 and FLAGS, Figure 4.10a), 400km by going to Flotta gas terminal in Orkney, Figure 4.10d), and 190km by going straight to Sullom Voe in Shetland Islands, Figure 4.10c). Table 4.8 - 4.11 show data and potential dimensions for new purpose-built pipelines.

4.4.3.1 St Fergus

Around 35% of UK natural gas terminates at St Fergus terminal [242]. There are currently two ongoing hydrogen projects, Acorn and Aberdeen Vision that identify St Fergus as a major hydrogen production site. Hydrogen at St Fergus can be directly fed into the gas grid starting at blending 2% of hydrogen into natural gas and going up to 100% hydrogen in planned new purpose-built hydrogen pipeline between St Fergus and Aberdeen [242].

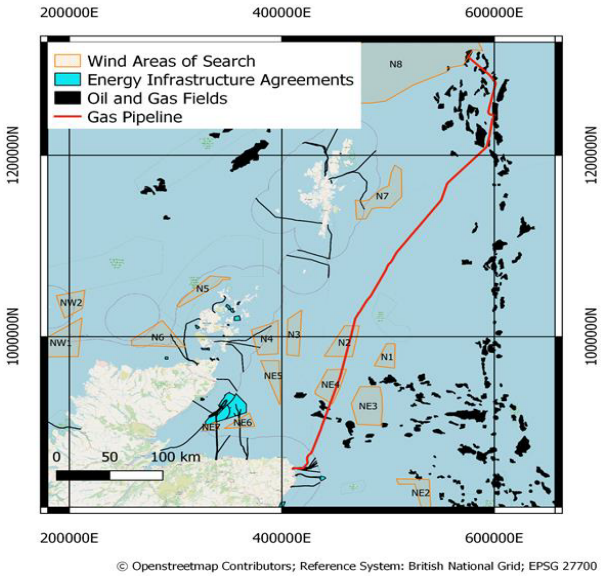

a) Existing Pipelines PL164 and Flotta

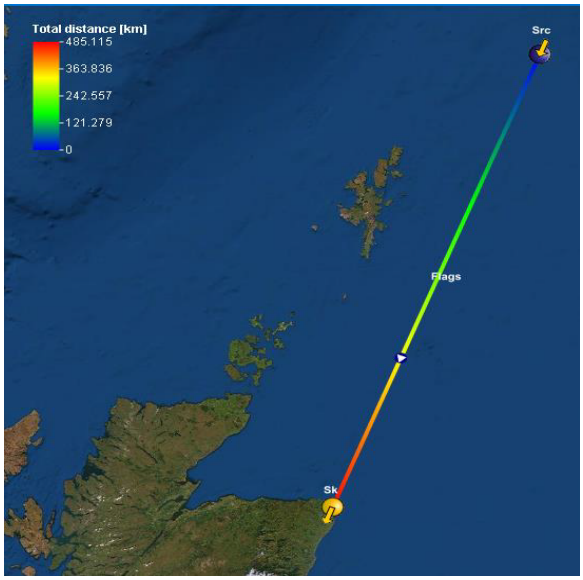

b) A New Pipeline to St Fergus

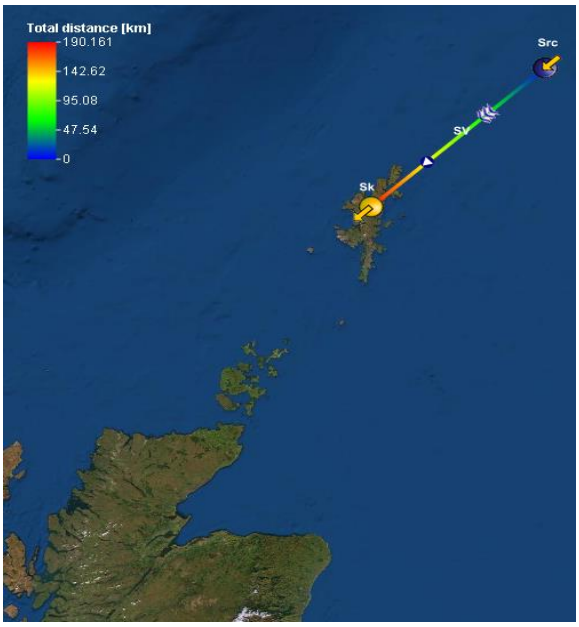

c) A New Pipeline to Sullom Voe

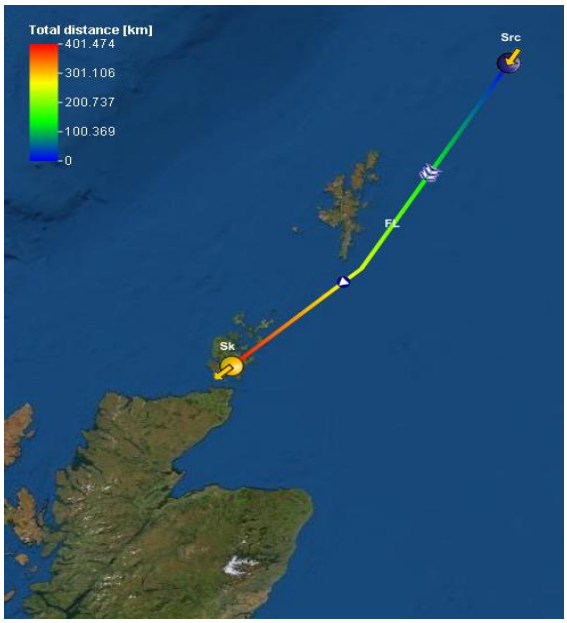

d) A New Pipeline to Flotta

Figure 4.10: Four different pipeline routes where a) are existing pipelines FLAGS and PL164, b) is a new pipeline from Magnus to St Fergus, c) is a new pipeline from Magnus to Sullom Voe and d) is a new pipeline to Flotta.

To serve the hydrogen production from a 1.5GW windfarm at 50 bar to St Fergus, a 22-24 inch (559-610 mm) outer diameter pipeline would be sufficient. Although the 22 inch pipeline delivers hydrogen faster, the 24 inch pipeline has a smaller pressure drop. Between the minimum and maximum production, the pressure drop would vary between 7-25 bar for the 22inch and 4-13 bar for the 24 inch pipeline, while the time to gas terminal would vary between 11 and 24 hours for 22 inch and 15 and 30 hours for 24 inch outer diameter pipeline (Table 4.8).

From the gas velocity and pressure drop perspective, even the purpose-built pipeline operates sub-optimally due to a large hydrogen mass flow rate difference between summer and winter production as well as the length of the pipeline. Thus, a hydrogen storage is of major importance to send larger volumes of hydrogen all at once, when transporting energy from a wind farm to land over a long distance.

Table 4.8: Purpose built pipeline to St Fergus.

	22 inch		***24 inch***	
	min	**max**	**min**	**max**
Mass flow rate (kgH_2/h)	17,227	30,000	17,227	30,000
ΔP (bar)	6.5	24.8	3.8	13
ΔP (bar/km)	0.013	0.051	0.0079	0.027
Maximum velocity at any point (m/s)	5.9	17.8	4.7	10.1
Average gas velocity (m/s)	5.6	12.2	4.5	8.7
Time to the gas terminal (hours)	24	11	30	15

4.4.3.2 Sullom Voe

Sullom Voe oil and gas terminal in Shetland receives natural gas from West of Shetland gas fields via 20-inch West of Shetland Gas Pipeline System, which is then used for onsite gas power station and enhanced oil recovery on Magnus platform. Currently there is no gas pipeline from Magnus to Sullom Voe (EnQuest, 2019). Magnus-Sullom Voe pipeline could complement Orion project, that is looking to build 200 floating wind turbines of the coast of Shetland to decarbonise oil and gas platforms and build hydrogen plant at Sullom Voe, which would produce green hydrogen from remaining wind power [114].

If a dedicated hydrogen pipeline was to be designed to Sullom Voe, it would be between 20 to 22 inch (508-559mm) outer diameter (See Table 4.9).This pipeline is much more efficient that the one going to St Fergus as it is much shorter, but again, in order to optimise the pipeline operation, significant hydrogen storage is required.

Table 4.9: Purpose built pipeline to Sullom Voe.

	20 inch		***22 inch***	
	min	**max**	**min**	**max**
Mass flow rate (kgH_2/h)	17,227	30,000	17,227	30,000
ΔP (bar)	4.3	15.3	2.4	8.1
ΔP (bar/km)	0.023	0.081	0.013	0.042
Maximum velocity at any point (m/s)	7.3	16.0	5.9	10.8
Average gas velocity (m/s)	6.8	13.7	5.5	10.3
Time to the gas terminal (hours)	8	4	10	5

4.4.3.3 Flotta

Flotta is another Scottish oil and gas terminal located in the Orkney Islands, closer to Magnus than St Fergus. The advantage of transporting hydrogen to Flotta is that the Orkney islands have many already pre-existing hydrogen projects and Flotta is a proposed location for the Hydrogen Hub Orkney [19]. Due to their remoteness, both Flotta and Sullom Voe can accommodate safety distance and potentially provide refuelling stations for hydrogen ships (Scottish Government, 2020). The purpose-built pipeline going to Flotta would have 22-24 inch (559-610 mm) outer diameter (See Table 4.10). It would face similar challenges as discussed for a pipeline going to St Fergus (Section 4.4.3.1) and Sullom Voe (Section 4.4.3.2).

Table 4.10: Purpose built pipeline to Flotta.

	22 inch		***24 inch***	
	min	**max**	**min**	**max**
Mass flow rate (kgH_2/h)	17,227	30,000	17,227	30,000
ΔP (bar)	5.3	19	3.1	10.5
ΔP (bar/km)	0.013	0.048	0.0078	0.026
Maximum velocity at any point (m/s)	5.9	14.6	4.9	9.5
Average gas velocity (m/s)	5.5	11.4	4.5	8.5
Time to the gas terminal (hours)	20	10	25	13

4.5 Conclusions and Future Work

This chapter investigates the technical feasibility of re-using gas pipelines for transportation of hydrogen from a material and thermo-hydraulic perspective. It takes flow rates from a theoretical 1.5 GW windfarm calculated in Chapter 3 and uses them to simulate hydrogen transportation in two North Sea pipelines case studies.

Based on an extensive literature search, it is concluded that it is possible to re-use oil and gas pipelines for hydrogen considering material as a single factor even if they are of higher grade than X52 as long as the operating pressure is reduced. However, the pipelines would then be able to carry only a fraction of the hydrogen that they could at higher pressures, which reduces the design energy supply of the pipelines when transporting hydrogen rather than natural gas. This chapter also demonstrates that it is possible to re-use gas pipelines from a thermo-hydraulic perspective even without requiring the use of a compressor on the platform. However, substantial summer and winter hydrogen production differences cause efficiency issues, leading to substantial storage requirements.

PIPESIM simulations showed that 20 bar would not be sufficient to transport the hydrogen produced from the 1.5GW windfarm through the shorter feeder pipelines such as PL164, while the maximum assumed pressure for the PEM electrolyser, 50 bar, allows the transportation of hydrogen from 1.5GW wind farm for both feeder and transmission pipelines such as PL164 and FLAGS.

For PL164, 50 bar is more suitable for the range of mass flow rates expectable from a 1.5 GW windfarm. The problem comes with the longer transmission pipeline, FLAGS, where transportation of hydrogen at 50bar takes anywhere between 38-67 hours, which increases even further at 100bar (75.6-133 hours) due to the line being underutilised, requiring higher hydrogen flow rate. This could be solved by including storage to be able to transport higher flow rates in periods with lower wind in the summer.

While 100 bar significantly increases the maximum mass flow rate transferred through the pipelines, which is important as hydrogen has lower heat capacity per volume in comparison to natural gas, it also significantly increases the transportation time, and would not be an optimal solution for a 1.5GW wind farm in current case study.

New shorter pipelines could be built to three gas terminals St Fergus, Flotta and Sullom Voe that would be suitable due to upcoming hydrogen utilisation projects in all three.

The advantage of building new pipelines is that new pipelines can be built from material with suitable steel grade operating at higher pressure and known pipeline integrity. The disadvantage of purpose build pipeline would be the limited capacity design, which would disable other future hydrogen production facilities in the vicinity to use it for hydrogen transport, unless it would be designed for larger amounts of hydrogen, which would increase the cost and decrease the efficiency.

For pressure drop and maximum capacity analysis such as the one carried out in this chapter, the steady-state simulator PIPESIM was sufficient. However, future work could include transient phenomena flow model analysing real time operation, hydrogen tracking, leakage, and metering for natural gas-hydrogen blends as well as pure hydrogen.

CHAPTER 5 - ECONOMIC ANALYSIS

5.1 Overview

This chapter describes the economic analysis conducted to estimate cost effectiveness of delivering energy to shore through hydrogen rather than electricity for windfarms located far offshore. It ties in results from Chapters 2-4 as per Figure 5.1. The Levelised cost of energy (LCOE) and Levelised cost of hydrogen (LCOH) results for a 1.5 GW floating offshore wind farm (FOWF) with a centrally located green hydrogen production platform (1.5GW and 957.5MW electrolyser capacity) was determined and compared with available literature. This chapter also includes a cost comparison between re-using existing oil and gas infrastructure and building new infrastructure.

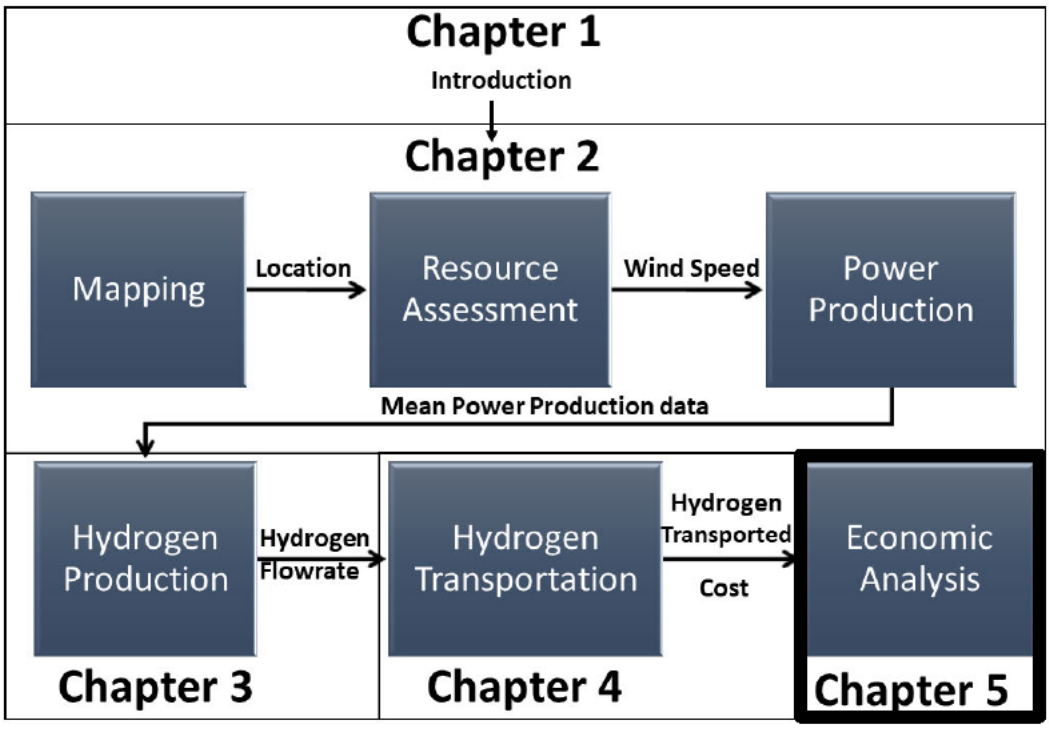

Figure 5.1: Thesis flow diagram.

5.2 Literature Review

5.2.1 Economic Analysis of Energy Systems

There are a number of methods which can be used to evaluate viability of energy projects some of which will be discussed in this section.

5.2.1.1 Simplified Methods

Simple payback period, Equation (5.1), and simple rate of return, Equation (5.2), are both very fast methods with outcomes that are easy to interpret [243]. Simple payback shows the amount of years it takes for the initial investment to be paid back, while simple rate of return is the inverse of simple payback and shows percentage of return on investment [243]. However, neither of them take into consideration the longevity of the system and thus they can both be misleading [243]. For their simplicity, they can be used as a first step in decision making to filter out least viable projects.

$$Simple\ Payback = \frac{Extra\ First\ Cost}{Annual\ Savings} \quad \textbf{(5.1)}$$

$$Simple\ Rate\ of\ Return = \frac{Annual\ Savings}{Extra\ First\ Cost} \quad \textbf{(5.2)}$$

5.2.1.2 Advanced Methods

The following methods take into consideration the fact that future cash flows do not have the same value as present cash flows and so they use discount rate, *r*, to discount future cash flows to their present value [243], [244]. The discount rate represents the opportunity cost of the capital, which increases with increased risk of the project, requiring riskier projects to have higher returns [245].

The discount rate used is usually weighted average cost of capital (WACC), which is calculated using Equation (5.3) [246]. Alternatively, a fixed r can be assigned based on the literature or the industry.

$$WACC = \frac{VE}{VE + VD} \times R_E \times \frac{VD}{VE + VD} \times R_D \times (1 - TR) \quad \textbf{(5.3)}$$

Where

$VE = value\ of\ equity$

$VD = market\ value\ of\ debt$

$R_E = the\ cost\ of\ equity$

$R_D = the\ cost\ of\ debt$

$TR = the\ asset\ tax\ rate$

However, like simple methods, the advanced methods also have some shortcomings. They do not include externalities such as environmental and health impact, so when applied in the energy sector, in some countries with cheap fossil fuels it would appear more beneficial to build a new coal power plant. However, the saved cost in energy would be spent on the deprived health of citizens living nearby and fines due to high CO_2 emissions.

They also do not estimate public support, so for example floating wind farms might have more public support than nuclear power plants although they are both GHG emission free during operation. Other factors missing in these calculations are possible project risks, fuel price fluctuations, power price fluctuation, safety, and regulatory risks. All the methods mentioned below have been used to evaluate offshore PtG projects in the past (see Table 5.1).

Table 5.1: Different economic analysis methods used for offshore PtG projects evaluation.

Economic Analysis	*Literature*
Net Present Value	[51]–[53], [137]
Internal Rate of Return	[137]
Levelised Cost of Hydrogen	[57], [136], [138], [141]

Net Present Value (NPV)

NPV is a discounted cash flow analysis that determines whether the sum of the net discounted cash income over the lifetime of the project exceeds the discounted costs. Jepma [52] describes the two cash flows of the NPV as the purchase of electricity to produce hydrogen (negative cash flow), and the market for the produced hydrogen (positive cash flow). NPV is calculated using Equation (5.4) [247].

$$NPV = \sum_{t=0}^{n} \frac{NCF_t}{(1+r)^t} \quad \textbf{(5.4)}$$

Where

$NCF_t = net\ cash\ flow\ generated\ by\ innovation\ project\ in\ year\ t$

$r = discount\ rate$

Internal Rate of Return (IRR)

Internal rate of return depicts the rate of return necessary for the project to break even, i.e. when present cash flowing in is equal to expected cash flowing out [53]. It allows the investment to be compared with returns on other competing investment [243]. When using Equation (5.4) IRR is the discount rate when NPV of the project is equal to zero, Equation (5.5) [243], [248].

$$0 = \sum_{t=0}^{n} \frac{NCF_t}{(1+IRR)^t} \quad \textbf{(5.5)}$$

Levelised Cost (LC)

Levelised cost analysis serves as a supporting decision-making tool for evaluating and comparing long-term investment projects. It allows adequate comparison between different sources of energy or energy vectors by providing cost per kWh or kg throughout the whole life cycle of the plant [243], [246], [249].

The result can be interpreted as the minimum price per kW at which energy needs to be sold to break even on the total investment [249]. Whether it is levelised cost of energy or hydrogen, to calculate it, it requires upfront fixed cost [243] also called capital expenditure or CAPEX. CAPEX consists of all the costs that need to be paid in order to start up the plant such as planning, individual equipment, construction, installation, etc [246], [250], [251].

Once the plant is operational, it requires annual investments also called operational expenditure or OPEX. OPEX consists of operational and maintenance costs, as well as any fuel costs, insurance, rent or land lease and any other costs occurring regularly or one off payments during the whole duration of the project lifecycle [251].

Even after the plant stops serving its purpose and ceases operation, the cash flow does not stop there. LC considers decommissioning expenditure or DECEX that includes all payments necessary to decommission the plant and return the land back to the original state.

Since LC considers cash flow throughout the whole life cycle of the plant, CAPEX is considered to be paid in 'year 0', i.e. a year before the operation and OPEX starts in year 1 [252]. DECEX is paid the year after last operational year, so if a plant operates for 30 years, DECEX is paid in year 31 [252].

Once all data are collected, LC can be calculated using Equation (5.4) to calculate NPV of total costs and then divide it by NPV of generation as shown in Equation (5.6**)** [251]. LC analysis specifically for floating offshore wind and hydrogen production is described later in this chapter in Sections 5.3.1 and 5.3.2.

$$LC = \frac{NPV\ of\ total\ costs}{NPV\ of\ generation} \quad \textbf{(5.6)}$$

5.3 Methodology

5.3.1 Levelised Cost of Energy (LCOE)

The LC analysis has been chosen for the economic analysis as it enables easy comparison between different technologies and is a widely used method within government bodies and industry for calculating the cost of energy [249]. In this work, LCOE has been calculated using the methodology outlined by Ebenhoch *et al.* [252] and BEIS [251] and adjusted to include DECEX as per Castro-Santos *et al.* [250] as shown in Equation (5.7).

$$LCoE = \frac{\sum_{t=1}^{n} \frac{C_0 + O_t + D_{31}}{(1+r)^t}}{\sum_{t=1}^{n} \frac{E_t}{(1+r)^t}} \quad \textbf{(5.7)}$$

$$C_0 = C_C + C_{FOWF} \quad \textbf{(5.8)}$$

$$D_{31} = D_C + D_{FOWF} \quad \textbf{(5.9)}$$

$$O_t = O_C + O_{FOWF} \quad \textbf{(5.10)}$$

Here C_0 stands for CAPEX at year 0 and consists of cable CAPEX (C_C) and FOWF CAPEX (C_{FOWF}), Equation (5.8), D_{31} is DECEX for year 31 and O_t is OPEX in year t. Both OPEX and DECEX include FOWF (O_{FOWF} and D_{FOWF}) and cables (O_C and D_C), Equations (5.9) and (5.10). For a diagram on contributions to LCOE, see Figure 5.2.

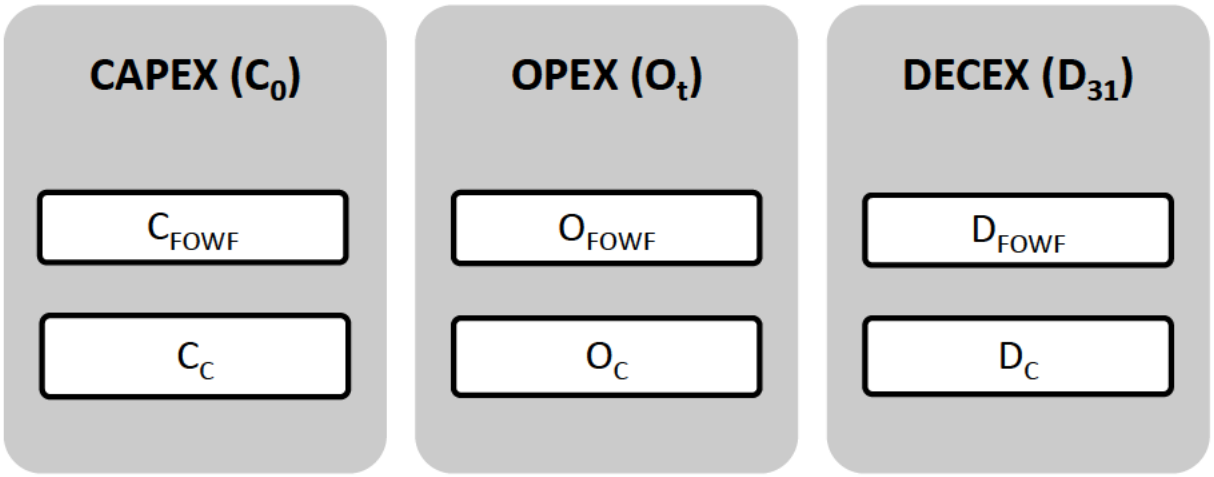

Figure 5.2: Diagram of LCOE contributions to FOWF.

Cable lifetime costs (C_C, O_C, and D_C) are separated from the rest of FOWF costs as FOWF costs are also included in the economic analysis of energy transportation through pipelines scenario. E_t is electricity output in year t, r is the discount rate in %, t is individual year from 1 to n, where n is total operational lifetime. The total operational lifetime has been set to 30 years [57], [253], [254].

A discount rate, r, is used in LCOE calculations in order to discount future cash flows to their present value [244]. Many recent studies indicate a significant effect of a discount rate on the LCOE [244], [255]. Based on the studies, the discount rate has a significant potential to reduce LCOE and thus, it is important to choose an accurate discount rate to represent the weighted average cost of capital for future commercial floating offshore wind projects.

Lerch [244] chooses 7% discount rate for future floating offshore wind projects, which is between 8% used by Spyroudi *et al.* [57]and 5% chosen by a study commissioned by the Scottish Government [136], and thus seems reasonable for this work. However, to study the effect of the discount rate on LCOE and LCOH, a sensitivity analysis has been carried out on both LCOE and LCOH with r varying between 3% and 12% in 2% increments and is presented later in Section 5.6.5.

5.3.1.1 Floating Offshore Wind Farm

Figure 5.3 and Figure 5.4 show CAPEX and OPEX estimations for floating offshore windfarms that were selected for LCOE calculations collected from the literature. These data are based on expert elicitations [256], existing offshore wind data [254], [257] and literature [253]. Figure 5.5 shows the cost components included in the CAPEX, the OPEX and the DECEX of a typical FOWF that were considered by the literature reviewed. While Wiser *et al*. [256] do not specify FOWF technology, California Public Utility Commission (CPUC) [257] and Beiter *et al.* [254], use semi-submersible floating offshore wind technology and Serri *et al.* [253] use average between spar buoy and semi-submersible for LCOE calculations. All FOWF CAPEX, OPEX and DECEX data that were collected from literature available publicly are listed in Figures C1, C2 and C3 in Appendix C as some of the data were excluded from the calculations. The data excluded are the ones that are not cost estimations for 2030 and are further discussed in Appendix C.

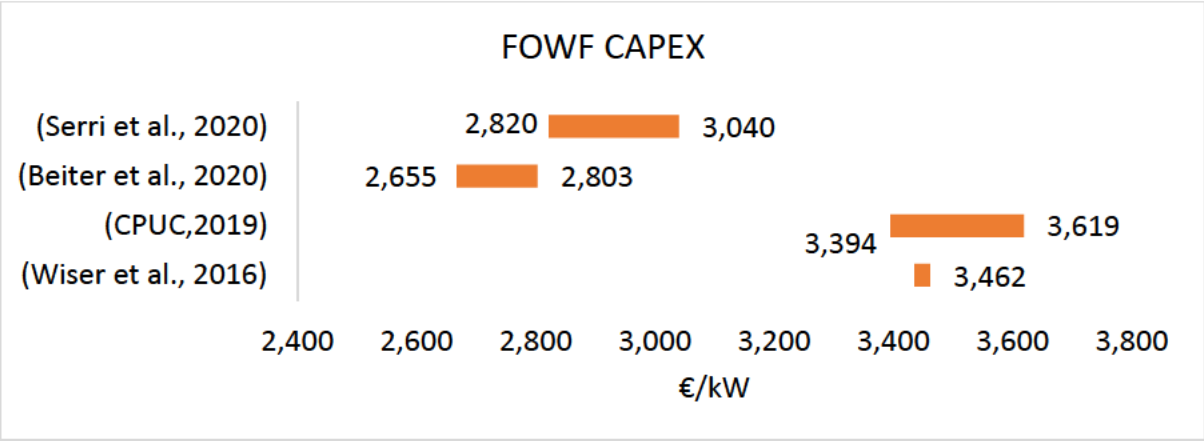

Figure 5.3: FOWF CAPEX data from the literature used in LCOE calculations.

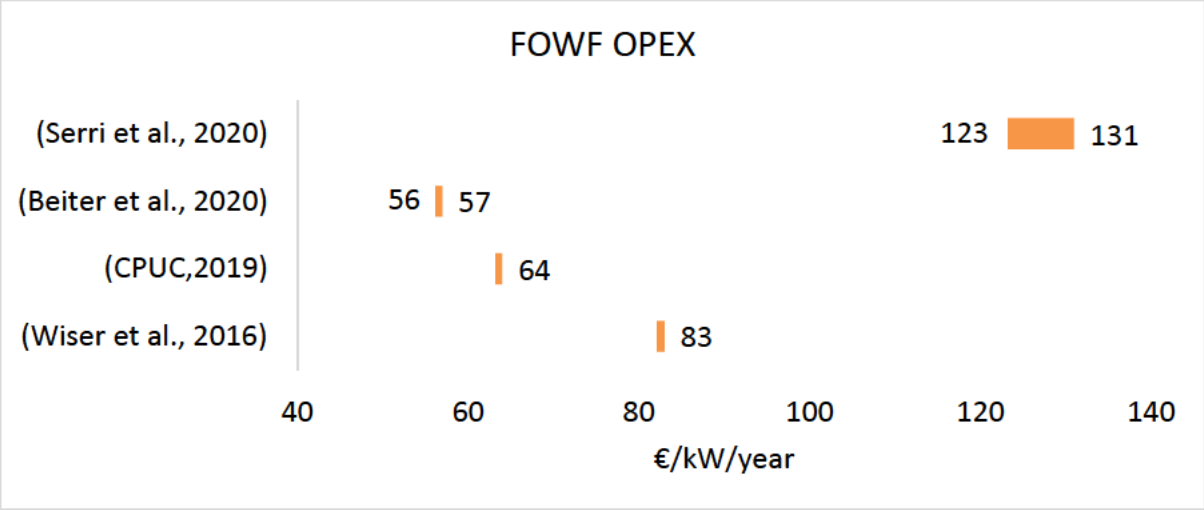

Figure 5.4: FOWF OPEX data from the literature used in LCOE calculations.

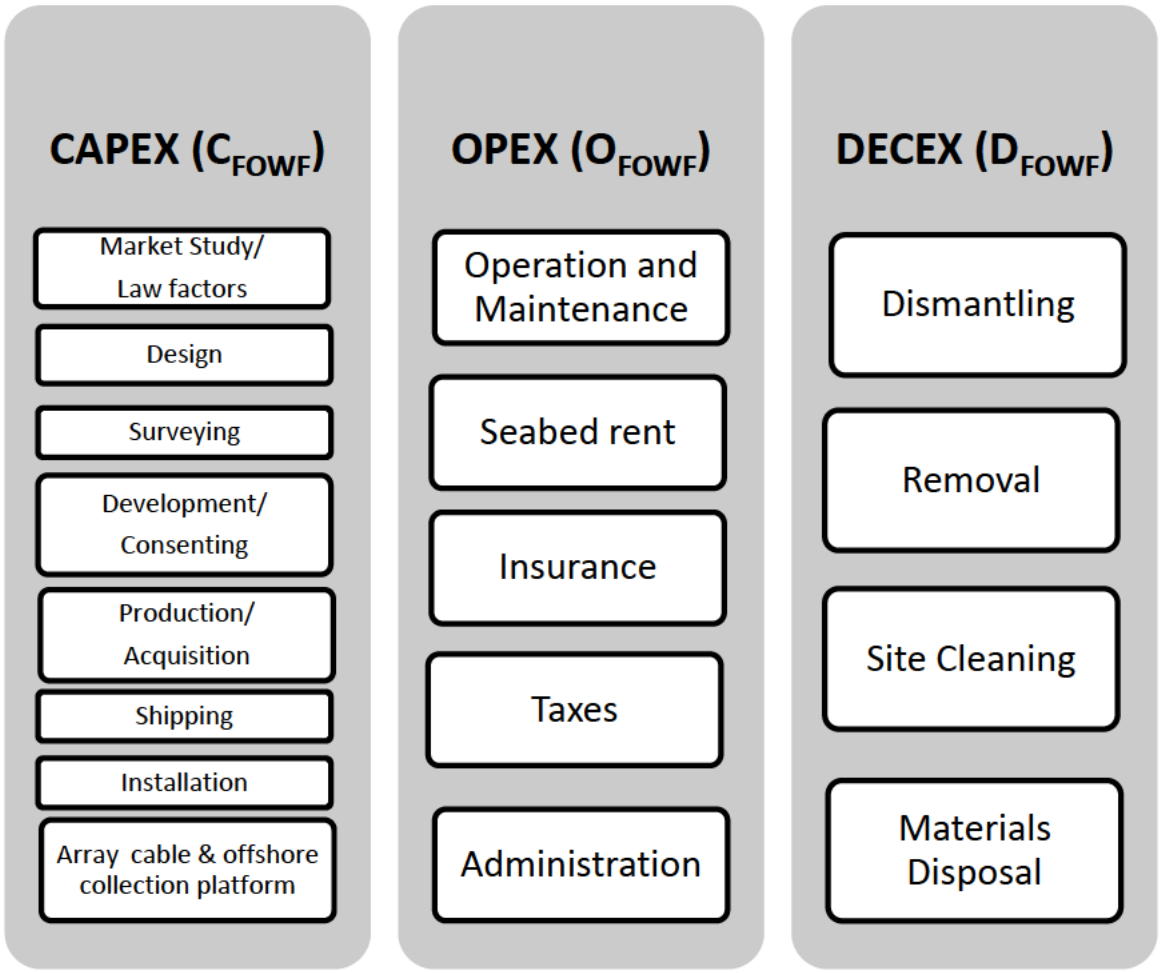

Figure 5.5: CAPEX, OPEX, and DECEX of typical FOWF [246], [250].

Figure 5.6 shows decommissioning values from the literature selected for LCOE calculations. All decommissioning values from the literature are presented in Figure C3 in Appendix C. Some analysis considers decommissioning as cost neutral such as Heidari [258], who did not include DECEX in their LCOE analysis. In 2018, 79% of UK based respondents to a Renewable Energy Discount Rate Survey from hydro, biomass, solar PV, onshore and offshore wind thought salvage will cover decommissioning cost [259]. This work includes decommissioning cost as it is a good practice to have a decommissioning reserve and thus, data sources were selected that also include decommissioning (Figure 5.6). Castro-Santos *et al.*

[250] contain scrap recovery, whilst the Wood plc [260] estimate does not include scrap recovery and is therefore more expensive. The DECEX figure in James & Costa Ros [261] is based on 3% of the CAPEX estimate and is more general and lower than Wood plc cost estimate that used long distance, greater depth and large scale windfarm in their estimate. Data for decommissioning costs used are all from the time of publication between 2015 and 2021 as there were no published estimations for 2030 available.

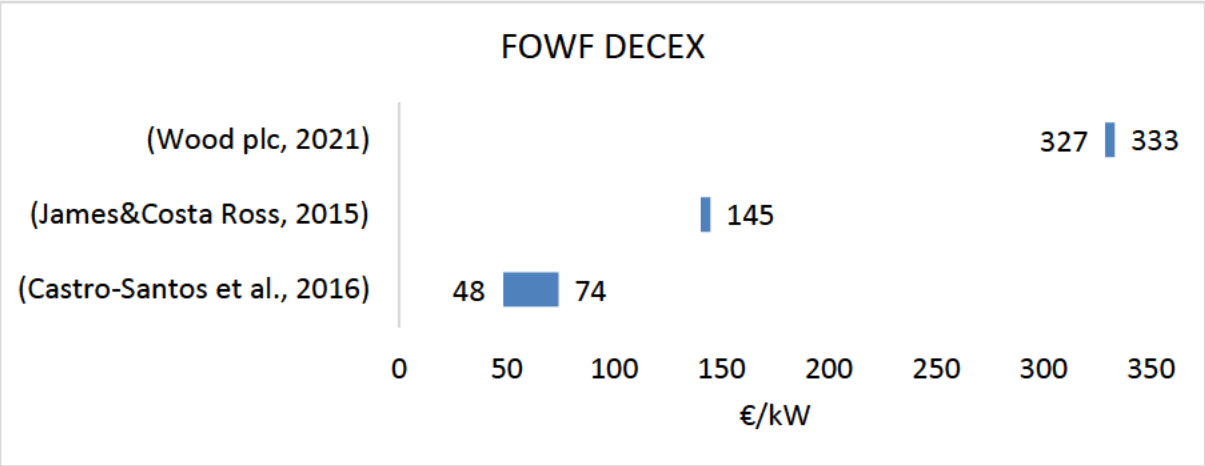

Figure 5.6: DECEX from the literature used for LCOE calculations.

5.3.1.2 Cables

When transferring power in the form of electrons, there are three ways to do this, HVAC (high voltage alternating current), HVDC (high voltage direct current), and LFAC (low frequency alternating current). Currently all offshore windfarms in the UK are connected to the grid via HVAC export cables. The first UK offshore wind farm to be connected through HVDC is the Dogger Bank Project, due to be operational in 2023 [262]. There is an argument to use HVDC for distances over 50km [263] to minimise losses as HVDC has a lower voltage drop in comparison to HVAC [264].

Figure 5.7 shows all the cost components contributing to CAPEX, OPEX and DECEX for cable scenario in typical FOWF. Inter-array cables and offshore substation for cable collection apply for both pipelines and cable scenario and thus are included in FOWF CAPEX (see Figure 5.5), while onshore station and export cable is considered only for cable scenario (refer back to Chapter 3, Section 3.4.2).

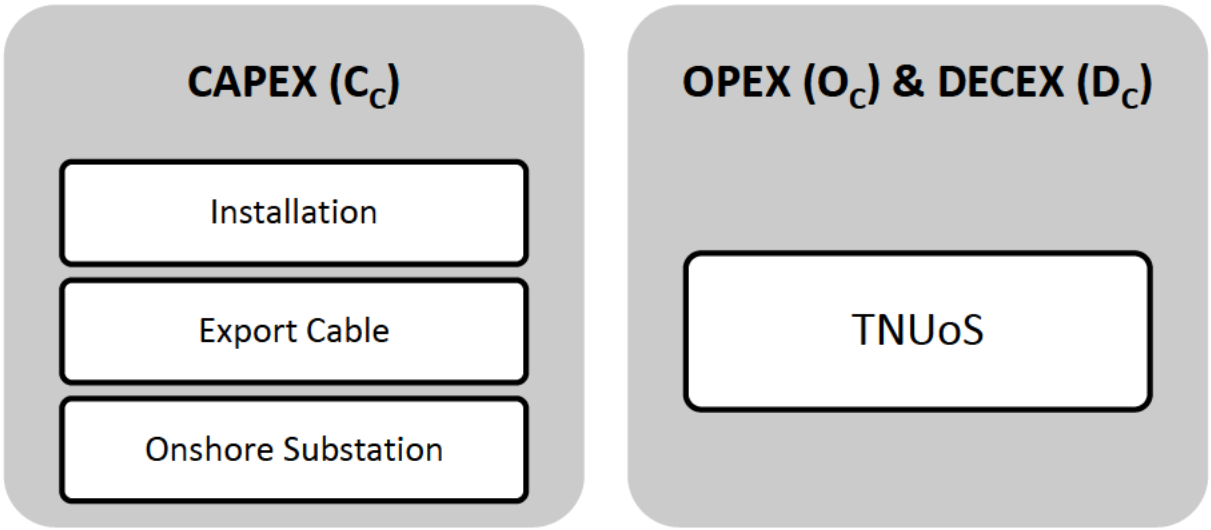

Figure 5.7: CAPEX, OPEX and DECEX of cable scenario for FOWF.

For the windfarm presented in Chapter 2 located close to the Magnus platform, there are three cable connection points available. Sandwick in Shetland, Banff on the Scottish mainland and Ayre of Cara on the Orkney Islands. These are shown in Figure 5.8. The connection to Shetland would be around 203km from the windfarm to Sandwick. However, current grid capacity is not sufficient for connecting a 1.5GW windfarm and the planned interconnector that should be fully commissioned between Shetland and Wick (mainland Scotland) by 2024 only has a capacity of 600MW [265].

A similar situation occurs for a 388km export cable to the Ayre of Cara as the planned new interconnector between Orkney and mainland Scotland that is due for completion in 2023 only has a capacity of 220MW [266]. This will be too small, so a cable link between the windfarm and Banff, which would be approximately 491km would have to be built.

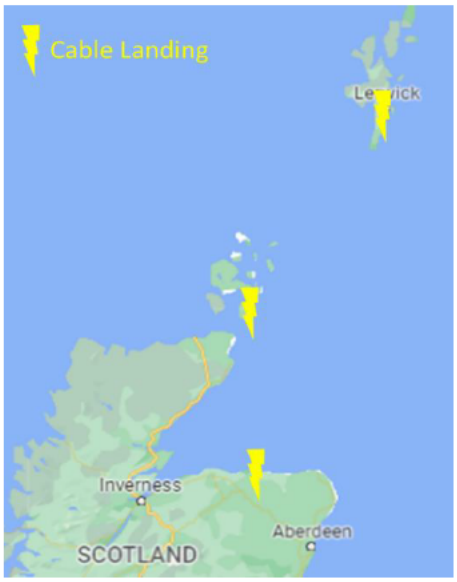

Figure 5.8: Map of cable landings around Magnus.

Figure C4 in the Appendix C shows all CAPEX data collected from the literature for long distance high-capacity export cables while Figure 5.9 shows only the data selected for LCOE calculations. Most of the cable data are for HVDC except for OWPB [267] that represents new HVAC technology system. The CAPEX data summarised in Figure 5.9 are costed for a 203km cable i.e. for a connection to the Shetland islands using Equation (5.11).

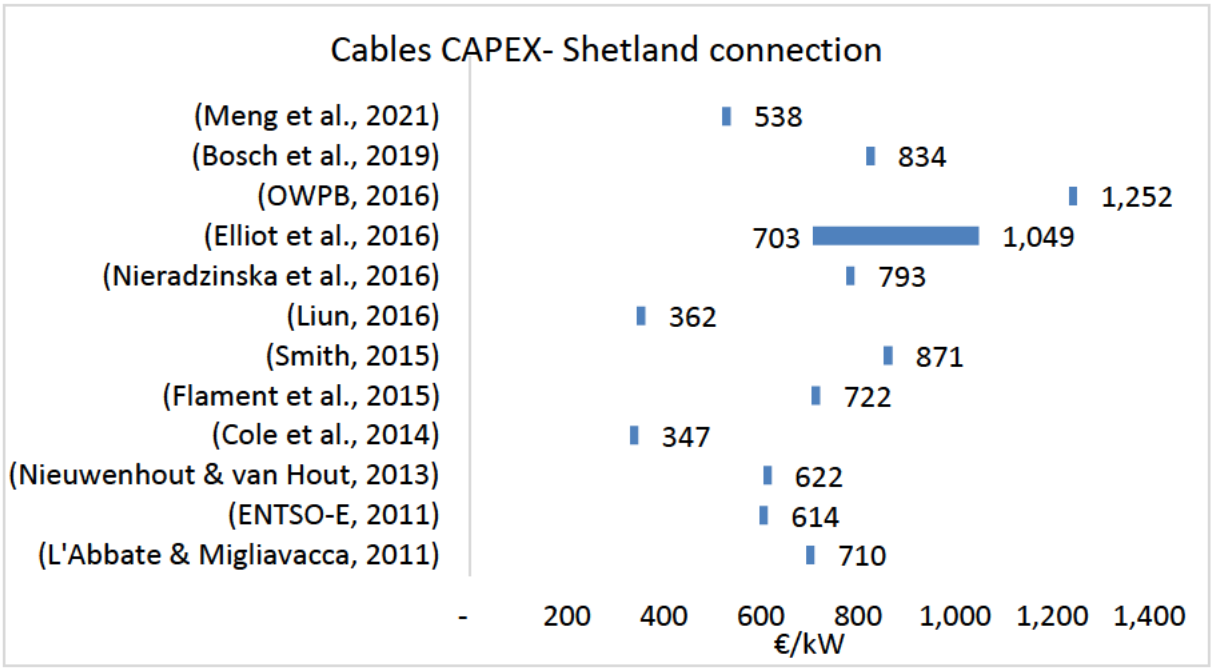

Figure 5.9: Cable CAPEX from the literature used in LCOE calculations.

$$C_C = \frac{(Installation\ Cost + Cable\ Cost) \times CL}{Cable\ Capacity} + (Converter\ Cost + Platform\ Cost) \quad \textbf{(5.11)}$$

Where

$C_C = CAPEX\ for\ cables\ in\ euros\ per\ kW$

$CL = cable\ length\ in\ km$

Installation Cost and *Cable Cost* are quoted per km for specific *Cable Capacity* in kW, and *Converter Cost* and *Platform Cost* are per kW.

Table C2 in Appendix C provides more information on data presented in Figure 5.9 such as cable length and capacity CAPEX is based on. Transmission costs presented in this section are from the date of publication between 2011 and 2021 as there were no 2030 estimation data available. As can be seen in Figure 5.9, in 10 years of cable CAPEX data, the cost is fairly stable and so the assumption was made that the cost is unlikely to change below minimum or above maximum cost presented in Figure 5.9

According to the Energy Act 2004, a wind farm developer is required to sell the transmission asset in the UK to OFTO (Offshore Transmission Operator), who is assigned by OFGEM (The Office of Gas and Electricity Markets) to operate the transmission asset. OFTO is also responsible for decommissioning of this asset after the end of its lifetime [268]. Thus, cable decommissioning and O&M costs are not included in the cost analysis, but transmission network use of system charges in £/kW (TNUoS) are, as these are the payments paid to OFTO for operating and decommissioning of the transmission assets. See Equation (5.12) for O_C and D_C calculations.

$$O_C + D_C = TNUoS \times Windfarm\ Capacity\ in\ kW \times n \quad \textbf{(5.12)}$$

Where

$O_C = OPEX\ of\ cables$

$D_C = DECEX\ of\ cables$

$n = total\ operational\ lifetime$

For the cable scenario (without hydrogen production), intermittent generation tariffs (type of TNUoS) for 2025/2026 were used [269]. As shown in Figure 5.10, TNUoS charges are currently one of the major issues for building offshore wind farms in the Northern part of the North Sea as they are significantly higher than TNUoS charges in North East England for example and even higher than South of England where TNUoS charges are negative and developers get paid for each kW of wind power generated.

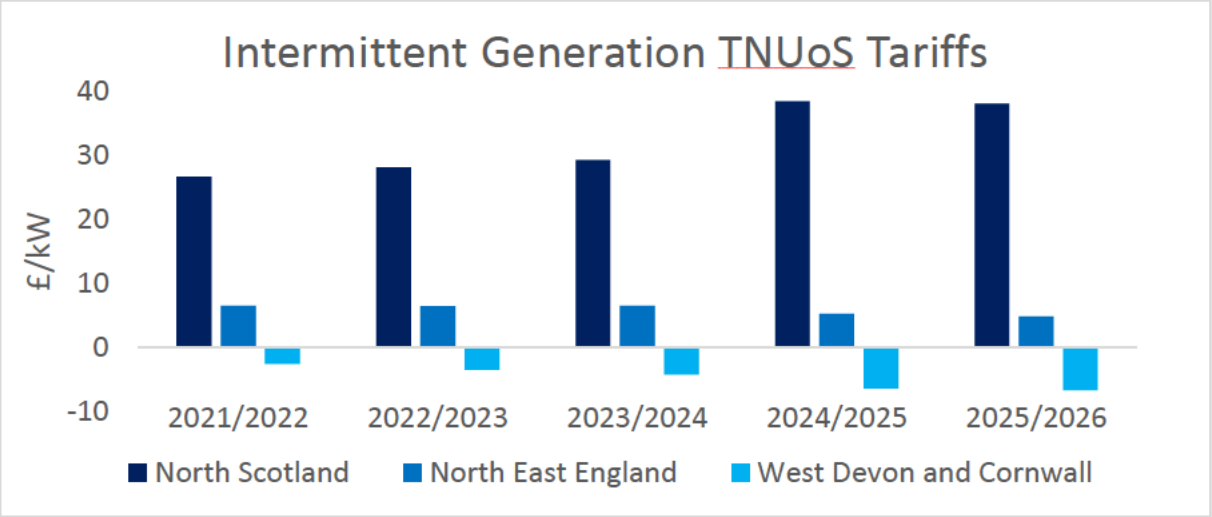

Figure 5.10: Five year view of TNUoS tariffs [269].

5.3.2 Levelised Cost of Hydrogen LCOH

For offshore hydrogen projects, LCOH can be calculated using Equation (5.13), which is similar to Equation (5.7) but instead of electricity output in year *t*, it contains hydrogen produced in year t (H_t) and adds onto LCOE without cables ($LCOE_{FOWF}$ consisting only of C_{FOWF}, O_{FOWF} and D_{FOWF}). Here the CAPEX (C_{H0}) consists of electrolyser CAPEX (C_E), desalination unit CAPEX (C_D), pipeline CAPEX (C_P) and topside CAPEX (C_T), Equation (5.14). O_{Ht} is OPEX in year t accounting for electrolyser (O_E), desalination unit (O_D), pipeline (O_P) and topside (O_T), Equation (5.15). D_{H31} is DECEX for year 31 and includes DECEX for pipelines (D_P) and topside (D_T), Equation(5.16). D_{H31} does not include decommissioning cost for desalination unit and the electrolyser as these will be removed together with the topside. Hydrogen production lifetime t is also set to 30 years [57], [136], [188] and discount rate r is set to 7% [188], which is between 8% from Spyroudi *et al.* [57] and 5% from study conducted for the Scottish Government [136]. As mentioned in Section 5.3.1, sensitivity analysis of both LCOH and LCOE to the discount rate can be found in Section 5.6.5.1.

$$LCOH = LCOE_{FOWF} + \frac{\sum_{t=1}^{n} \frac{C_{H0} + O_{Ht} + D_{H31}}{(1+r_H)^t}}{\sum_{t=1}^{n} \frac{H_t}{(1+r_H)^t}} \quad \textbf{(5.13)}$$

$$C_{H0} = C_E + C_D + C_P + C_T \quad \textbf{(5.14)}$$

$$O_{Ht} = O_E + O_D + O_P + O_T \quad \textbf{(5.15)}$$

$$D_{H31} = D_P + D_T \quad \textbf{(5.16)}$$

5.3.2.1 PEM Electrolyser

As described in Chapter 3, Section 3.2.2, PEM electrolyser technology has been chosen for this work mostly due to the intermittent power supply and pressurised hydrogen production. The LCOH for maximum (1500MW) and minimum (least windy day, 957.5 MW) electrolyser capacities has been calculated. Figure 5.11 shows the aspects contributing to full CAPEX and OPEX as considered by the literature referenced in Figure 5.12 and Figure 5.13. Both figures show the PEM electrolyser CAPEX and OPEX data for 2030 collected from available literature used for LCOH calculations. As can be seen in Figure 5.12 some CAPEX values have a wide range of cost, significantly influencing the maximum and average cost of PEM electrolysers. However, these cost ranges come from relevant literature with data based on expert elicitations [270], interviews with relevant stakeholders [271], a significant literature review [272] or a combination of both, literature review and interviews with manufacturers [273] and thus have been included in the final CAPEX. While FCH 2 JU [130] does not contain 'real' CAPEX data it lists key performance indicators for PEM electrolysis for 2030, which the EU will be aiming to reach and thus the cost has been included in the data as a good guide for future price estimates.

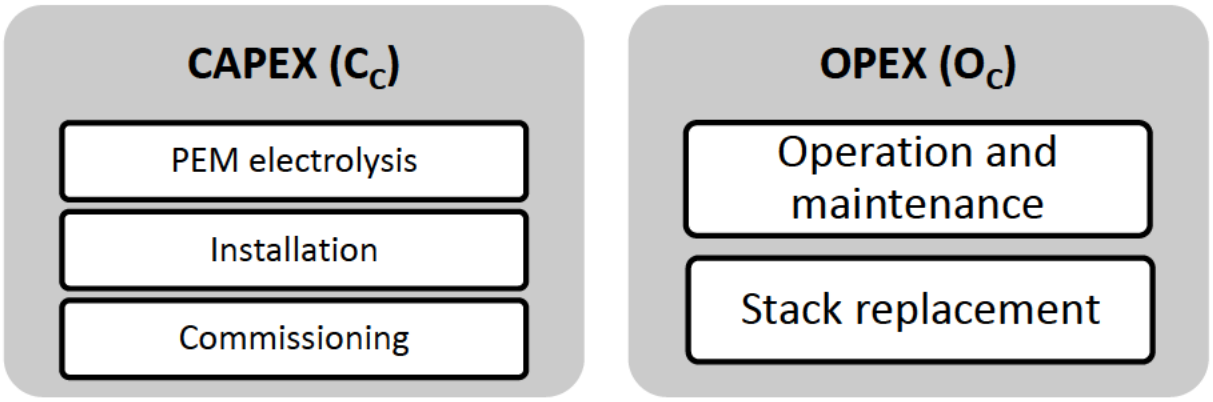

Figure 5.11: Electrolysis contributions to LCOH.

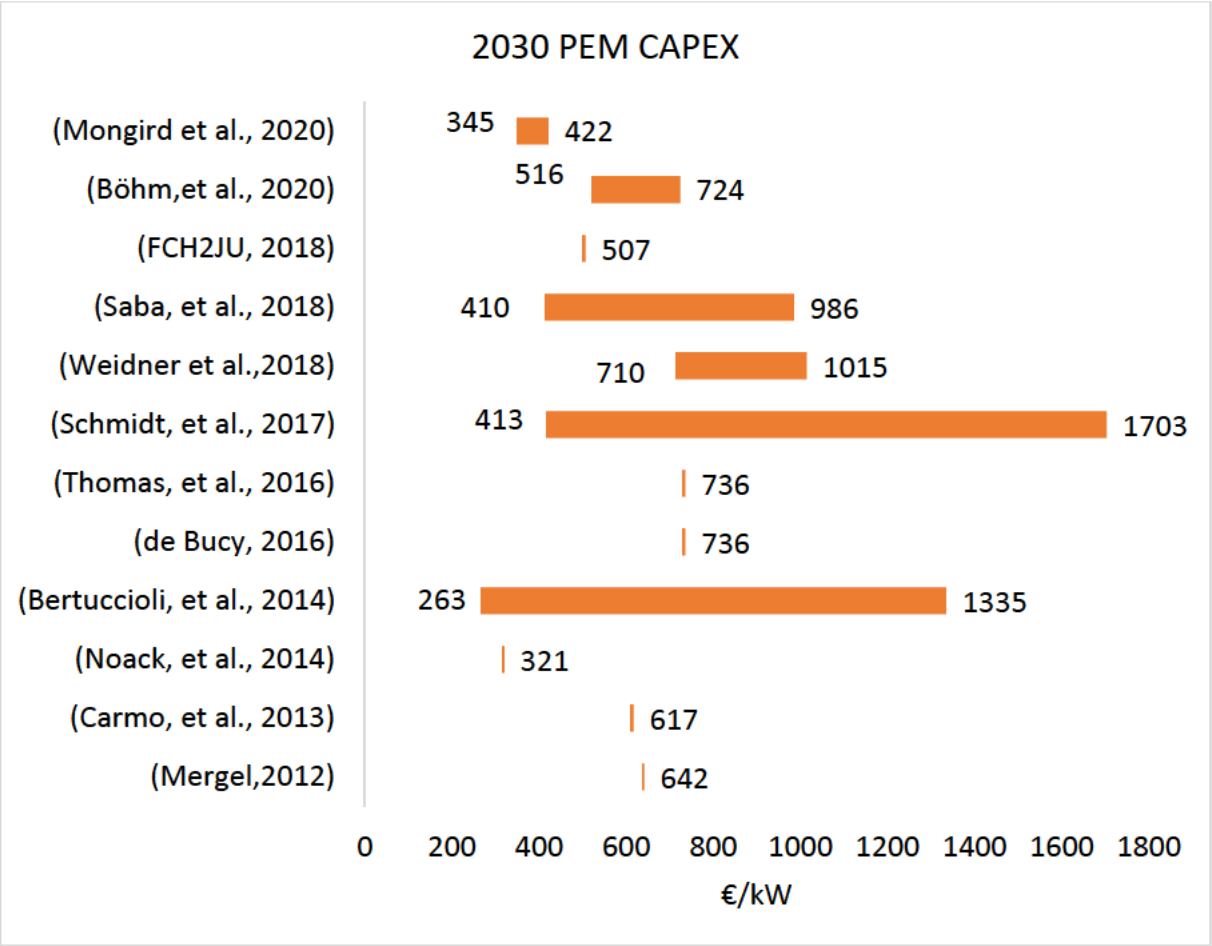

Figure 5.12: Capital expenditure values for PEM electrolyser from the literature used for LCOH calculation.

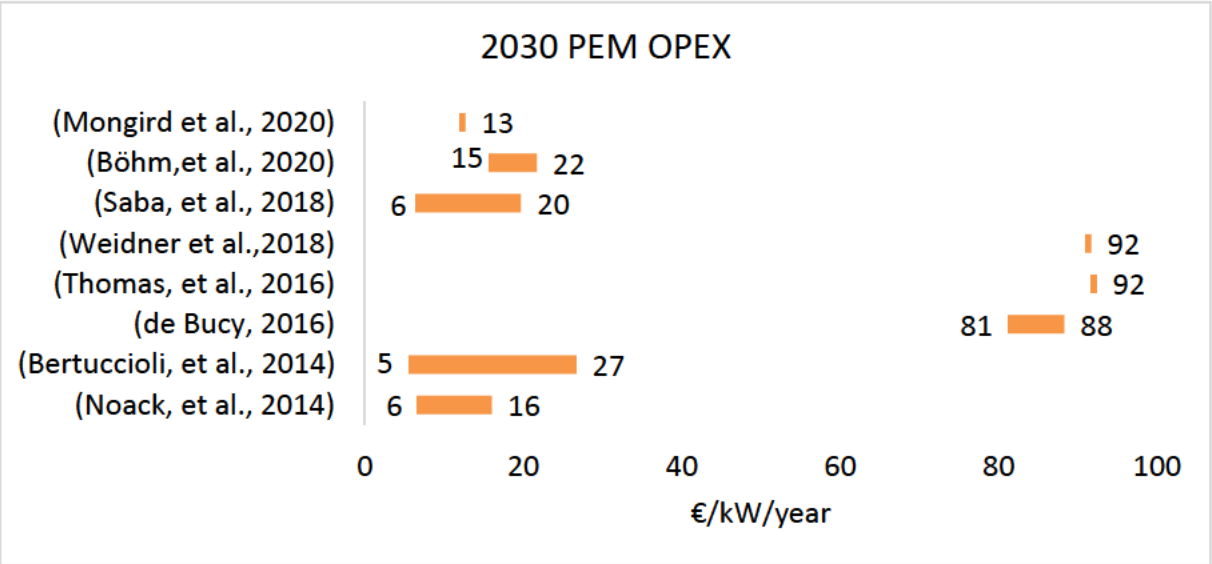

Figure 5.13: OPEX PEM electrolyser cost used for LCOH calculation.

While some studies included OPEX as a % of CAPEX [271], [272], [274]–[276], others included specific price per kW [273], [277], [278]. Carmo *et al.* [152] and Mergel [279] did not mention any OPEX information and thus have not been included in the overall OPEX. The OPEX estimate also includes a stack replacement cost after 40,000h [276] or 50,000h [278]. Noack *et al.* [275] expects 2030 electrolysers to be able to run for 70,000h prior to stack replacement. Where stack replacement was specified, Equation (5.17) was used to calculate figures presented in Figure 5.13. Decommissioning for both electrolyser and desalination unit is included within the topside decommissioning costs.

$$SR = \frac{\left(\frac{n}{\frac{n_{STACK}}{E_O}}\right) \times C_{PEM} \times SRC}{n} \quad \textbf{(5.17)}$$

Where

$SR = Stack\ replacement\ contribution\ to\ O_{PEM}\ \ in\ €\ per\ kW\ per\ year$

$n = total\ operational\ lifetime\ in\ years$

$n_{STACK} = operational\ lifetime\ of\ one\ stack\ in\ hours$

$E_O = typical\ electrolyser\ operation\ per\ year\ in\ hours\ (assumed\ 8000h)$

$C_{PEM} = CAPEX\ of\ electrolyser\ in\ €\ per\ kW$

$SRC = stack\ replacement\ cost\ as\ fraction\ of\ C_{PEM}$

5.3.2.2 Desalination

Since electrolysis takes place far offshore, treated sea water is used for hydrogen production and thus a zero cost for water is assumed. Figure 5.14 and Figure 5.15 show CAPEX and OPEX of desalination equipment used for LCOH calculations where the orange bar represents assumption for 2030 and the blue bar represents cost estimations for the year when the publication was written.

The data sources are a mix of data from academia [160], [162] and industry [280], [281]. All desalination cost data were used due to lack of 2030 cost estimations. Figure 5.16 shows individual desalination cost contributions to LCOH.

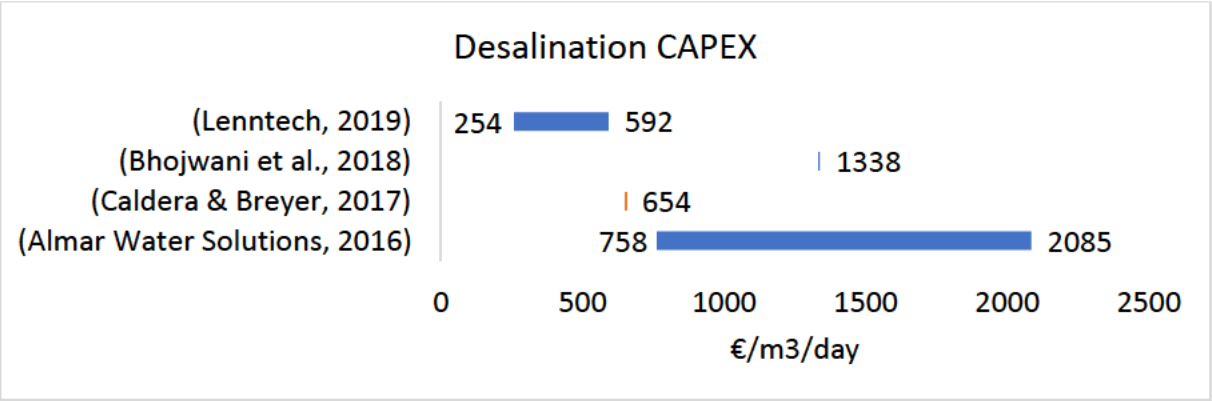

Figure 5.14: Desalination capital expenditure from the literature.

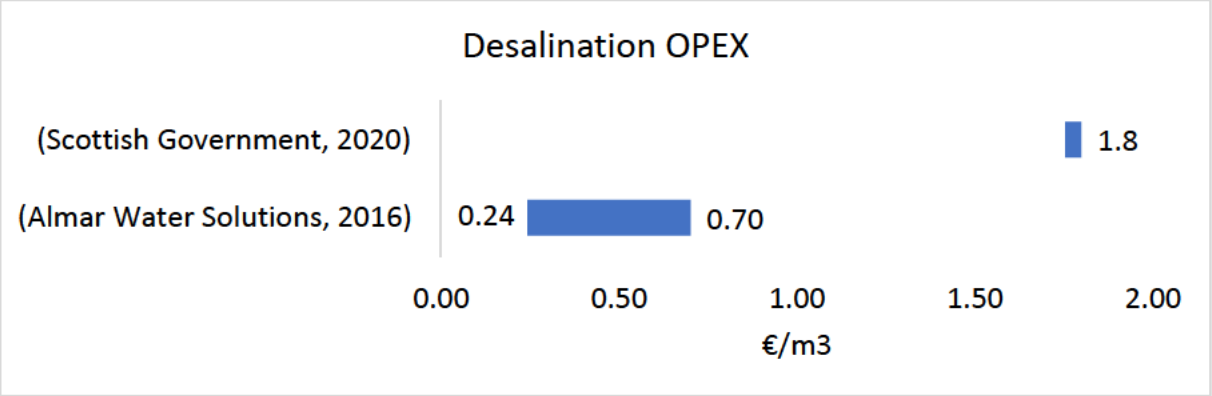

Figure 5.15: Desalination operation and maintenance expenditure from the literature.

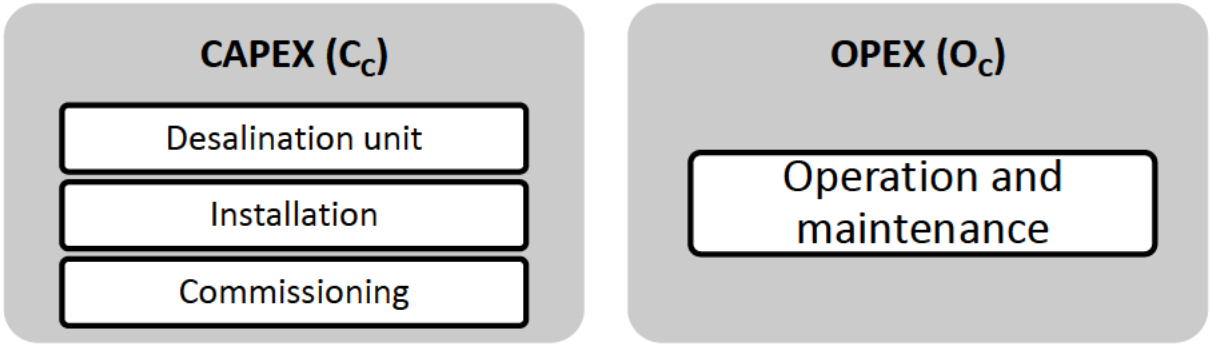

Figure 5.16: Desalination contributions to LCOH.

5.3.2.3 Pipelines

Figure 5.17 shows the individual costs adding up to CAPEX, OPEX and DECEX of pipelines [282], [283]. Figure C5 in the Appendix C shows all collected CAPEX data for building new pipelines, while Figure 5.18 shows the one used for LCOH calculations. These data are not 2030 estimations and are based on either quadratic equation models using diameter and length, Equations (5.18) to (5.22) [282], [284]–[287] respectively, weight based models, Equation (5.23) [288] or a cost estimation per km [57]. All the equations used for CAPEX calculations assume plain carbon steel as higher grades would not be used due to hydrogen cracking.

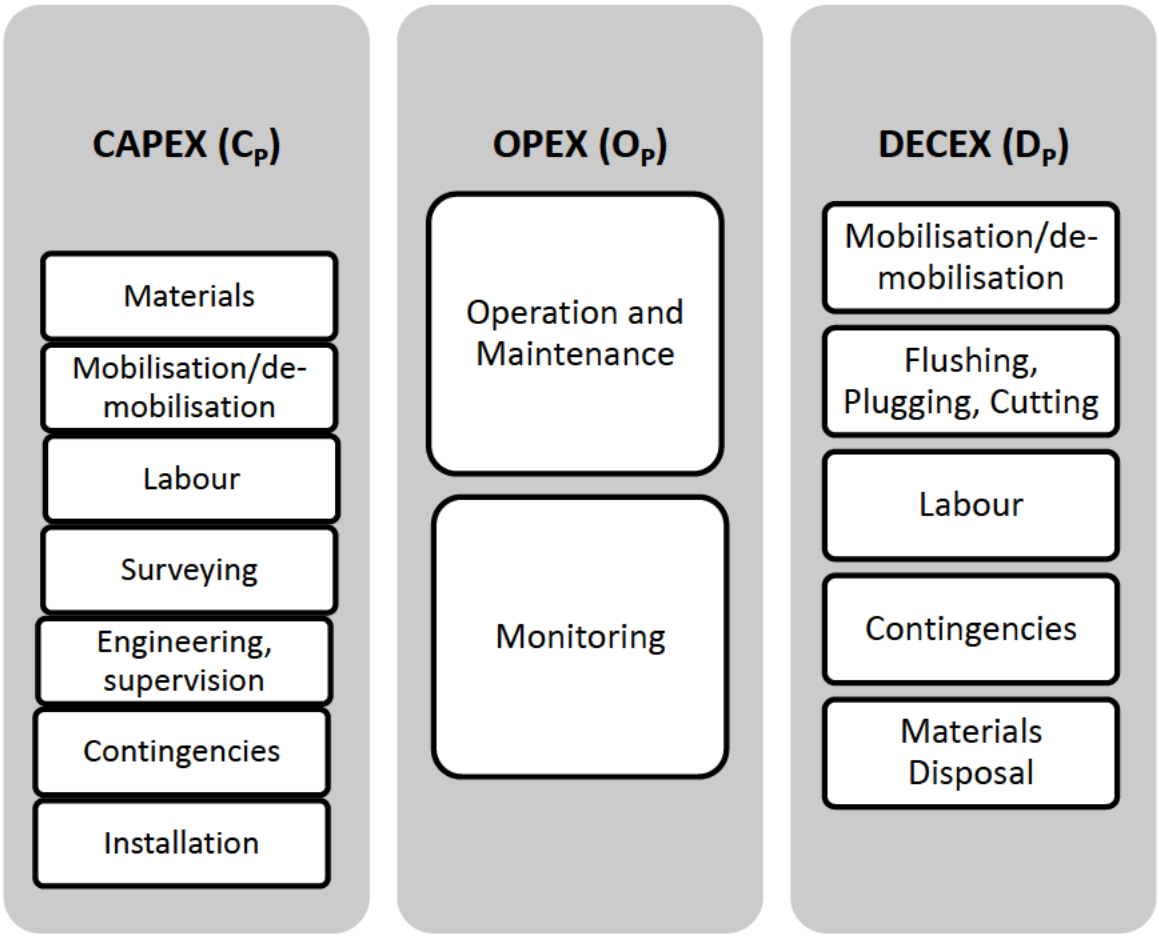

Figure 5.17: Diagram of pipeline contributions to LCOH.

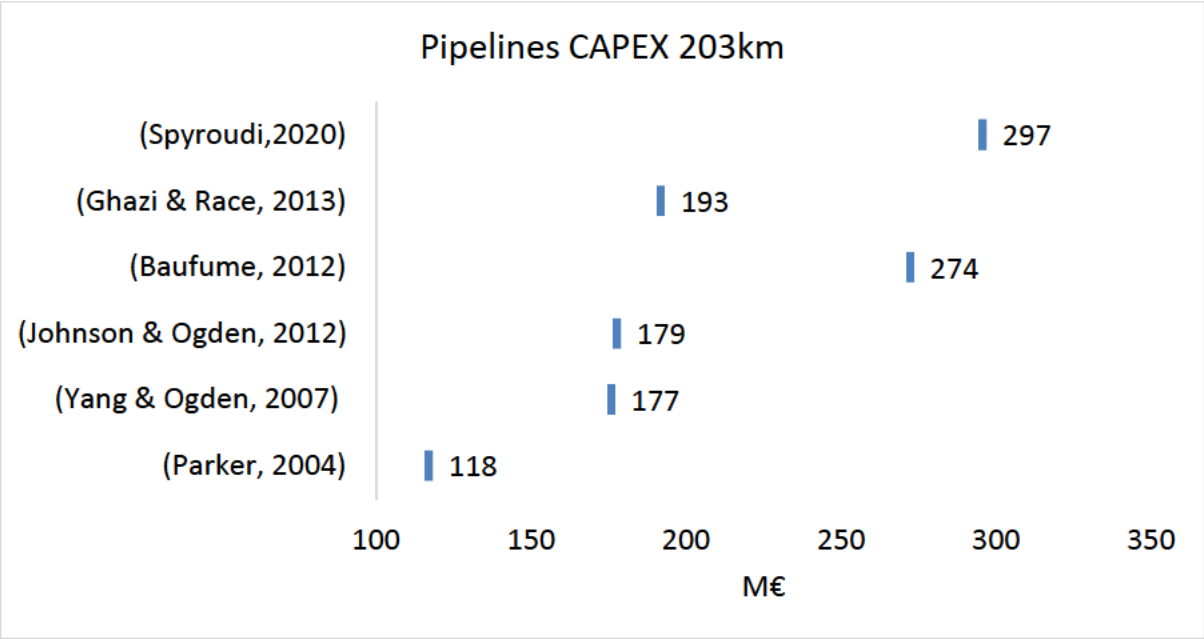

Figure 5.18: Pipeline CAPEX from the literature used in LCOH calculations.

$$C_P = [1{,}500{,}000 \times OD^2 + 860{,}500 \times OD + 247{,}500] \times L \quad \textbf{(5.18)}$$

Where

L=pipeline length in km

OD= outer diameter in m

$$C_P = F \times 10^6 \times [(0.4048L + 4.6964) - 0.00153L + 0.0113) \times OD + (0.000511L + 0.00024) \times OD^2] \quad \textbf{(5.19)}$$

Where

F= location factor, 1.2

L=pipeline length in km

OD= outer diameter in inches

$$C_P = [L \times 0.621371 \times (818.64 \times OD^2 + 14{,}288.2 \times OD + 284{,}530.3) + 431502.5] \quad \textbf{(5.20)}$$

Where

L=*pipeline length in km*

OD= *outer diameter in inches*

$$C_P = [674 \times OD^2 + 11{,}754 \times OD + 234{,}085] \times L + 405{,}000 \quad \textbf{(5.21)}$$

Where

L=*pipeline length in miles*

OD= *outer diameter in inches*

$$C_P = CAPEX \times OD^2 \times L \quad \textbf{(5.22)}$$

Where

$CAPEX$= *pipeline CAPEX per km*

L=*pipeline length in km*

OD= *outer diameter in inches*

$$C_P = V_P \times \rho_{PM} \times Cost_{PM} \times L \quad \textbf{(5.23)}$$

Where

V_P = *pipeline volume in* m^3

$\rho_{PM} = density\ of\ the\ pipeline\ material\ kg/m^3$

$Cost_{PM} = cost\ of\ pipeline\ material\ per\ kg\ per\ m$

$L = pipeline\ length\ in\ m$

The Wood plc [288] data point was removed from the selection because it doesn't include installation cost and thus CAPEX is significantly lower than the rest of the data points.

OPEX estimation ranges presented in Figure 5.19 have been calculated using 2-5% of CAPEX [284]. Johnson & Ogden [286] and Yang & Ogden [285] use 4% of CAPEX for OPEX.

All cost estimations used for CAPEX and OPEX are specific to hydrogen pipelines [285]–[287] or adjusted from natural gas for hydrogen [282], except for Ghazi & Race [284] that adjusts oil and gas pipeline costs for CO_2 pipelines. It has been included as it is still relevant especially in regard to OPEX and DECEX of existing pipelines and the data point is not an outlier, so has minimal effect on average cost of pipelines.

While hydrogen scenario that re-uses old oil and gas pipelines does not include CAPEX, OPEX and DECEX are both included (Figure 5.19 and Figure 5.20).

203km length (cable length from the windfarm to the nearest cable landing in Shetland) was used for new pipeline and for OPEX and DECEX of re-used pipelines to make the comparison equivalent to cable scenario.

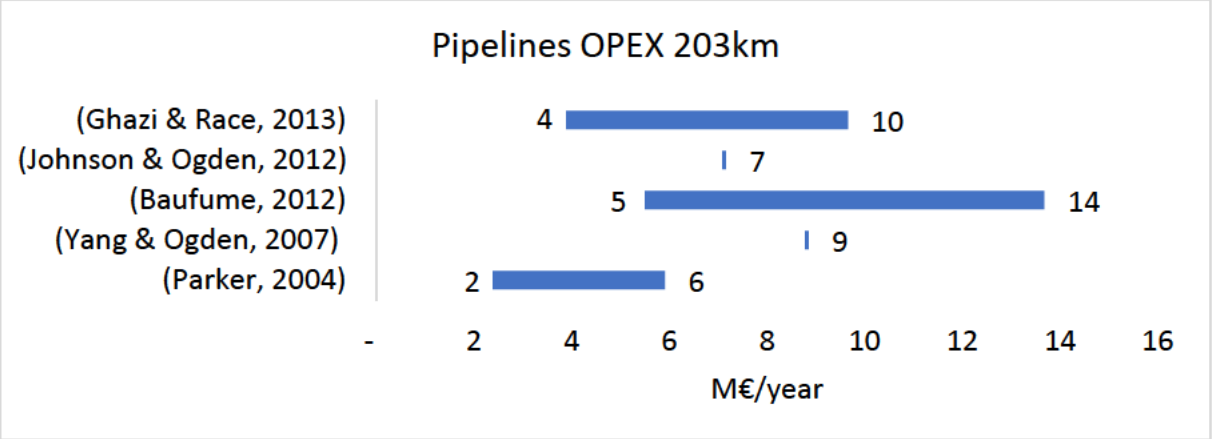

Figure 5.19: All collected pipeline OPEX data.

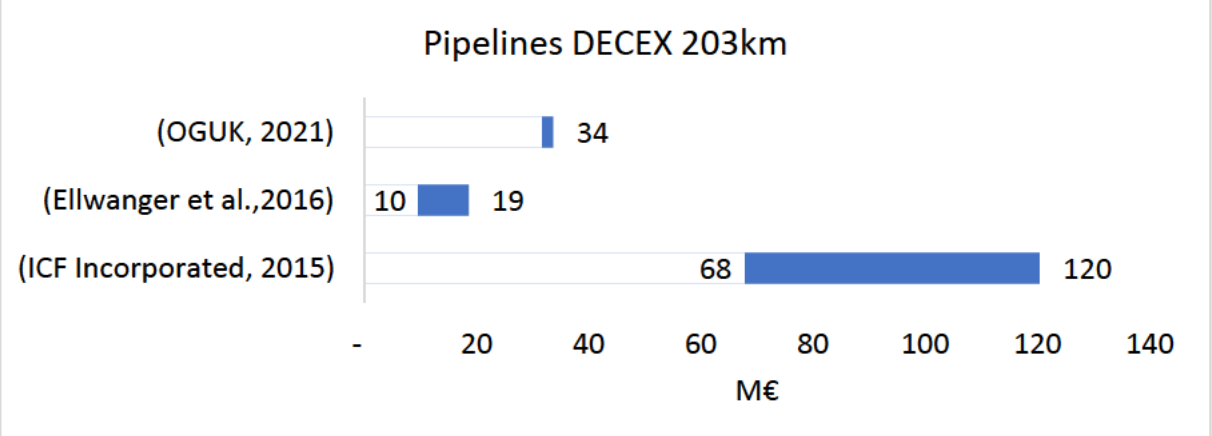

Figure 5.20: All collected pipeline DECEX data.

The decommissioning data used is based on past projects [289], industry [283] and government body estimates [50]. The data is summarised in Table C3 in the Appendix C.

5.3.2.4 Topside

CAPEX, OPEX and DECEX for the topsides were costed by industry experts at Wood plc, by adding up the costs of individual contributions (see Figure 5.21) for CAPEX and estimating 5% of CAPEX for annual OPEX, and 10% of CAPEX for DECEX at the end of the lifetime. Including bulk materials, equipment, fabrication, installation, commissioning, engineering and project management, the cost for large topsides per tonne was estimated.

To estimate the weight of the platform per MW, the weight of the entire balance of plant consisting of electrolyser, desalination unit, power equipment (refer back to Chapter 3 to read about the balance of plant), plus roof, cranes and helideck was estimated and summed. Using this ratio of topside tonnes/ MW of electrolysis with cost of topside/ ton mentioned above, CAPEX, OPEX and DECEX costs listed in Table 5.4 in Results section were determined. As mentioned in Chapter 3, due to confidentiality of the individual cost and weight data used, only final CAPEX, OPEX and DECEX data specific to 1500MW and 957.5MW electrolyser are provided. The cost for substructure was not included as substructures for large platforms weighing more than 10,000 tonnes in air, can be left in situ and potentially re-used as indicated in Chapter 3 of this thesis.

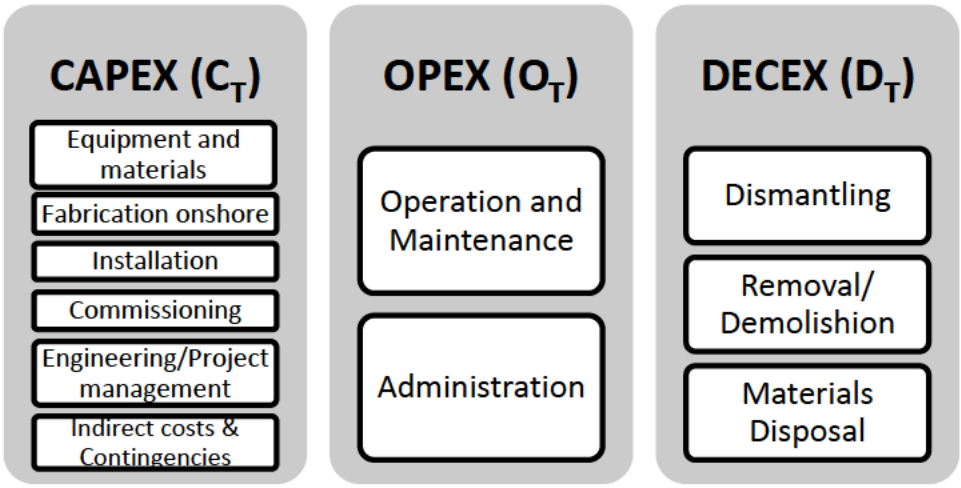

Figure 5.21: Diagram of topside contributions to LCOH.

5.3.3 Inflation and Currency Adjustments

All costs are quoted in 2020 euros as the economic analysis was carried out in 2021, so 2020 was most recent full year at the time of the analysis. Where price was quoted in different currency or year, the currency was converted to euros using average historical exchange rate for that year, Equation (5.24) and adjusted for inflation using Equation (5.25) adjusted from Thompson [290].

$$\begin{aligned} &Cost\ in\ euros \\ &\quad = cost\ in\ original\ currency\ for\ year\ t \\ &\quad \times\ exchange\ rate\ for\ year\ t \end{aligned} \tag{5.24}$$

$$IAC_{\ t+x} = PC_t\ \times \left(1 + \frac{IR_{t+1}}{100}\right) \times \left(1 + \frac{IR_{t+2}}{100}\right) \times \ldots \times \left(1 + \frac{IR_{t+x}}{100}\right) \tag{5.25}$$

Where

$IAC_{\ t+x} = Inflation\ Adjusted\ Cost\ in\ year\ t + x$

$PC_t = Past\ cost\ in\ year\ t$

$IR_{t+1} = Inflation\ rate\ for\ year\ t + 1\ in\ \%$

The average annual historical exchange rates for all currencies between 2010 and 2020 were sourced from Exchange Rates UK [291] and any exchange rates before 2010 were sourced from UKForex Limited [292]. The annual historical inflation rates were taken from Rate Inflation website [293]. The exchange rates and inflation rates used are listed in Table C4 in the Appendix C.

5.3.4 Cost Scenarios

Table 5.2 shows general scenarios for which LCOE and LCOH were calculated in order to compare cost of transportation of energy via cable versus transportation of energy via pipelines. Both cables and pipelines are 203km (length from Magnus windfarm to closest cable landing in Shetland). Table 5.3 shows Magnus case study specific scenarios. All LCOH are based on 1500MW electrolyser capacity unless otherwise indicated with a subscript.

Table 5.2: General scenarios.

Short form	*Scenario*	*Description*
$LCOE_{FOWF}$	FOWF	FOWF no cables
$LCOE$	FOWF+Cable	FOWF with cable connection
$LCOE_{TNUoS}$	FOWF+Cable+TNUoS	FOWF with cable connection including TNUoS charges
$LCOH_{RU}$	FOWF+re-used pipeline	Pipeline connection re-using existing pipelines (same length as cable scenario)
$LCOH_{RUT}$	FOWF+ re-used pipeline+topside	Pipeline connection re-using existing pipelines including new topside (same length as cable scenario)
$LCOH_{RUT957.5MW}$ $LCOH_{RUT1100MW}$ $LCOH_{RUT1300MW}$	FOWF+ re-used pipeline+topside	Pipeline connection re-using existing pipelines (same length as cable scenario) including new topside with 957.5MW/1100MW/1300MW electrolyser
$LCOH_{NP}$	FOWF+new-pipeline	Pipeline connection with new purpose-built pipelines (same length as cable scenario)
$LCOH_{NPT}$	FOWF+new-pipeline+topside	Pipeline connection with new purpose-built pipelines (same length as cable scenario) including new topside

Table 5.3: Magnus case study specific scenarios.

Short form	*Scenario*	*Description*
LCOE-Magnus	FOWF+Cable 491km	Cable to mainland Scotland as Shetland and Orkney do not have sufficient grid capacity for 1.5GW windfarm (Section 5.3.1.2)
LCOE-Magnus $_{TNUoS}$	FOWF+Cable 491km+TNUoS	Cable to mainland Scotland including TNUoS charges for Aberdeenshire
LCOH-Magnus $_{RU}$	FOWF+Re-used existing pipelines PL164+FLAGS	Re-used pipeline PL164 and FLAGS
LCOH-Magnus $_{RUT}$	FOWF+ Re-used existing pipelines PL164+FLAGS+ new topside	Re-used pipeline PL164 and FLAGS including new topside installed on Magnus substation
LCOH-Magnus $_{NP}$	FOWF+new-pipeline	New built 190 km pipeline to Shetland, 1500MW electrolyser
LCOH-Magnus $_{NPT}$	FOWF+new-pipeline+topside	New built 190km pipeline to Shetland including new topside installed on existing magnus substation

LCOH-Magnus *NPT957.5MW*	FOWF+new-pipeline+topside	New built 190km pipeline to Shetland including new topside installed on existing magnus substation, 957.5MW electrolyser

Three cost scenarios were calculated for CAPEX, OPEX, and DECEX data to calculate high, average and low cost scenarios for LCOE and LCOH. High cost scenario contains the maximum value and low cost scenario contains the minimum value of CAPEX, OPEX, and DECEX. The average scenario as implied by the name, is the average of all the values that were collected from the literature, and which have not been excluded. Equation (5.26) shows C_{FOW} average scenario calculations. Same principle was applied to CAPEX, OPEX, and DECEX for all other parameters.

$$C_{FOW} = \frac{\sum FOWF\ CAPEX\ Estimations}{Number\ of\ FOWF\ CAPEX\ Estimations} \quad \textbf{(5.26)}$$

5.4 Results

Table 5.4 summarises the LCOE and LCOH expenditure inputs from literature review described in the Methodology section that were calculated using methodology described in Section 5.3.4. Table 5.5 presents LCOE and LCOH results in 2020 €/MWh obtained by substituting values from Table 5.4 into Equation (5.7) to calculate LCOE and into Equation (5.13) to calculate LCOH.

Table 5.4: Levelised cost of electricity and hydrogen inputs.

Asset	*Expenditure*	*Low Cost Scenario*	*Average Cost Scenario*	*High Cost Scenario*
Floating Offshore Wind Farm	C_{FOWF} (€/kW)	2,655	3,113	3,619
	O_{FOWF} (€/kW/y)	56	86	131
	D_{FOWF} (€/kW)	48	150	333
Cables (203km)	C_C (€/kW)	347	724	1,252
	O_C & D_C (€/kW/y)	42.8	42.8	42.8
Cables (491km)	C_C (€/kW)	630	1,173	1,845
	O_C & D_C (€/kW/y)	34	34	34
PEM Electrolyser	C_{PEM} (€/kW)	263	689	1,335
	O_{PEM}(€/kW/y)	5	37	92
Desalination unit	C_D (€/m^3)	254	947	2,085
	O_D (€/m^3)	0.24	0.91	1.8
New Pipelines (203km)	C_P (M€)	118	206	297
	O_P (M€/y)	2	7	14
	D_P (M€)	10	50	120
	C_P (M€)	315	544	765
	O_P (M€/y)	6	19	38

New Pipelines (491km)	D_P (M€)	25	165	488
Topsides (957.5 MW)	C_T (M€)	1,714	1,714	1,714
	O_T(M€/y)	86	86	86
	D_T (M€)	171	171	171
Topsides (1500 MW)	C_T (M€)	2,685	2,685	2,685
	O_T(M€/y)	134	134	134
	D_T (M€)	268	268	268

Table 5.5: Levelised cost of electricity and levelised cost of hydrogen results.

Levelised Cost (€/MWh)	*Low Cost Scenario €/MWh*	*Average Cost Scenario €/MWh*	*High Cost Scenario €/MWh*
$LCOE_{TNUoS}$	98.11	126.30	163.80
$LCOE_{FOWF}$	77.76	97.21	122.48
$LCOH_{RU}$	83.95	119.24	169.54
$LCOH_{RUT957.5MW}$	118.74	149.81	193.26
$LCOH_{RUT1100MW}$	122.5	154.5	199.48
$LCOH_{RUT1300MW}$	127.51	160.75	203.35
$LCOH_{RUT}$	135.43	170.72	221.02
$LCOH_{NPT}$	136.82	173.82	224.51
$LCOH_{NP}$	85.33	122.72	173.02

5.4.1 Magnus Case Study

Table 5.6: LCOE and LCOH results specific to Magnus case study.

	Low Cost Scenario €/MWh	*Average Cost Scenario* €/MWh	*High Cost Scenario* €/MWh
LCOE-Magnus	92.36	124.39	165.23
LCOE-Magnus $_{TNUoS}$	102.14	134.17	175.01
LCOH-Magnus $_{RU}$	85.30	123.42	177.21
LCOH-Magnus $_{RUT}$	136.79	174.59	228.70
LCOH-Magnus $_{NP}$	86.85	126.51	181.92
LCOH-Magnus $_{NPT}$	136.64	173.64	225.88
LCOH-Magnus $_{NPT957.5MW}$	120.19	152.20	196.71

5.6 Discussion

5.6.1 LCOE

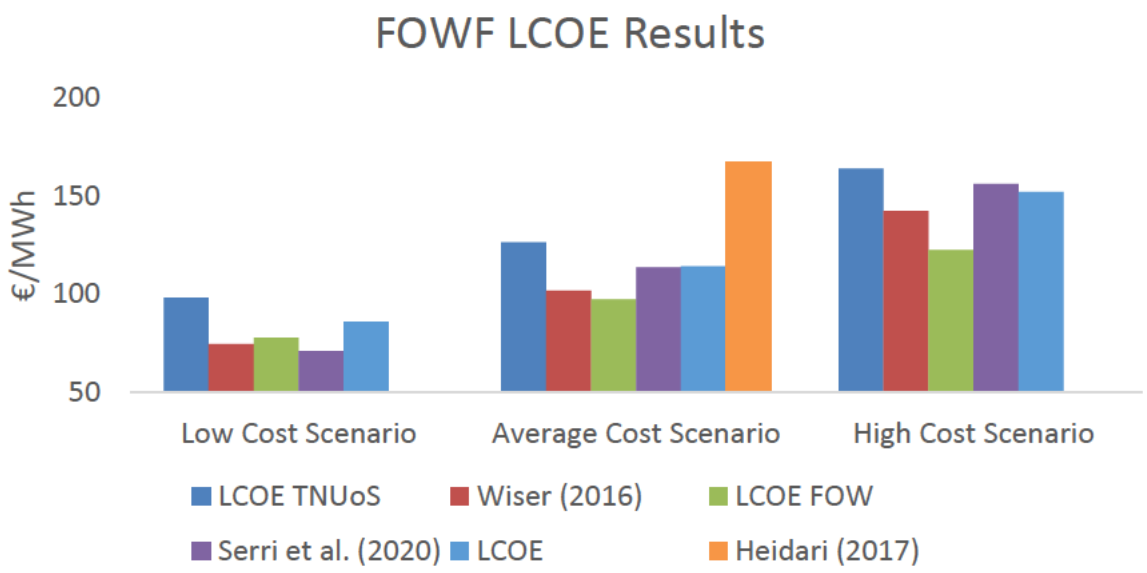

Figure 5.22: Low, Average and High LCOE scenario for FOWF compared to literature.

The $LCOE_{TNUoS}$ for floating far-offshore wind in 2030 was calculated to range between 98.11-163.80 €/ MWh. This compares well with Wiser *et al.* [256] (red bar), who had estimated floating offshore wind LCOE for 2030 based on an expert elicitation survey. However, Wiser *et al.* [256] does not include transmission connection and thus should be compared with the green bar, that represents results from this work, without cable costs (Figure 5.22). The difference is less than 5% for low and average scenario and around 14% for high scenario. Heidari [258] represents much higher cost estimation as the LCOE is calculated for 2017, rather than 2030. It has been included in the comparison to serve as a sense check as major cost reduction is expected for floating offshore wind between now and 2030 [294]. Thus, FOWF LCOE for 2030 should be lower than value by Heidari [258], which is the case as can be seen in Figure 5.22. Serri *et al.* [253] (purple bar) does not contain transmission charges and thus compares with light blue bar that represents LCOE without TNUoS charges. These values are also comparable with less than 1% on average, less than 3% on high and 21% on low cost scenario.

5.6.2 LCOH

Figure 5.23 shows CAPEX, OPEX and DECEX breakdown of the average cost scenario for hydrogen production with 1,500MW electrolyser capacity. Figure 5.23 indicates that the FOWF is the most costly, while the desalination unit is the least costly item in CAPEX. For OPEX, the topside and FOWF have similarly significant expected spending, while DECEX expenditure is mostly made of topside removal, which was expected as the wind turbines have floating substructures and can be towed back to shore.

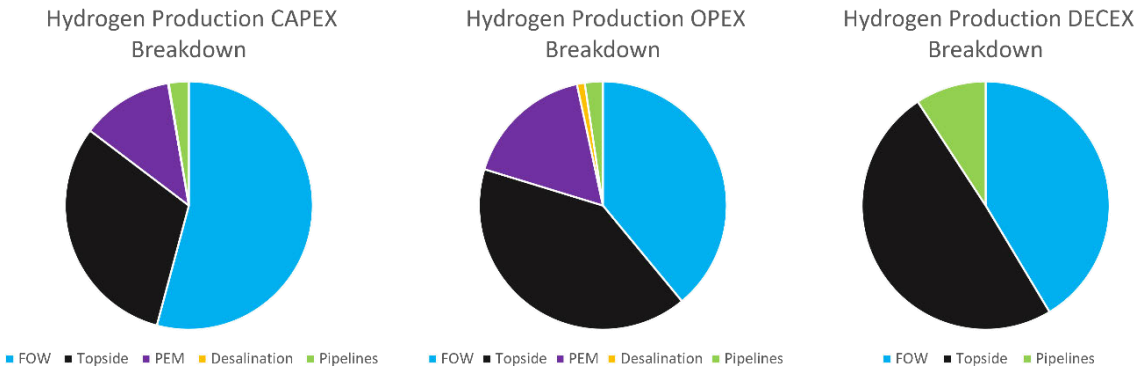

Figure 5.23: Offshore hydrogen production CAPEX, OPEX and DECEX average cost scenario breakdown.

Figure 5.24 shows comparison of the average scenario LCOH produced from offshore wind in this work with different values published in the literature. All of the values are for 2030 except for O'Kelly-Lynch *et al.* [138]. Most of the 2030 cost projections are around 100 €/MWh and above, where [295] produces hydrogen onshore and thus, does not include the cost for the offshore platform. Scottish Government [136] includes offshore hydrogen production in their scenarios, but there is no CAPEX, OPEX or DECEX for the offshore platform. Spyroudi *et al.* [57] includes the topside with 960 MW electrolyser capacity. Their value is 7% lower than the value presented for offshore hydrogen produced in this research using 957.5MW electrolyser, which is comparable.

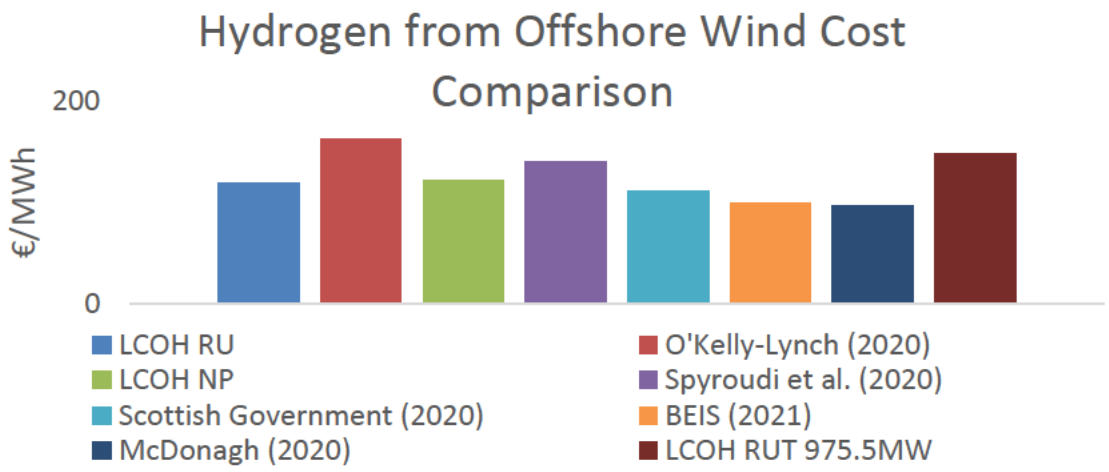

Figure 5.24: Cost comparison for offshore hydrogen.

Figure 5.25 shows comparison of LCOH calculated within this research with LCOHs produced by different hydrogen production methods published by BEIS [27]. All values are estimations for 2030. While the graph indicates blue hydrogen (SMR + CCUS) to be the most cost effective, the values do not include the gas price spike in 2021, nor the recent gas price increase due to Russian invasion on Ukraine in 2022. Since then, gas prices have spiked threefold [296], which would have an effect on the LCOH of blue hydrogen. Another cost that is not included in other hydrogen production costs is transportation to gas terminal as included in offshore hydrogen cost calculated in this work. Including this distribution cost would increase the hydrogen costs for other production methods and make them more comparable to LCOH RU and LCOH NP.

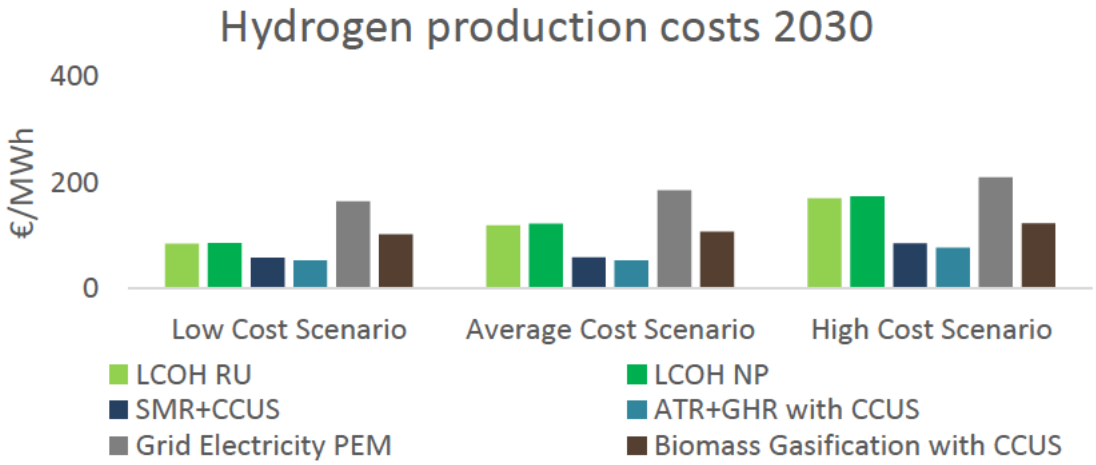

Figure 5.25: Comparison for 2030 cost projections for hydrogen by production source [27].

By 2030, EU estimates that the cost of green hydrogen could be less than 1.80 €/kg [297]. The cheapest cost calculated for offshore green hydrogen in this work is 2.72-5.17€ for $LCOH_{RU975.5MW}$. Although the 2030 price estimations calculated for offshore green hydrogen are higher right now, there will be likely improvements over the time in electrolysis technology, floating offshore wind technology and economies of scale for large scale production that have not been included in this work due to novelty and lack of available information on offshore hydrogen production.

As can be seen in Figure 5.26, building new pipelines offshore (purple bar) in comparison to re-using old pipelines offshore (red and green bar) only adds extra 2% to LCOH. This is because the old pipelines still have to be maintained and decommissioned as well as the new pipelines. The only difference in cost is CAPEX which converts into 2% increase in LCOH.

Regarding the comparison between the two ways of power transmission, hydrogen is shown to be cheaper than electricity in low and average cost scenarios for both, reused and new pipelines. However, when the cost of building a new topside is included, the cost of offshore hydrogen increases significantly above the cost of electricity for all cost scenarios.

Adding a new topside to accommodate 1500MW electrolysis capacity (light blue bar) increases LCOH between 19 and 36% across the three cost scenarios. For topsides accommodating 957.5MW electrolyser (orange bar) it’s between 8 and 28% increase in LCOH.

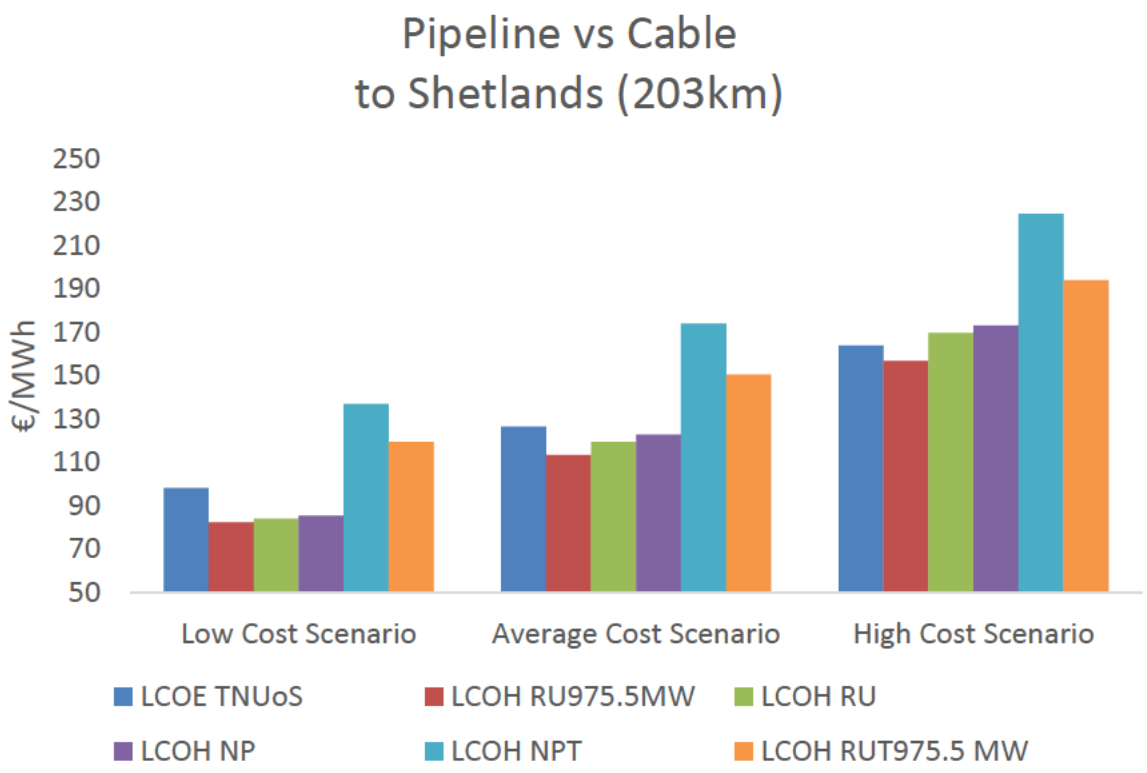

Figure 5.26: Cost comparison for energy transportation.

Figure 5.26 also shows the effect of size of the electrolyser on the size of the topside. The bigger the electrolysis capacity, the heavier the topside and thus the more expensive are the manufacturing costs and the cost of offshore operations involved in heavy topside installation. By installing smaller electrolyser capacity, there can be a smaller topside installed, which is cheaper. For example, a topside accommodating a 957.5MW electrolyser is 36% cheaper than topside accommodating 1,500MW electrolyser. However, as mentioned in Chapter 3, there is currently no platform big enough to accommodate large scale hydrogen production and an artificial island or several large platforms would be required for all hydrogen production equipment. It is expected that the centralised model will reduce footprint as the need for many individual systems such as desalination units, dryers, rectifiers, etc. will be removed. Unfortunately, at this early stage, the scale effect of footprint reduction with centralised model is yet to be explored as there is no such large-scale hydrogen production even onshore.

Another factor influencing the cost of cables vs hydrogen pipelines is TNUoS charge. It adds between 7-12% to LCOE across the three cost scenarios. TNUoS charge could be disregarded in cases where the windfarm is operating on a private cable (no grid connection, e.g. onshore hydrogen production) or the project was built elsewhere in Europe, where TNUoS charges are significantly lower, or non-existent (20 European countries including Germany, Poland and Baltic Region States) [298]. When deducting TNUoS the LCOE is comparable to LCOH (without topsides) and even 12% lower in the high cost scenario for LCOH with new built pipelines.

5.6.3 Electrolyser Size

As can be seen in Table 5.7, larger the capacity of the electrolyser, higher the LCOH. This is mostly due to the cost of the topside and the electrolyser as both these costs are proportional to the increasing capacity of the electrolyser as discussed in Sections 5.3.2.1 and 5.3.2.4. Thus, although 1300MW electrolyser annually produces slightly more kg of hydrogen than the rest (refer back to Chapter 3), LCOH does not show any benefit to this due to the increasing cost of topsides and electrolyser with increasing capacity of the electrolyser.

Table 5.7: $LCOH_{RUT}$ comparison based on electrolyser size.

Scenario	*Electrolyser size in MW*	*Hydrogen Produced t/year*	*Low Cost Scenario €/MWh*	*Average Cost Scenario €/MWh*	*High Cost Scenario €/MWh*
$LCOH_{RUT957.5MW}$	957.5	145,000	119.43	150.49	193.94
$LCOH_{RUT1100MW}$	1100	152,000	122.5	154.5	199.48
$LCOH_{RUT1300MW}$	1300	162,000	127.51	160.75	203.35
$LCOH_{RUT}$	1500	161,000	135.43	170.72	221.02

5.6.4 Magnus Case Study

While in previous sections the length of cable, re-used pipeline and new-built pipeline was 203km for all, in real life projects, this will hardly be the case. As mentioned in Section 5.3.1.2, the closest transmission cable connection for the 1.5 GW Magnus windfarm, would have to be Banff in mainland Scotland (approximately 491km), while a new pipeline connection could go to the existing Sullom Voe gas terminal in Shetland Islands (approximately 190km). Figure 5.27 shows the comparison of results for the Magnus case study.

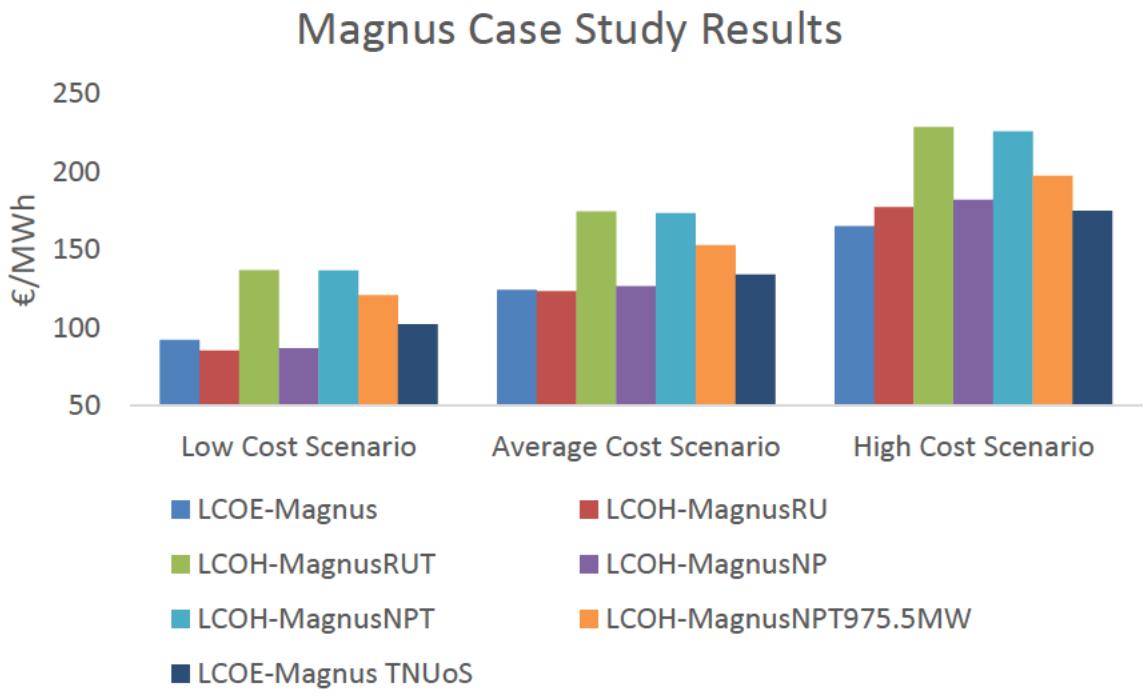

Figure 5.27: Magnus case study results.

When comparing re-using pipelines vs building new, the difference is within 3% mostly due to OPEX and DECEX being distance dependent. As the combination of PL164 and FLAGS is significantly longer than pipeline to Shetland, from an economic perspective, there is not much difference between re-using or building new. From the environmental perspective, it would be favourable to re-use existing pipelines (if in a good state) to avoid disrupting marine life with construction noise and damage to the sea bed. Additionally, existing substructures serve as artificial reefs creating nurseries for marine life that will be disrupted when these structures are removed. From a structural integrity point of view, it might be beneficial to build new pipelines as they will have a known structural integrity, they will be purpose built and will last longer. The existing pipelines could be used in the meantime while the new ones are being built depending on their current usage. Even hydrogen blending in existing pipelines could help speed up hydrogen economy.

The low cost scenario shows that LCOH (without building new topsides) is lower than LCOE even without TNUoS charges. The results are similar for the average scenario as well except this time LCOE without TNUoS is comparable. In the high cost scenario, $LCOH\text{-}Magnus_{RU,}$ $LCOH\text{-}Magnus_{NP}$ and $LCOE_{TNUoS}$ become comparable.

When adding costs for building the topside, LCOH becomes significantly more expensive increasing the cost of energy transportation by 8-28% using 957.5MW electrolyser or 19-36% using 1500MW electrolyser. This suggests that while large-scale non-grid connected centralised offshore hydrogen production is expected to be more expensive than LCOE in 2030, co-locating hydrogen production with wind turbines might be competitive with the cable alternative. However, O&M within this work does not include serving several individual units in different locations, which should be considered in any future work investigating WTG co-located hydrogen production.

5.6.5 Sensitivity Analysis

5.6.5.1 Discount Rate

Table 5.8 shows sensitivity to discount rate across different cost scenarios, while Figure 5.28 shows the sensitivity of the average cost scenario LCOE to discount rate varying between 3-12%. Table 5.8 indicates that changing discount rate has similar effect across the different cost scenarios (8-9% change). As can be seen in Figure 5.28, 2% increase in discount rate results in 9% increase in LCOE and 3% increase in discount rate, translates into 13% increase in LCOE.

Table 5.8: Change in LCOE for floating offshore wind (203km cable) with changing discount rate.

LCOE/r	*5%*	*7%*	*%change*
High/€/MWh	150.03	163.80	8
Average/€/MWh	115.15	126.30	9
Low/€/MWh	89.27	98.11	9

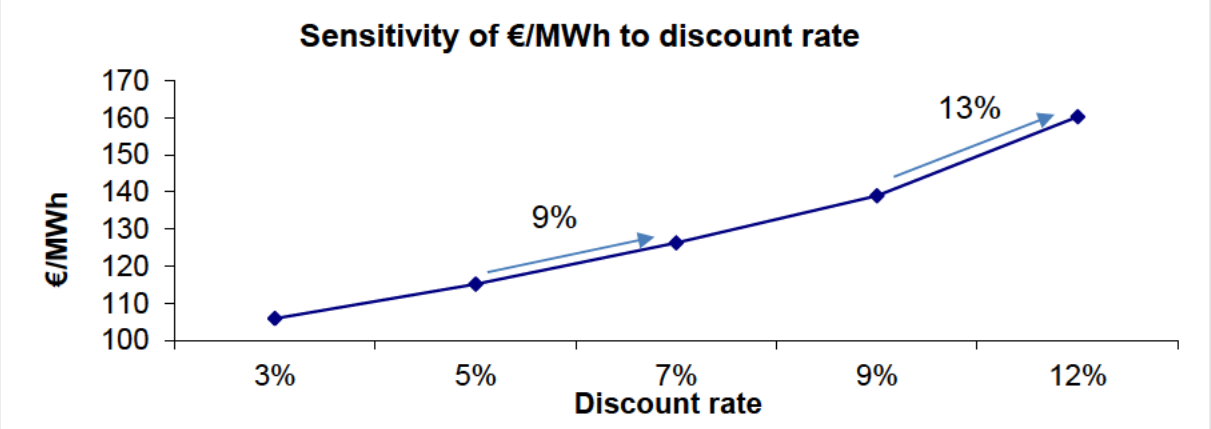

Figure 5.28: LCOE sensitivity to discount rate.

Figure 5.29 presents varying discount rates for both floating wind and hydrogen production in sensitivity analysis. Both Spyroudi *et al.* [57] and Scottish Government [136] use the same value of r for both the LCOE and LCOH calculation, which might be disputable as floating offshore wind is more established than offshore hydrogen production and thus is likely to involve less risk. As shown in Figure 5.29, 2% change in discount rate for hydrogen production, causes around 3% change in LCOH while 2% change in discount rate for floating offshore wind, causes 5-6 % change in LCOH.

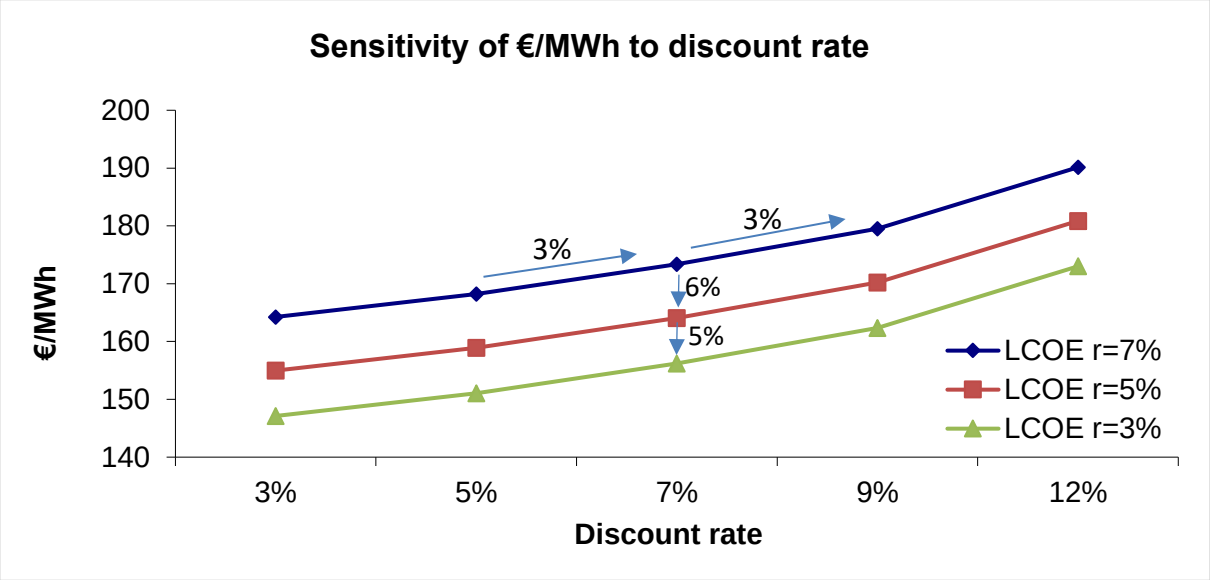

Figure 5.29: LCOH sensitivity to r with different LCOE discount rates.

5.6.6 Limitations

There are limitations to this work due to the breadth of the research topic and limited time available for completion. One such limitation is the design life for pipelines as it was assumed to be the entire lifetime of the hydrogen production project for both re-used and new pipelines. While this is possible for the new pipelines, it is questionable for the re-used pipelines. This could have been included as an extra O&M cost for re-used pipelines, but O&M was calculated based on length and wall thickness only, which limits this work and makes LCOH for re-used pipelines more favourable. Thus, future work could calculate and include a percentage of added O&M cost to allow for safe re-use of pipelines.

5.7 Conclusion and Future Work

This chapter compares economic feasibility of two routes to transfer energy to shore. A more conventional way through cables in the form of electricity, and a more novel route, by using pipelines to transfer renewable electricity in the form of green hydrogen.

Both hydrogen scenarios whether re-using oil and gas pipelines or building new pipelines are cheaper than using cables in low and average cost scenarios for large scale floating offshore wind farm. The cost for offshore green hydrogen has been calculated to range between 84-170 €/MWh for 1500MW electrolysis capacity, re-using pipelines and 137-225 €/MWh for 1500MW electrolysis capacity including new pipelines and a platform.

However, cables become a cheaper option in the high cost scenario and as soon as building a new topside is involved. Adding a new topside to accommodate 1500MW electrolysis capacity increases LCOH between 19 and 36% across the three cost scenarios. For a topside accommodating a 957.5MW electrolyser there is between 8 and 28% increase in LCOH.

When considering building new pipelines rather than re-using old pipelines due to pressure limitations, to avoid hydrogen embrittlement in high grade steel pipelines, or unknown structural integrity of old pipelines, it has been found that building new pipelines does not add much to LCOH. This is because the old pipelines still have to be maintained and decommissioned as well as the new pipelines. The only difference in cost is CAPEX which converts into 2% increase in LCOH. The arguments for re-using gas pipelines would be the environment and time. From the environmental perspective, it would be favourable to re-use existing pipelines (if in a good state) to avoid disrupting marine life with construction noise and damage to the sea bed, while re-using already available existing pipelines would speed up decarbonisation by stimulating earlier uptake of hydrogen by increasing supply.

While this work used levelised cost of energy to compare the two energy transfer methods and help developers to decide on building far offshore windfarms, future work could include economic analysis looking more into profitability of a projected investment. This could be in the form of net present value calculations including further market and policy tools analysis such as hydrogen contracts for difference.

Another aspect not covered by this research is transportation via other means such as shipping. Future work could involve techno-economic comparison between transportation of hydrogen through pipelines and ships as well as direct use of hydrogen offshore.

While this thesis slightly touches the centralised versus co-located hydrogen production question, future work could take the basis introduced within and look in greater depth at advantages and disadvantages of each method. Aspects such as economies of scale, footprint reduction, control systems, O&M, and efficiency should be considered to compare the two.

Although it was concluded that in 2030, LCOH for centralised hydrogen production is higher than LCOE, offshore green hydrogen is still an interesting commodity, and such project might still go forward for several reasons such as:

- Significant amount of hydrogen needed to decarbonise hard to electrify sectors
- Increasing amount of RE connected to the grid, causing less buildable RE projects in the future, unless alternative methods of power transportation, such as hydrogen and its derivatives, are proposed
- Hydrogen can enable international renewable energy export
- Local island communities might not support projects that take their renewable resources and send them to different parts of the country rather than supporting local decarbonisation projects

CHAPTER 6 - CONCLUSION

This section summarises the work done in this thesis, underlines major outcomes and highlights those areas that need further work done, to enable large scale offshore green hydrogen production re-using oil and gas infrastructure.

The work presented in Chapter 2 mapped possible sites for offshore hydrogen production in Scotland, outlined the methodology for detailed resource assessment, wind farm design and introduced losses and uncertainty that need to be considered. The major outcomes of the chapter were:

- The four areas identified where existing O&G infrastructure coincides with already existing or potential offshore wind sites.
- The observation that the sites are in deep water indicating the use of floating wind technology for production of offshore hydrogen on O&G infrastructure and that none of the draft plan options for tidal and wave developments were located in proximity of O&G infrastructure, which is going to change with the upcoming INTOG.
- Some of the platforms identified especially in Area A have foundations heavier than 10,000 tonnes meaning there might not be any economic advantage to re-using the foundations. However, there might be an economic advantage to hydrogen production operator not having to build new ones. The opposite applies to Areas C and D.
- The importance of discussion between RE and O&G industry to utilise the O&G infrastructure for hydrogen production before suitable sites identified are decommissioned.
- The importance of integrating the design of the hydrogen plant with the windfarm at an early stage to optimise the performance of both as the availability of the electrolyser can have significant impact on CF when no grid is available.

Chapter 3 looked into available literature investigating offshore hydrogen production, provided insights into balance of plant for offshore green hydrogen production and methodology to calculate the size of the electrolyser and hydrogen flow rate.

Major findings include:

- PEM electrolysis in combination with reverse osmosis desalination is currently the most suitable way to produce green hydrogen offshore.
- For large scale non grid connected windfarms that are located far offshore, a scenario where electrolysers are located on a wind turbine could be more suitable, as this would allow for bigger electrolysis capacity, albeit individual electrolysers with their BoP would be required to fit on the turbine platforms.
- Hourly hydrogen flow rate was calculated to vary between 30,000-17,230 kg/h for a 1500MW electrolyser, and 19,150-17,227 kg/h for 957.5MW electrolyser.

Chapter 4 investigates the technical feasibility of re-using gas pipelines for transportation of hydrogen from a material and thermo-hydraulic perspective. It takes flow rates from a 1.5 GW theoretical windfarm calculated in Chapter 3 and uses them to simulate hydrogen transportation in two case study North Sea pipelines. Major conclusions of this chapter are:

- Based on an extensive literature search, it is concluded that it is possible to re-use oil and gas pipelines for hydrogen considering material as a single factor even if they are of higher grade than X52 as long as the operating pressure is reduced. However, the pipelines would then be able to carry only a fraction of the hydrogen that they could at higher pressures, which reduces the design energy supply of the pipelines when transporting hydrogen rather than natural gas.
- It is possible to re-use gas pipelines from a thermo-hydraulic perspective even without requiring the use of a compressor on the platform. However, substantial summer and winter hydrogen production differences cause efficiency issues, leading to substantial storage requirements.
- PIPESIM simulations showed that 20 bar would not be sufficient to transport the hydrogen produced from the 1.5GW windfarm through the shorter feeder pipelines such as PL164, while the maximum assumed pressure for the PEM electrolyser, 50 bar, allows the transportation of hydrogen from 1.5GW wind farm for both feeder and transmission pipelines such as PL164 and FLAGS.

- For PL164, 50 bar is more suitable for the range of mass flow rates expectable from a 1.5 GW windfarm. The problem comes with the longer transmission pipeline, FLAGS, where transportation of hydrogen at 50bar takes anywhere from 38-67 hours, which increases even further at 100bar (75.6-133 hours) due to the line being underutilised, requiring higher hydrogen flow rate. This could be solved by including storage to be able to transport higher flow rates in periods with lower wind in the summer.
- While 100 bar significantly increases the maximum mass flow rate transferred through the pipelines, which is important as hydrogen has lower heat capacity per volume in comparison to natural gas, it also significantly increases the transportation time, and would not be an optimal solution for a 1.5GW wind farm in current case study.
- New shorter pipelines could be built to three gas terminals St Fergus, Flotta and Sullom Voe that would all be suitable due to upcoming hydrogen projects in all three.
- The advantage of building new pipelines is that new pipelines can be built from material with suitable steel grade operating at higher pressure and known pipeline integrity. The disadvantage of purpose build pipeline would be the limited capacity design, which would disable other future hydrogen production facilities in the vicinity to use it for hydrogen transport, unless it would be designed for larger amounts of hydrogen, which would increase the cost and decrease the efficiency.

Chapter 5 compares economic feasibility of two routes to transfer energy to shore. A more conventional way through cables in the form of electricity, and a more novel route, by using pipelines to transfer renewable electricity in the form of green hydrogen. The major conclusions are:

- Both hydrogen scenarios whether re-using oil and gas pipelines or building new pipelines are cheaper than using cables in low and average cost scenarios for large scale floating offshore wind farm. The cost for offshore green hydrogen has been calculated to range between 84-170 €/MWh for 1500MW electrolysis capacity, re-using pipelines and 137-225 €/MWh for 1500MW electrolysis capacity including new pipelines and a platform.

- Cables become a cheaper option in the high cost scenario and as soon as building a new topside is involved. Adding a new topside to accommodate 1500MW electrolysis capacity increases LCOH between 19 and 36% across the three cost scenarios. For a topside accommodating a 957.5MW electrolyser there is between 8 and 28% increase in LCOH.
- The advantages of building new pipelines rather than re-using old pipelines are avoiding pressure limitations and hydrogen embrittlement in high grade steel pipelines, as well as unknown structural integrity of old pipelines.
- It has been found that building new pipelines to shore does not add much to LCOH because the old pipelines still have to be maintained and decommissioned as well as the new pipelines. The only difference in cost is CAPEX which converts into 2% increase in LCOH.
- The arguments for re-using gas pipelines are the environment and time. From the environmental perspective, it would be favourable to re-use existing pipelines (if in a good state) to avoid disrupting marine life with construction noise and damage to the sea bed, while re-using already available existing pipelines would speed up decarbonisation by stimulating earlier uptake of hydrogen by increasing supply.

Although it was concluded that in 2030, LCOH for centralised hydrogen production is higher than LCOE, offshore green hydrogen is still an interesting commodity, and such project might still go forward for several reasons such as:

- Significant amount of hydrogen needed to decarbonise hard to electrify sectors
- Increasing amount of RE connected to the grid, causing less buildable RE projects in the future, unless alternative methods of power transportation, such as hydrogen and its derivatives, are proposed
- Hydrogen can enable international renewable energy export
- Local island communities might not support projects that take their renewable resources and send them to different parts of the country rather than supporting local decarbonisation projects

6.1 Future Work

As identified within the individual chapters, there are still many areas that require further research to enable large scale offshore green hydrogen production re-using oil and gas infrastructure.

Chapter 2 suggests that future research should include QGIS analysis with INTOG areas, or a completely new user accountancy map including areas that were under O&G exclusion zones during the time of this research. Future work could also include tidal and wave energy converters as this technology is evolving and could provide smaller hydrogen production for the use of decarbonisation of O&G platforms or to fuel O&M ships. Last challenge identified within Chapter 2 that would benefit from further work was the effect of connecting hydrogen plant to a wind farm on CF with further research looking into connection issues, losses and availability issues in more detail.

Chapter 3 recommends that techno economic analysis into different hydrogen carriers such as ammonia, synthetic natural gas, and liquid hydrocarbons should be investigated in the future research. Other areas of offshore hydrogen production that would benefit from further research are direct sea water electrolysis, investigation into electrolysers suitable for offshore environment, and investigation into advantages and disadvantages of centralised electrolysis on a platform versus wind turbine co-located electrolysers. Further work into challenges such as black start, AC to DC conversion and system stability as well as research into offshore hydrogen storage to help to offset the difference between summer and winter hydrogen production, would also allow for faster commercialisation of offshore hydrogen production.

Chapter 4 concludes that future work could include transient phenomena flow model analysing real time operation, hydrogen tracking, leakage, and metering for natural gas-hydrogen blends as well as pure hydrogen. This is the natural next step after feasibility studies, to enable safe hydrogen pipeline operation.

Both Chapter 3 and 4 would also benefit from further research work on safety aspects associated with hydrogen production and transportation. These could be sourced from existing oil and gas safety aspects as well as standards such as Hydrogen Technologies Code by National Fire Protection Association (NFPA) [299].

Chapter 5 proposes economic analysis looking more into profitability of a projected investment to be further investigated. This could be in the form of net present value calculations including further market and policy tools analysis such as hydrogen contracts for difference. Another aspect not covered by this research is transportation via other means such as shipping. Future work could involve techno-economic comparison between transportation of hydrogen through pipelines and ships as well as direct use of hydrogen offshore and further investigate centralised and co-located hydrogen production taking into consideration aspects such as economies of scale, footprint reduction, control systems, O&M, and efficiency. Lastly, future work could use information from this research and make a decision based tool to determine at what distance it is better to transfer power through cables, pipelines or shipping including different hydrogen derivatives.

BIBLIOGRAPHY

[1] IPCC, “Climate change 2022: Impacts, adaptation, vulnerability,” 2022. Accessed: May 24, 2022. [Online]. Available: https://www.ipcc.ch/report/ar6/wg2/downloads/report/IPCC_AR6_WGII_FinalDraft_FullReport.pdf.

[2] CCC, “Net Zero. The UK’s contribution to stopping global warming.,” Committee on Climate Change, London, 2019.

[3] COP, “Glasgow Climate Pact,” Glasgow, 2021. Accessed: Jun. 11, 2022. [Online]. Available: https://unfccc.int/sites/default/files/resource/cop26_auv_2f_cover_decision.pdf.

[4] European Commission, “The European Green Deal.” European Comission, Brussels, 2019, Accessed: May 20, 2022. [Online]. Available: https://eur-lex.europa.eu/legal-content/EN/TXT/?qid=1576150542719&uri=COM%3A2019%3A640%3AFIN.

[5] European Commission, “REPowerEU plan.” European Comission, Brussels, 2022, Accessed: May 20, 2022. [Online]. Available: https://eur-lex.europa.eu/legal-content/EN/TXT/?uri=COM%3A2022%3A230%3AFIN&qid=1653033742483.

[6] HM Government, “British energy security strategy,” 2022. Accessed: May 23, 2022. [Online]. Available: https://assets.publishing.service.gov.uk/government/uploads/system/uploads/attachment_data/file/1069969/british-energy-security-strategy-web-accessible.pdf.

[7] BEIS, “The ten point plan for a green industrial revolution,” 2020. Accessed: May 23, 2022. [Online]. Available: https://assets.publishing.service.gov.uk/government/uploads/system/uploads/attachment_data/file/936567/10_POINT_PLAN_BOOKLET.pdf.

[8] HM Government, “Net Zero Strategy: Build back greener,” 2021. Accessed: May 23, 2022. [Online]. Available: https://assets.publishing.service.gov.uk/government/uploads/system/uploads/attachment_data/file/1033990/net-zero-strategy-beis.pdf.

[9] Scottish Parliament, “Climate change (emissions reduction targets) (Scotland) bill.” 2019, Accessed: Feb. 28, 2019. [Online]. Available: https://www.parliament.scot/parliamentarybusiness/Bills/108483.aspx.

[10] Scottish Government, “Scottish greenhouse gas statistics: 1990-2019,” 2021. Accessed: May 26, 2022. [Online]. Available: https://www.gov.scot/publications/scottish-greenhouse-gas-statistics-1990-2019/#:~:text=The Baseline Period uses 1990,sulphur hexafluoride and nitrogen trifluoride.

[11] CCC, “Progress reducing emissions in Scotland – 2021 Report to Parliament,” 2021. Accessed: May 23, 2022. [Online]. Available: https://www.theccc.org.uk/publication/progress-reducing-emissions-in-scotland-2021-report-to-parliament/.

[12] IEA Hydrogen, “Global trends and outlook for hydrogen,” 2017. Accessed: Oct. 29, 2019. [Online]. Available: https://iea.blob.core.windows.net/assets/9e3a3493-b9a6-4b7d-b499-7ca48e357561/The_Future_of_Hydrogen.pdf.

[13] Ministerial Council on Renewable Energy Hydrogen and Related Issues, “Basic hydrogen strategy,” 2017. Accessed: Jun. 10, 2022. [Online]. Available: https://policy.asiapacificenergy.org/sites/default/files/Basic Hydrogen Strategy %28EN%29.pdf.

[14] J. Eun Ha, “Hydrogen economy plan in Korea,” 2019. Accessed: Jun. 10, 2022. [Online]. Available: https://www.rvo.nl/sites/default/files/2019/03/Hydrogen-economy-plan-in-Korea.pdf.

[15] Council of Australian Government, “Australia’s National Hydrogen Strategy,” 2019. Accessed: Jun. 10, 2022. [Online]. Available: https://www.industry.gov.au/sites/default/files/2019-11/australias-national-hydrogen-strategy.pdf.

[16] Government of Canada, “Hydrogen strategy for Canada,” 2020. Accessed: Jun. 10, 2022. [Online]. Available: https://www.nrcan.gc.ca/sites/nrcan/files/environment/hydrogen/NRCan_Hydrogen Strategy for Canada Dec 15 2200 clean_low_accessible.pdf.

[17] Ministry of Energy, “National Green Hydrogen Strategy,” 2020. Accessed: Jun. 10, 2022. [Online]. Available: https://energia.gob.cl/sites/default/files/national_green_hydrogen_strategy_-_chile.pdf.

[18] IEA, “Global hydrogen review 2021,” 2021. Accessed: May 20, 2022. [Online]. Available: https://iea.blob.core.windows.net/assets/5bd46d7b-906a-4429-abda-e9c507a62341/GlobalHydrogenReview2021.pdf.

[19] The Scottish Government, “Scottish Government Hydrogen Policy Statement,” 2020. Accessed: May 26, 2022. [Online]. Available: https://www.gov.scot/publications/scottish-government-hydrogen-policy-statement/.

[20] HM Government, “UK hydrogen strategy,” 2021. doi: 10.1002/cind.859_6.x.

[21] M.-R. de Valladares, “Global trends and outlook for hydrogen.” 2017, Accessed: Mar. 28, 2019. [Online]. Available: http://ieahydrogen.org/pdfs/Global-Outlook-and-Trends-for-Hydrogen_Dec2017_WEB.aspx.

[22] Wood, “Assessing the cost reduction potential and competitiveness of novel (next generation) UK carbon capture technology,” 2018. Accessed: May 06, 2019. [Online]. Available: https://assets.publishing.service.gov.uk/government/uploads/system/uploads/attachment_data/file/864688/BEIS_Final_Benchmarks_Report_Rev_4A.pdf.

[23] M. Ball and M. Weeda, “The hydrogen economy – Vision or reality?,” *Int. J. Hydrogen Energy*, vol. 40, no. 25, pp. 7903–7919, 2015, doi: https://doi.org/10.1016/j.ijhydene.2015.04.032.

[24] D. Sadler *et al.*, “H21 Leeds city gate.” p. 382, 2016, Accessed: Mar. 29, 2019. [Online]. Available: https://www.northerngasnetworks.co.uk/wp-content/uploads/2017/04/H21-Report-Interactive-PDF-July-2016.compressed.pdf.

[25] Sturgeon Refinery, “Carbon capture and storage,” 2022. https://nwrsturgeonrefinery.com/project/carbon-capture-and-storage/ (accessed Sep. 29, 2022).

[26] IEA, “Energy technology perspectives 2020 - Special report on carbon capture utilisation and storage,” 2020. doi: 10.1787/208b66f4-en.

[27] BEIS, “Hydrogen production costs by production source,” 2021. Accessed: Mar. 07, 2022. [Online]. Available: https://www.iea.org/data-and-statistics/charts/hydrogen-production-costs-by-production-source-2018.

[28] A. Velazquez Abad and P. E. Dodds, “Green hydrogen characterisation initiatives: Definitions, standards, guarantees of origin, and challenges,” *Energy Policy*, vol. 138, p. 111300, 2020, doi: https://doi.org/10.1016/j.enpol.2020.111300.

[29] M. M. Rashid, M. K. Al Mesfer, H. Naseem, and M. Danish, “Hydrogen production by water electrolysis: A review of alkaline water electrolysis, PEM water electrolysis and high temperature water electrolysis,” *Int. J. Eng. Adv. Technol.*, vol. 4, no. 3, pp. 2249–8958, 2015.

[30] A. Buttler and H. Spliethoff, “Current status of water electrolysis for energy storage, grid balancing and sector coupling via power-to-gas and power-to-liquids: A review,” *Renew. Sustain. Energy Rev.*, vol. 82, no. February 2017, pp. 2440–2454, 2018, doi: 10.1016/j.rser.2017.09.003.

[31] National Grid, “The hydrogen colour spectrum,” 2022. https://www.nationalgrid.com/stories/energy-explained/hydrogen-colour-spectrum (accessed May 25, 2022).

[32] IEA, “Iron and steel technology roadmap,” 2020. Accessed: May 20, 2022. [Online]. Available: https://www.iea.org/reports/iron-and-steel-technology-roadmap.

[33] Hybrit, “Hybrit fossil-free steel.” 2019, Accessed: Mar. 29, 2019. [Online]. Available: http://www.hybritdevelopment.com/steel-making-today-and-tomorrow.

[34] J. Braennberg Fogelstroem, “Experimental study of the temperature profile in an iron ore pellet during reduction using hydrogen gas,” KTH Royal Institute of Technology, Stockholm, 2020. Accessed: Jun. 17, 2022. [Online]. Available: http://www.diva-portal.org/smash/get/diva2:1389477/FULLTEXT02.pdf.

[35] IEA, “Chemicals,” Paris, 2021. Accessed: May 20, 2022. [Online]. Available: https://www.iea.org/reports/chemicals.

[36] A. M. Bazzanella and F. Ausfelder, “Low carbon energy and feedstock for the European chemical industry,” 2017. Accessed: Mar. 29, 2019. [Online]. Available: https://cefic.org/app/uploads/2019/01/Low-carbon-energy-and-feedstock-for-the-chemical-industry-DECHEMA_Report-energy_climate.pdf.

[37] R. Markillie, “World’s largest hydrogen electrolysis in Shell’s Rhineland refinery.” 2018, Accessed: Mar. 29, 2019. [Online]. Available: http://www.itm-power.com/news-item/worlds-largest-hydrogen-electrolysis-in-shells-rhineland-refinery.

[38] Z. Byrum, H. Pilorge, and J. Wilcox, “Technological pathways for decarbonizing petroleum refining.,” Washington DC, 2021. Accessed: Jun. 17, 2022. [Online]. Available: https://files.wri.org/d8/s3fs-public/2021-10/technological-pathways-decarbonizing-petroleum-refining.pdf?VersionId=oCHsIJ44.gemRzzrXlix7dYSIQD0OFrW.

[39] Energy Networks Association, “Britains hydrogen blending delivery plan,” London, 2021. Accessed: May 23, 2022. [Online]. Available: https://www.energynetworks.org/industry-hub/resource-library/britains-hydrogen-blending-delivery-plan.pdf.

[40] SGN, “A world-first green hydrogen gas network in the heart of Fife,” 2022. https://h100fife.co.uk/ (accessed May 26, 2022).

[41] BEIS, “Hy4Heat report,” 2022. Accessed: May 30, 2022. [Online]. Available: https://static1.squarespace.com/static/5b8eae345cfd799896a803f4/t/626aa96961a39b380f82717d/1651157358782/Final+Final+Report.pdf.

[42] Innovate UK, “HyDime,” 2018. https://hydime.co.uk/ (accessed May 26, 2022).

[43] H2Bus, “Presenting H2 bus consortium,” 2022. https://h2bus.eu/ (accessed May 26, 2022).

[44] ZeroAvia, “The future of flight is renewable hydrogen,” 2022. https://www.zeroavia.com/ (accessed May 26, 2022).

[45] Alstom, “Coradia iLint^{TM} – the world’s 1st hydrogen powered train,” 2022. https://www.alstom.com/solutions/rolling-stock/coradia-ilinttm-worlds-1st-hydrogen-powered-train (accessed May 26, 2022).

[46] IEA, “The future of hydrogen,” 2019. Accessed: May 20, 2022. [Online]. Available: https://iea.blob.core.windows.net/assets/9e3a3493-b9a6-4b7d-b499-7ca48e357561/The_Future_of_Hydrogen.pdf.

[47] Orkney Islands Council, “Big Hit,” 2018. https://www.orkney.gov.uk/Service-Directory/Renewable/big-hit.htm#:~:text=Hydrogen will be produced in,fuels traditionally used for heat. (accessed Apr. 28, 2022).

[48] FCHJU, “The Hypster project,” 2020. https://hypster-project.eu/ (accessed May 27, 2022).

[49] SHFCA, “Green hydrogen for green distilleries,” 2021. http://www.shfca.org.uk/news/2021/1/8/green-hydrogen-for-green-distilleries (accessed May 27, 2022).

[50] OGUK, “Decommissioning insight 2021,” 2021. Accessed: Jan. 24, 2022. [Online]. Available: https://oilandgasuk.cld.bz/OGUK-Decom-Insight-Report-2021/35/.

[51] C. Jepma, G.-J. Kok, M. Renz, M. van Schot, and K. Wouters, “North Sea Energy D3.6 Towards sustainable energy production on the North Sea-Green hydrogen production and CO 2 storage: onshore or offshore?,” 2018. Accessed: Oct. 29, 2019. [Online]. Available: https://www.north-sea-energy.eu/documents/North Sea Energy I - D3.1.2-3.1.4, D3.1.6 Towards sustainable energy production on the North Sea_final-public.pdf.

[52] C. J. Jepma, “Smart sustainable combinations in the North Sea Area (NSA),” Energy Delta Institute, Groningen, 2015.

[53] C. Jepma and M. Van Schot, “On the economics of offshore energy conversion: smart combinations_Converting offshore wind energy into green hydrogen on existing oil and gas platforms in the North Sea,” 2017. Accessed: Oct. 19, 2019. [Online]. Available: https://www.gasmeetswind.eu/wp-content/uploads/2017/05/EDI-North-Sea-smart-combinations-final-report-2017.pdf.

[54] North Sea Energy, “Synthesis paper NSE II Hybrid offshore energy transition options-The merits and challenges of combining offshore system integration options,” 2019. Accessed: Jun. 03, 2019. [Online]. Available: https://www.north-sea-energy.eu/results-nse2.htm.

[55] World Energy Council, “Bringing North Sea energy ashore efficiently,” World Energy Council Netherlands, Tilburg, 2017.

[56] A. van Wijk and C. Hellinga, “Hydrogen, the key to the energy transition,” 2018. Accessed: Oct. 05, 2019. [Online]. Available: http://edepot.wur.nl/333952.

[57] A. Spyroudi, K. Stefaniak, D. Wallace, S. Mann, G. Smart, and Z. Kurban, “Offhore wind and hydrogen. Solving the integration challenge.,” 2020. Accessed: Aug. 25, 2020. [Online]. Available: https://ore.catapult.org.uk/wp-content/uploads/2020/09/Solving-the-Integration-Challenge-ORE-Catapultr.pdf.

[58] Element Energy, “Gigastack phase 2: Pioneering UK renewable hydrogen,” 2021. Accessed: Jun. 14, 2022. [Online]. Available: https://gigastack.co.uk/content/uploads/2021/11/Gigastack-Phase-2-Public-Report_FINAL_.pdf.

[59] L. Collins, “Offshore wind to power giant green-hydrogen carbon-neutral aviation-fuel plant,” 2020. https://www.rechargenews.com/transition/offshore-wind-to-power-giant-green-hydrogen-carbon-neutral-aviation-fuel-plant/2-1-696907 (accessed May 27, 2022).

[60] Neptune Energy, “The world’s first offshore green hydrogen plant,” 2019. https://www.neptuneenergy.com/esg/climate-change-and-environment/poshydon-hydrogen-pilot (accessed Oct. 07, 2020).

[61] Neptune Energy, “PosHYdon pilot offshore green hydrogen,” 2019. Accessed: Oct. 07, 2020. [Online]. Available: https://www.nstauthority.co.uk/media/6220/ogauthoritysharepointcom-ssl-davwwwroot-sites-ecm-tbw3-documents-files-exchange-malcolm-workshop-slides-301019-neptune.pdf.

[62] GCE Ocean Technology, “Deep Purple Project collaboration,” 2020. https://www.gceocean.no/news/posts/2020/july/deep-purple-project-collaboration/ (accessed May 27, 2022).

[63] ERM, “Dolphyn hydrogen phase 1 - Final report,” 2019. Accessed: Sep. 25, 2020. [Online]. Available: https://www.gov.uk/government/publications/hydrogen-supply-competition.

[64] A. S. Bull and M. S. Love, “Worldwide oil and gas platform decommissioning: A review of practices and reefing options,” *Ocean Coast. Manag.*, vol. 168, no. October 2018, pp. 274–306, 2019, doi: 10.1016/j.ocecoaman.2018.10.024.

[65] J. M. Lawrence and P. G. Fernandes, “A typology of North Sea oil and gas platforms,” *Sci. Rep.*, vol. 12, no. 1, pp. 1–7, 2022, doi: 10.1038/s41598-022-11975-2.

[66] OGUK, “Decommissioning insight 2018,” 2018. Accessed: Oct. 29, 2019. [Online]. Available: https://oilandgasuk.cld.bz/Decommissioning-Insight-2018.

[67] BEIS, “Decommissioning of offshore oil and gas installations and pipelines,” 2018. Accessed: Mar. 25, 2020. [Online]. Available: https://www.gov.uk/beis.

[68] ABB, “Offshore oil and gas decommissioning,” 2015. Accessed: Mar. 25, 2020. [Online]. Available: https://library.e.abb.com/public/d689c2f70f0c447586610ac566c9aa7e/ABB-Offshore-Oil-and-Gas-Decommissioning-2015.pdf.

[69] Arup, “Decommissioning in the North Sea. Review of decommissioning capacity,” 2014. Accessed: Mar. 24, 2020. [Online]. Available: https://www.arup.com/perspectives/publications/research/section/decommissioning-in-the-north-sea.

[70] BEIS, “Re-use of oil and gas assets for carbon capture usage and storage,” London, 2020. Accessed: Aug. 21, 2020. [Online]. Available: https://assets.publishing.service.gov.uk/government/uploads/system/uploads/attachment_data/file/909642/CCUS-government-response-re-use-of-oil-and-gas.pdf.

[71] D. Jelenova, A. Mortimer, J. Race, P. Thies, and D. Mignard, “Resource Assessment for Offshore Green Hydrogen Production,” in *Wind Europe Offshore 2019*, 2019, p. 12, [Online]. Available: https://pure.strath.ac.uk/ws/portalfiles/portal/111396352/Jelenova_etal_WindEurope_2019_Resource_assessment_for_offshore_green_hydrogen_production.pdf.

[72] F. Baldi *et al.*, “Optimisation-based system designs for deep offshore wind farms including power to gas technologies,” *Appl. Energy*, vol. 310, no. December 2021, p. 118540, 2022, doi: 10.1016/j.apenergy.2022.118540.

[73] Marine Scotland, “Energy resources Areas of Search refined from offshore wind scoping study 2018,” 2018. Accessed: Mar. 13, 2019. [Online]. Available: https://spatialdata.gov.scot/geonetwork/srv/eng/catalog.search#/metadata/Marine_Scotland_FishDAC_12106.

[74] Scottish Power, “Outdoor Pursuits,” 2022. https://www.whiteleewindfarm.co.uk/outdoor-pursuits (accessed Jun. 18, 2022).

[75] ESRI, “ArcGIS Online,” 2022. https://www.esri.com/en-us/arcgis/products/arcgis-online/overview (accessed Jun. 18, 2022).

[76] Marine Scotland, “Marine Scotland,” 2022. https://marinescotland.atkinsgeospatial.com/nmpi/ (accessed Jun. 18, 2022).

[77] M. Kennedy, *Introducing geographic information systems with ArcGIS*, 2nd ed. Hoboken: John Wiley & Sons, Inc, 2009.

[78] E. Cantero *et al.*, “Energy yield Prediction of offshore wind farm clusters at the EERA-DTOC European project,” *Energy Procedia*, vol. 53, no. C, pp. 324–341, 2014, doi: 10.1016/j.egypro.2014.07.241.

[79] I. Arrambide, I. Zubia, and A. Madariaga, “Critical review of offshore wind turbine energy production and site potential assessment,” *Electr. Power Syst. Res.*, vol. 167, no. October 2018, pp. 39–47, 2019, doi: 10.1016/j.epsr.2018.10.016.

[80] M. R. Patel, *Wind and solar power systems*. New York: CRC Press, 1999.

[81] M. L. Thøgersen, L. Svenningsen, T. Sørensen, and M. Jogararu, “Technical note, EMD-WRF global on-demand mesoscale services, ERA5, ERA-Interim, MERRA2 and CFSR,” EMD International A/S, Aalbrog, 2018.

[82] R. P. Patel, G. Nagababu, S. S. Kachhwaha, and V. V. A. K. Surisetty, “A revised offshore wind resource assessment and site selection along the Indian coast using ERA5 near-hub-height wind products,” *Ocean Eng.*, vol. 254, no. March, p. 111341, 2022, doi: 10.1016/j.oceaneng.2022.111341.

[83] L. Ramirez Camargo, K. Gruber, and F. Nitsch, “Assessing variables of regional reanalysis data sets relevant for modelling small-scale renewable energy systems,” *Renew. Energy*, vol. 133, pp. 1468–1478, 2019, doi: https://doi.org/10.1016/j.renene.2018.09.015.

[84] K. Hennermann, “ERA5: data documentation,” 2019. https://confluence.ecmwf.int//display/CKB/ERA5+data+documentation#ERA5datadocumentation-Observations (accessed May 10, 2019).

[85] D. D. Hans Hersbach, “ERA5 reanalysis is in production.” 2016, Accessed: May 10, 2019. [Online]. Available: https://confluence.ecmwf.int/display/CKB/What+is+ERA5?preview=/58140637/58140636/16299-newsletter-no147-spring-2016_p7.pdf.

[86] A. N. Celik, “Energy output estimation for small-scale wind power generators using Weibull-representative wind data,” *J. Wind Eng. Ind. Aerodyn.*, vol. 91, no. 5, pp. 693–707, 2003, doi: https://doi.org/10.1016/S0167-6105(02)00471-3.

[87] H. Shi, Z. Dong, N. Xiao, and Q. Huang, “Wind Speed Distributions Used in Wind Energy Assessment: A Review,” *Front. Energy Res.*, vol. 9, no. November, pp. 1–14, 2021, doi: 10.3389/fenrg.2021.769920.

[88] C. G. Justus, W. R. Hargraves, and A. Yalcin, “Nationwide assessment of potential output from wind-powered generators,” *J. Appl. Meteorol.*, vol. 15, no. 7, pp. 673–678, 1976.

[89] J. V. Seguro and T. W. Lambert, “Modern estimation of the parameters of the Weibull wind speed distribution for wind energy analysis,” *J. Wind Eng. Ind. Aerodyn.*, vol. 85, no. 1, pp. 75–84, 2000, doi: 10.1016/S0167-6105(99)00122-1.

[90] A. K. Resen, A. A. Mahmood, and J. S. Nmr, “Statistical calculations of wind data utilizing WAsP model,” in *AIP Conference Proceedings*, 2019, vol. 2123, no. July, doi: 10.1063/1.5116956.

[91] Y. Jiang, X. Yuan, X. Cheng, and X. Peng, “Wind potential assessment using the Weibull model at the Inner Mongolia of China,” *Energy Explor. Exploit.*, vol. 24, no. 3, pp. 211–221, 2006, doi: 10.1260/014459806779367509.

[92] A. K. Azad, M. G. Rasul, M. M. Alam, S. M. Ameer Uddin, and S. K. Mondal, “Analysis of wind energy conversion system using Weibull distribution,” *Procedia Eng.*, vol. 90, pp. 725–732, 2014, doi: 10.1016/j.proeng.2014.11.803.

[93] M. Satir, F. Murphy, and K. McDonnell, “Feasibility study of an offshore wind farm in the Aegean Sea, Turkey,” *Renew. Sustain. Energy Rev.*, vol. 81, pp. 2552–2562, 2018, doi: https://doi.org/10.1016/j.rser.2017.06.063.

[94] L. Hayes, M. Stocks, and A. Blakers, “Accurate long-term power generation model for offshore wind farms in Europe using ERA5 reanalysis,” *Energy*, vol. 229, p. 120603, 2021, doi: 10.1016/j.energy.2021.120603.

[95] M. Lydia, S. S. Kumar, A. I. Selvakumar, and G. E. Prem Kumar, “A comprehensive review on wind turbine power curve modeling techniques,” *Renew. Sustain. Energy Rev.*, vol. 30, pp. 452–460, 2014, doi: https://doi.org/10.1016/j.rser.2013.10.030.

[96] X. Sun, D. Huang, and G. Wu, “The current state of offshore wind energy technology development,” *Energy*, vol. 41, no. 1, pp. 298–312, 2012, doi: 10.1016/j.energy.2012.02.054.

[97] R. Shakoor, M. Y. Hassan, A. Raheem, and Y.-K. Wu, “Wake effect modeling: A review of wind farm layout optimization using Jensen′s model,” *Renew. Sustain. Energy Rev.*, vol. 58, pp. 1048–1059, 2016, doi: https://doi.org/10.1016/j.rser.2015.12.229.

[98] P. Hou, J. Zhu, K. Ma, G. Yang, W. Hu, and Z. Chen, “A review of offshore wind farm layout optimization and electrical system design methods,” *J. Mod. Power Syst. Clean Energy*, vol. 7, no. 5, pp. 975–986, 2019, doi: 10.1007/s40565-019-0550-5.

[99] I. Katic, J. Højstrup, and N. O. Jensen, “A Simple Model for Cluster Efficiency,” in *European wind energy association conference and exhibition*, 1987, vol. 1, pp. 407–410, [Online]. Available: https://backend.orbit.dtu.dk/ws/portalfiles/portal/106427419/A_Simple_Model_for_Cluster_Efficiency_EWEC_86_.pdf.

[100] DTU Wind Energy, “Wake effect model,” 2021. https://www.wasp.dk/wasp/wake-effect-model (accessed May 09, 2022).

[101] P. Lakshmanan, J. Liang, and N. Jenkins, “Assessment of collection systems for HVDC connected offshore wind farms,” *Electr. Power Syst. Res.*, vol. 129, pp. 75–82, 2015, doi: https://doi.org/10.1016/j.epsr.2015.07.015.

[102] N. G. Mortensen, D. N. Heathfield, O. Rathmann, and M. Nielsen, “Wind atlas analysis and application program: WAsP 10. Help facility,” Technical University of Denmark, Roskilde, 2011.

[103] W. P. Beach, R. P. Benedict, R. B. Dowdell, and M. Asme, “ASME measurement uncertainty,” *J. Fluids Eng.*, vol. 107, no. 83, pp. 161–164, 1985.

[104] A. P. Dobos, M. Kasberg, and P. Gilman, “WREF 2012: P50/P90 analysis for solar energy systems using the system advisor model,” *World Renew. Energy Forum, WREF 2012, Incl. World Renew. Energy Congr. XII Color. Renew. Energy Soc. Annu. Conf.*, vol. 4, no. June, pp. 2561–2566, 2012.

[105] Marine Scotland, “Energy resources offshore wind areas of search.” Marine Scotland, Edinburgh, 2018, Accessed: Mar. 13, 2019. [Online]. Available: http://marine.gov.scot/themes/renewable-energy-and-power-cables.

[106] NSTA and OceanWise, “Oil and gas - Hydrocarbon pipelines.” Marine Scotland, Edinburgh, 2019, Accessed: May 08, 2019. [Online]. Available: http://marine.gov.scot/maps/515.

[107] OPRED, “Oil and gas: decommissioning of offshore installations and pipelines,” 2013. https://www.gov.uk/guidance/oil-and-gas-decommissioning-of-offshore-installations-and-pipelines (accessed May 15, 2019).

[108] QGIS development team, “QGIS Geographic Information System.” Open Source Geospatial Foundation, 2009, Accessed: Feb. 19, 2019. [Online]. Available: https://qgis.org.

[109] Marine Scotland Science, “Scoping ‘Areas of Search’ Study for offshore wind energy in Scottish waters, 2018.,” Marine Scotland Science, Edinburgh, 2018.

[110] Scottish Government, “Offshore wind energy in Scottish waters - Darft regional locational guidance,” 2012. doi: 10.7489/1686-1.

[111] Rystad Energy, “Rystad Energy’s upstream database UCube.” Rystad 2019, Oslo, 2019.

[112] OSPAR, “OSPAR offshore installations inventory.” 2017, Accessed: Mar. 24, 2020. [Online]. Available: https://odims.ospar.org/en/maps/map-inventory-of-offshore-installations-2017/.

[113] A. Harrington, “Shetland Islands: A driving force in clean, renewable energy,” *The Herald*, The Herald, May 05, 2021.

[114] C. Cope, “Energy developer wants to install 200 offshore wind turbines and create Sullom Voe hydrogen plant,” *Shetland News*, Jun. 01, 2021.

[115] P. Nielsen *et al.*, “WindPro.” EMD International A/S, Aalbrog, 2018.

[116] Equinor, “Wind farm being considered at Snorre and Gullfaks.” 2018, Accessed: May 09, 2019. [Online]. Available: https://www.equinor.com/en/news/27aug2018-hywind-tampen.html.

[117] MHI Vestas Offshore Wind, “MHI Vestas to supply five V164-9.5 MW turbines for Kincardine floating offshore wind park in Scotland.” 2019, Accessed: May 09, 2019. [Online]. Available: http://www.mhivestasoffshore.com/mhi-vestas-to-supply-five-v164-9-5-mw-turbines-for-kincardine-floating-offshore-wind-park-in-scotland/.

[118] P. Dvorak, “Principle Power and Senvion plan to float a 10-MW turbine.” 2018, Accessed: May 09, 2019. [Online]. Available: https://www.windpowerengineering.com/design/floating-turbines/principle-power-and-senvion-plan-to-float-a-10-mw-turbine/.

[119] A. Durakovic, “Europe’s first 10MW wind turbine stands offshore Scotland,” Dec. 2021.

[120] C. Tejon, “Vestas secures offshore order with Ocean Winds for floating wind project in France,” 2022. https://www.vestas.com/en/media/company-news/2022/vestas-secures-offshore-order-with-ocean-winds-for-floa-c3537414 (accessed Jun. 21, 2022).

[121] MHI Vestas Offshore Wind, “MHI Vestas launches the first 10 MW wind turbine in history,” 2018. http://www.mhivestasoffshore.com/mhi-vestas-launches-the-first-10-mw-wind-turbine-in-history/ (accessed May 09, 2019).

[122] The Crown Estate, “Offshore wind new leasing market engagement event 26th November 2018.” 2018, Accessed: Apr. 04, 2019. [Online]. Available: https://www.thecrownestate.co.uk/media/2797/20181126-new-leasing-engagement-event-slides-published.pdf.

[123] P. Nielsen, “Recommendations for wake loss calculation for offshore wind farms.,” EMD International A/S, Aalborg, 2019.

[124] R. J. Barthelmie *et al.*, “Modelling and measuring flow and wind turbine wakes in large wind farms offshore,” *Wind Energy*, vol. 12, no. 5, pp. 431–444, 2009, doi: 10.1002/we.348.

[125] DTU Wind Energy, “WAsP 11.” Technical University of Denmark, Roskilde, 2014.

[126] C. Bak *et al.*, “Description of the DTU 10 MW reference wind turbine,” Technical University of Denmark, Roskilde, 2013.

[127] E. Lundtang Petersen, I. Troen, S. T. Frandsen, and K. Hedegaard, *Danish Windatlas: A rational method of wind energy siting*, no. 428. Roskilde: RisøNational Laboratory, 1981.

[128] S. Obara, “Energy and exergy flows of a hydrogen supply chain with truck transportation of ammonia or methyl cyclohexane,” *Energy*, vol. 174, pp. 848–860, 2019, doi: 10.1016/j.energy.2019.01.103.

[129] The Crown Estate, “Offshore wind operational report,” 2019. Accessed: Nov. 12, 2019. [Online]. Available: www.thecrownestate.co.uk.

[130] FCH 2 JU, “Multi-annual work plan 2014-2020,” 2018. Accessed: Oct. 30, 2019. [Online]. Available: http://hydrogencouncil.com/wp-content/uploads/2017/11/Hydrogen-Scaling-up_Hydrogen-.

[131] Repsol Sinopec, “Beatrice decommissioning programmes,” Repsol Sinopec, Aberdeen, 2018.

[132] OSPAR Commission, “Ministerial meeting of the OSPAR Commission Sintra, 22-23 July 1998 Programmes and measures,” 1998. Accessed: Oct. 31, 2019. [Online]. Available: https://www.ospar.org/documents?v=6877.

[133] Marine Scotland, “Sectoral marine plan for offshore wind for Innovation and Targeted Oil and Gas decarbonisation (INTOG),” 2021. Accessed: May 20, 2022. [Online]. Available: https://marine.gov.scot/sites/default/files/sectoral_marine_plan_for_offshore_wind_for_intog_-_project_spec-context_report_-_confidential_-_25_august_2021.pdf.

[134] I. Komusanac, D. Fraile, and G. Brindley, “Wind energy in Europe in 2018,” Wind Europe, Brussels, 2019.

[135] C. Chardonnet *et al.*, “Study on early business cases for H2 in energy storage and more broadly power to H2 applications,” Brussels, 2017. Accessed: Oct. 30, 2019. [Online]. Available: https://www.fch.europa.eu/sites/default/files/P2H_Full_Study_FCHJU.pdf.

[136] Xodus, “Scottish offshore wind to green hydrogen opportunity assessment,” The Scottish Government, Edinburgh, 2020. Accessed: Sep. 29, 2021. [Online]. Available: https://www.gov.scot/binaries/content/documents/govscot/publications/research-and-analysis/2020/12/scottish-offshore-wind-green-hydrogen-opportunity-assessment2/documents/scottish-offshore-wind-green-hydrogen-opportunity-assessment/scottish-offshore-wind-.

[137] M. Leporini, B. Marchetti, F. Corvaro, and F. Polonara, “Reconversion of offshore oil and gas platforms into renewable energy sites production: Assessment of different scenarios,” *Renew. Energy*, vol. 135, pp. 1121–1132, 2019, doi: 10.1016/j.renene.2018.12.073.

[138] P. D. O’Kelly-Lynch, P. D. Gallagher, A. G. L. Borthwick, E. J. McKeogh, and P. G. Leahy, “Offshore conversion of wind power to gaseous fuels: Feasibility study in a depleted gas field,” *Proc. Inst. Mech. Eng. Part A J. Power Energy*, vol. 234, no. 2, pp. 226–236, 2020, doi: 10.1177/0957650919851001.

[139] D. K. Sedlar, D. Vulin, G. Krajačić, and L. Jukić, “Offshore gas production infrastructure reutilisation for blue energy production,” *Renew. Sustain. Energy Rev.*, vol. 108, no. April, pp. 159–174, 2019, doi: 10.1016/j.rser.2019.03.052.

[140] J. Mathur, N. Agarwal, R. Swaroop, and N. Shah, “Economics of producing hydrogen as transportation fuel using offshore wind energy systems,” *Energy Policy*, vol. 36, no. 3, pp. 1212–1222, 2008, doi: 10.1016/j.enpol.2007.11.031.

[141] K. Meier, “Hydrogen production with sea water electrolysis using Norwegian offshore wind energy potentials: Techno-economic assessment for an offshore-based hydrogen production approach with state-of-the-art technology,” *Int. J. Energy Environ. Eng.*, vol. 5, no. 2–3, pp. 1–12, 2014, doi: 10.1007/s40095-014-0104-6.

[142] P. Blanco-Fernández and F. Pérez-Arribas, “Offshore facilities to produce hydrogen,” *Energies*, vol. 10, no. 6, 2017, doi: 10.3390/en10060783.

[143] Á. Serna and F. Tadeo, “Offshore hydrogen production from wave energy,” *Int. J. Hydrogen Energy*, vol. 39, no. 3, pp. 1549–1557, 2014, doi: 10.1016/j.ijhydene.2013.04.113.

[144] I. A. Gondal, “Offshore renewable energy resources and their potential in a green hydrogen supply chain through power-to-gas,” *Sustain. Energy Fuels*, vol. 3, no. 6, pp. 1468–1489, 2019, doi: 10.1039/c8se00544c.

[145] I. A. Gondal and S. A. Masood, “Synergies in offshore wind and oil industry for carbon capture and utilization,” *Greenh. Gases Sci. Technol.*, vol. 9, no. 5, pp. 856–871, 2019, doi: 10.1002/ghg.1921.

[146] I. A. Gondal, “Hydrogen integration in power-to-gas networks,” *Int. J. Hydrogen Energy*, vol. 44, no. 3, pp. 1803–1815, 2019, doi: 10.1016/j.ijhydene.2018.11.164.

[147] R. D’Amore-Domenech and T. J. Leo, “Sustainable hydrogen production from offshore marine renewable farms: Techno-energetic insight on seawater electrolysis technologies,” *ACS Sustain. Chem. Eng.*, vol. 7, no. 9, pp. 8006–8022, 2019, doi: 10.1021/acssuschemeng.8b06779.

[148] A. Abarnou and L. Miossec, “Chlorinated waters discharged to the marine environment chemistry and environmental impact. An overview,” *Sci. Total Environ.*, vol. 126, no. 1, pp. 173–197, 1992, doi: https://doi.org/10.1016/0048-9697(92)90490-J.

[149] W. A. Brungs, “Effects of Residual Chlorine on Aquatic Life,” *J. (Water Pollut. Control Fed.*, vol. 45, no. 10, pp. 2180–2193, Jun. 1973, [Online]. Available: http://www.jstor.org/stable/25038016.

[150] N. Ahmad and R. E. Baddour, “A review of sources, effects, disposal methods, and regulations of brine into marine environments,” *Ocean Coast. Manag.*, vol. 87, pp. 1–7, 2014, doi: https://doi.org/10.1016/j.ocecoaman.2013.10.020.

[151] Gilman Industries, “Introducing Evolve,” 2018. https://gilmanindustries.com/ (accessed Apr. 20, 2019).

[152] M. Carmo, D. L. Fritz, J. Mergel, and D. Stolten, “A comprehensive review on PEM water electrolysis,” *Int. J. Hydrogen Energy*, vol. 38, no. 12, pp. 4901–4934, 2013, doi: 10.1016/j.ijhydene.2013.01.151.

[153] Ø. Ulleberg, T. Nakken, and A. Eté, “The wind/hydrogen demonstration system at Utsira in Norway: Evaluation of system performance using operational data and updated hydrogen energy system modeling tools,” *Int. J. Hydrogen Energy*, vol. 35, no. 5, pp. 1841–1852, 2010, doi: 10.1016/j.ijhydene.2009.10.077.

[154] G. Gahleitner, “Hydrogen from renewable electricity: An international review of power-to-gas pilot plants for stationary applications,” *Int. J. Hydrogen Energy*, vol. 38, no. 5, pp. 2039–2061, 2013, doi: 10.1016/j.ijhydene.2012.12.010.

[155] C. Rakousky *et al.*, “Polymer electrolyte membrane water electrolysis: Restraining degradation in the presence of fluctuating power,” *J. Power Sources*, vol. 342, pp. 38–47, 2017, doi: 10.1016/j.jpowsour.2016.11.118.

[156] R. D’amore-Domenech, E. Navarro, E. Mora, and T. J. Leo, “Alkaline electrolysis at sea for green hydrogen production. A solution to electrolyte deterioration,” 2018. Accessed: Jan. 27, 2020. [Online]. Available: https://asmedigitalcollection.asme.org/OMAE/proceedings-pdf/OMAE2018/51319/V010T09A014/2537110/v010t09a014-omae2018-77209.pdf.

[157] P. Schulze and F. de Groot, “Re-use of North Sea offshore assets for power-to-gas,” DNV GL Oil & Gas, Groningen, 2015.

[158] Power Technology, “Oyster Project consortium to investigate offshore hydrogen production,” 2021. https://www.power-technology.com/news/oyster-project-consortium-investigate-hydrogen-production-ec-european-commission-funding/ (accessed Dec. 02, 2021).

[159] X. Jia, J. J. Klemeš, P. S. Varbanov, and S. R. W. Alwi, “Analyzing the energy consumption, GHG emission, and cost of seawater desalination in China,” *Energies*, vol. 12, no. 3, pp. 1–16, 2019, doi: 10.3390/en12030463.

[160] S. Bhojwani, K. Topolski, R. Mukherjee, D. Sengupta, and M. M. El-Halwagi, “Technology review and data analysis for cost assessment of water treatment systems,” *Sci. Total Environ.*, vol. 651, pp. 2749–2761, 2018, doi: 10.1016/j.scitotenv.2018.09.363.

[161] A. Al-Karaghouli and L. L. Kazmerski, “Energy consumption and water production cost of conventional and renewable-energy-powered desalination processes,” *Renew. Sustain. Energy Rev.*, vol. 24, pp. 343–356, 2013, doi: 10.1016/j.rser.2012.12.064.

[162] U. Caldera and C. Breyer, “Learning curve for seawater reverse osmosis desalination plants: Capital cost trend of the past, present, and future,” *Water Resour. Res.*, vol. 53, no. 12, pp. 10523–10538, 2017, doi: 10.1002/2017WR021402.

[163] W. Priest, “Future mining energy solutions-Hydrogen hybrid remote area power systems (RAPS),” Hydrogen and Mines, Perth, 2019.

[164] M. Quante *et al.*, “Introduction to the assessment- Characteristics of the region,” in *North Sea Region Climate Change Assessment*, no. October, E. Quante and F. Colijn, Eds. Cham: Springer, 2016, pp. 1–52.

[165] U. Caldera, D. Bogdanov, and C. Breyer, “Local cost of seawater RO desalination based on solar PV and wind energy: A global estimate,” *Desalination*, vol. 385, pp. 207–216, 2016, doi: 10.1016/j.desal.2016.02.004.

[166] N. Ghaffour, T. M. Missimer, and G. L. Amy, “Technical review and evaluation of the economics of water desalination: Current and future challenges for better water supply sustainability,” *Desalination*, vol. 309, pp. 197–207, 2013, doi: 10.1016/j.desal.2012.10.015.

[167] L. F. Greenlee, D. F. Lawler, B. D. Freeman, B. Marrot, and P. Moulin, “Reverse osmosis desalination: Water sources, technology, and today’s challenges,” *Water Res.*, vol. 43, no. 9, pp. 2317–2348, 2009, doi: 10.1016/j.watres.2009.03.010.

[168] V. G. Gude, “Energy consumption and recovery in reverse osmosis,” *Desalin. Water Treat.*, vol. 36, no. 1–3, pp. 239–260, 2011, doi: 10.5004/dwt.2011.2534.

[169] M. W. Shahzad, M. Burhan, D. Ybyraiymkul, and K. C. Ng, “Desalination processes’ efficiency and future roadmap,” *Entropy*, vol. 21, no. 1, 2019, doi: 10.3390/e21010084.

[170] Lenntech, “Ultra-high recovery 3 stage seawater desalination,” 2021. https://www.lenntech.com/processes/desalination/general/3-stage-recovery.htm (accessed Jan. 25, 2021).

[171] N. Voutchkov, “Desalination – Past, present and future,” 2016. https://iwa-network.org/desalination-past-present-future/ (accessed Feb. 05, 2021).

[172] Lenntech, “Water treatment solutions,” 2016. https://www.lenntech.com/Data-sheets/ES_LennRO_SW_M_cont_rev01.pdf (accessed Feb. 05, 2021).

[173] J. A. Cotruvo, “Rolling revision of the WHO guidelines for drinking water quality desalination guidelines development for drinking water,” World Health Organisation, Geneva, 2004. Accessed: Jan. 15, 2021. [Online]. Available: http://www.who.int/water_sanitation_health/dwq/nutwaterrequir.pdf.

[174] EPA, “Secondary drinking water standards: Guidance for nuisance chemicals,” 2021. https://www.epa.gov/sdwa/secondary-drinking-water-standards-guidance-nuisance-chemicals (accessed Jan. 15, 2021).

[175] K. Hyde and A. Ellis, “DUAL ports. De-carbonising port business today. Feasibility of hydrogen bunkering,” 2019. Accessed: Apr. 28, 2022. [Online]. Available: https://northsearegion.eu/media/9385/feasibility-of-hydrogen-bunkering-final-080419.pdf.

[176] D. Thomas, “Large scale PEM electrolysis : technology status and upscaling strategies,” Hydrogenics, Brussels, 2019. Accessed: Apr. 27, 2022. [Online]. Available: http://hybalance.eu/wp-content/uploads/2019/10/Large-scale-PEM-electrolysis.pdf.

[177] Siemens AG, “Silyzer 300,” Siemens AG 2018, Erlangen, 2018. Accessed: Apr. 28, 2022. [Online]. Available: https://northsearegion.eu/media/9385/feasibility-of-hydrogen-bunkering-final-080419.pdf.

[178] H. K. Ju, S. Badwal, and S. Giddey, “A comprehensive review of carbon and hydrocarbon assisted water electrolysis for hydrogen production,” *Appl. Energy*, vol. 231, no. August, pp. 502–533, 2018, doi: 10.1016/j.apenergy.2018.09.125.

[179] S. Shiva Kumar and V. Himabindu, “Hydrogen production by PEM water electrolysis – A review,” *Mater. Sci. Energy Technol.*, vol. 2, no. 3, pp. 442–454, 2019, doi: 10.1016/j.mset.2019.03.002.

[180] DNV GL, “Power-to-hydrogen,” 2018. Accessed: Oct. 29, 2019. [Online]. Available: https://www.tennet.eu/fileadmin/user_upload/Company/Publications/Technical_Publications/Dutch/P2H_IJmuiden_Ver_-_Final_Report_-_Public.pdf.

[181] D. McCool, “Private communication.” 2021.

[182] O. Anaya-Lara, “Private communication.” 2021.

[183] P. Judge, “Private communication.” 2021.

[184] Ö. Göksu, O. Saborío-Romano, N. A. Cutululis, and P. Sørensen, “Black start and island operation capabilities of wind power plants,” in *Proc. 16th Wind Integration Workshop*, 2017, no. October, pp. 25–27, [Online]. Available: https://www.promotion-offshore.net/fileadmin/PDFs/Conference_Paper_Black_Start_and_Island_Operation_Capabilities_of_Wind_Power_Plants_with_note.pdf.

[185] T. Edenfeld, “Use of pitch battery power to start wind turbine during grid loss/black start capability.,” 2011.

[186] Carbon Trust, “Electrical Systems,” 2021. https://www.carbontrust.com/our-projects/offshore-wind-accelerator-owa/electrical-systems (accessed Aug. 18, 2021).

[187] S. M. Muyeen, R. Takahashi, T. Murata, and J. Tamura, “Integration of hydrogen generator into wind farm interconnected HVDC system,” *2009 IEEE Bucharest PowerTech Innov. Ideas Towar. Electr. Grid Futur.*, no. August 2017, 2009, doi: 10.1109/PTC.2009.5282050.

[188] J. L. B. Ferguson, “Technoeconomic modelling of renewable hydrogen supply chains on islands with constrained grids,” EngD thesis, The University of Edinburgh, 2021.

[189] M. Mohitpour, H. Golshan, and A. Murray, “Specialty fluid transmission,” in *Pipeline design & construction: A practical approach, Third edition*, M. Mohitpour, H. Golshan, and A. Murray, Eds. New York: ASME, 2010, pp. 565–681.

[190] E. Ohaeri, U. Eduok, and J. Szpunar, “Hydrogen related degradation in pipeline steel: A review,” *Int. J. Hydrogen Energy*, vol. 43, no. 31, pp. 14584–14617, 2018, doi: https://doi.org/10.1016/j.ijhydene.2018.06.064.

[191] K. Poorhaydari, “A comprehensive examination of high-temperature hydrogen attack—A review of over a century of investigations,” *J. Mater. Eng. Perform.*, vol. 30, no. 11, pp. 7875–7908, 2021, doi: 10.1007/s11665-021-06045-z.

[192] N. Gallon, “Hydrogen pipelines - Design and materials challenges and mitigations,” European Pipeline Research Group, Duisburg, 2020.

[193] L. Jemblie, V. Olden, P. Mainçon, and O. M. Akselsen, “Cohesive zone modelling of hydrogen induced cracking on the interface of clad steel pipes,” *Int. J. Hydrogen Energy*, vol. 42, no. 47, pp. 28622–28634, 2017, doi: https://doi.org/10.1016/j.ijhydene.2017.09.051.

[194] T. J. Carter and L. A. Cornish, “Hydrogen in metals,” *Eng. Fail. Anal.*, vol. 8, no. 2, pp. 113–121, 2001, doi: https://doi.org/10.1016/S1350-6307(99)00040-0.

[195] W. T. Becker and R. J. Shipley, “Hydrogen damage and embrittlement,” in *Failure Analysis and Prevention*, vol. 11, ASM Handbook, 2002, pp. 809–822.

[196] G. F. Vander Voort, “Embrittlement of steels,” in *Properties and selection: Irons, steels, and high-performance alloys*, vol. 1, ASM International, 1990, pp. 689–736.

[197] D. P. Dunne, D. Hejazi, A. A. Saleh, A. J. Haq, A. Calka, and E. V Pereloma, “Investigation of the effect of electrolytic hydrogen charging of X70 steel: I. The effect of microstructure on hydrogen-induced cold cracking and blistering,” *Int. J. Hydrogen Energy*, vol. 41, no. 28, pp. 12411–12423, 2016, doi: https://doi.org/10.1016/j.ijhydene.2016.04.114.

[198] EIGA, “Hydrogen pipeline systems,” European Industrial Gases Association, Brussels, 2014. Accessed: Aug. 05, 2020. [Online]. Available: https://www.eiga.eu/index.php?eID=dumpFile&t=f&f=2532&token=17b3cf7479e0b3ebf9a602a522c7be5b25aa5f22.

[199] OGTC, “Delivery of an offshore hydrogen supply programme via industrial trials at Flotta terminal.,” 2020. Accessed: Jun. 22, 2020. [Online]. Available: http://www.kawarthasnaturally.ca/phaseone/.

[200] OGTC, “Subsea decommissioning call for ideas : Technical documentation,” 2019. Accessed: Nov. 06, 2020. [Online]. Available: https://www.netzerotc.com/media/2771/subsea-decommissioning-technical-document.pdf.

[201] A. J. Slifka *et al.*, “Fatigue measurement of pipeline steels for the application of transporting gaseous hydrogen,” *J. Press. Vessel Technol.*, vol. 140, no. 1, Dec. 2018, doi: 10.1115/1.4038594.

[202] R. L. Amaro, R. M. White, C. P. Looney, E. S. Drexler, and A. J. Slifka, “Development of a model for hydrogen-assisted fatigue crack growth of pipeline steel,” *J. Press. Vessel Technol. Trans. ASME*, vol. 140, no. 2, pp. 1–13, 2018, doi: 10.1115/1.4038824.

[203] W. R. Hoover, S. L. Robinson, R. E. Stoltz, and J. R. Spingarn, “Hydrogen compatibility of structural materials for energy storage and transmission.,” Sandia National Laboratories, Livermore, 1981.

[204] M. L. Martin, M. Connolly, Z. N. Buck, P. E. Bradley, D. Lauria, and A. J. Slifka, “Evaluating a natural gas pipeline steel for blended hydrogen service,” *J. Nat. Gas Sci. Eng.*, vol. 101, p. 104529, 2022, doi: https://doi.org/10.1016/j.jngse.2022.104529.

[205] C. San Marchi, B. P. Somerday, K. A. Nibur, D. G. Stalheim, T. Boggess, and S. Jansto, “Fracture resistance and fatigue crack growth of X80 pipeline steel in gaseous hydrogen,” 2011, vol. Volume 6:, pp. 841–849, doi: 10.1115/PVP2011-57684.

[206] J. A. Ronevich, B. P. Somerday, and C. W. San Marchi, “Effects of microstructure banding on hydrogen assisted fatigue crack growth in X65 pipeline steels,” *Int. J. Fatigue*, vol. 82, pp. 497–504, 2016, doi: https://doi.org/10.1016/j.ijfatigue.2015.09.004.

[207] ASME, “Hydrogen piping and pipelines. ASME code for pressure piping B31,” The American Society of Mechanical Engineers, New York, 2019.

[208] L. Briottet, R. Batisse, G. De Dinechin, P. Langlois, and L. Thiers, “Recommendations on X80 steel for the design of hydrogen gas transmission pipelines,” *Int. J. Hydrogen Energy*, vol. 37, no. 11, pp. 9423–9430, 2012, doi: 10.1016/j.ijhydene.2012.02.009.

[209] S. Mokhatab and W. A. Poe, “Sales gas transmission,” in *Handbook of natural gas transmission and processing*, S. Mokhatab and W. A. Poe, Eds. Amsterdam: Elsevier Science Ltd, 2012, pp. 425–450.

[210] M. Stewart, “6 - Fluid flow and pressure drop,” in *Surface Production Operations*, M. Stewart, Ed. Boston: Gulf Professional Publishing, 2016, pp. 343–470.

[211] M. Mohitpour, H. Golshan, A. Murray, M. Mohitpour, H. Golshan, and A. Murray, “Natural gas transmission,” in *Pipeline design & construction: A practical approach, Third edition*, M. Mohitpour, H. Golshan, and A. Murray, Eds. New York: ASME, 2010, pp. 57–128.

[212] T. R. Weymouth, “Problems in natural gas engineering,” *Trans. Am. Soc. Mech. Eng.*, vol. 34, no. 1349, pp. 185–231, 1912.

[213] T. Włodek, M. Łaciak, K. Kurowska, and Ł. Węgrzyn, “Thermodynamic analysis of hydrogen pipeline transportation – selected aspects,” *AGH Drilling, Oil, Gas*, vol. 33, no. 2, p. 379, 2016, doi: 10.7494/drill.2016.33.2.379.

[214] K. Nasrifar, “Comparative study of eleven equations of state in predicting the thermodynamic properties of hydrogen,” *Int. J. Hydrogen Energy*, vol. 35, no. 8, pp. 3802–3811, 2010, doi: 10.1016/j.ijhydene.2010.01.032.

[215] N. B. Vargaftik, Y. K. Vinogradov, and V. S. Yargin, *Handbook of physical properties of liquids and gases. Pure substances and mixtures.*, 3rd ed. New York: Begell House Inc, 1996.

[216] D. Y. Peng and D. B. Robinson, “A new two-constant equation of state,” *Ind. Eng. Chem. Fundam.*, vol. 15, no. 1, pp. 59–64, 1976, doi: 10.1021/i160057a011.

[217] H. D. Beggs, *Gas production operations*. Tulsa: OGCI Publications, 1991.

[218] N. G. Diez, S. van der Meer, J. Bonetto, and A. Herwijn, “North Sea Energy Technical assessment of Hydrogen transport, compression, processing offshore,” 2020. Accessed: Jul. 14, 2021. [Online]. Available: https://north-sea-energy.eu/static/7ffd23ec69b9d82a7a982b828be04c50/FINAL-NSE3-D3.1-Final-report-technical-assessment-of-Hydrogen-transport-compression-processing-offshore.pdf.

[219] Schlumberger, “Pipesim 2019,” Schlumberger, Houston, 2020.

[220] B. Wetenhall, J. M. Race, and M. J. Downie, “The effect of CO2 purity on the development of pipeline networks for carbon capture and storage schemes,” *Int. J. Greenh. Gas Control*, vol. 30, pp. 197–211, 2014, doi: 10.1016/j.ijggc.2014.09.016.

[221] H. Haghighi, D. Erickson, and J. Holbeach, “Realtime operation of a hydrogen enhanced natural gas grid.” Gastech, Dubai, 2021.

[222] Simerics, “Hydrogen and SIMERICS-The future starts now,” 2022. https://simerics.de/anwendungen/hydrogen/?lang=en (accessed Apr. 06, 2022).

[223] Flownex, “Flownex,” 2022. https://flownex.com/industries/hydrogen/ (accessed Apr. 06, 2022).

[224] NREL, “H2FillS: Hydrogen filling simulation,” 2021. https://www.nrel.gov/hydrogen/h2fills.html (accessed Apr. 06, 2022).

[225] OceanWise; OGA, “Oil & gas pipelines,” 2019. https://marinescotland.atkinsgeospatial.com/nmpi/ (accessed Nov. 06, 2020).

[226] EIC, “Asset Map,” 2020. https://eicassetmap.the-eic.com/ (accessed Nov. 06, 2020).

[227] Y. Bai and Q. Bai, “Chapter 18 - Hydraulics,” Y. Bai and Q. B. T.-S. P. and R. Bai, Eds. Oxford: Elsevier Science Ltd, 2005, pp. 277–316.

[228] Schlumberger, “PIPESIM software version 2018.1.” Schlumberger, Houston, 2018.

[229] Infochem, “Multiflash, version 3.7 ed.” Infochem Computer Services Ltd, London, 2011.

[230] A. Züttel, “Materials for hydrogen storage,” *Mater. Today*, vol. 6, no. 9, pp. 24–33, 2003, doi: 10.1016/S1369-7021(03)00922-2.

[231] P. J. Knight, J. Falconer, and M. J. Howarth, “Current meter records.,” 1990. Accessed: Apr. 09, 2022. [Online]. Available: nora.nerc.ec.uk/id/eprint/3874.

[232] Simorc, “Simorc formats,” 2007. http://www.simorc.com/content/content.asp?menu=0020014_000000 (accessed Apr. 08, 2022).

[233] National Oceanic and Atmospheric Administration, “World ocean atlas 2009,” 2015. www.nodc.noaa.gov/OC5/WOA09/pr_woa09.html (accessed Apr. 08, 2022).

[234] F. Kreith and M. Bohn, *Principles of heat transfer*. Eagan: PWS Publishing Company, 1997.

[235] K. S. Pedersen, A. Fredenslund, P. L. Christensen, and P. Thomassen, “Viscosity of crude oils,” *Chem. Eng. Sci.*, vol. 39, no. 6, pp. 1011–1016, 1984, doi: https://doi.org/10.1016/0009-2509(84)87009-8.

[236] J. Lohrenz, B. G. Bray, and C. R. Clark, “Calculating viscosities of reservoir fluids from their compositions,” *J. Pet. Technol.*, vol. 16, no. 10, pp. 1171–1176, Oct. 1964, doi: 10.2118/915-PA.

[237] C. H. Twu, “An internally consistent correlation for predicting the critical properties and molecular weights of petroleum and coal-tar liquids,” *Fluid Phase Equilib.*, vol. 16, no. 2, pp. 137–150, 1984, doi: https://doi.org/10.1016/0378-3812(84)85027-X.

[238] M. L. Huber, “NIST standard reference database 4 (SUPERTRAPP).” National Institute of Standards and Technology, Maryland, 2007.

[239] R. D. McCarty, *Hydrogen, its technology and implications*, no. v. 4. Boca Raton: CRC Press, 1979.

[240] G. Soave, “Equilibrium constants from a modified Redkh-Kwong EOS,” *Chem. Eng. Sci.*, vol. 27, no. 6, pp. 1197–1203, 1972.

[241] Schlumberger, “PIPESIM 2018.1 Manual.” 2018.

[242] SGN, “Aberdeen Vision Project,” 2020. [Online]. Available: https://www.sgn.co.uk/sites/default/files/media-entities/documents/2020-11/SGN-Aberdeen-Vision-Project_Final-Report_0520.pdf.

[243] G. M. Masters, “Economics of distributed resources,” in *Renewable and Efficient Electric Power Systems*, John Wiley & Sons, Inc, 2004, pp. 231–305.

[244] M. Lerch, “Qualification of innovative floating substructures for 10MW wind turbines and water depths greater than 50m.,” 2019. Accessed: Jan. 28, 2022. [Online]. Available: https://ec.europa.eu/research/participants/documents/downloadPublic?documentIds=080166e5c3ac71f4&appId=PPGMS.

[245] O. Žižlavský, “Net present value approach: Method for economic assessment of innovation projects,” *Procedia - Soc. Behav. Sci.*, vol. 156, no. April, pp. 506–512, 2014, doi: 10.1016/j.sbspro.2014.11.230.

[246] A. Myhr, C. Bjerkseter, A. Ågotnes, and T. A. Nygaard, “Levelised cost of energy for offshore floating wind turbines in a life cycle perspective,” *Renew. Energy*, vol. 66, pp. 714–728, 2014, doi: https://doi.org/10.1016/j.renene.2014.01.017.

[247] P. K. Jain and M. Y. Khan, *Theory and problems in financial management*. New York: Tata McGraw-Hill Education, 1999.

[248] M. Bruseva, “Financial - economic assessment of innovative projects,” *Innov. Descrete Prod.*, vol. 27, no. 2, pp. 25–27, 2015.

[249] J. Aldersey-Williams and T. Rubert, “Levelised cost of energy – A theoretical justification and critical assessment,” *Energy Policy*, vol. 124, pp. 169–179, 2019, doi: https://doi.org/10.1016/j.enpol.2018.10.004.

[250] L. Castro-Santos, E. Martins, and C. Guedes Soares, “Methodology to calculate the costs of a floating offshore renewable energy farm,” *Energies*, vol. 9, no. 5, 2016, doi: 10.3390/en9050324.

[251] BEIS, “Electricity generation cost report 2020,” 2020. Accessed: Jun. 03, 2022. [Online]. Available: https://assets.publishing.service.gov.uk/government/uploads/system/uploads/attachment_data/file/911817/electricity-generation-cost-report-2020.pdf.

[252] R. Ebenhoch, D. Matha, S. Marathe, P. C. Muñoz, and C. Molins, “Comparative levelized cost of energy analysis,” in *Energy Procedia*, 2015, vol. 80, pp. 108–122, doi: 10.1016/j.egypro.2015.11.413.

[253] L. Serri, L. Colle, B. Vitali, and T. Bonomi, “Floating offshore wind farms in Italy beyond 2030 and beyond 2060: Preliminary results of a techno-economic assessment,” *Appl. Sci.*, vol. 10, no. 24, pp. 1–19, 2020, doi: 10.3390/app10248899.

[254] P. Beiter *et al.*, “The cost of floating offshore wind energy in California between 2019 and 2032 cost and performance results data,” National Renewable Energy Laboratory, Golden, 2020. Accessed: Jan. 28, 2022. [Online]. Available: www.nrel.gov/publications.

[255] L. Castro-Santos, A. Filgueira-Vizoso, I. Lamas-Galdo, C. Alvarez-Feal, and L. Carral-Couce, “Influence of the discount rate in the economic analysis of a floating offshore wind farm in the Galician region of the European Atlantic Area,” in *Proceedings of the ASME 2018 37th International Conference on Ocean, Offshore and Arctic Engineering*, 2018, no. January 2021, p. 6, doi: 10.1115/OMAE2018-78727.

[256] R. Wiser *et al.*, “Expert elicitation survey on future wind energy costs,” *Nat. Energy*, vol. 1, no. 10, p. 16135, 2016, doi: 10.1038/nenergy.2016.135.

[257] CPUC, “2019-20 IRP: Proposed Reference System Plan,” 2019. [Online]. Available: https://docs.cpuc.ca.gov/PublishedDocs/Efile/G000/M319/K128/319128759.PDF.

[258] S. Heidari, “Economic modelling of floating offshore wind power,” Master thesis, Maelardalen University, 2017.

[259] T. Freyman and T. Tran, “Renewable energy discount rate survey results -2018 | Grant Thornton,” 2019. Accessed: Feb. 21, 2022. [Online]. Available: https://www.grantthornton.co.uk/globalassets/1.-member-firms/united-kingdom/pdf/documents/renewable-energy-discount-rate-survey-results-2018.pdf.

[260] Wood plc, “Floating offshore wind LCOE calculator.” Wood plc, Aberdeen, 2021.

[261] R. James and M. Costa Ros, “Floating offshore wind: Market and technology review,” The Carbon Trust, London, 2015.

[262] O. D. Adeuyi *et al.*, “Grid-access technologies for GB offshore wind industry,” 2020. Accessed: Mar. 23, 2022. [Online]. Available: https://www.hvdccentre.com/wp-content/uploads/2020/01/Grid-Access-Technologies_V3.pdf.

[263] R. Ryndzionek and Ł. Sienkiewicz, “Evolution of the HVDC link connecting offshore wind farms to onshore power systems,” *Energies*, vol. 13, no. 8, 2020, doi: 10.3390/en13081914.

[264] Y. Meng *et al.*, “Comparative economic analysis of low frequency AC transmission system for the integration of large offshore wind farms,” *Renew. Energy*, vol. 179, pp. 1955–1968, 2021, doi: https://doi.org/10.1016/j.renene.2021.07.137.

[265] NS Energy, “Shetland interconnector,” 2020. https://www.nsenergybusiness.com/projects/shetland-interconnector/ (accessed Mar. 15, 2022).

[266] Energy Voice, “SSE’s £260m Orkney energy transmission link given go-ahead by Ofgem,” 2019. https://www.energyvoice.com/renewables-energy-transition/207807/sses-260m-orkney-renewable-energy-transmission-link-given-go-ahead-by-ofgem/ (accessed Mar. 15, 2022).

[267] OWPB, “Transmission costs for offshore wind,” 2016. Accessed: Feb. 22, 2022. [Online]. Available: https://ore.catapult.org.uk/app/uploads/2018/02/Transmission-Costs-for-Offshore-Wind.pdf.

[268] UK Government, “Energy Act 2004,” 2004. Accessed: Mar. 24, 2022. [Online]. Available: https://www.legislation.gov.uk/ukpga/2004/20/contents.

[269] National Grid Electricity System Operator, “Five-year view of TNUoS tariffs for 2021/22 to 2025/26,” 2020. Accessed: May 07, 2022. [Online]. Available: https://www.nationalgrideso.com/document/176486/download.

[270] O. Schmidt, A. Gambhir, I. Staffell, A. Hawkes, J. Nelson, and S. Few, “Future cost and performance of water electrolysis: An expert elicitation study,” *Int. J. Hydrogen Energy*, vol. 42, no. 52, pp. 30470–30492, 2017, doi: 10.1016/j.ijhydene.2017.10.045.

[271] L. Bertuccioli, A. Chan, D. Hart, F. Lehner, B. Madden, and E. Standen, “Development of water electrolysis in the European Union,” 2014. Accessed: Mar. 21, 2022. [Online]. Available: https://www.fch.europa.eu/sites/default/files/study electrolyser_0-Logos_0_0.pdf.

[272] S. M. Saba, M. Müller, M. Robinius, and D. Stolten, “The investment costs of electrolysis – A comparison of cost studies from the past 30 years,” *Int. J. Hydrogen Energy*, vol. 43, no. 3, pp. 1209–1223, 2018, doi: https://doi.org/10.1016/j.ijhydene.2017.11.115.

[273] S. Weidner, M. Faltenbacher, I. François, D. Thomas, J. B. Skùlason, and C. Maggi, “Feasibility study of large scale hydrogen power-to-gas applications and cost of the systems evolving with scaling up in Germany, Belgium and Iceland,” *Int. J. Hydrogen Energy*, vol. 43, no. 33, pp. 15625–15638, 2018, doi: https://doi.org/10.1016/j.ijhydene.2018.06.167.

[274] H. Böhm, A. Zauner, D. C. Rosenfeld, and R. Tichler, “Projecting cost development for future large-scale power-to-gas implementations by scaling effects,” *Appl. Energy*, vol. 264, p. 114780, 2020, doi: https://doi.org/10.1016/j.apenergy.2020.114780.

[275] C. Noack *et al.*, “Studie über die planung einer demonstrationsanlage zur wasserstoff-kraftstoffgewinnung durch elektrolyse mit zwischenspeicherung in salzkavernen unter druck,” Stuttgart, 2014. Accessed: Mar. 25, 2022. [Online]. Available: https://elib.dlr.de/94979/1/2014_DLR_ISE_KBB_LBST_PlanDelyKaD.pdf.

[276] J. de Busy, “The potential of power-to-gas,” Paris, 2016. Accessed: Mar. 21, 2022. [Online]. Available: https://www.enea-consulting.com/static/3663dbb115f833de23e4c94c8fa399ec/enea-the-potential-of-power-to-gas.pdf.

[277] K. Mongird, V. Viswanathan, J. Alam, C. Vartanian, V. Sprenkle, and R. Baxter, “2020 grid energy storage technology cost and performance assessment,” 2020. Accessed: Mar. 25, 2022. [Online]. Available: https://www.pnnl.gov/sites/default/files/media/file/Hydrogen_Methodology.pdf.

[278] D. Thomas, D. Mertens, M. Meeus, W. Van der Laak, and I. Francois, “Power-to-gas. Roadmap for Flanders.,” Brussels, 2016. Accessed: Mar. 21, 2022. [Online]. Available: https://www.waterstofnet.eu/_asset/_public/powertogas/P2G-Roadmap-for-Flanders.pdf.

[279] J. Mergel, “Anforderungen an die wasserelektrolyse und deren entwicklungspotenzial als schlüsseltechnologie für erneuerbare energien,” Juelich Forschungszentrum, Berlin, 2012.

[280] Lenntech, “Seawater desalination golf course,” 2019. https://www.lenntech.com/Data-sheets/2019-Seawater-Desalination-for-Golf-Course-Curacao.pdf (accessed Mar. 24, 2022).

[281] Almar Water Solutions, “Desalination technologies and economics: CAPEX, OPEX and technological game changers,” 2016. Accessed: Mar. 25, 2022. [Online]. Available: http://www.cmimarseille.org/sites/default/files/newsite/library/files/en/1.6. C. Cosin_ Desalination technologies and economics_ capex%2C opex and technological game changers to come -ilovepdf-compressed.pdf.

[282] N. Parker, “Using natural gas transmission pipeline costs to estimate hydrogen pipeline costs,” California Digital Library, Davis, 2004. Accessed: Oct. 18, 2021. [Online]. Available: http://escholarship.org/uc/item/9m40m75r.

[283] ICF International, “Decommissioning methodology and cost evaluation,” 2015. Accessed: Mar. 25, 2022. [Online]. Available: https://www.bsee.gov/sites/bsee.gov/files/tap-technical-assessment-program/738aa.pdf.

[284] N. Ghazi and J. M. Race, “Techno-economic modelling and analysis of CO2 pipelines,” Sep. 2012, pp. 189–198, doi: 10.1115/IPC2012-90455.

[285] C. Yang and J. Ogden, “Determining the lowest-cost hydrogen delivery mode,” *Int. J. Hydrogen Energy*, vol. 32, no. 2, pp. 268–286, 2007, doi: 10.1016/j.ijhydene.2006.05.009.

[286] N. Johnson and J. Ogden, “A spatially-explicit optimization model for long-term hydrogen pipeline planning,” *Int. J. Hydrogen Energy*, vol. 37, no. 6, pp. 5421–5433, 2012, doi: 10.1016/j.ijhydene.2011.08.109.

[287] S. Baufumé *et al.*, “GIS - based scenario calculations for a nationwide German hydrogen pipeline infrastructure,” *Int. J. Hydrogen Energy*, pp. 1–33, 2012.

[288] Wood plc, “Wood internal pipeline model.” Wood plc, Aberdeen, 2018.

[289] K. Ellwanger, E. A. Nascimento, S. F. Mohammadi, and N. S. Galgoul, “Regulations and cost estimation for the decommissioning of a sample fixed offshore platform in Brazil,” *Int. J. Civ. Environ. Eng.*, vol. 16, no. 5, pp. 69–81, 2016.

[290] G. Thompson, “Statistical literacy guide: How to adjust for inflation,” London, 2009. Accessed: Jun. 03, 2022. [Online]. Available: http://www.parliament.uk/briefing-papers/sn04962.pdf.

[291] Exchange Rates UK, “Exchange Rates UK - Compare live foreign currency exchange rate & history,” 2022. https://www.exchangerates.org.uk/ (accessed Feb. 03, 2022).

[292] UKForex Limited, “Ofx,” 2022. ofx.com (accessed Feb. 03, 2022).

[293] RI, “Euro area inflation rates: 1997 to 2022,” 2022. https://www.rateinflation.com/inflation-rate/euro-area-historical-inflation-rate/ (accessed Feb. 03, 2022).

[294] ORE Catapult, “Floating offshore wind : Cost reduction pathways to subsidy free,” 2021. Accessed: Mar. 23, 2022. [Online]. Available: https://ore.catapult.org.uk/?orecatapultreports=floating-offshore-windcost-reduction-pathways-subsidy-free.

[295] S. McDonagh, S. Ahmed, C. Desmond, and J. D. Murphy, “Hydrogen from offshore wind: Investor perspective on the profitability of a hybrid system including for curtailment,” *Appl. Energy*, vol. 265, no. February, p. 114732, 2020, doi: 10.1016/j.apenergy.2020.114732.

[296] Clifford Talbot Partnership Ltd, “Energy prices,” 2022. https://www.cliffordtalbot.co.uk/energy-prices/ (accessed Mar. 23, 2022).

[297] Euroactive and Reuters, “‘Let’s reach for the stars’: EU aims for green hydrogen below €2/kg by 2030,” 2021. https://www.euractiv.com/section/energy/news/lets-reach-for-the-stars-eu-aims-for-green-hydrogen-below-e2-kg-by-2030/ (accessed Nov. 05, 2022).

[298] M. Smeed, “Charging the wrong way,” 2021. [Online]. Available: https://cdn.ymaws.com/www.renewableuk.com/resource/resmgr/210524_tnuos_paper_final_for.pdf.

[299] NFPA, “Hydrogen technologies Code,” NFPA, Quincy, 2020.

[300] Crown Estate Scotland, “Energy Infrastructure Agreements.” 2019.

[301] P. Beiter *et al.*, “A spatial-economic cost- Reduction pathway analysis for U.S. offshore wind energy development from 2015–2030,” National Renewable Energy Laboratory, Golden, 2016.

[302] T. Adedipe and M. Shafiee, “An economic assessment framework for decommissioning of offshore wind farms using a cost breakdown structure,” *Int. J. Life Cycle Assess.*, vol. 26, no. 2, pp. 344–370, 2021, doi: 10.1007/s11367-020-01793-x.

[303] A. Spyroudi, “End-of-life planning in offshore wind,” 2021. Accessed: Mar. 15, 2022. [Online]. Available: https://ore.catapult.org.uk/analysisinsight/end-of-life-planning-offshore-wind/.

[304] A. Madariaga and N. MacLeod, “Offshore HVDC risk perceptions: are they driving investments appropriately?,” Energynautics GmbH, Brussels, 2015.

[305] T. Stehly, P. Beiter, and P. Duffy, “2019 cost of wind energy review,” National Renewable Energy Laboratory, Golden, 2020.

[306] G. Rubio-Domingo and P. Linares, “The future investment costs of offshore wind: An estimation based on auction results,” *Renew. Sustain. Energy Rev.*, vol. 148, p. 111324, 2021, doi: https://doi.org/10.1016/j.rser.2021.111324.

[307] I. Elzemeity, I. Elsayeed, and A. Elzemeity, “Feasibility study of an offshore wind farm with the Egyptian-Saudi Arabia HVDC link,” in *2021 6th International Conference on Renewable Energy: Generation and Applications (ICREGA)*, 2021, pp. 168–172, doi: 10.1109/ICREGA50506.2021.9388222.

[308] C. Maienza, A. M. Avossa, F. Ricciardelli, D. Coiro, G. Troise, and C. T. Georgakis, “A life cycle cost model for floating offshore wind farms,” *Appl. Energy*, vol. 266, p. 114716, 2020, doi: https://doi.org/10.1016/j.apenergy.2020.114716.

[309] A. Ioannou, A. Angus, and F. Brennan, “A lifecycle techno-economic model of offshore wind energy for different entry and exit instances,” *Appl. Energy*, vol. 221, pp. 406–424, 2018, doi: https://doi.org/10.1016/j.apenergy.2018.03.143.

[310] J. Bosch, I. Staffell, and A. D. Hawkes, “Global levelised cost of electricity from offshore wind,” *Energy*, vol. 189, p. 116357, 2019, doi: https://doi.org/10.1016/j.energy.2019.116357.

[311] D. Elliott *et al.*, “A Comparison of AC and HVDC Options for the Connection of Offshore Wind Generation in Great Britain,” *IEEE Trans. Power Deliv.*, vol. 31, no. 2, pp. 798–809, 2016, doi: 10.1109/TPWRD.2015.2453233.

[312] K. Nieradzinska, C. MacIver, S. Gill, G. A. Agnew, O. Anaya-Lara, and K. R. W. Bell, “Optioneering analysis for connecting Dogger Bank offshore wind farms to the GB electricity network,” *Renew. Energy*, vol. 91, pp. 120–129, 2016, doi: https://doi.org/10.1016/j.renene.2016.01.043.

[313] E. Liun, “Stochastic Methodology to Estimate Costs of HVDC Transmission System,” *J. Energy Power Sources*, vol. 2, no. 3, pp. 90–98, 2015.

[314] P. Härtel, T. K. Vrana, T. Hennig, M. von Bonin, E. J. Wiggelinkhuizen, and F. D. J. Nieuwenhout, “Review of investment model cost parameters for VSC HVDC transmission infrastructure,” *Electr. Power Syst. Res.*, vol. 151, pp. 419–431, 2017, doi: https://doi.org/10.1016/j.epsr.2017.06.008.

[315] R. Smith, “Electricity Ten Year Statement--Appendix E,” 2015.

[316] A. Flament *et al.*, “NorthSeaGrid Final Report,” 2015.

[317] S. Cole, P. Martinot, S. Rapoport, G. Papaefthymiou, and V. Gori, “Study of the benefits of a meshed offshore grid in Northern Seas region,” 2014.

[318] F. D. J. Nieuwenhout and M. van Hout, “Cost, benefits, regulations and policy aspects of a North Sea Transnational Grid,” 2013. [Online]. Available: https://www.nstg-project.nl/uploads/media/9_ECN-E-13-065_NSTG_WP7_Cost_benefits_regulations_policy_aspects.pdf.

[319] ENTSOE, “Offshore Transmission Technology,” ENTSOE, 2011. Accessed: Mar. 25, 2022. [Online]. Available: https://eepublicdownloads.entsoe.eu/clean-documents/pre2015/publications/entsoe/SDC/European_offshore_grid_-_Offshore_Technology_-_FINALversion.pdf.

[320] A. L’Abbate and G. Migliavacca, “Review of costs of transmission infrastructures, including cross border connections,” 2011.

APPENDIX A

The information within this part of Appendix was accurate at the time of writing (2019) and has been updated regularly within 2020, 2021 and 2022. However, due to fast paced changes in the industry and world decarbonisation ambitions, the accuracy of these data especially status should be confirmed with other sources before use.

Appendix A lists all oil and gas infrastructure identified within the Areas selected in Section 2.3.1 of Chapter 2. The oil and gas platforms listed are within 50 km radius from the Areas of Search. The weights of the platforms were sourced from OSPAR [112]. and the status and estimated cease of production were sourced from the Rystad database [111]. The O&G pipelines listed start at the platforms identified, but the tables also contain information on other pipelines in case the original pipelines do not connect directly to shore. For example, the pipeline PL 164 that was selected for the case study for Chapter 4, does not end in a gas terminal. It ends at Brent A platform, which is connected to shore through FLAGS pipeline terminating at St Fergus gas terminal. Thus, FLAGS pipeline, as a line connecting the previous pipeline to shore, is also listed in the table.

Since Area D also contains existing or planned wind farms, Table A9 lists information on these windfarms.

Table A1: Area A oil and gas platforms. [111], [112]

Platform	*Status*	*Estimated Cease of Production*	*Weight of Substructure (t)*	*Weight of Topside (t)*
Magnus	Producing	2026	35,057	34,600
Tern	Producing	-	20,500	19,300
Eider	Abandoned	2018	17,100	11,200

Table A2: Area A pipelines [225].

Pipeline	*Status*	*Fluid*	*From*	*To*	*Connection with Shore*	*Diameter (inch)*
PL139	Active	Oil	Magnus	Ninian	No (further line Ninian to Sullom Voe, PL10)	24
PL164	Active	Gas	Magnus	Brent A	No (further line Brent A to St Fergus, FLAGS)	20
PL477	Active	Oil	Tern	Cormorant	No (further line North Cormorant to Cormorant A, PL113, Cormorant A to Sullom Voe PL4)	16

Table A3: Area B oil and gas platforms [111], [112].

Platform	*Status*	*Estimated Cease of Production*	*Weight of Substructure (t)*	*Weight of topside (t)*
Piper	Producing	2026	22,555	28,000
Saltire	Abandoned	2015	15,000	14,744
Captain	Producing	-	5,500/ 5,500	4,900/7,600
Claymore	Producing	2029	17,000/3,400	18,000/4,600
Tartan	Producing	2023	14,090	14,400
Scott	Producing	2023	16,130/8,800	20,839/15,477

Golden Eagle	Producing	2024	6,200/6,200	11,500/4,800	
Goldeneye	Abandoned	2018	3,000	1,000	
Buzzard	Producing	2026	5,569/5,130/4,720/3,500	10,950/9,651/3,608/5,300	

Table A4: Area B pipelines [225].

Pipeline	*Status*	*Fluid*	*From*	*To*	*Connection with Shore*	*Diameter (inch)*
PL1744	Active	Gas	Captain	Frigg	No (further line Frigg to St Fergus PL 6S)	8
PL2072	Active	Gas	Buzzard	Captain T	No (further line Frigg to St Fergus PL 6S)	10
PL2074	Active	Oil	Buzzard	Forties	No (further line Forties to Cruden Bay PL721, 36 inch or abandoned PL8)	18
PL11	Active	Oil	Claymore	Flotta	Yes	30
PL14	Not in use	Gas	Tartan	MCP01	No (further line Frigg to St Fergus PL 6S)	18
PL18	Active	Oil	Tartan	Claymore	No (further line PL11)	30

PL820	Active	Oil	Piper	Claymore	No (further line PL11)	30
PL822	Active	Oil	Scott	Forties	No (further line Forties to Cruden Bay PL721, or abandoned PL8)	24
PL823	Active	Gas	Scott	Sage T	No (further line PL762, Sage export line)	14
PL3036	Active	Oil	Golden Eagle	Claymore	No (further line PL11)	6
PL3037	Active	Gas	Golden Eagle	Ettrick	No (connects to Sage export line through PL2448 hot tap jumper)	20
PL1978	Active	Gas	Goldeneye	St Fergus	Yes	20

Table A5: Area C oil and gas platforms [111], [112].

Platform	*Status*	*Estimated Cease of Production*	*Weight of Substructure (t)*	*Weight of Topside (t)*
Kittiwake	Producing	-	5,370	9,000
Gannet A	Producing	2023	7,750	12,350

Table A6: Area C pipelines [225].

Pipeline	*Status*	*Fluid*	*From*	*To*	*Connection with Shore*	*Diameter (inch)*

PL673	Active	Gas	Kittiwake	Fulmar receiver T	No (further line Fulmar A to St Fergus PL208)	4
PL2403	Active	Oil	Kittiwake		No (further line Forties to Cruden Bay PL721)	10
PL764	Active	Gas	Gannet A	Gannet Diverter	No (further line Fulmar A to St Fergus PL208)	20
PL763	Active	Oil	Gannet A	Fulmar A	No (further line from Fulmar a to Teeside through Norpipe system)	16

Table A7: Area D oil and gas platforms [111], [112].

Platform	*Status*	*Estimated Cease of Production*	*Weight of Substructure (t)*	*Weight of Topside (t)*
Beatrice	Abandoned	2015	3,225/1,976/1,537/730	8,157/6,349/5,360/415
Jacky	Abandoned	2014	596	663

Table A8: Area D pipeline [225].

Pipeline	*Status*	*Fluid*	*From*	*To*	*Connection with Shore*	*Diameter (inch)*

PL1838	Active	Oil	Beatrice	Shandwick Bay	Yes	16

Table A9: Information on wind developments in Area D [300].

Name	*Status*	*Capacity (MW)*	*No of turbines*	*First Power (Year)*
Beatrice demonstrator	Abandoned	10	2	2007
Beatrice	Fully Commissioned	588	84	2019
Moray East	Under Construction	950	100	2022
Moray West	Consent Authorised	850	72-85	2024

APPENDIX B

Appendix B shows supporting data for Chapter 3. Figure B1 shows hourly mean wind speed data in m/s over 21 years for the area around Magnus platform. The data is colour scaled with green representing the lowest mean wind speed and red the highest.

Figure B2 shows the mean power production in kW per hour per individual 10MW wind turbine data as described in Section 3.3.2 in Chapter 3. The least windy hour with the lowest mean power production, which was used to size the electrolyser with the smallest capacity, is highlighted.

Figure B3 shows the average windfarm utilisation (AWFu) when connected to 957.5 MW electrolyser calculated as per Section 3.3.2 in Chapter 3. As the electrolyser is sized according to the wind resource in the summer months, windfarm is fully utilised in the summer. However, this is not the case in the winter months when windfarm produces at full capacity and thus being utilised on average around 64%.

Figure B4 shows the 1500 MW electrolyser utilisation (AEu) when connected to the 1500MW windfarm as per Section 3.3.2 in Chapter 3. The electroyser is fully utilised during the winter when windfarm is producing at full capacity (note no losses are included yet) and utilised at around 65% in the summer, when the wind resource is lower.

As highlighted in Chapter 3, utilisation factors are only based on the wind resource ie they are gross percentages. To gain net percentage of operation, losses have to be applied as discussed in Section 3.3.3.3 in Chapter 3.

	Mean of WS_ERA-5 (m/s)											
Hour	Jan	Feb	Mar	Apr	May	Jun	Jul	Aug	Sep	Oct	Nov	Dec
00:00 - 01:00	12.662	11.913	10.798	9.704	8.501	8.148	8.015	8.166	9.835	11.075	11.924	12.033
01:00 - 02:00	12.735	11.921	10.775	9.69	8.463	8.143	8.001	8.148	9.766	11.079	11.93	12.053
02:00 - 03:00	12.797	11.966	10.733	9.678	8.472	8.188	7.97	8.122	9.712	11.08	11.98	12.029
03:00 - 04:00	12.834	11.937	10.722	9.632	8.457	8.23	7.976	8.107	9.701	11.058	11.965	12.079
04:00 - 05:00	12.836	11.952	10.754	9.575	8.448	8.266	7.983	8.106	9.723	11.042	11.908	12.116
05:00 - 06:00	12.805	11.932	10.798	9.557	8.411	8.285	8.003	8.132	9.767	11.016	11.882	12.144
06:00 - 07:00	12.755	11.92	10.821	9.534	8.358	8.295	8.009	8.156	9.864	11.016	11.889	12.194
07:00 - 08:00	12.703	11.9	10.843	9.528	8.369	8.295	8.027	8.191	9.935	11.045	11.838	12.288
08:00 - 09:00	12.677	11.919	10.952	9.568	8.405	8.287	8.032	8.222	10.006	11.113	11.781	12.411
09:00 - 10:00	12.679	11.999	11.078	9.635	8.434	8.299	8.041	8.252	10.053	11.127	11.774	12.533
10:00 - 11:00	12.672	11.976	11.103	9.615	8.319	8.231	8.009	8.161	10.043	11.099	11.598	12.52
11:00 - 12:00	12.52	11.973	11.052	9.646	8.251	8.212	7.996	8.131	10.04	11.037	11.508	12.514
12:00 - 13:00	12.486	12.038	11.018	9.662	8.265	8.222	7.979	8.124	10.005	10.928	11.509	12.554
13:00 - 14:00	12.555	12.111	11.003	9.704	8.281	8.227	8.001	8.148	9.952	10.884	11.556	12.557
14:00 - 15:00	12.556	12.145	10.976	9.765	8.291	8.225	7.984	8.178	9.932	10.869	11.598	12.559
15:00 - 16:00	12.554	12.134	10.942	9.769	8.277	8.219	7.971	8.203	9.904	10.855	11.608	12.529
16:00 - 17:00	12.503	12.127	10.942	9.777	8.26	8.221	7.939	8.226	9.852	10.862	11.648	12.528
17:00 - 18:00	12.459	12.113	10.904	9.749	8.277	8.202	7.928	8.245	9.843	10.89	11.635	12.52
18:00 - 19:00	12.514	12.102	10.873	9.733	8.315	8.192	7.93	8.254	9.78	10.983	11.638	12.566
19:00 - 20:00	12.605	12.052	10.872	9.749	8.348	8.199	7.912	8.27	9.791	11.063	11.691	12.621
20:00 - 21:00	12.695	12.064	10.891	9.797	8.396	8.204	7.934	8.28	9.871	11.151	11.774	12.655
21:00 - 22:00	12.771	12.139	10.917	9.855	8.467	8.236	7.983	8.304	9.924	11.256	11.905	12.597
22:00 - 23:00	12.569	12.007	10.89	9.807	8.523	8.221	8.026	8.298	10.013	11.197	11.909	12.333
23:00 - 24:00	12.527	11.969	10.811	9.713	8.508	8.206	8.013	8.277	9.961	11.164	11.932	12.176

Figure B1: Hourly mean wind speed data for the area around Magnus platform.

Hour	Jan	Feb	Mar	Apr	May	Jun	Jul	Aug	Sep	Oct	Nov	Dec
00:00 - 01:00	10000	9923	8937	7970	6906	6594	6476	6610	8086	9182	9933	10000
01:00 - 02:00	10000	9930	8917	7957	6872	6589	6464	6594	8025	9186	9938	10000
02:00 - 03:00	10000	9970	8880	7947	6880	6629	6436	6571	7977	9187	9982	10000
03:00 - 04:00	10000	9944	8870	7906	6867	6666	6442	6558	7967	9167	9969	10000
04:00 - 05:00	10000	9958	8898	7856	6859	6698	6448	6557	7987	9153	9919	10000
05:00 - 06:00	10000	9940	8937	7840	6826	6715	6466	6580	8025	9130	9896	10000
06:00 - 07:00	10000	9929	8957	7819	6779	6724	6471	6601	8111	9130	9902	10000
07:00 - 08:00	10000	9912	8977	7814	6789	6724	6487	6632	8174	9156	9857	10000
08:00 - 09:00	10000	9928	9073	7849	6821	6717	6491	6659	8237	9216	9806	10000
09:00 - 10:00	10000	9999	9185	7909	6847	6727	6499	6686	8278	9228	9800	10000
10:00 - 11:00	10000	9979	9207	7891	6745	6667	6471	6605	8270	9203	9645	10000
11:00 - 12:00	10000	9976	9162	7918	6685	6650	6459	6579	8267	9148	9565	10000
12:00 - 13:00	10000	10000	9132	7933	6697	6659	6444	6573	8236	9052	9566	10000
13:00 - 14:00	10000	10000	9118	7970	6711	6664	6464	6594	8189	9013	9607	10000
14:00 - 15:00	10000	10000	9095	8024	6720	6662	6449	6620	8171	9000	9645	10000
15:00 - 16:00	10000	10000	9064	8027	6708	6657	6437	6642	8147	8988	9653	10000
16:00 - 17:00	10000	10000	9064	8034	6693	6658	6409	6663	8101	8994	9689	10000
17:00 - 18:00	10000	10000	9031	8010	6708	6642	6399	6680	8093	9018	9677	10000
18:00 - 19:00	10000	10000	9003	7995	6741	6633	6401	6688	8037	9101	9680	10000
19:00 - 20:00	10000	10000	9003	8010	6771	6639	6385	6702	8047	9171	9727	10000
20:00 - 21:00	10000	10000	9019	8052	6813	6643	6405	6711	8117	9249	9800	10000
21:00 - 22:00	10000	10000	9042	8103	6876	6672	6448	6732	8164	9342	9916	10000
22:00 - 23:00	10000	10000	9018	8061	6925	6658	6486	6726	8243	9290	9920	10000
23:00 - 24:00	10000	9973	8949	7978	6912	6645	6474	6708	8197	9261	9940	10000

Figure B2: Mean power production per hour per individual 10MW wind turbine, with highlighted least windy hour.

	Mean of power_production_data (kW)				% utilisation of the windfarm							
Hour	Jan	Feb	Mar	Apr	May	Jun	Jul	Aug	Sep	Oct	Nov	Dec
00:00 - 01:00	63.83	64.33	71.42	80.09	92.43	96.81	98.57	96.58	78.95	69.52	64.26	63.83
01:00 - 02:00	63.83	64.28	71.59	80.22	92.88	96.87	98.76	96.81	79.55	69.49	64.23	63.83
02:00 - 03:00	63.83	64.03	71.89	80.33	92.78	96.29	99.18	97.15	80.02	69.49	63.95	63.83
03:00 - 04:00	63.83	64.19	71.97	80.74	92.96	95.76	99.09	97.34	80.12	69.63	64.03	63.83
04:00 - 05:00	63.83	64.11	71.74	81.26	93.06	95.30	99.00	97.36	79.93	69.74	64.36	63.83
05:00 - 06:00	63.83	64.22	71.42	81.42	93.51	95.06	98.73	97.02	79.54	69.92	64.51	63.83
06:00 - 07:00	63.83	64.29	71.26	81.63	94.16	94.94	98.65	96.70	78.70	69.92	64.47	63.83
07:00 - 08:00	63.83	64.40	71.11	81.69	94.02	94.94	98.41	96.25	78.09	69.72	64.76	63.83
08:00 - 09:00	63.83	64.29	70.35	81.32	93.58	95.04	98.34	95.86	77.50	69.27	65.09	63.83
09:00 - 10:00	63.83	63.84	69.50	80.71	93.23	94.89	98.22	95.48	77.11	69.17	65.13	63.83
10:00 - 11:00	63.83	63.97	69.33	80.89	94.64	95.74	98.65	96.64	77.19	69.36	66.19	63.83
11:00 - 12:00	63.83	63.99	69.67	80.61	95.49	95.98	98.82	97.03	77.22	69.77	66.74	63.83
12:00 - 13:00	63.83	63.83	69.90	80.47	95.31	95.86	99.05	97.12	77.51	70.52	66.73	63.83
13:00 - 14:00	63.83	63.83	70.00	80.09	95.11	95.79	98.76	96.81	77.95	70.82	66.44	63.83
14:00 - 15:00	63.83	63.83	70.19	79.56	94.99	95.82	98.99	96.42	78.12	70.93	66.19	63.83
15:00 - 16:00	63.83	63.83	70.42	79.52	95.16	95.90	99.16	96.10	78.36	71.02	66.13	63.83
16:00 - 17:00	63.83	63.83	70.42	79.45	95.38	95.87	99.60	95.81	78.80	70.98	65.88	63.83
17:00 - 18:00	63.83	63.83	70.68	79.70	95.16	96.11	99.75	95.57	78.88	70.78	65.96	63.83
18:00 - 19:00	63.83	63.83	70.90	79.84	94.69	96.24	99.72	95.45	79.42	70.14	65.94	63.83
19:00 - 20:00	63.83	63.83	70.91	79.70	94.28	96.15	99.97	95.25	79.33	69.60	65.63	63.83
20:00 - 21:00	63.83	63.83	70.77	79.28	93.69	96.09	99.67	95.12	78.64	69.01	65.13	63.83
21:00 - 22:00	63.83	63.83	70.59	78.77	92.84	95.68	99.00	94.82	78.19	68.33	64.37	63.83
22:00 - 23:00	63.83	63.83	70.78	79.19	92.17	95.87	98.42	94.90	77.44	68.71	64.35	63.83
23:00 - 24:00	63.83	64.01	71.33	80.01	92.35	96.06	98.59	95.16	77.87	68.93	64.22	63.83

Figure B3: Windfarm utilisation results at 957.5MW electrolyser.

	electrolyser % utilisation if max hour mean power production used											
Hour	Jan	Feb	Mar	Apr	May	Jun	Jul	Aug	Sep	Oct	Nov	Dec
00:00 - 01:00	100.00	99.23	89.37	79.70	69.06	65.94	64.76	66.10	80.86	91.82	99.33	100.00
01:00 - 02:00	100.00	99.30	89.17	79.57	68.72	65.89	64.64	65.94	80.25	91.86	99.38	100.00
02:00 - 03:00	100.00	99.70	88.80	79.47	68.80	66.29	64.36	65.71	79.77	91.87	99.82	100.00
03:00 - 04:00	100.00	99.44	88.70	79.06	68.67	66.66	64.42	65.58	79.67	91.67	99.69	100.00
04:00 - 05:00	100.00	99.58	88.98	78.56	68.59	66.98	64.48	65.57	79.87	91.53	99.19	100.00
05:00 - 06:00	100.00	99.40	89.37	78.40	68.26	67.15	64.66	65.80	80.25	91.30	98.96	100.00
06:00 - 07:00	100.00	99.29	89.57	78.19	67.79	67.24	64.71	66.01	81.11	91.30	99.02	100.00
07:00 - 08:00	100.00	99.12	89.77	78.14	67.89	67.24	64.87	66.32	81.74	91.56	98.57	100.00
08:00 - 09:00	100.00	99.28	90.73	78.49	68.21	67.17	64.91	66.59	82.37	92.16	98.06	100.00
09:00 - 10:00	100.00	99.99	91.85	79.09	68.47	67.27	64.99	66.86	82.78	92.28	98.00	100.00
10:00 - 11:00	100.00	99.79	92.07	78.91	67.45	66.67	64.71	66.05	82.70	92.03	96.45	100.00
11:00 - 12:00	100.00	99.76	91.62	79.18	66.85	66.50	64.59	65.79	82.67	91.48	95.65	100.00
12:00 - 13:00	100.00	100.00	91.32	79.33	66.97	66.59	64.44	65.73	82.36	90.52	95.66	100.00
13:00 - 14:00	100.00	100.00	91.18	79.70	67.11	66.64	64.64	65.94	81.89	90.13	96.07	100.00
14:00 - 15:00	100.00	100.00	90.95	80.24	67.20	66.62	64.49	66.20	81.71	90.00	96.45	100.00
15:00 - 16:00	100.00	100.00	90.64	80.27	67.08	66.57	64.37	66.42	81.47	89.88	96.53	100.00
16:00 - 17:00	100.00	100.00	90.64	80.34	66.93	66.58	64.09	66.63	81.01	89.94	96.89	100.00
17:00 - 18:00	100.00	100.00	90.31	80.10	67.08	66.42	63.99	66.80	80.93	90.18	96.77	100.00
18:00 - 19:00	100.00	100.00	90.03	79.95	67.41	66.33	64.01	66.88	80.37	91.01	96.80	100.00
19:00 - 20:00	100.00	100.00	90.03	80.10	67.71	66.39	63.85	67.02	80.47	91.71	97.27	100.00
20:00 - 21:00	100.00	100.00	90.19	80.52	68.13	66.43	64.05	67.11	81.17	92.49	98.00	100.00
21:00 - 22:00	100.00	100.00	90.42	81.03	68.76	66.72	64.48	67.32	81.64	93.42	99.16	100.00
22:00 - 23:00	100.00	100.00	90.18	80.61	69.25	66.58	64.86	67.26	82.43	92.90	99.20	100.00
23:00 - 24:00	100.00	99.73	89.49	79.78	69.12	66.45	64.74	67.08	81.97	92.61	99.40	100.00

Figure B4: Electrolyser utilisation results at 1500MW electrolyser size.

APPENDIX C

While Chapter 5 only presents selection of cost data used in LCOE and LCOH calculations, more cost data has been collected from the literature. Whenever cost data points were excluded, a graph with all collected cost data was included within this Appendix. Figures C1 – C5 represent such graphs. The orange bar in these figures represents published cost estimations for 2030, and the blue bar represents cost estimations for the year of publication.

As can be seen in Figure C1, most of the data for FOWF CAPEX range around similar values. Beiter *et al.* [301] and Heidari [258] provide the widest CAPEX and OPEX range due to including different types of floating offshore wind substructures such as semi-submersible and spar buoy and do not include price reductions due to industry gaining experience as it is not a 2030 estimation. Castro-Santos *et al.* [250] on the other hand is lower as it is based on a smaller windfarm size, closer to land. Wood plc [260] also estimate higher costs as they are based on 2021, for a full 1500MW windfarm, which is far offshore. Blue data ranges have been excluded for FOWF CAPEX and OPEX as this work is looking at year 2030 and beyond. Thus, Figure C1 and Figure 5.4 in Chapter 5 only show CAPEX and OPEX estimations for floating offshore windfarms that were selected for LCOE calculations collected.

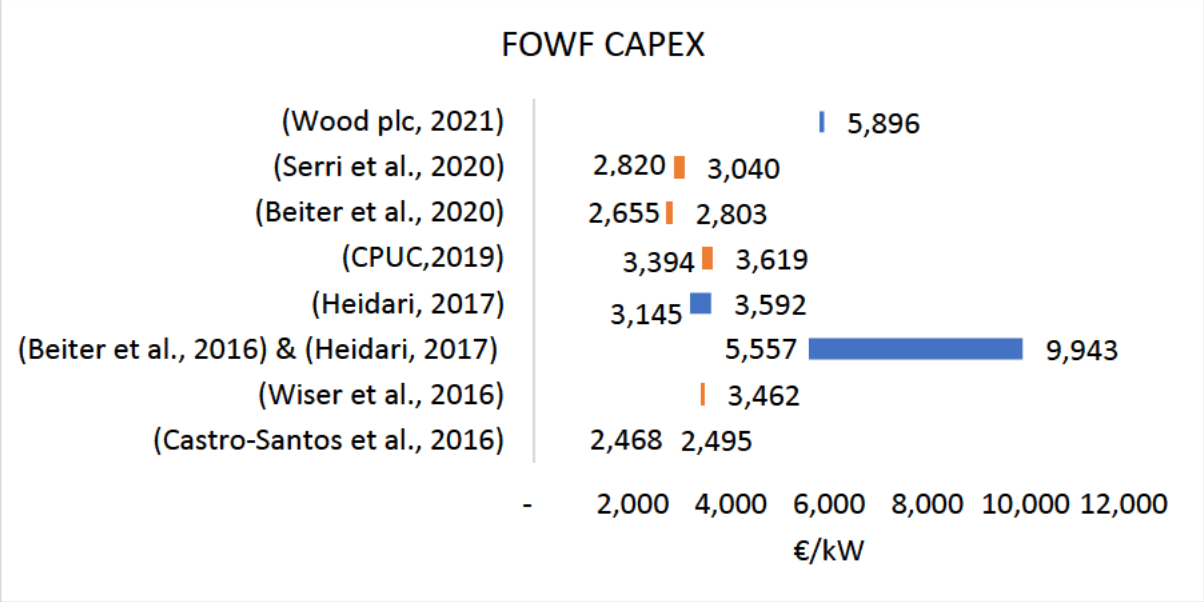

Figure C1: All FOWF capital expenditure costs from the literature.

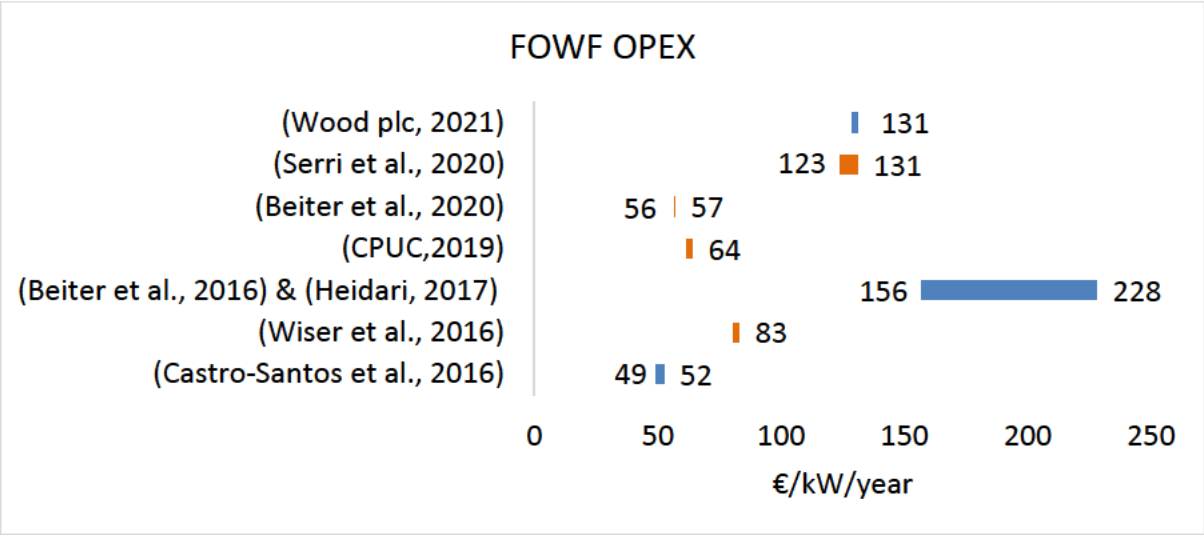

Figure C2: Operations and maintenance expenditure cost from the literature.

Table C1 lists the properties the data is based on that could impact the CAPEX ranges such as turbine size, distance from shore, and water depth. It also contains information on the data source to help the selection process.

Table C1: FOWF data properties description.

Type	*Turbine (MW)*	*Windfarm Size (MW)*	*Distance from shore (km)*	*Depth (m)*	*Country*	*Data Source*	*Source*
semi-submersible	5.075	106.58	25.5-43.60	90	Portugal	Literature, expert consultation, extrapolation	[250]
TLP, semi-sub and Spar buoy	9-11	N/A	N/A	N/A	North America and Europe	Expert elicitation	[256]
TLP, semi-sub and Spar buoy	10	600	190	186	variety including Europe and US	Estimations based on fixed bottom OWT data	[301] & [258]
TLP, semi-sub and Spar buoy	10	600	50	100	variety including	Estimations based on	[258]

					Europe and US	fixed bottom OWT data	
N/A	N/A	1,000	30-49	640-1013	US	OWF data	[257]
semi-submersible	8-15	1,000	30-49	640-1013	US	OWF data	[254]
Semi-submersible	10	1,000	100 and 200	150	Italy	Literature	[253]
Semi-submersible	10	1,500	190	186	UK	Project work	[260]

Figure C3 represents all collected DECEX estimations including Adedipe and Shafiee [302] and Spyroudi [303] that have been excluded from the data used for the LCOE calculation. This is because they include costs for fixed bottom offshore wind turbines rather than floating, which would skew the results as it is more expensive to decommission fixed bottom wind turbine rather than tow a FOWT.

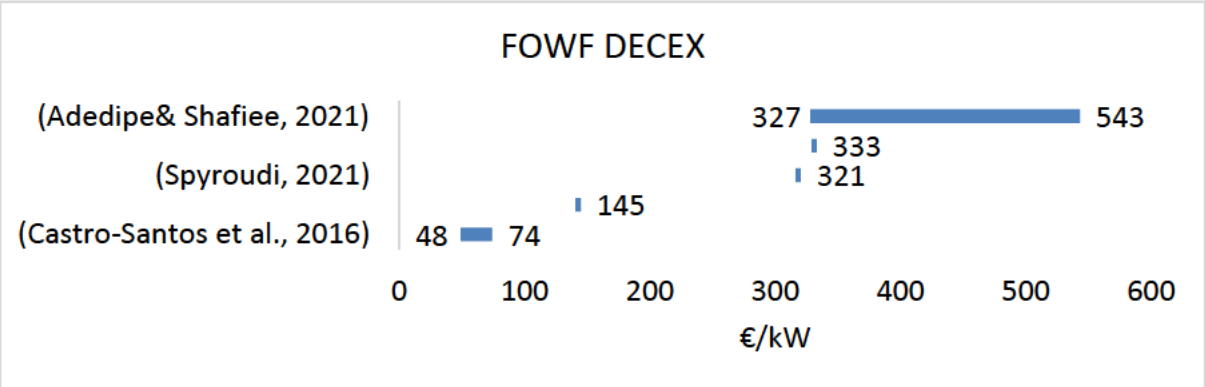

Figure C3: All FOWF DECEX data from the literature.

Figure C4 shows all cable CAPEX estimations collected from the literature including excluded data such as data that were not distance dependent [250], [258], [304]–[307] and those for cables connecting windfarms with small capacity or close to shore [250], [258], [305], [307]–[309] Table C2 provides information on data that were selected for LCOE calculations presented in Figure 5.9 in Chapter 5 such as cable length and capacity CAPEX is based on.

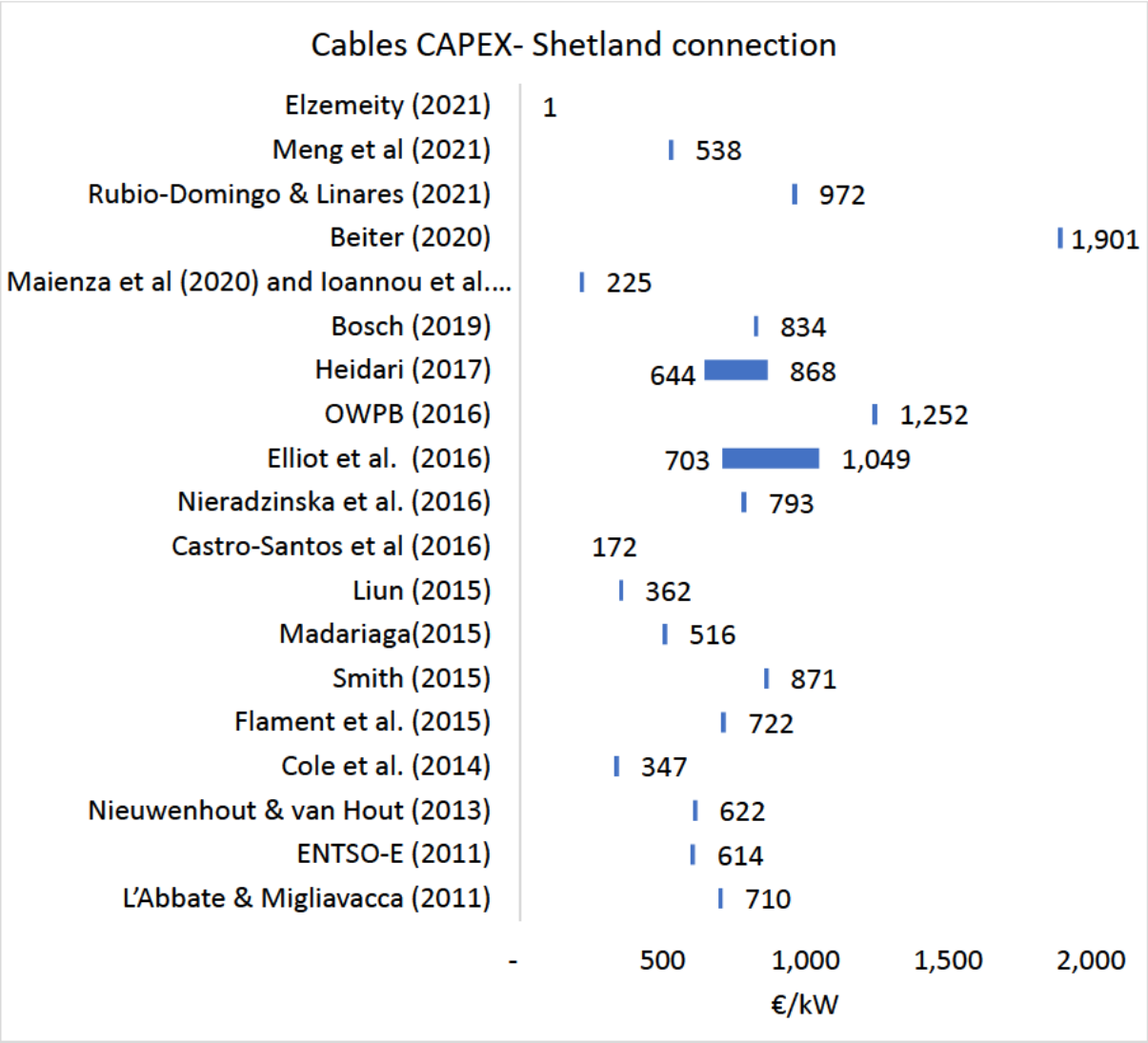

Figure C4: All cable CAPEX costs from the literature.

Table C2: Summary of cable cost data used for LCOE.

Length (km)	*Capacity (MW)*	*Notes*	*Source*
203	1500	Literature review	[264]
203	500-1000	Literature review	[310]
203	1500	Future HVAC technology	[267]
200	1000	Literature review	[311]

203	2400	Data from UK based engineering design firms	[312]
203	1500	Energy market operator estimations	[313]
203	1200	Technology cost data based on updated project information from suppliers [314]	[315]
203	1400	EU co-funded project, with range of sources and stakeholders [314]	[316]
203	2000	European Commission project with input from previous studies and a consultancy firm [314]	[317]
203	1200	North Sea Transnational Grid project [314]	[318]
203	1133	Technology cost report including suppliers and manufacturers [314]	[319]
203	1200	Data based on technical, scientific literature, and interviews with TSOs [314]	[320]

Figure C5 shows all data collected for CAPEX of pipelines including the Wood plc [288] data point. This CAPEX estimation was removed from the selection because it does not include installation cost, which makes it significantly lower than the rest of the data points.

Table C3 summarises information impacting DECEX such as mobilisation distance, water depth internal diameter and the length of the pipeline.

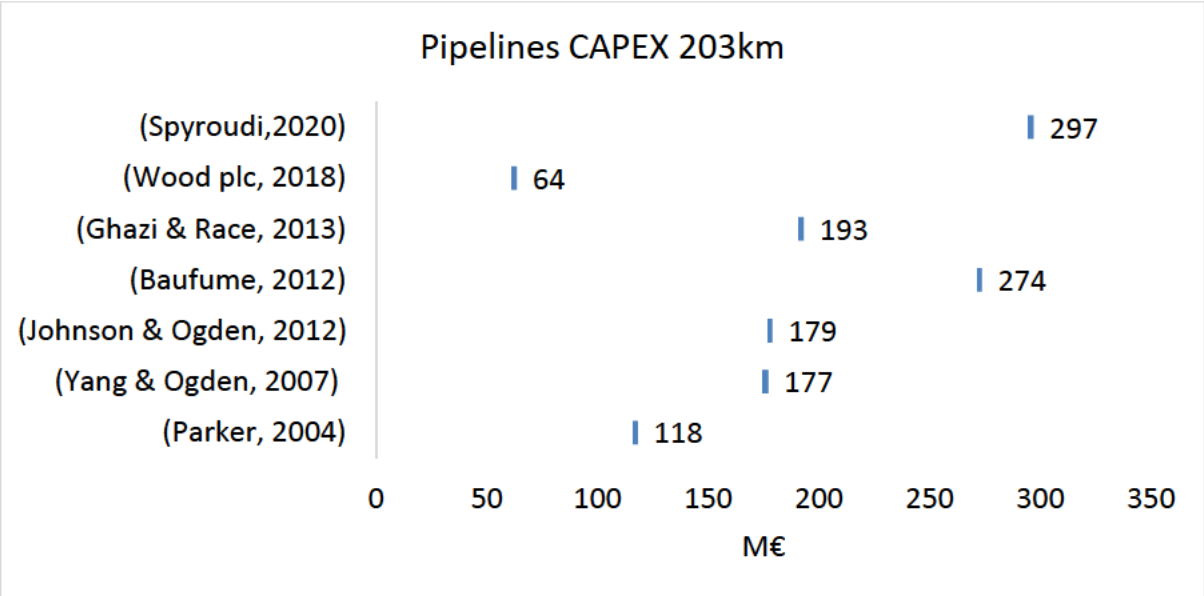

Figure C5: All pipeline CAPEX data from the literature.

Table C3: Data used to calculate pipeline DECEX.

Mobilisation Distance (km)	*Water Depth (m)*	*ID (inch)*	*L (km)*	*Cost (USD/inch/km)*	*Source*
178	211	12	4	36.1k	[283]
		13	4	34.4k	
139	190	6	13	20.3k	
		10	7	22.1k	
226	122	16	21	4.2k	[289]
		8	59	2.8k	

		6	31	5.4k	
-	-	-	1807	166.4M£/km	[50]

Table C4 shows the exchange rates and inflation rates used to convert all values into € 2020 as discussed in Section 5.3.3 of Chapter 5,.

Table C4: Average annual exchange and inflation rates.

Year	*USD to Euro (€)* [291], [292]	*GBP to Euro (€)*	*Euro inflation rate (%)* [293]
2009	0.7190	1.1225	0.29
2010	0.7551	1.166	1.62
2011	0.719	1.1527	2.71
2012	0.7781	1.2332	2.5
2013	0.7531	1.1778	1.35
2014	0.7541	1.2411	0.43
2015	0.9015	1.3777	0.03
2016	0.904	1.2242	0.24
2017	0.8865	1.1414	1.54
2018	0.8475	1.1301	1.74
2019	0.8931	1.1405	1.21
2020	0.877	1.1248	0.25